*Supplementary Material (2) to accompany* ***Investigating the Influence of Diffusional Coupling on Mixture Permeation across Porous Membranes***

# Characteristics of Maxwell-Stefan Diffusivities $Đ_1$, $Đ_2$, and $Đ_{12}$ in Nanoporous Crystalline Materials

**Rajamani Krishna*, Jasper M. van Baten**

Van 't Hoff Institute for Molecular Sciences, University of Amsterdam, Science Park 904,

1098 XH Amsterdam, The Netherlands

CORRESPONDING AUTHOR *Tel +31 20 6270990; Fax: + 31 20 5255604;

email: r.krishna@uva.nl

**Table of Contents**

# 1. Abstract

Mixture diffusion within nanoporous crystalline materials such as zeolites, and metal-organic frameworks (MOFs), is often strongly influenced by the extent to which the diffusivity of one species is *correlated* to that of its partner. Most commonly, the less-mobile species *slows* down its more mobile partner by not vacating an adsorption site quick enough for its more mobile partner to occupy that position. Such slowing-down effects, also termed *correlation effects*, are quantified by the exchange coefficient $Đ_{12}$ in the Maxwell-Stefan (M-S) diffusion formulation. With increasing concentrations of guest molecules inside the pores, the $Đ_{12}$ tends to decrease significantly, implying that correlation effects become increasingly important for separation processes operating at high pressures. The exchange coefficients $Đ_{12}$ are not accessible directly from experiments, and there is a need for developing reliable procedures for estimating $Đ_{12}$ for any given guest-mixture/host-material combination.

Molecular Dynamics (MD) simulations were carried out to determine the M-S diffusivities, $Đ_1$, $Đ_2$, and $Đ_{12}$ for a wide variety of binary mixtures ($H_2/CO_2$, $H_2/CH_4$, $CO_2/N_2$, $CH_4/CO_2$, $CH_4/C_2H_6$, $CH_4/C_3H_8$, $CH_4/nC_4H_{10}$, Ne/Ar, $H_2$/Ar, $CH_4$/Ar, Ne/$CO_2$, Ar/Kr) in several different nanoporous host materials (MFI, FAU, LTA, BEA, CHA, IRMOF-1, CuBTC, MOF-177, MgMOF-74, COF-102, COF-103, COF-108, and BTP-COF) covering a wide range of pore dimensions, pore topologies, and connectivities. For the systems that do no exhibit hydrogen bonding effects, M-S diffusivities, $Đ_1$, $Đ_2$ are in good agreement with the corresponding unary diffusivities, when compared at the total concentration, $c_t$, within the pores of the structures. the Additionally, MD simulations were also performed to determine the corresponding values of M-S diffusivity in the fluid phase, $Đ_{12,fl}$, in the absence of the restraining influence of the pore walls. For each guest/host combination, over the entire range of pore concentrations, it was found that $Đ_{12}$ is a constant fraction, $F$, of the fluid phase value, $Đ_{12,fl}$ when compared at the same value of pore concentration, $c_t$. The $Đ_{12,fl}$ can be estimated reliably

from the molecular properties using established correlation methods in the literature. This fraction, $F$, is primarily dependent on the host material, and has values in the range of 0.1 – 1. For mesopores, and for porous structures such as COF-102, COF-103, and COF-108 with large voidages and pore volumes, $F \approx 1$. For intersecting channels structures of MFI, with channels of 5.5 Å, the value of $F$ is in the narrow range of 0.1 – 0.15. For structures such as FAU, MgMOF-74, and IRMOF-1 the values of $F$ fall in range of 0.4 – 0.7.

**Keywords**: Maxwell-Stefan diffusion; correlations; zeolites; metal-organic frameworks; fluid phase diffusivity; clustering; hydrogen bonding; mutual-slowing down;

## 2. Introduction

A wide variety of crystalline nanoporous materials is used in membrane separations and pressure swing adsorption (PSA) devices [1-8]. These materials include zeolites (crystalline aluminosilicates), metal-organic frameworks (MOFs), zeolitic imidazolate frameworks (ZIFs), covalent organic frameworks (COFs), periodic mesoporous organosilicas (PMOs), SBA-16, and MCM-41. The characteristic pore dimensions of these structures are either in the *micro*-porous ($d_p$ < 2 nm), or *meso*-porous ranges (2 nm < $d_p$ < 50 nm). Several types of channel topologies are encountered, including one-dimensional (1D) channels (e.g. AFI, MIL-47, MIL-53(Cr), MgMOF-74, and BTP-COF), intersecting channels (e.g. MFI, BEA), cavities with large windows (e.g. FAU, IRMOF-1, CuBTC), and cages separated by narrow windows (e.g. LTA, CHA).

For separation process design and development it is necessary to have a reliable *quantitative* description of the diffusion of mixtures of guest molecules inside the porous materials. For binary mixture diffusion, the fluxes $N_i$ of species $i$ are commonly related to the chemical potential gradients $\nabla\mu_i$ by use of the set of two *coupled* Maxwell-Stefan (M-S) equations, that apply equally for micro- and meso-porous frameworks [9-11]

$$\begin{aligned} -\phi\frac{c_1}{RT}\nabla\mu_1 &= \frac{x_2N_1 - x_1N_2}{Đ_{12}} + \frac{N_1}{Đ_1}; \\ -\phi\frac{c_2}{RT}\nabla\mu_2 &= \frac{x_1N_2 - x_2N_1}{Đ_{12}} + \frac{N_2}{Đ_2} \end{aligned} \qquad (1)$$

where $\phi$ represents the fractional pore volume, and the concentrations $c_i$ are defined in terms of moles per $m^3$ of accessible pore volume. The fluxes $N_i$ are defined in terms of the cross-sectional area of the crystalline framework. The $x_i$ in eq. (1) are the component mole fractions of the adsorbed phase within the micropores

$$x_i = c_i / c_t; \quad i = 1,2 \qquad (2)$$

Formally speaking, the M-S equations (1) serve only to *define* the phenomenological coefficients $Đ_1$, $Đ_2$, and $Đ_{12}$ and the estimation of the fluxes $N_i$ in the mixture requires reliable procedures for estimation of these three diffusivities.

The coefficients $Đ_1$, and $Đ_2$ characterize species $i$ – pore wall interactions in the broadest sense; these can in most, but not all, cases be determined from unary diffusion experiments or simulations.

The exchange coefficients $Đ_{12}$ quantify interaction between components $i$ with component $j$. At the molecular level, the $Đ_{12}$ reflect how the facility for transport of species $i$ *correlates* with that of species $j$. The value of $Đ_{12}$, relative to that of $Đ_1$, determines the extent to which the flux of species 1 is influenced by the chemical potential gradient of species 2. The larger the *degree of correlation*, $Đ_1/Đ_{12}$, the stronger is the influence of coupling. Generally speaking, the more-strongly-adsorbed-tardier partner species will have the effect of slowing down the less-strongly-adsorbed-more-mobile partner in the mixture. The proper estimation of $Đ_{12}$ is of vital importance, for example, in modeling $CO_2/H_2$ separations across MgMOF-74 membranes; in this case the tardier $CO_2$ slows down the mobile partner $H_2$ in sufficient measure to result in $CO_2$-selective separations [12].

The exchange coefficients $Đ_{12}$ cannot be determined directly from unary experiments and, therefore, its estimation requires more careful attention and analysis.

In this second of two Supplementary Materials to accompany our article *Investigating the Influence of Diffusional Coupling on Mixture Permeation across Porous Membranes*, we summarize, and analyse, published Molecular Dynamics (MD) simulation data for unary and binary mixture diffusion of a wide variety of guest species in several different nanoporous host materials, listed in Table 1, along with salient structural details, with the overall objective of suggesting practical estimation procedures for $Đ_1$, $Đ_2$, and $Đ_{12}$.

## 3. Estimating $Đ_1$ and $Đ_2$

The persuasive advantages for use of the M-S equations (1) in preference to the alternative Onsager or Fickian formulations is that in most cases the coefficients $Đ_1$, and $Đ_2$, that characterize species $i$ – pore wall interactions in the broadest sense, can be identified with those determined for *unary* systems [13].

To illustrate this, Figure 1 provides data on the M-S diffusivity of $CO_2$, $Đ_i$, determined MD simulation data for diffusion of a variety of equimolar ($c_1 = c_2$) binary mixtures of $CO_2$ and different partner species in six different host materials. For any host material, we note that the diffusivity of $CO_2$ in a binary mixture is practically independent of the partner species. Furthermore, when compared at the same total pore concentration of the adsorbed phase within the pores, $c_t = c_1 + c_2$, the values of $Đ_i$ are nearly the same in the mixture as those determined for *unary* diffusion, indicated by the red circles in Figure 1. Similar conclusions hold for the diffusivity of $CH_4$ in mixture containing different partner species; see Figure 2. These conclusions are of general validity for mixtures in which no cluster formation occurs; exceptional circumstances are discussed in Sections 9 and 10.

## 4. Relating $Đ_{12}$ in *meso*-porous materials to fluid phase $Đ_{12,fl}$

In the absence of pore walls, i.e. in *fluid phase* mixtures, the molecule-molecule interactions are quantified by the M-S diffusivity $Đ_{12,fl}$. As illustration, Figure 3 presents MD simulation data on $Đ_{12,fl}$ for $H_2/CH_4$, $CO_2/H_2$, $CH_4/CO_2$, $CH_4$/Ar, $CH_4/C_2H_6$, and $CH_4/C_3H_8$ mixtures as a function of the total molar concentration $c_t$; these simulations were carried out with the methodology described in the literature [14]. MD simulations of $Đ_{12}$ in BTP-COF, that consists of one-dimensional (1D) hexagonal shaped channels of 3.4 nm size are in excellent agreement with the values of $Đ_{12,fl}$ over the range of $c_t$. This conclusion also holds for cylindrical mesopores of 2 nm, 3 nm, 4 nm, and 5.8 nm. This leads us to conclude that the assumption that molecule-molecule interactions in mesoporous hosts is practically the same as that within the same *fluid phase* mixture at the same total molar concentration, $c_t$, i.e. $Đ_{12} = Đ_{12,fl}$.

Reliable procedures for estimation of $Đ_{12,fl}$ from molecular properties of the individual species are available in the literature, offering the possibility of *a priori* estimations of correlations. As illustration, the continuous solid lines in Figure 3 show the estimations of $Đ_{12,fl}$ using the method of Fuller, Schettler and Giddings (FSG) [15], developed for *ideal gas* mixtures. We note that for concentrations $c_t < 6$ kmol $m^{-3}$, the MD simulated $Đ_{12,fl}$ values are in excellent agreement with the FSG estimations. For

concentrations $c_t > 6$ kmol m$^{-3}$, the $Đ_{12,fl}$ values reflect those in dense condensed fluids, for which some estimation procedures are also available in the literature [16].

## 5. Relating $Đ_{12}$ in *micro*-porous materials to fluid phase $Đ_{12,fl}$

For micro-porous materials, the exchange coefficient $Đ_{12}$ cannot be directly identified with the corresponding fluid phase diffusivity $Đ_{12,fl}$ because the molecule-molecule interactions are also significantly influenced by molecule-wall interactions. This is underscored by MD data for $Đ_{12}$ for six binary mixtures in a variety of micro-porous hosts; see Figure 4. For every guest/host combination, at any specific $c_t$, the $Đ_{12}$ is lower than the value of $Đ_{12,fl}$. The extent of lowering can be quantified by defining the fraction $F$

$$F \equiv Đ_{12} / Đ_{12,fl} \tag{3}$$

Every guest/host combination can be characterized by a constant fraction $F$, that are determined by data fitting; the complete data sets are available in the accompanying Figures B1-B126. For "open" structures, with large pore volumes, $V_p$, the values of $F$ are closer to unity. For example, for $CH_4$/Ar diffusion in IRMOF-1, COF-102, COF-103, and COF-108, the values are $F$ = 0.6, 0.65, 0.65, and 0.8, respectively, increasing with increasing void fractions, $\phi$. Remarkably, for IRMOF-1, the fraction $F$ is in the narrow range of 0.6 – 0.7 for every guest mixture investigated.

At the other end of the spectrum, materials with low pore volumes, the values of the fraction $F$ lie significantly below unity. In MFI that has a set of intersecting channels, $F$ lies in the range of 0.1 – 0.15 for all mixtures. For BEA, also with intersecting channels, but with a slightly higher void fraction, we obtain $F$ = 0.2. For materials such as FAU, NaX, NaY, LTA, and MgMOF-74 with intermediate void fractions, the values of $F$ fall in range 0.3 – 0.6.

Figure 5a presents a plot of $F$ as a function of the pore volume $V_p$ of different micro-porous host materials for nine different binary mixtures. The correlation is not perfect, suggesting that other aspects such as channel dimensions, and pore connectivity are also determinants of the exchange coefficient $Đ_{12}$.

## 6. Relating $Đ_{ii}$ in *micro*-porous materials to fluid phase $Đ_{ii,fl}$

The self-exchange diffusivity, $Đ_{ii}$, is defined by applying the M-S equations (1) to a binary mixture, that consists of identical species, tagged and un-tagged. In this special case, the M-S equations (1) can be used to derive the following relation between the self-diffusivity, $D_{i,self}$, and the M-S diffusivity, $Đ_i$, for *unary* diffusion [11]

$$\frac{1}{D_{i,self}} = \frac{1}{Đ_i} + \frac{1}{Đ_{ii}}; \quad i = 1,2 \tag{4}$$

Equation (4) can be used to determine the self-exchange coefficients $Đ_{ii}$ from MD simulations of $D_{i,self}$, and $Đ_i$. These self-exchange $Đ_{ii}$ were determined for several species from unary MD simulations. In each case the $Đ_{ii}$ is also a fraction, $F \equiv Đ_{ii}/Đ_{ii,fl}$, of the corresponding value of the fluid phase $Đ_{ii,fl}$; see data in Figure 6 for some selected guest/host combinations. The fraction $F$ exhibits the same dependence on the pore volume; see Figure 5b.

## 7. Estimating $Đ_{12}$ from information on self-exchange coefficients $Đ_{ii}$

For a fluid phase mixture, the Vignes [14, 17] interpolation formula is commonly used in practice for estimation of the $Đ_{12,fl}$

$$Đ_{12,fl} = \left(Đ_{11,fl}\right)^{x_1} \left(Đ_{22,fl}\right)^{x_2} \tag{5}$$

where the $Đ_{ii,fl}$ represent the self-exchange coefficients for *unary* fluid phase diffusion. The validation of this interpolation formula is demonstrated in Figure 7 for six different equimolar fluid mixtures; the complete data sets are available in the accompanying Figures B1-B126. This interpolation formula can be extended to apply to porous materials in the following manner

$$Đ_{12} = \left(Đ_{11}\right)^{x_1} \left(Đ_{22}\right)^{x_2} \tag{6}$$

Figure 8 provides a comparison of the predictions of the interpolation equation (6) with MD simulations of $Đ_{12}$ for six different guest/host combinations. A more extensive set of comparisons is to be found in the Supplementary material.

The results presented in Figure 5 for unary and binary mixtures, provides an alternative, independent rationalization for the interpolation formula suggested in earlier works [11, 18, 19] for estimation of the binary exchange $Đ_{12}$ using unary diffusion data on self-exchange coefficients $Đ_{ii}$

Equation (6) follows from Equation (5) since the binary and self-exchange coefficients share the same dependence on the structural parameters of relevance.

## 8. Degree of correlations $Đ_1/Đ_{12}$

The results of Figures 4 and 5 might lead us to conclude that correlation effects are less important in structures with large pore volumes because the values of $F$ are larger; this conclusion is fallacious as we shall explain below. The importance of correlations is dictated by the *degree of correlations* defined by ($Đ_1/Đ_{12}$). Figure 9 shows MD data on $Đ_1/Đ_{12}$ for diffusion of six different mixtures. For any guest/host combination, $Đ_1/Đ_{12}$ is seen to increase as the pore concentration increases; this implies that correlation effects are expected to be stronger for operations at higher pressures. Correlations are strongest in one-dimensional (1D) channel structures (e.g. BTP-COF, NiMOF-74), intersecting channels (e.g. MFI), and "open" structures (e.g. IRMOF-1, FAU, NaX) consisting of large cages separated by wide windows. The degree of correlations is weakest in cage-type structures such as CHA, DDR and LTA; the reason is that the molecules jump one-at-a-time across the narrow windows separating adjacent cages.

## 9. Influence of cluster formation due to hydrogen bonding

Exceptional circumstances prevail in cases of severe molecular segregation [13, 20] or cluster formation [21-24]; in such situations, the coefficients $Đ_1$, and $Đ_2$ in the mixture are significantly different to those determined from unary experiments or simulations. For water/alcohol mixture diffusion, the diffusivity of each component is lowered due to molecular clusters being formed as a consequence of hydrogen bonding. This is illustrated in Figure 10 that present MD simulations of $Đ_1$, and $Đ_2$ for water/alcohol mixture diffusion in FAU, MFI, LTA, DDR, and CHA zeolites. In all cases, the diffusivity of water is reduced with increasing proportion of alcohol. Hydrogen bonding between

water and alcohol molecule pairs serves to act as a "flexible leash" linking the motion of the more mobile (water) and tardier (alcohol) species. The net result is that the motion of water is retarded due to cluster formation. For MFI, the diffusivity of methanol is practically independent of composition, while that for water shows a dramatic decrease with increasing methanol concentration (cf. Figure 10c); this trend is the same as determined in the NMR experiments data of Caro et al. [25]. For LTA, and DDR the $D_{i,self}$ of methanol decreases with increasing proportion of water; see Figures 10d, and 10e. For CHA, the self-diffusivities for methanol show a decreasing trend for low water concentrations, till a minimum is reached; see Figure 10f. A similar minimum in the alcohol self-diffusivity is observed for FAU zeolite; see Figures 10a, and 10b. The general conclusion to be drawn from the MD data in Figure 10 is that at either ends of the composition range, there is slowing down of either component, due to increasing proportion of its partner species.

A number of experimental data on pervaporation of water/alcohol, mixtures can be interpreted using the MD data presented in Figure 10.

The NMR spectroscopy data of Hallberg et al.[26] on self-diffusivities in water-methanol mixtures across a Nafion membrane shows that the methanol diffusivity decreases significantly with increasing water composition; see Figure 11.

For water/alcohol pervaporation across CHA zeolite membrane, the experimental data of Hasegawa et al. [27] show that the alcohol fluxes *decrease* with increasing water composition in the feed; see Figure 12. Indeed, *both* water and alcohol fluxes are reduced with increasing concentrations of partner species in the mixture. Similar experimental data for water/alcohol pervaporation across DDR membranes are reported [28]. The decrease in the alcohol fluxes with increasing water concentration in the feed mixture observed experimentally in the CHA pervaporation experimental data presented in Figures 12, and 13, must be ascribed, in part at least, to a reduction in the alcohol diffusivities observed in the MD simulation results presented in Figure 10f.

For industrial scale water/NMP pervaporation across CHA membrane, the NMP flux also shows a decreasing trend with increasing feed water composition; see Figure 13a. The component permeances,

as reported by Sato et al. [29], show that NMP permeance decreases for water concentrations < 10 wt%, and tends to increases when the water feed concentrations > 15 wt%; see Figure 13b. Since permeances are closely related to the diffusivities, the NMP diffusivities will either decrease or increase depending on the feed composition.

The experimental data on pervaporation of water/ethanol mixtures across LTA-4A membrane [30], shown in Figure 14, can also be interpreted in terms of mutual-slowing down effects.

## 10. Intersection blocking and traffic-junction effects

Branched and cyclic hydrocarbons locate preferentially at the intersections of the channel structures of MFI zeolite [31]. This is illustrated in the snapshots in Figure 15 showing the location of molecules in mixtures of n-butane(nC4)/iso-butane(iC4), n-hexane(nC6)/2,2dimethylbutane (22DMB), and ethene/benzene mixtures. The preferential location is because of molecular configuration effects; the intersections afford extra "leg room".

In the PFG NMR investigation of Fernandez et al.[32] the self-diffusivity in MFI of n-butane (nC4), in mixtures with iso-butane (iC4), was found to decreases to nearly zero as the loading of iC4 is increased from $\Theta_{iC4} = 0$ to 2 molecules per unit cell; see Figure 16a. The reason for this strong decline can be understood on the basis of the preferential location of iC4 at the channel intersections of MFI. For $\Theta_{iC4} = 2$, half the total number of intersections are occupied by iC4, that has a diffusivity which is about three orders of magnitude lower than that of nC4. Since the occupancy of the intersections is distributed randomly, each of the straight channels has an iC4 molecule ensconced somewhere along the channels; this is evident from the snapshot in Figure 15a. This is tantamount to blockage and leads to severe reduction in the molecular traffic of the intrinsically more mobile nC4. Uptake experiments of Chmelik et al.[33] provide further evidence of the influence iC4 has on co-diffusion of nC4 in MFI crystals.

PFG NMR studies of Förste et al.[34] found that the self-diffusivity of $CH_4$ in MFI is significantly reduced as the loading of the co-adsorbed benzene increases; see Figure 16b. The explanation is again to be found in the hindering of $CH_4$ diffusion due to blocking of the intersections by benzene [34].

For analogous reasons, the branched alkanes 2-methylpentane (2MP), causes the reduction in the self-diffusivity of the n-hexane (nC6) in nC6/ 2MP mixtures [35]; see Figure 16c.

When intersection blocking effects occur, the pure component diffusivities of the more mobile partner, that locates anywhere along the channels of MFI, cannot be identified with those in the mixture.

The preferential location of branched alkanes at the intersections of MFI leads to other unusual adsorption and diffusion phenomena that can be exploited to achieve separation of hydrocarbon isomers. For illustration, consider for example, a mixture of nC6 and 2,2 dimethyl butane (22DMB). Configurational-bias Monte Carlo (CBMC) simulations of the adsorbed phase loadings of the components in MFI in equilibrium with bulk fluid phase partial fugacities $f_2 = 4\, f_1$ are shown in Figure 17a. Up to a total hydrocarbons fugacity $f$ of 1 kPa, the component loadings increase in an expected manner. At $f \approx 2$ kPa, the total loading in the zeolite $\approx$ 4 molecules per unit cell. All the intersection sites are fully occupied; see snapshot in Figure 17b. To further adsorb 22DMB, we need to provide an extra "push". Energetically, it is more efficient to obtain higher mixture loadings by "replacing" the 22DMB with nC6; this *configurational entropy* effect is the reason behind the curious maxima in the 22DMB loading in the mixture at $f \approx 2$ kPa. For $f > 2$ kPa, we have unusual phenomenon that increasing the fugacity of 22DMB in the bulk fluid phase has the effect of reducing the loading in the adsorbed phase. Experimental evidence of the curious maximum in the loading of the branched isomer is available from mixture adsorption data [36-39]. A further consequence is that for permeation of nC6-22DMB mixtures across an MFI membrane, the flux of 22DMB decreases when the upstream hydrocarbons pressures $f > 2$ kPa as observed in one set of the experiments of Gump et al.[40]; see Figure 17c.

The configuration entropy effect can be exploited to separate hydrocarbon isomers in a chromatographic column, or in a simulated moving bed adsorber [41-45].

Traffic junction effects are of vital importance in modeling reactors alkylation of benzene with ethene using MFI zeolite catalyst (in the acidic form H-ZSM-5) to produce ethylbenzene[46]. Both benzene (reactant) and ethylbenzene (product) are preferentially located at the intersections of MFI; see

Figure 18a. The blocking of intersections causes effective diffusivity of ethene inside the catalyst to reduce five-fold as the total mixture loading approaches 2 molecules per unit cell; see Figure 18.

## 11. Conclusions

The major conclusions of the present study are summarized below.

(1) When no cluster formation occurs, the M-S diffusivities of constituent species in a binary mixture, $Đ_1$, and $Đ_2$ are practically the same as that for unary diffusion, when determined at the total pore concentration in the mixture, $c_t$. This implies that the experimental data on unary permeation across membranes, say, can be used to predict the corresponding values for mixture permeation.

(2) For mixtures in which cluster formation occurs, say due to hydrogen bonding, $Đ_1$, and $Đ_2$ in the mixture cannot be identified with the unary values.

(3) For mixture diffusion inside cylindrical silica meso-pores, $d_p > 2$ nm, the binary exchange coefficient $Đ_{12}$, is found to be equal to the corresponding value in the binary fluid mixture, $Đ_{12,fl}$, over the entire range of mixture concentrations, $c_t$.

(4) For mixture diffusion inside zeolites, MOFs, and COFs, with channel dimensions smaller than 2 nm, $Đ_{12}$ is found to be lower than $Đ_{12,fl}$, by a constant factor $F$.

(5) Analogously, the self-exchange coefficient for unary diffusion $Đ_{ii}$ inside micro-porous structures is related to the fluid phase self-diffusivity $Đ_{ii,fl}$ by a constant factor $F$.

(6) The factor $F$ is primarily dependent on the pore volume or void fraction; the larger the void fraction, the closer is the value of $F$ to unity.

(7) The degree of correlations effects, as quantified by the ratio $Đ_1/Đ_{12}$, are *stronger* in open structures with larger pore volumes, and in 1D channels. Correlations are relatively insignificant in cage-type structures in which adjacent cages are separated by narrow windows.

(8) Due to cluster formation, the Maxwell-Stefan diffusivity, $Đ_i$, of either component in water-alcohol mixtures is lowered below the corresponding values of the pure components. In practice we need to take account of the influence of mixture composition on the $Đ_i$.

(9) Within the intersecting channels of MFI zeolite, branched and cyclic hydrocarbons locate preferentially at the intersections. This causes intersection blocking of more mobile partners that locate within the channels. The M-S diffusivity of the more mobile partner cannot be identified with the pure component values.

# 12. Notation

| | |
|---|---|
| $c_i$ | pore concentration of species *i*, mol $m^{-3}$ |
| $c_t$ | total pore concentration in mixture, mol $m^{-3}$ |
| $d_p$ | pore diameter, m |
| $Đ_i$ | M-S diffusivity of species *i*, $m^2$ $s^{-1}$ |
| $Đ_{ii}$ | self-exchange coefficient, $m^2$ $s^{-1}$ |
| $Đ_{ii,fl}$ | self-diffusivity of species *i* in fluid phase, $m^2$ $s^{-1}$ |
| $Đ_{12}$ | M-S exchange coefficient, $m^2$ $s^{-1}$ |
| $Đ_{12,fl}$ | M-S diffusivity in binary fluid mixture, $m^2$ $s^{-1}$ |
| $D_{i,self}$ | self-diffusivity of species *i*, $m^2$ $s^{-1}$ |
| $F$ | factor defined by equation (3), dimensionless |
| $N_i$ | molar flux of species *i* defined in terms of the cross-sectional area of the crystalline framework, mol $m^{-2}$ $s^{-1}$ |
| $R$ | gas constant, 8.314 J $mol^{-1}$ $K^{-1}$ |
| $T$ | absolute temperature, K |
| $V_p$ | accessible pore volume, $m^3$ $kg^{-1}$ |
| $x_i$ | mole fraction of species *i* based on loading within pore, dimensionless |

***Greek letters***

| | |
|---|---|
| $\phi$ | fractional pore volume of microporous material, dimensionless |
| $\mu_i$ | molar chemical potential, J $mol^{-1}$ |
| $\Theta_i$ | loading of *i*, molecules per unit cell |

***Subscripts***

| | |
|---|---|
| i | referring to component *i* |
| fl | referring to fluid phase |
| t | referring to total mixture |

# 13. References


[1] J. Kärger, D.M. Ruthven, D.N. Theodorou, Diffusion in Nanoporous Materials, Wiley - VCH, Weinheim, 2012.

[2] J. Caro, Are MOF membranes better in gas separation than those made of zeolites?, Curr. Opin. Chem. Eng. 1 (2011) 77-83.

[3] J. Gascon, F. Kapteijn, Metal-Organic Framework Membranes—High Potential, Bright Future?, Angew. Chem. Int. Ed. 49 (2010) 1530-1532.

[4] R. Krishna, J.M. van Baten, In Silico Screening of Zeolite Membranes for $CO_2$ Capture, J. Membr. Sci. 360 (2010) 323-333.

[5] R. Krishna, J.M. van Baten, In silico screening of metal-organic frameworks in separation applications, Phys. Chem. Chem. Phys. 13 (2011) 10593-10616.

[6] R. Krishna, J.R. Long, Screening metal-organic frameworks by analysis of transient breakthrough of gas mixtures in a fixed bed adsorber, J. Phys. Chem. C 115 (2011) 12941-12950.

[7] Y. He, R. Krishna, B. Chen, Metal-Organic Frameworks with Potential for Energy-Efficient Adsorptive Separation of Light Hydrocarbons, Energy Environ. Sci. 5 (2012) 9107-9120.

[8] D. Dubbeldam, R. Krishna, S. Calero, A.Ö. Yazaydın, Computer-Assisted Screening of Ordered Crystalline Nanoporous Adsorbents for Separation of Alkane Isomers, Angew. Chem. Int. Ed. 51 (2012) 11867-11871.

[9] R. Krishna, Describing the diffusion of guest molecules inside porous structures, J. Phys. Chem. C 113 (2009) 19756-19781.

[10] R. Krishna, Diffusion in Porous Crystalline Materials, Chem. Soc. Rev. 41 (2012) 3099-3118.

[11] R. Krishna, J.M. van Baten, Unified Maxwell-Stefan description of binary mixture diffusion in micro- and meso- porous materials, Chem. Eng. Sci. 64 (2009) 3159-3178.

[12] R. Krishna, J.M. van Baten, Investigating the potential of MgMOF-74 membranes for $CO_2$ capture, J. Membr. Sci. 377 (2011) 249-260.

[13] R. Krishna, J.M. van Baten, Onsager coefficients for binary mixture diffusion in nanopores, Chem. Eng. Sci. 63 (2008) 3120-3140.

[14] R. Krishna, J.M. van Baten, The Darken relation for multicomponent diffusion in liquid mixtures of linear alkanes. An investigation using Molecular Dynamics (MD) simulations, Ind. Eng. Chem. Res. 44 (2005) 6939-6947.

[15] E.N. Fuller, P.D. Schettler, J.C. Giddings, A new method for prediction of binary gas-phase diffusion coefficients, Ind. Eng. Chem. 58 (1966) 19-27.

[16] B.E. Poling, J.M. Prausnitz, J.P. O'Connell, The Properties of Gases and Liquids, McGraw-Hill, 5th Edition, New York, 2001.

[17] A. Vignes, Diffusion in binary solutions, Ind. Eng. Chem. Fundamentals 5 (1966) 189-199.

[18] A.I. Skoulidas, D.S. Sholl, R. Krishna, Correlation effects in diffusion of $CH_4/CF_4$ mixtures in MFI zeolite. A study linking MD simulations with the Maxwell-Stefan formulation, Langmuir 19 (2003) 7977-7988.

[19] S. Chempath, R. Krishna, R.Q. Snurr, Nonequilibrium MD simulations of difusion of binary mixtures containing short n-alkanes in faujasite, J. Phys. Chem. B 108 (2004) 13481-13491.

[20] R. Krishna, J.M. van Baten, Segregation effects in adsorption of $CO_2$ containing mixtures and their consequences for separation selectivities in cage-type zeolites, Sep. Purif. Technol. 61 (2008) 414-423.

[21] R. Krishna, J.M. van Baten, Investigating cluster formation in adsorption of $CO_2$, $CH_4$, and Ar in zeolites and metal organic frameworks at sub-critical temperatures, Langmuir 26 (2010) 3981-3992.
[22] R. Krishna, J.M. van Baten, Highlighting a variety of unusual characteristics of adsorption and diffusion in microporous materials induced by clustering of guest molecules, Langmuir 26 (2010) 8450-8463.
[23] R. Krishna, J.M. van Baten, Hydrogen bonding effects in adsorption of water-alcohol mixtures in zeolites and the consequences for the characteristics of the Maxwell-Stefan diffusivities, Langmuir 26 (2010) 10854-10867.
[24] R. Krishna, J.M. van Baten, Mutual slowing-down effects in mixture diffusion in zeolites, J. Phys. Chem. C 114 (2010) 13154-13156.
[25] J. Caro, M. Bülow, J. Richter-Mendau, J. Kärger, M. Hunger, D. Freude, Nuclear Magnetic Resonance Self-diffusion Studies of Methanol-Water Mixtures in Pentasil-type Zeolites, J. Chem. Soc., Faraday Trans. 83 (1987) 1843-1849.
[26] F. Hallberg, T. Vernersson, E.T. Pettersson, S.V. Dvinskikh, G. Lindbergh, I. Furó, Electrokinetic transport of water and methanol in Nafion membranes as observed by NMR spectroscopy, Electrochim. Acta 55 (2010) 3542-3549.
[27] Y. Hasegawa, C. Abe, M. Nishioka, K. Sato, T. Nagase, T. Hanaoka, Formation of high flux CHA-type zeolite membranes and their application to the dehydration of alcohol solutions, J. Membr. Sci. 364 (2010) 318-324.
[28] J. Kuhn, J.M. Castillo-Sanchez, J. Gascon, S. Calero, D. Dubbeldam, T.J.H. Vlugt, F. Kapteijn, J. Gross, Adsorption and Diffusion of Water, Methanol, and Ethanol in All-Silica DD3R: Experiments and Simulation, J. Phys. Chem. C 113 (2009) 14290-14301.
[29] K. Sato, K. Sugimoto, N. Shimosuma, T. Kikuchi, T. Kyotani, T. Kurata, Development of practically available up-scaled high-silica CHA-type zeolite membranes for industrial purpose in dehydration of N-methyl pyrrolidone solution, J. Membr. Sci. 409-410 (2012) 82-95.
[30] M. Pera-Titus, C. Fité, V. Sebastián, E. Lorente, J. Llorens, F. Cunill, Modeling Pervaporation of Ethanol/Water Mixtures within 'Real' Zeolite NaA Membranes, Ind. Eng. Chem. Res. 47 (2008) 3213-3224.
[31] R. Krishna, J.M. van Baten, Diffusion of hydrocarbon mixtures in MFI zeolite: Influence of intersection blocking, Chem. Eng. J. 140 (2008) 614-620.
[32] M. Fernandez, J. Kärger, D. Freude, A. Pampel, J.M. van Baten, R. Krishna, Mixture diffusion in zeolites studied by MAS PFG NMR and molecular simulation, Microporous Mesoporous Mater. 105 (2007) 124-131.
[33] C. Chmelik, L. Heinke, J.M. van Baten, R. Krishna, Diffusion of *n*-butane/*iso*-butane mixtures in silicalite-1 investigated using infrared (IR) microscopy, Microporous Mesoporous Mater. 125 (2009) 11-16.
[34] C. Förste, A. Germanus, J. Kärger, H. Pfeifer, J. Caro, W. Pilz, A. Zikánóvá, Molecular mobility of methane adsorbed in ZSM-5 containing co-adsorbed benzene, and the location of benzene molecules, J. Chem. Soc., Faraday Trans. 1. 83 (1987) 2301-2309.
[35] A.O. Koriabkina, A.M. de Jong, D. Schuring, J. van Grondelle, R.A. van Santen, Influence of the acid sites on the intracrystalline diffusion of hexanes and their mixtures within MFI-zeolites, J. Phys. Chem. B 106 (2002) 9559-9566.
[36] D.S. Santilli, Pore probe: A new technique for measuring the concentration of molecules inside porous materials at elevated temperatures, J. Catal. 99 (1986) 335-341.
[37] S. Calero, B. Smit, R. Krishna, Configurational entropy effects during sorption of hexane isomers in silicalite, J. Catal. 202 (2001) 395-401.
[38] S. Calero, B. Smit, R. Krishna, Separation of linear, mono-methyl and di-methyl alkanes in the 5-7 carbon atom range by exploiting configurational entropy effects during sorption on silicalite-1, Phys. Chem. Chem. Phys. 3 (2001) 4390-4398.
[39] M. Yu, J.L. Falconer, R.D. Noble, Adsorption of Liquid Mixtures on Silicalite-1 Zeolite: A Density-Bottle Method, Langmuir 21 (2005) 7390-7397.

[40] C.J. Gump, R.D. Noble, J.L. Falconer, Separation of hexane isomers through nonzeolite pores in ZSM-5 zeolite membranes, Ind. Eng. Chem. Res. 38 (1999) 2775-2781.
[41] E. Jolimaître, K. Ragil, M. Tayakout-Fayolle, C. Jallut, Separation of Mono- and Dibranched Hydrocarbons on Silicalite, A.I.Ch.E.J. 48 (2002) 1927-1937.
[42] R. Krishna, B. Smit, S. Calero, Entropy effects during sorption of alkanes in zeolites, Chem. Soc. Rev. 31 (2002) 185-194.
[43] R. Krishna, R. Baur, On the Langmuir-Hinshelwood formulation for zeolite catalysed reactions, Chem. Eng. Sci. 60 (2005) 1155 - 1166.
[44] R. Baur, R. Krishna, A moving bed reactor concept for alkane isomerization, Chem. Eng. J. 109 (2005) 107-113.
[45] B. Smit, R. Krishna, Molecular simulations in zeolitic process design, Chem. Eng. Sci. 58 (2003) 557-568.
[46] N. Hansen, R. Krishna, J.M. van Baten, A.T. Bell, F.J. Keil, Analysis of Diffusion Limitation in the Alkylation of Benzene over H-ZSM-5 by Combining Quantum Chemical Calculations, Molecular Simulations, and a Continuum Approach, J. Phys. Chem. C 113 (2009) 235-246.
[47] R. Krishna, Adsorptive separation of $CO_2/CH_4/CO$ gas mixtures at high pressures, Microporous Mesoporous Mater. 156 (2012) 217-223.
[48] R. Krishna, J.M. van Baten, Diffusion of alkane mixtures in zeolites. Validating the Maxwell-Stefan formulation using MD simulations, J. Phys. Chem. B 109 (2005) 6386-6396.
[49] R. Krishna, J.M. van Baten, Diffusion of alkane mixtures in MFI zeolite, Microporous Mesoporous Mater. 107 (2008) 296-298.
[50] R. Krishna, J.M. van Baten, Insights into diffusion of gases in zeolites gained from molecular dynamics simulations, Microporous Mesoporous Mater. 109 (2008) 91-108.
[51] R. Krishna, J.M. van Baten, Investigating the Relative Influences of Molecular Dimensions and Binding Energies on Diffusivities of Guest Species Inside Nanoporous Crystalline Materials J. Phys. Chem. C 116 (2012) 23556-23568.
[52] R. Krishna, J.M. van Baten, Maxwell-Stefan modeling of slowing-down effects in mixed gas permeation across porous membranes, J. Membr. Sci. 383 (2011) 289-300.
[53] R. Krishna, J.M. van Baten, Investigating the validity of the Knudsen prescription for diffusivities in a mesoporous covalent organic framework, Ind. Eng. Chem. Res. 50 (2011) 7083-7087.
[54] R. Krishna, J.M. van Baten, Investigating the validity of the Bosanquet formula for estimation of diffusivities in mesopores, Chem. Eng. Sci. 69 (2012) 684-688.
[55] R. Krishna, J.M. van Baten, Highlighting Pitfalls in the Maxwell-Stefan Modeling of Water-Alcohol Mixture Permeation across Pervaporation Membranes, J. Membr. Sci. 360 (2010) 476-482.
[56] R. Krishna, J.M. van Baten, A rationalization of the Type IV loading dependence in the Kärger-Pfeifer classification of self-diffusivities, Microporous Mesoporous Mater. 142 (2011) 745-748.
[57] D. Schuring, A.O. Koriabkina, A.M. de Jong, B. Smit, R.A. van Santen, Adsorption and diffusion of n-hexane/2-methylpentane mixtures in zeolite silicalite: Experiments and modeling, J. Phys. Chem. B 105 (2001) 7690-7698.
[58] R. Krishna, J.M. van Baten, Screening of zeolite adsorbents for separation of hexane isomers: A molecular simulation study, Sep. Purif. Technol. 55 (2007) 246-255.

Table 1. Salient structural information on zeolites, MOFs and COFs.

| Structure | Topology | Fractional pore volume, $\phi$ | Pore volume/ $cm^3/g$ | Framework density/ $kg/m^3$ |
|---|---|---|---|---|
| AFI | 12-ring 1D channels of 7.3 Å size | 0.274 | 0.159 | 1730 |
| BEA | Intersecting channels of two sizes: 12-ring of 7.1 Å - 7.3 Å and 10-ring of 5.6 – 5.6 Å | 0.408 | 0.271 | 1509 |
| BOG | Intersecting channels: 12-ring 7.0 Å -7.0 Å and 10-ring of 5.5 Å - 5.8 Å | 0.374 | 0.241 | 1996 |
| CHA | 316 $Å^3$ cages separated by 3.77 Å × 4.23 Å size windows | 0.382 | 0.264 | 1444 |
| DDR | 277.8 $Å^3$ cages separated by 3.65 Å × 4.37 Å size windows | 0.245 | 0.139 | 1760 |
| FAU-Si | 790 $Å^3$ cages separated by 7.4 Å size windows | 0.439 | 0.328 | 1338 |
| NaY | 790 $Å^3$ cages separated by 7.4 Å size windows | 0.41 | 0.303 | 1347 |
| NaX | 790 $Å^3$ cages separated by 7.4 Å size windows | 0.40 | 0.280 | 1421 |
| ISV | Intersecting channels of two sizes: 12-ring of 6.1 Å -6.5 Å and 12-ring of 5.9 Å - 6.6 Å | 0.426 | 0.278 | 1533 |
| LTA-Si | 743 $Å^3$ cages separated by 4.11 Å × 4.47 Å size windows | 0.399 | 0.310 | 1285 |
| MFI | 10-ring intersecting channels of 5.1 Å – 5.5 Å and 5.3 Å – 5.6 Å size | 0.297 | 0.165 | 1796 |
| CuBTC | Large cages are inter-connected by 9 Å windows of square cross-section. The large cages are also connected to tetrahedral-shaped pockets of ca. 6 Å size through triangular-shaped windows of 4.6 Å size | 0.759 | 0.863 | 879 |
| IRMOF1 | Two alternating, inter-connected, cavities of 10.9 Å and 14.3 Å with window size of 8 Å. | 0.812 | 1.369 | 593 |
| MOF-177 | Six diamond-shaped channels (upper) with diameter of 10.8 Å surround a pore containing eclipsed $BTB^{3-}$ moieties. | 0.840 | 1.968 | 427 |
| MgMOF-74 | 1D hexagonal-shaped channels of 11 Å | 0.708 | 0.782 | 905 |
| MIL-47 | 1D diamond-shaped channels of 8.5 Å | 0.608 | 0.606 | 1004 |
| MIL-53 (Cr)-lp | 1D lozenge-shaped channels of 8.5 Å | 0.539 | 0.518 | 1041 |
| BTP-COF | 1D hexagonal-shaped channels of 34 Å | 0.752 | 1.79 | 420 |
| COF-102 | Cavity of size 8.9 Å | 0.8 | 1.875 | 426 |
| COF-103 | Cavity of size 9.6 Å | 0.82 | 2.040 | 400 |
| COF-108 | Two cavities, of sizes 15.2 Å and 29.6 Å | 0.93 | 5.467 | 170 |

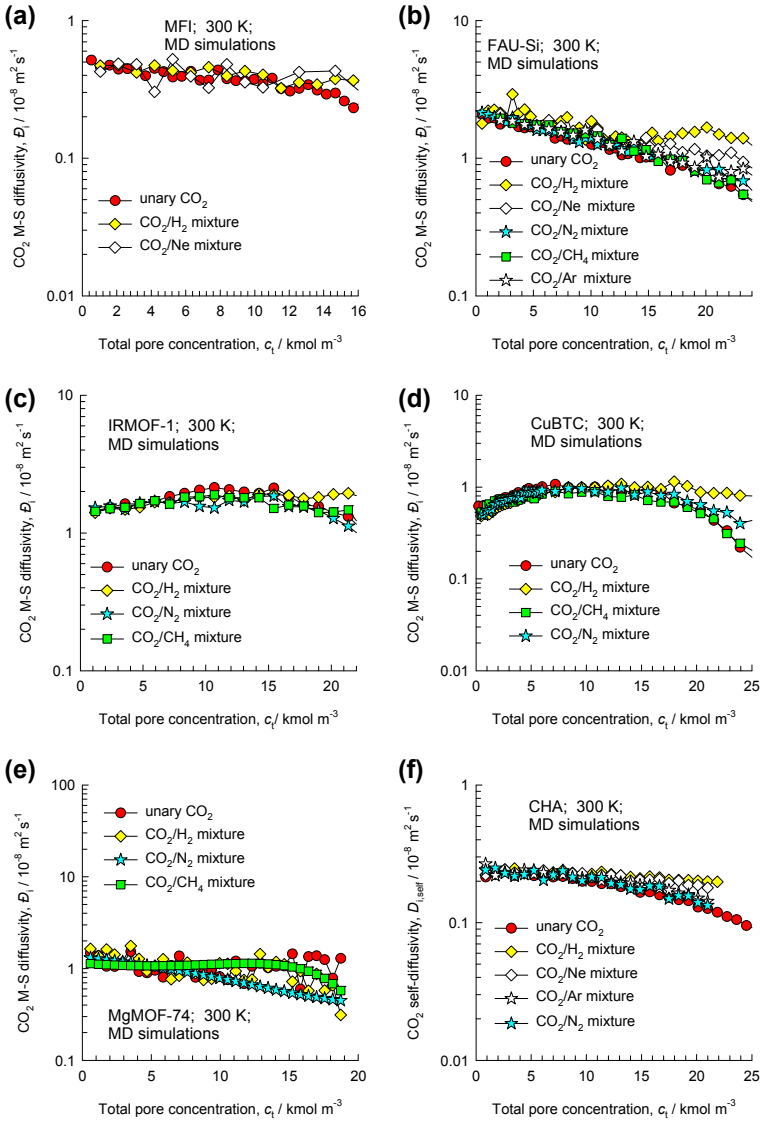


Figure 1. Maxwell-Stefan diffusivity of $CO_2$, $Đ_i$, determined MD simulation data for diffusion of a variety of equimolar ($c_1 = c_2$) binary mixtures of $CO_2$ and different partner species in (a) MFI, (b) FAU-Si, (c) IRMOF-1, (d) CuBTC, (e) MgMOF-74, and (f) CHA. The $x$- axis represent the total pore concentration of the adsorbed phase within the pores, $c_t = c_1 + c_2$. Also shown in red circles are the MD simulations of $Đ_i$, for unary diffusion. For CHA, the plotted diffusivities are the self-diffusivities, $D_{i,self}$, that are more accurate to determine for CHA and provide good approximations of the M-S diffusivities, i.e. $D_{i,self} \approx Đ_i$. The MD data are culled from our previous publications [10-13, 47-52]. For convenience, the pure component MD data are also summarized in the accompanying Figures A1 – A92.

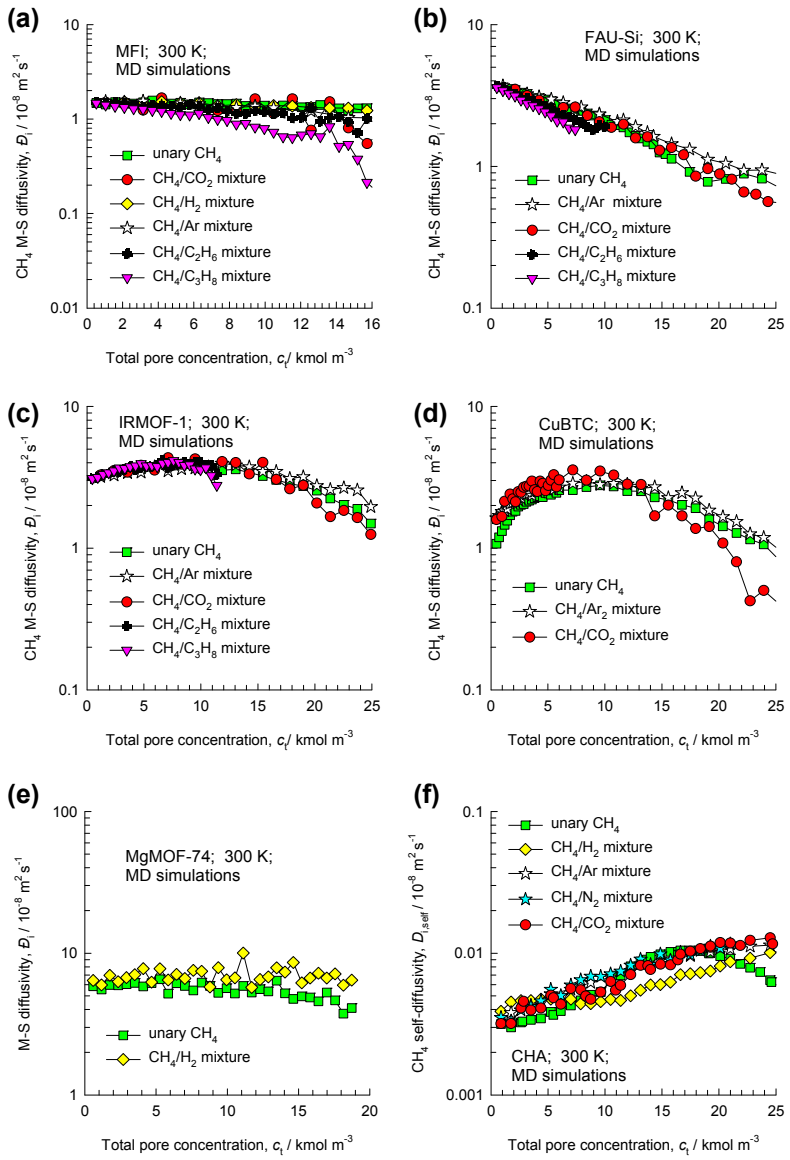


Figure 2. Maxwell-Stefan diffusivity of $CH_4$, $Đ_i$, determined MD simulation data for diffusion of a variety of equimolar ($c_1 = c_2$) binary mixtures of $CH_4$ and different partner species in (a) MFI, (b) FAU-Si, (c) IRMOF-1, (d) CuBTC, (e) MgMOF-74, and (f) CHA. The $x$- axis represent the total pore concentration of the adsorbed phase within the pores, $c_t = c_1 + c_2$. Also shown in green squares are the MD simulations of $Đ_i$, for unary diffusion. For CHA, the plotted diffusivities are the self-diffusivities, $D_{i,self}$, that are more accurate to determine for CHA and provide good approximations of the M-S diffusivities, i.e. $D_{i,self} \approx Đ_i$. The MD data are culled from our previous publications [10-13, 47-52]. For convenience, the pure component MD data are also summarized in the accompanying Figures A1 – A92.

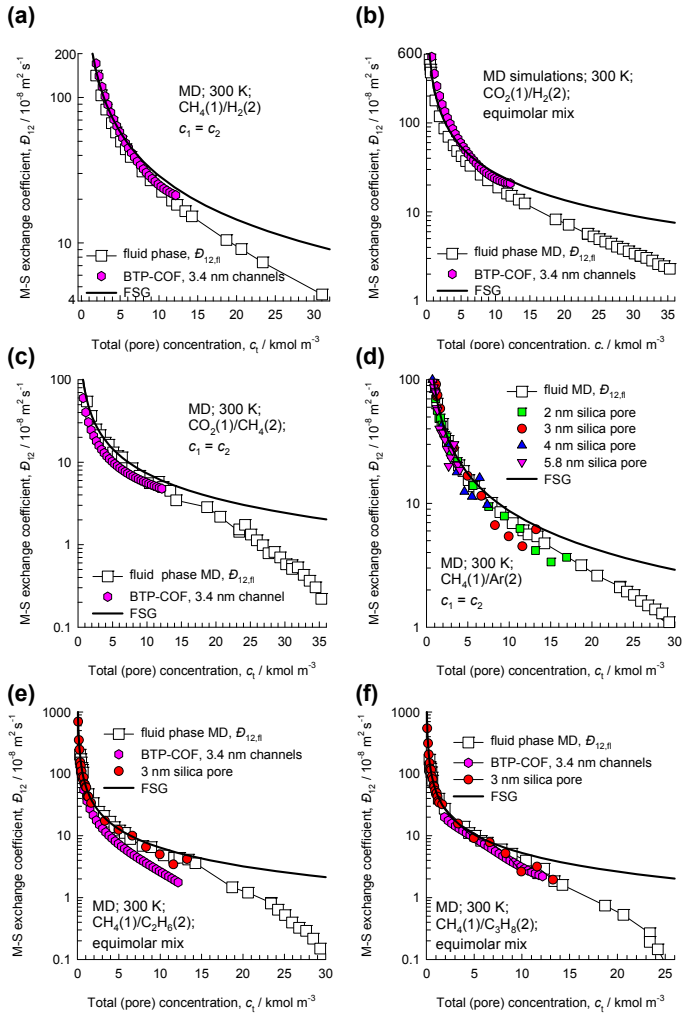


Figure 3. The MD simulations for fluid phase diffusivity $Đ_{12,fl}$ (square symbols) for equimolar ($c_1 = c_2$) (a) $H_2/CH_4$, (b) $CO_2/H_2$, (c) $CH_4/CO_2$, (d) $CH_4$/Ar, (e) $CH_4/C_2H_6$, and (f) $CH_4/C_3H_8$ mixtures as a function of the total fluid phase molar concentration $c_t$. The calculation of $Đ_{12,fl}$ using correlation of Fuller, Schettler and Giddings (FSG) [15], developed for *binary* gas mixtures, is indicated by the continuous solid line. Also indicated are MD data for the exchange coefficients $Đ_{12}$ in cylindrical silica mesopores (of diameters 3 nm, 4 nm, and 5.8 nm), and BTP-COF (with 3.4 nm size 1D hexagonal-shaped channels). The MD data are culled from our previous publications [10-13, 47-54]. For convenience, the MD data are also summarized in the accompanying Figures B1 – B118, arranged according to the guest mixtures.

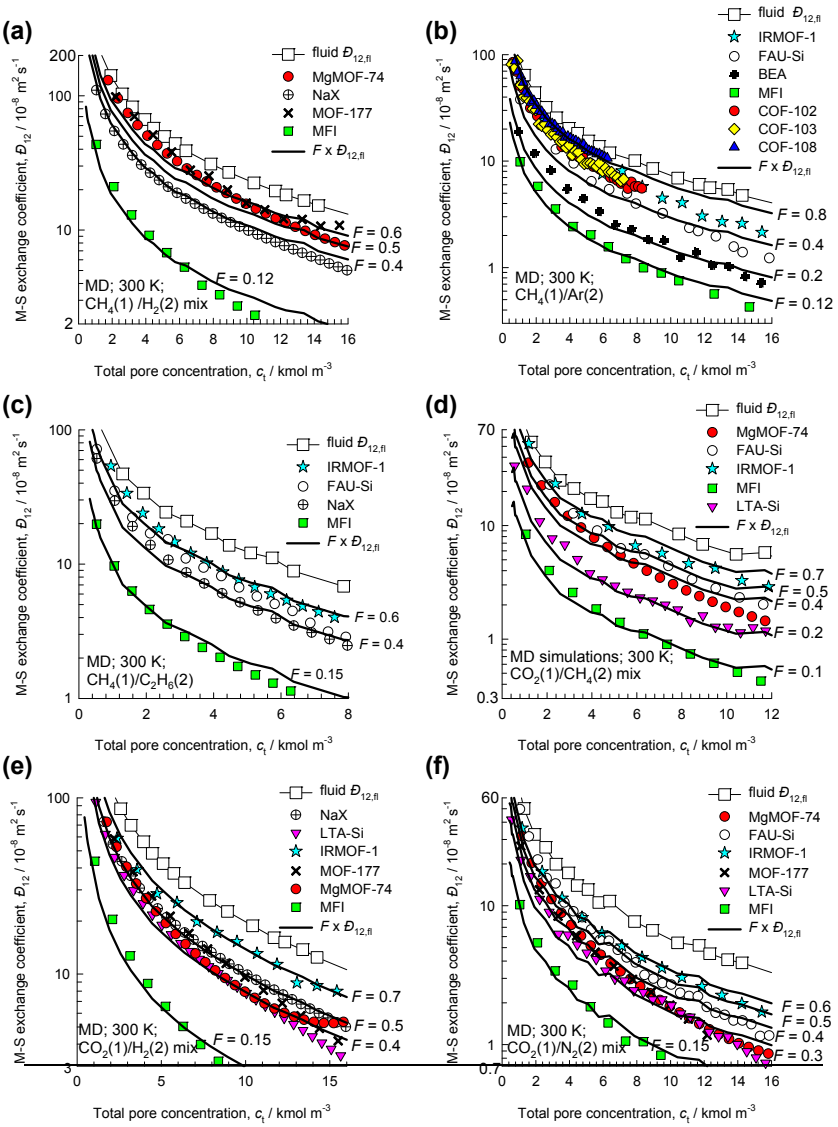


Figure 4. The M-S binary exchange coefficients $Đ_{12}$, for diffusion of equimolar ($c_1 = c_2$) binary mixtures (a) $H_2/CH_4$, (b) $CH_4/Ar$, (c) $CH_4/C_2H_6$, (d) $CH_4/CO_2$, (e) $H_2/CO_2$, and (f) $CO_2/N_2$ at 300 K in a variety of host materials as a function of the total pore concentration, $c_t$. The $Đ_{12,fl}$ for binary *fluid phase* mixture diffusion, obtained from independent MD simulations, are also presented in square symbols, along with continuous solid lines that represent the fraction $F$ times $Đ_{12,fl}$. The MD data are culled from our previous publications [10-13, 47-54]. For convenience, the MD data are also summarized in the accompanying Figures B1 – B118, arranged according to the guest mixtures.

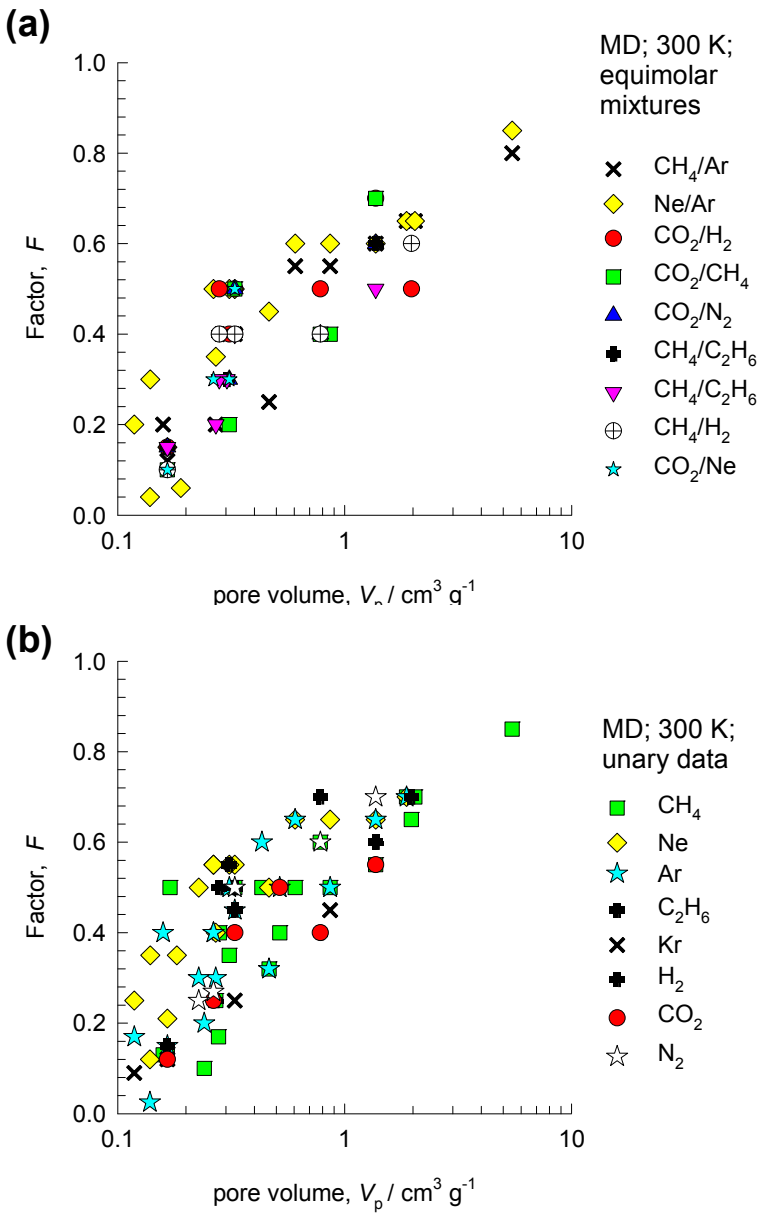


Figure 5. Fraction $F$ determined from (a) binary mixture, and (b) unary MD simulations, expressed as a function of the pore volume of the micro-porous host structures, $V_p$. The data used for constructing (a) are from the accompanying Figures B1 – B118, arranged according to the guest mixtures. The data used for constructing (b) are from the accompanying Figures A1 – A92, arranged according to the guest species.

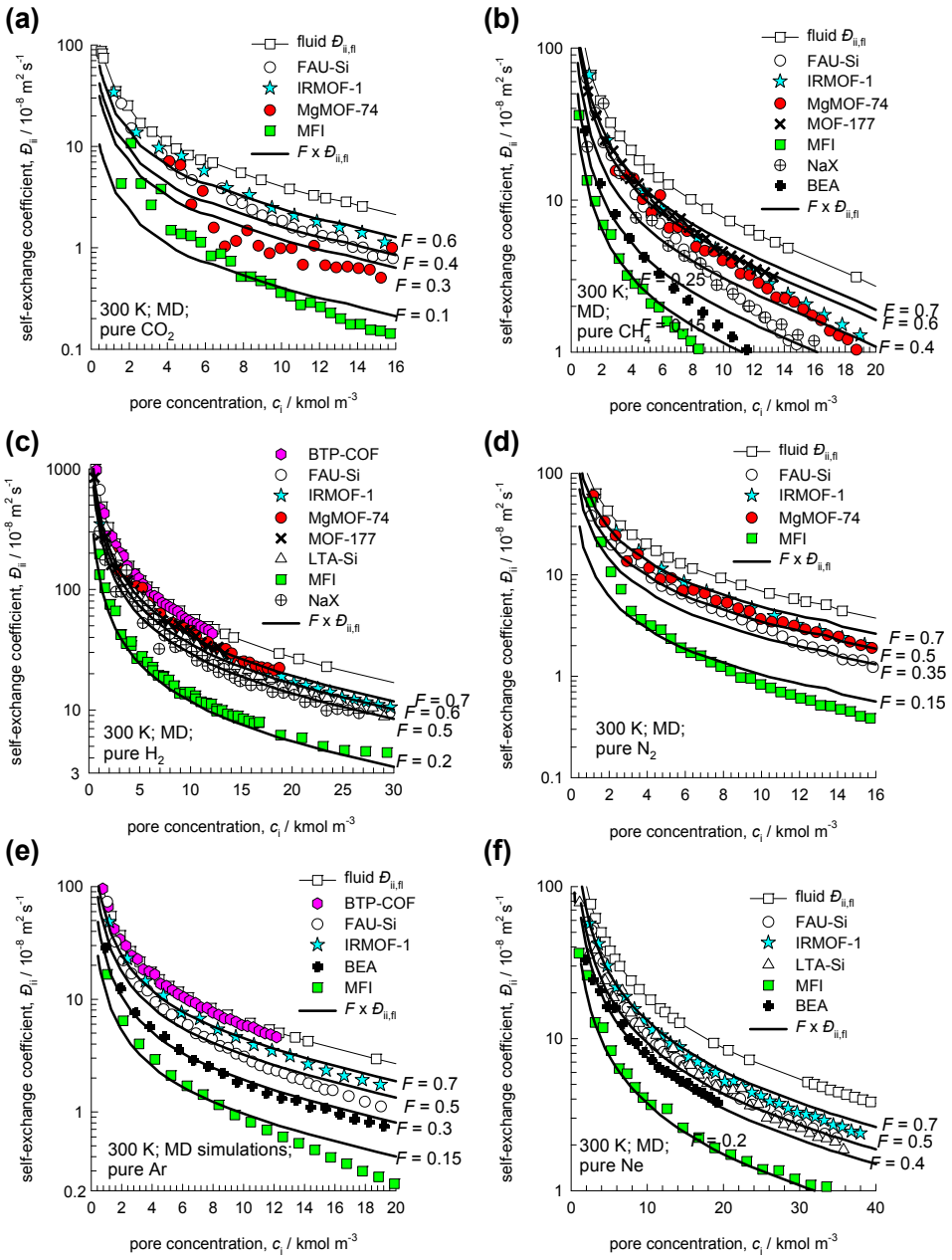


Figure 6. The self-exchange coefficients $Đ_{ii}$, for unary diffusion of (a) $CO_2$, (b) $CH_4$, (c) $H_2$, (d) $N_2$, (e) Ar, and (f) Ne at 300 K in a variety of host materials as a function of the pore concentration, $c_i$. The $Đ_{ii,fl}$ for self-diffusivity in the *fluid phase*, obtained from independent MD simulations, are also presented in square symbols, along with continuous solid lines that represent the fraction $F$ times $Đ_{ii,fl}$. The MD data are culled from our previous publications [10-13, 47-54]. For convenience, the MD data are also summarized in the accompanying Figures A1 – A92, arranged according to the guest species.

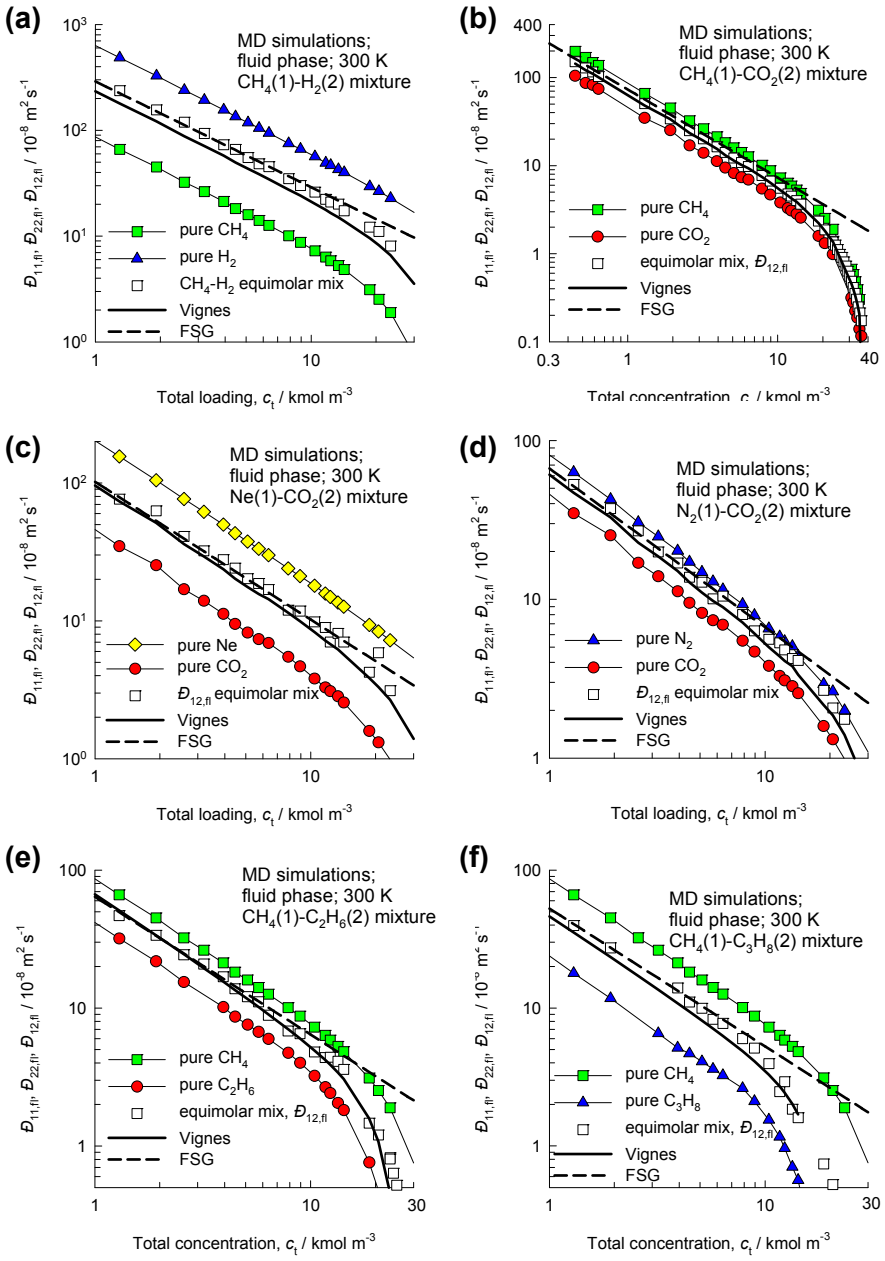


Figure 7. MD simulations of self-diffusivities, $Đ_{ii,fl}$, along with the $Đ_{12,fl}$ for diffusion in a variety of equimolar binary fluid mixtures as a function of the total fluids concentration, $c_t$. The calculations of $Đ_{12,fl}$ following Equation (5) are shown by the continuous solid lines. The calculation of $Đ_{12,fl}$ using correlation of Fuller, Schettler and Giddings (FSG) [15], developed for *binary* gas mixtures, is indicated by the dashed lines. The MD data are culled from our previous publications [10-13, 47-54]. A more complete compilation of data is presented in the accompanying Figures A1 – A92.

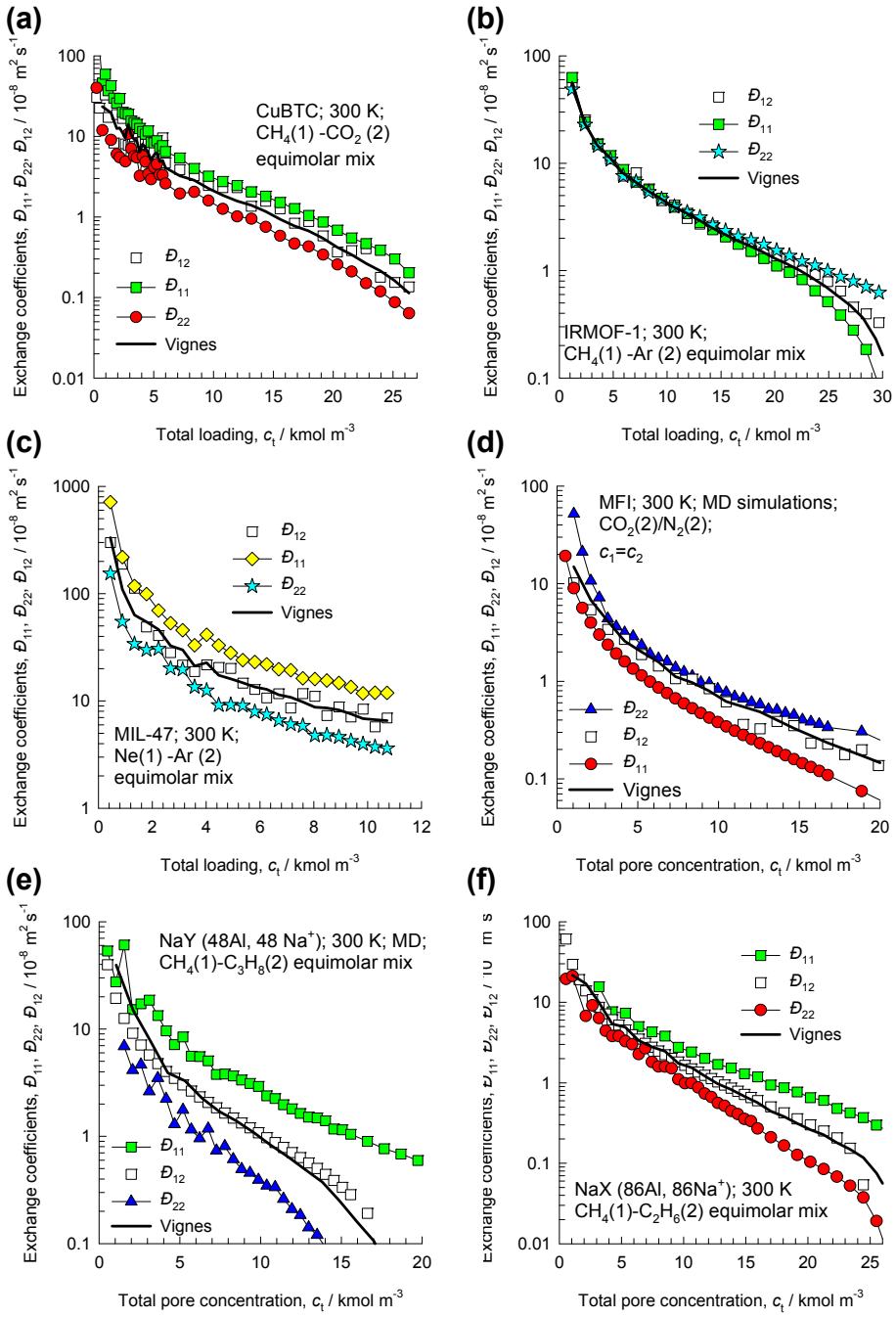


Figure 8. Test of the interpolation Equation (6) for diffusion in a variety of binary mixtures in different microporous hosts. The MD data are culled from our previous publications [10-13, 47-54]. A more complete compilation of the validation of the interpolation formula is presented in the accompanying Figures Figures B1 – B118.

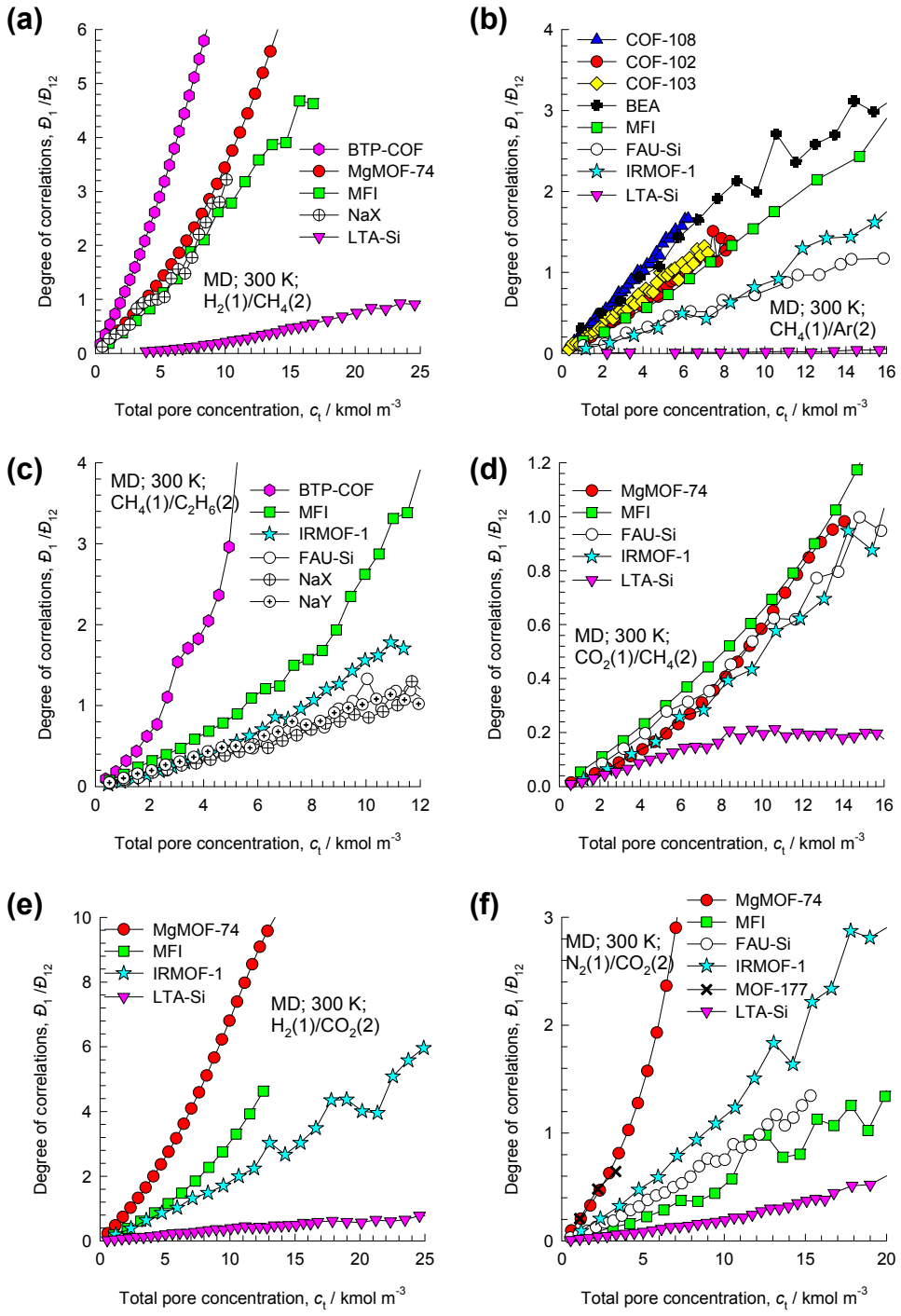


Figure 9. MD simulation data for the degree of correlations, $Đ_1/Đ_{12}$, for diffusion of equimolar ($c_1 = c_2$) binary mixtures (a) $H_2/CH_4$, (b) $CH_4/Ar$, (c) $CH_4/C_2H_6$, (d) $CH_4/CO_2$, (e) $H_2/CO_2$, and (f) $CO_2/N_2$ at 300 K in a variety of host materials, as a function of the total pore concentration. The MD data are culled from our previous publications [10-13, 47-54]. For convenience, the MD data are also summarized in the accompanying Figures B1 – B118.

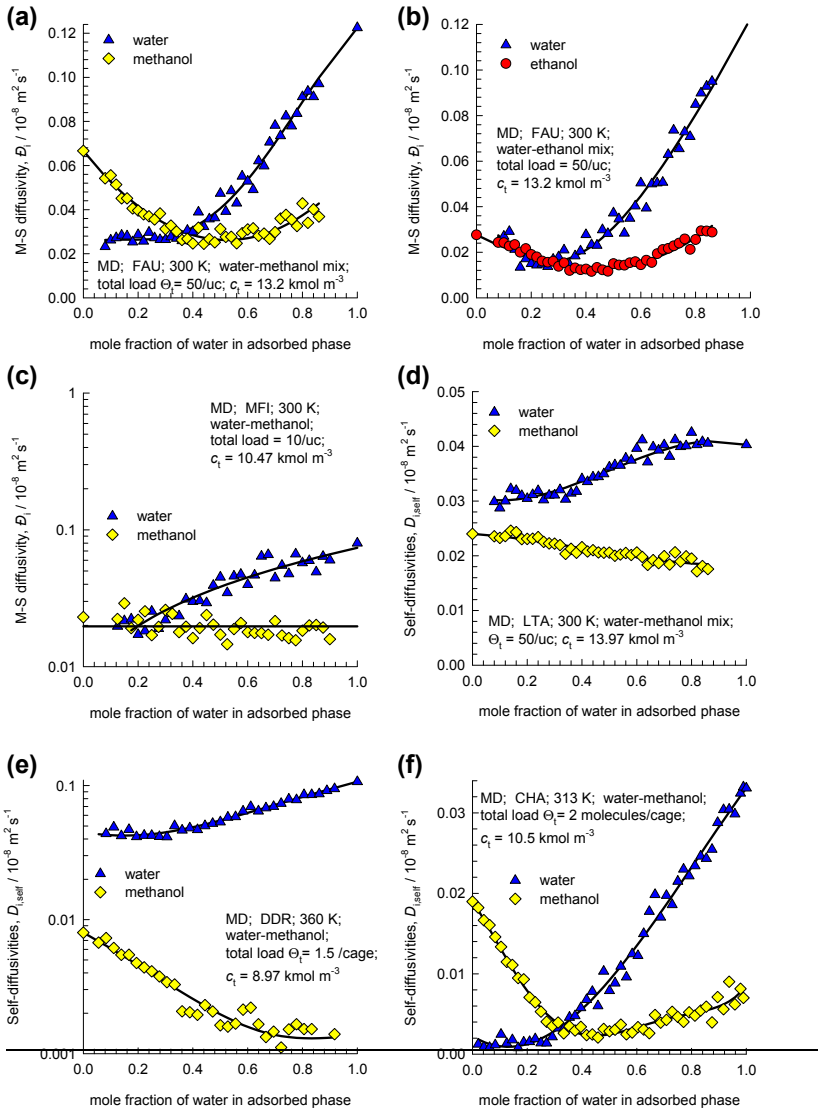


Figure 10. Maxwell-Stefan diffusivities, $Đ_i$, in water/methanol, and water/ethanol mixtures of varying composition in (a, b) FAU, (c) MFI, (d) LTA, (e) DDR, and (f) CHA zeolites. The data are compiled from MD simulation results published in the literature [23, 24, 55]. In all cases the MD simulations were carried out under conditions in which the total concentration within the pores, $c_t$, is held constant; the values $c_t$ are specified in each case and are based on the accessible pore volume in the various zeolites. In some cases the corresponding loadings per unit, $\Theta_t$, are also specified. For CHA, DDR, and LTA the plotted diffusivities are the self-diffusivities, $D_{i,self}$, that are more accurate to determine and provide good approximations of the M-S diffusivities, i.e. $D_{i,self} \approx Đ_i$. The MD data are culled from our previous publications [21-24, 55, 56].

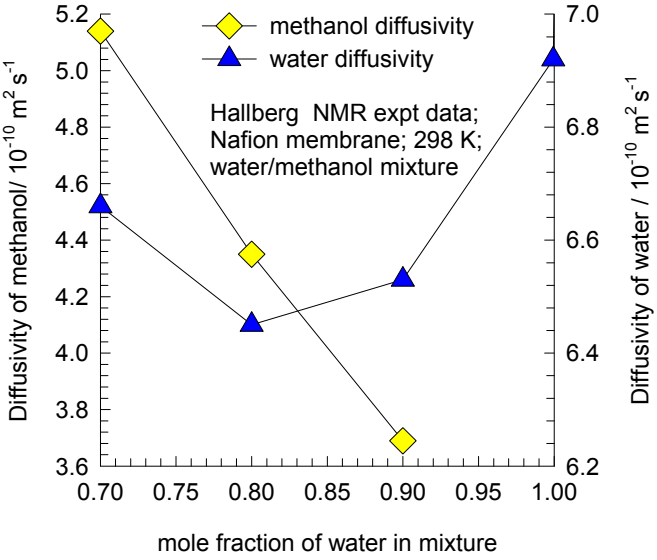


Figure 11. The NMR spectroscopy data of Hallberg et al. [26] on self-diffusivities in water-methanol mixtures across a Nafion membrane at 298 K.

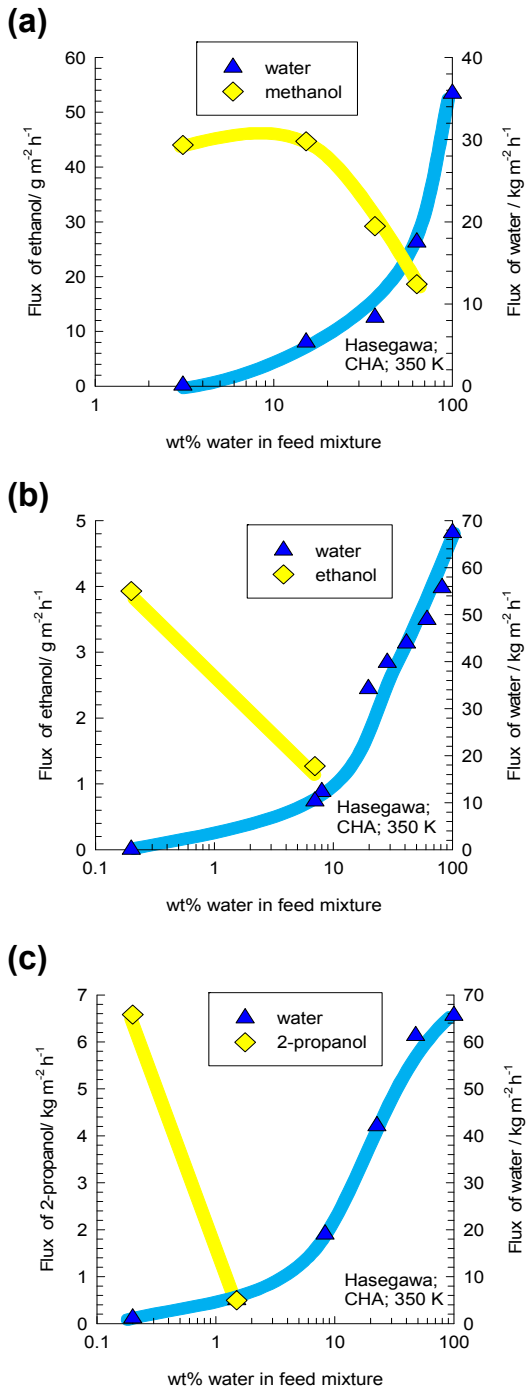


Figure 12. Experimental data of Hasegawa et al.[27] for permeation fluxes across CHA membrane as a function of the wt% water in (a) water/methanol, (b) water/ethanol, and (c) water/2-propanol mixtures.

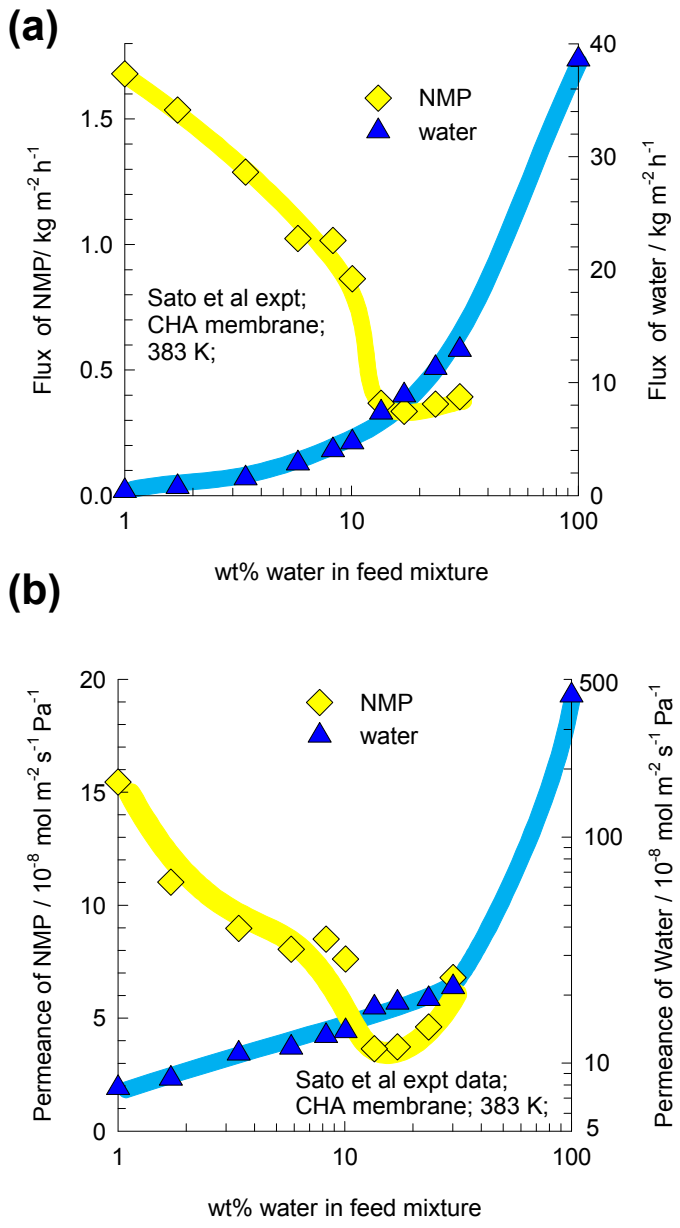


Figure 13. (a) Fluxes, and (b) permeances of water and NMP across for water/NMP pervaporation across CHA membrane [29].

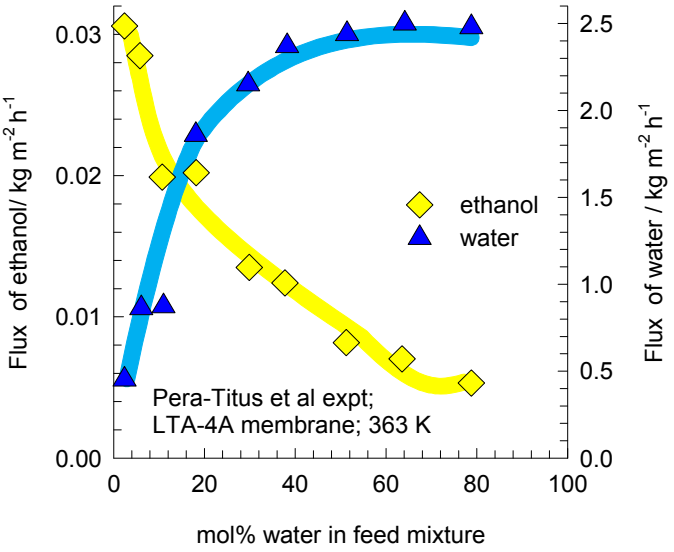


Figure 14. Fluxes of ethanol and water for water/ethanol pervaporation across LTA-4A membrane [30].

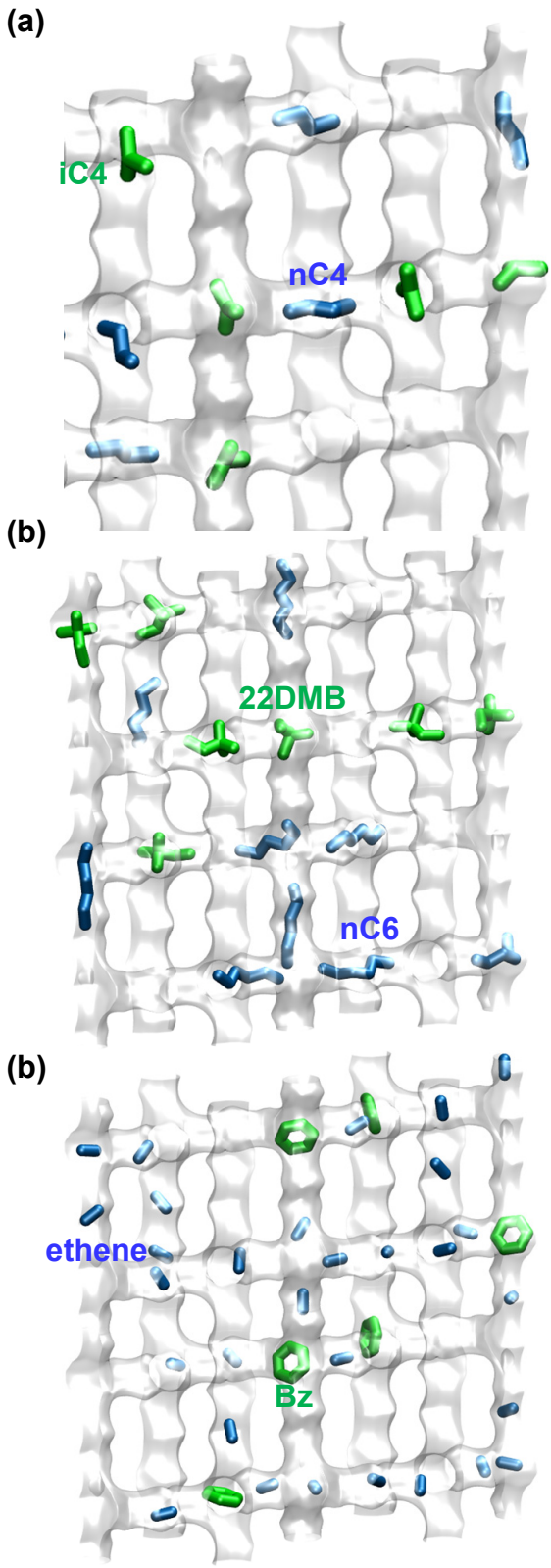


Figure 15. Snapshots showing the location of molecules of (a) nC4/iC4, (b) nC6/22DMB, and (c) ethene/benzene mixtures in MFI.

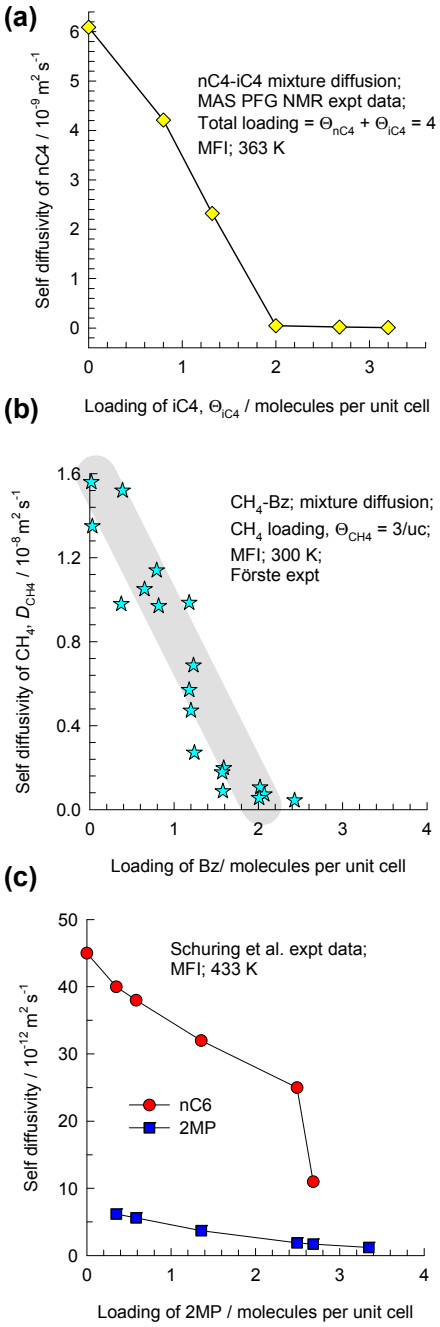


Figure 16. (a) PFG NMR experimental data [32] on self-diffusion coefficients of nC4 in nC4/iC4 mixtures in MFI as a function of the loading of iC4 in the mixture. (b) PFG NMR experimental data [34] on self-diffusion coefficients of $CH_4$ in $CH_4$/Benzene mixtures in MFI as a function of the loading of Benzene in the mixture. (c) Experimental data [57] on self-diffusivities of nC6 and 2methylpentane (2MP) as a function of the loading of 2MP in MFI zeolite

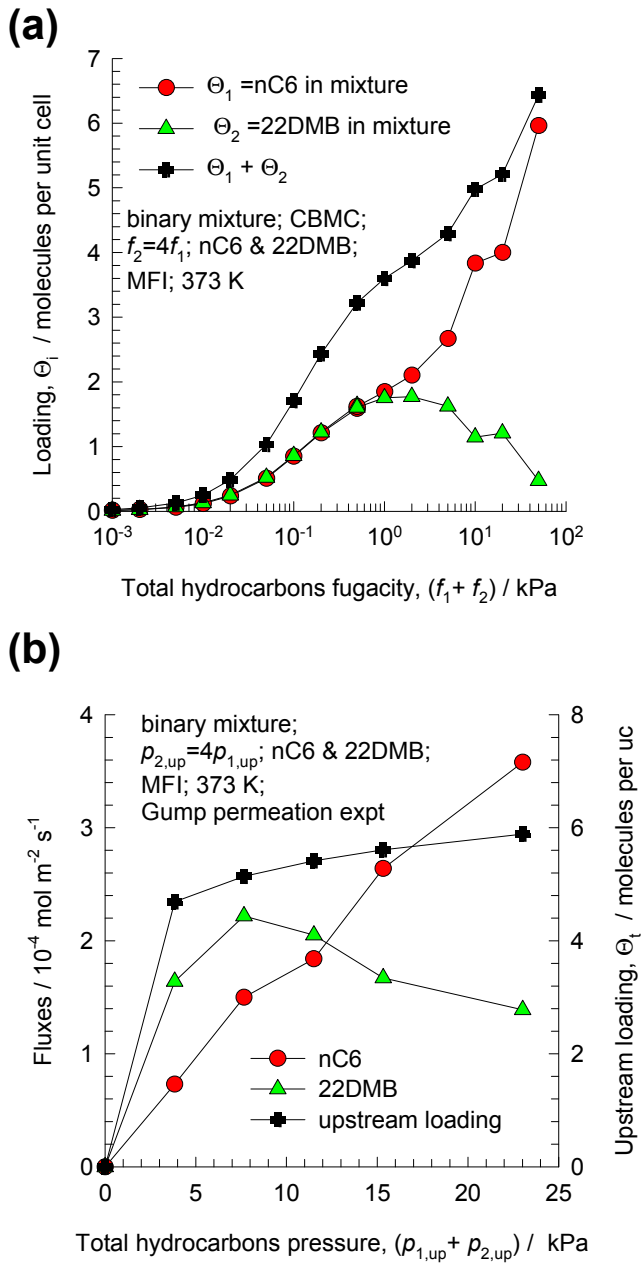


Figure 17. (a) CBMC simulations of loadings in the adsorbed phase in equilibrium with binary fluid phase containing nC6 (1) - 22DMB (2) in MFI, with bulk fluid fugacities $f_2 = 4\,f_1$. (b) Experimental data for nC6 - 22DMB binary mixture permeation across MFI membrane, with upstream partial pressures $f_2 = 4\,f_1$. Graphs are re-constructed using the data from refs [40, 58].

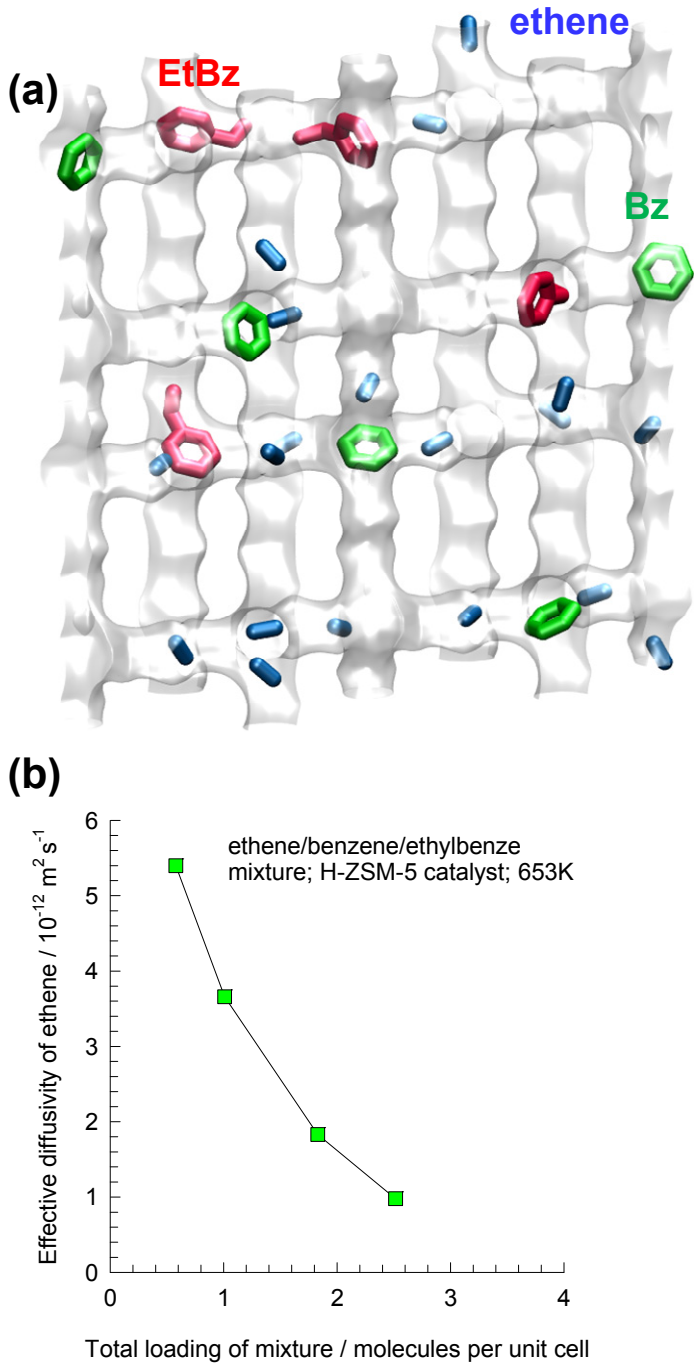


Figure 18. (a) Snapshot showing the location of reactants and products in the alkylation of benzene with ethene to produce ethylbenzene within the intersecting channel topology of MFI catalyst. (b) Effective diffusivity of ethene within MFI catalyst as a function of the mixture loading [46].

# 14. Listing of additional Figures containing MD data

Figures A1 – A92: Unary MD data, arranged according to guest molecules in the following order:

$CO_2$

$CH_4$

$H_2$

Ar

Ne

Kr

$N_2$

$C_2H_6$

$C_3H_8$

$nC_4H_{10}$

water

methanol

ethanol

iso-butane in MFI

in-pentane MFI

n-hexane in MFI

n-heptane in MFI

2,2 dimethylbutane in MFI

2-methylpentane in MFI

3-methylpentane in MFI

Benzene in MFI

Figures B1 – B118: Binary mixture MD data, including validation of Vignes interpolation formula, arranged according to guest mixtures in the following order:

$H_2/CO_2$

$CH_4/CO_2$

$CO_2/N_2$

$CH_4/C_2H_6$

$CH_4/C_3H_8$

$CH_4/nC_4H_{10}$

$H_2/CH_4$

$N_2/CH_4$

Ne/Ar

$H_2$/Ar

$CH_4$/Ar

Ne/$CO_2$

Ar/Kr

water/methanol, and water/ethanol

$CH_4/iC_4H_{10}$ in MFI zeolite

$C_2H_6/iC_4H_{10}$ in MFI zeolite

$C_3H_8/iC_4H_{10}$ in MFI zeolite

$nC_4H_{10}/iC_4H_{10}$ in MFI zeolite

$CH_4$/Benzene in MFI zeolite

$CH_4$/22MB in MFI zeolite

$C_3H_8$/Benzene in MFI zeolite

nC6/22MB in MFI zeolite

nC6/2MP in MFI zeolite

nC6/3MP in MFI zeolite

nC6/Benzene in MFI zeolite

$C_2H_4$/Benzene in MFI zeolite

nC6/3MP/22MB in MFI zeolite

$C_2H_4$/Benzene/Ethylbenzene in MFI zeolite

Figure A1

Figures A1 – A92:
Unary MD data, arranged according to guest molecules in the following order:
$CO_2$
$CH_4$
$H_2$
Ar
Ne
Kr
$N_2$
$C_2H_6$
$C_3H_8$
$nC_4H_{10}$
water
methanol
ethanol
iso-butane in MFI
in-pentane MFI
n-hexane in MFI
n-heptane in MFI
2,2 dimethylbutane in MFI
2-methylpentane in MFI
3-methylpentane in MFI
Benzene in MFI

Figure A2

# Guest Molecule: $CO_2$

Figure A3

# Pure component isotherms and Thermodynamic Factor

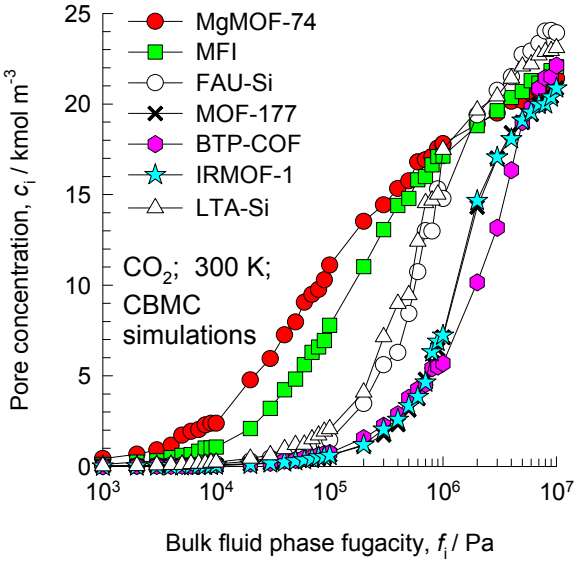


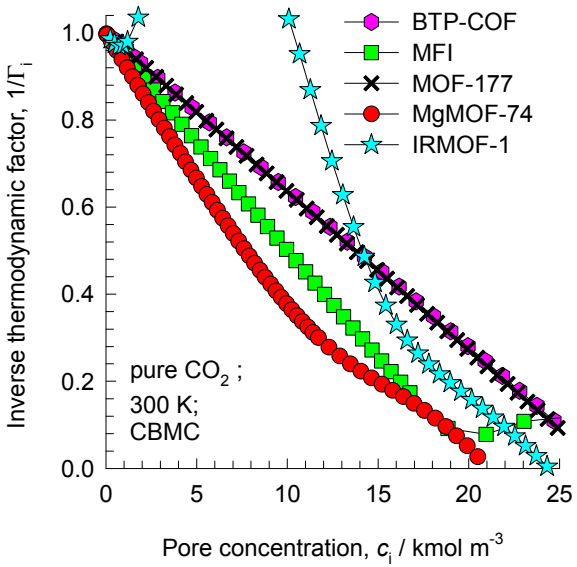


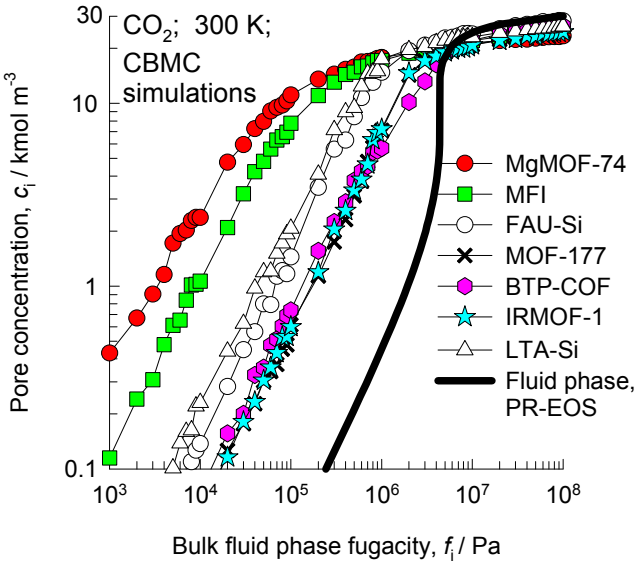


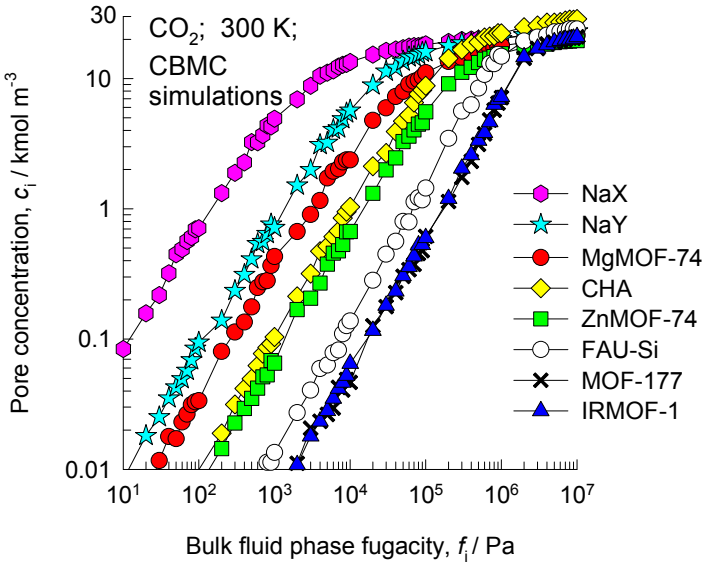

Figure A4

# Isosteric heats of adsorption

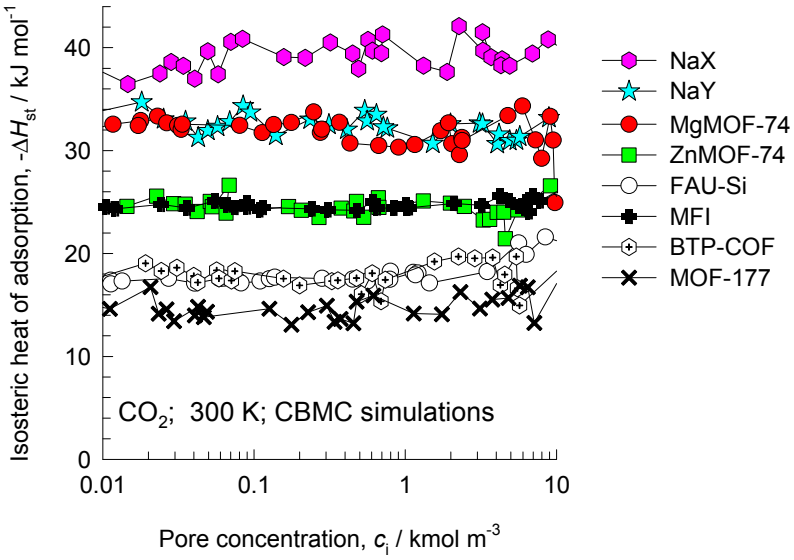


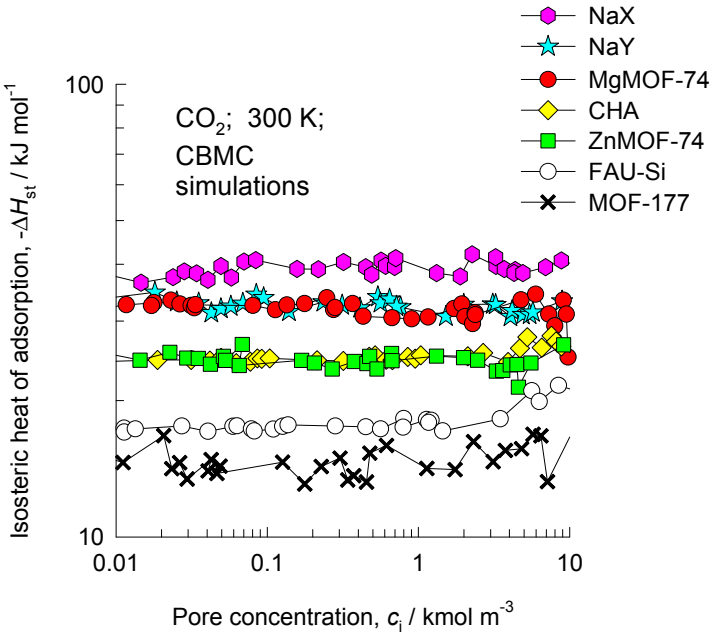

Figure A5

# Self-, and Maxwell-Stefan diffusivities

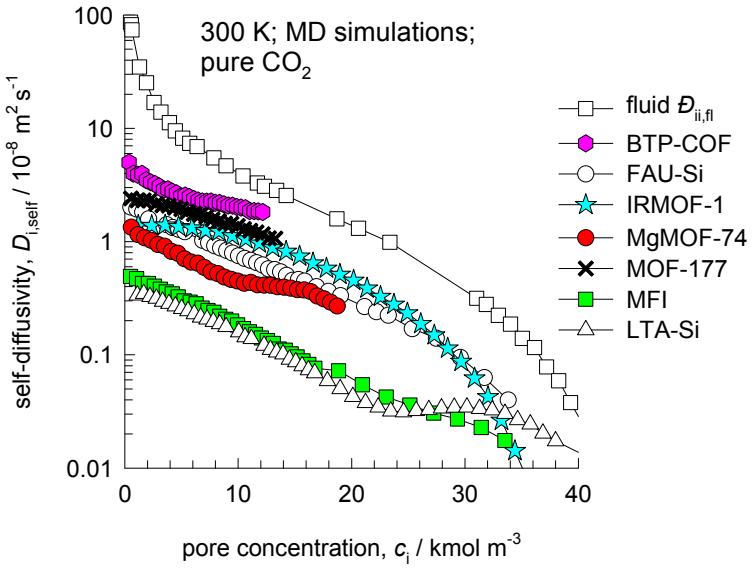


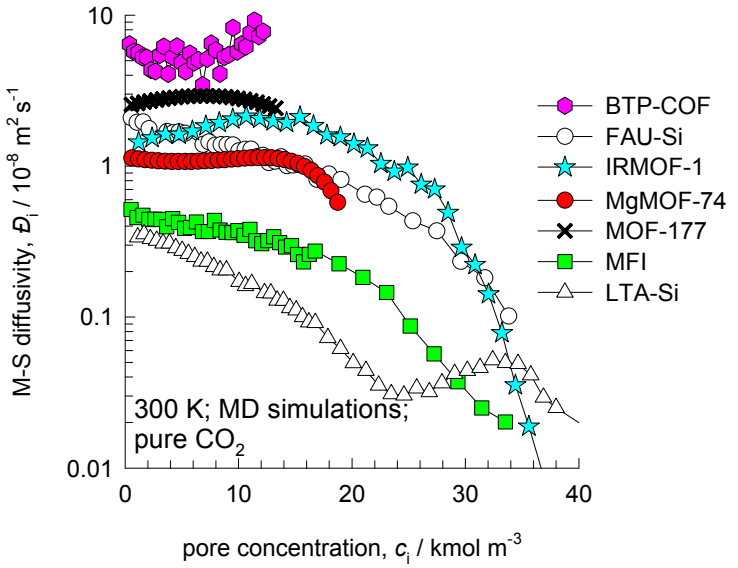


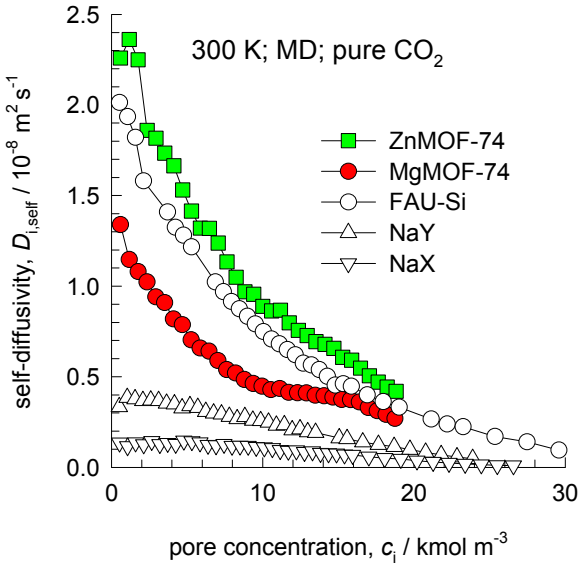

Figure A6

# Self-exchange coefficients and Degrees of correlations

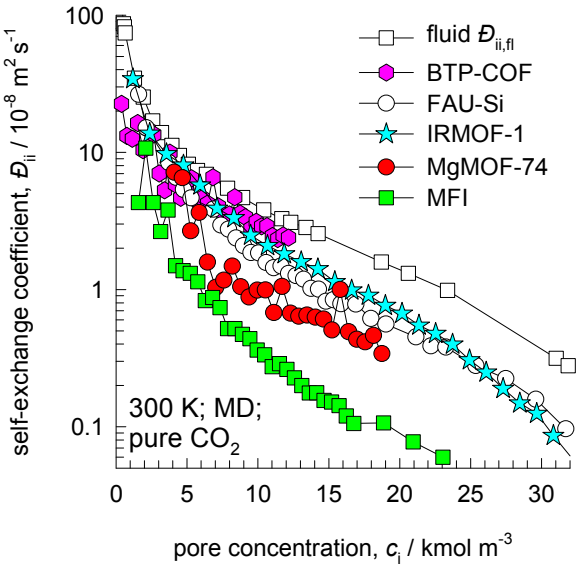


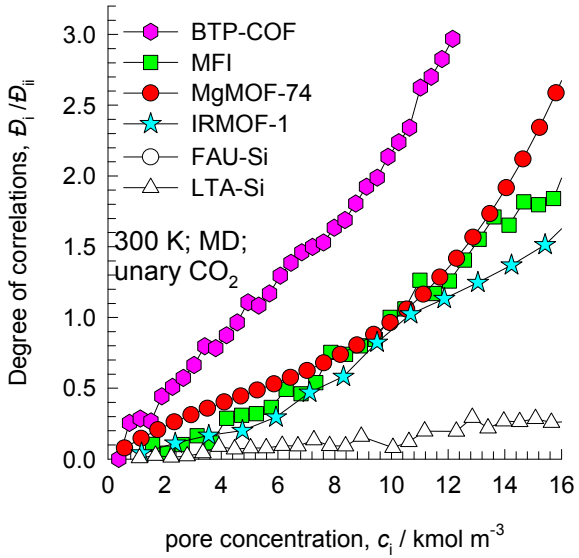


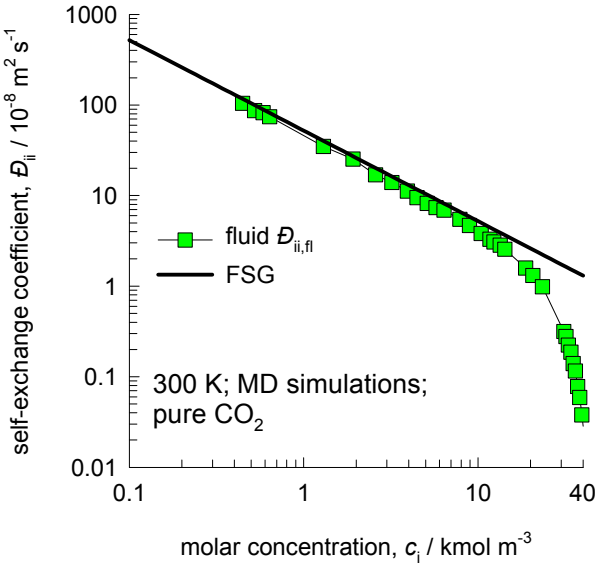


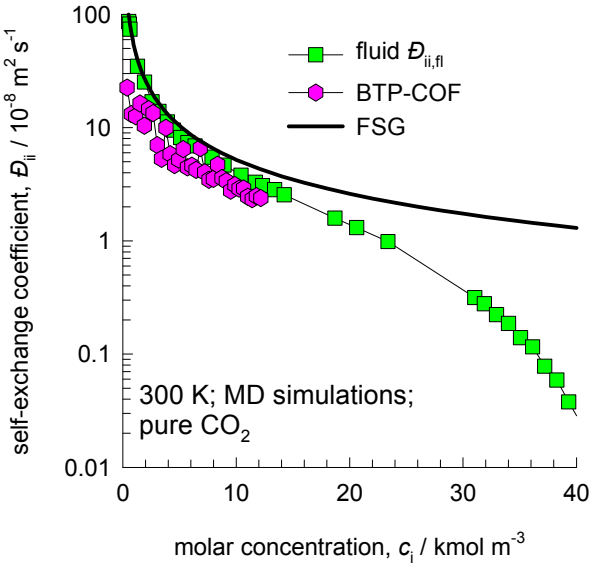

Figure A7

# Exchange coefficients as fraction of fluid phase $Đ_{ii,fl}$

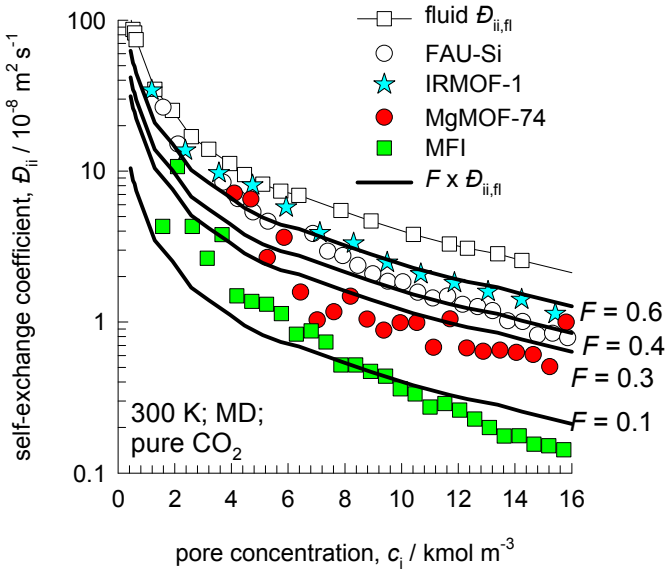


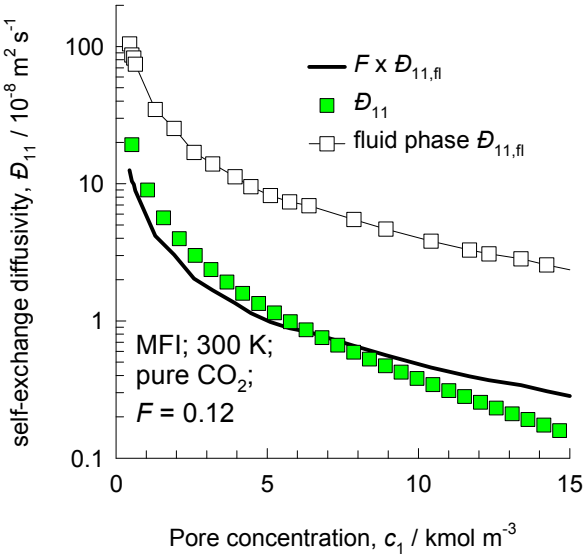


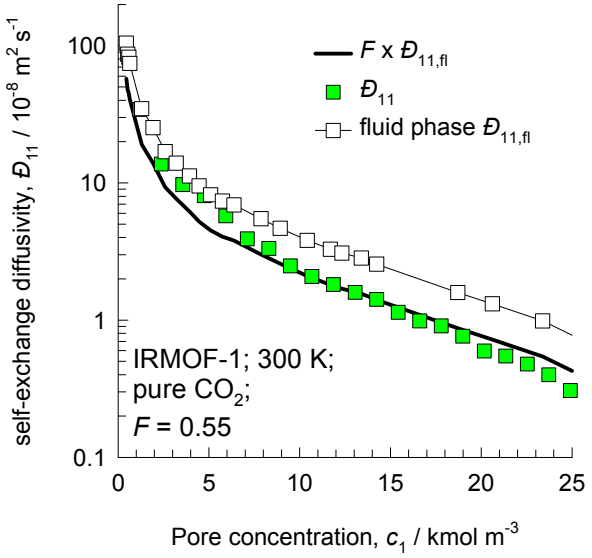


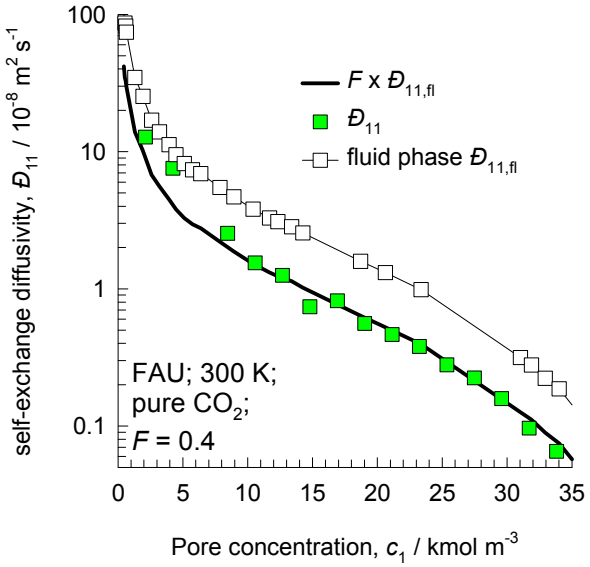


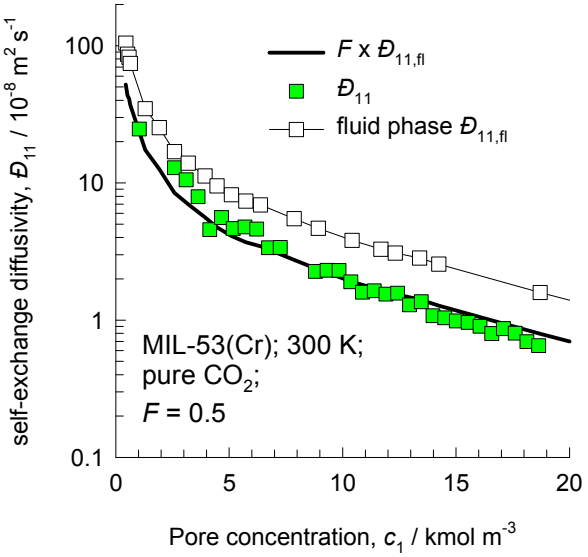


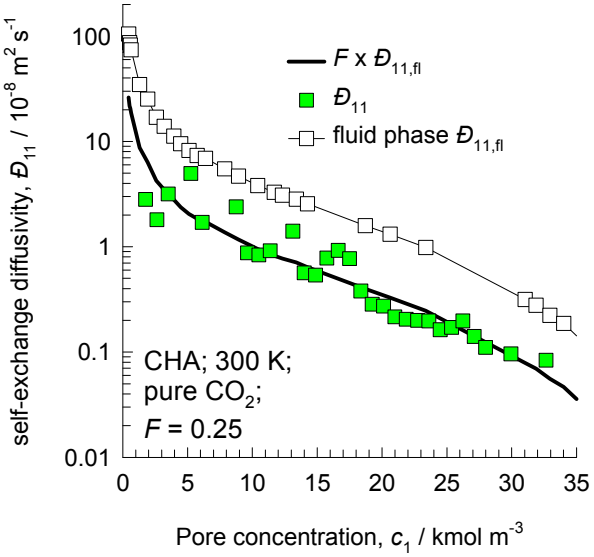

Figure A8

# Guest Molecule: $CH_4$

Figure A9

# Pure component isotherm and Thermodynamic Factor

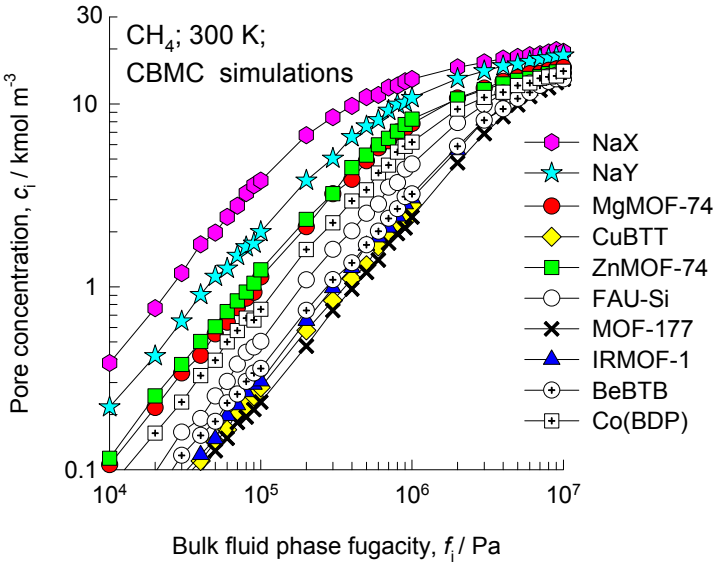


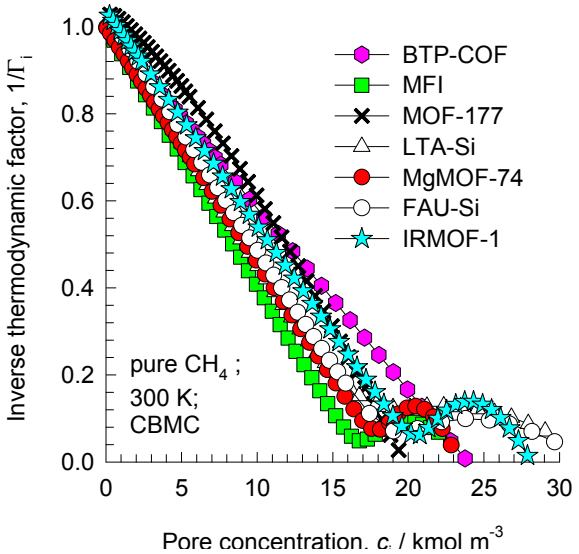


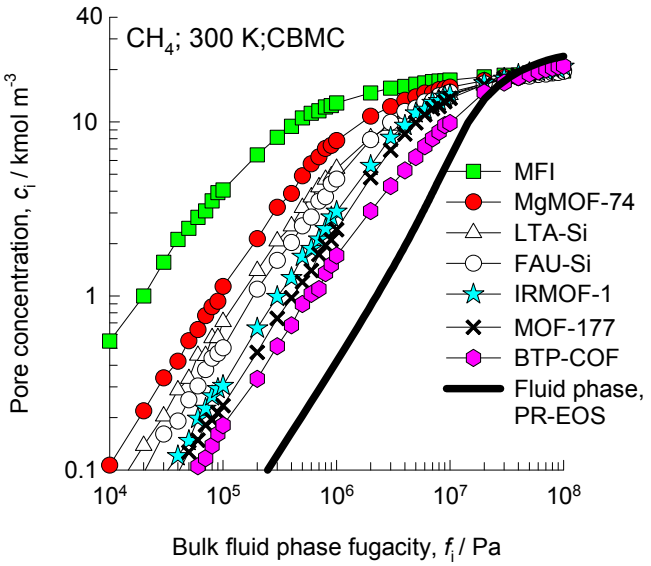


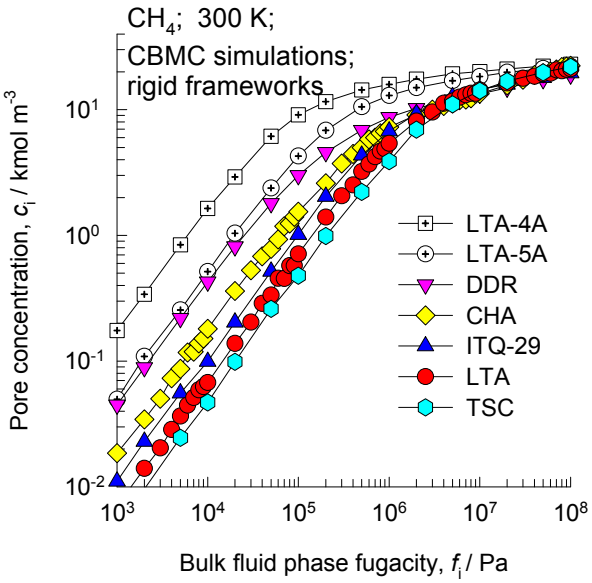


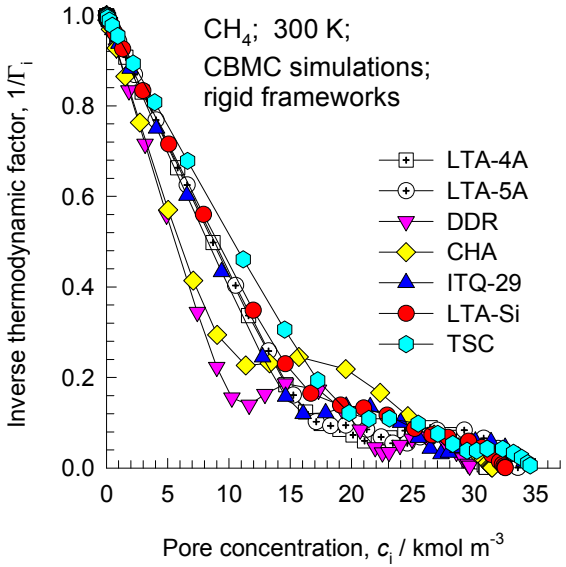

Figure A10

# Isosteric heats of adsorption

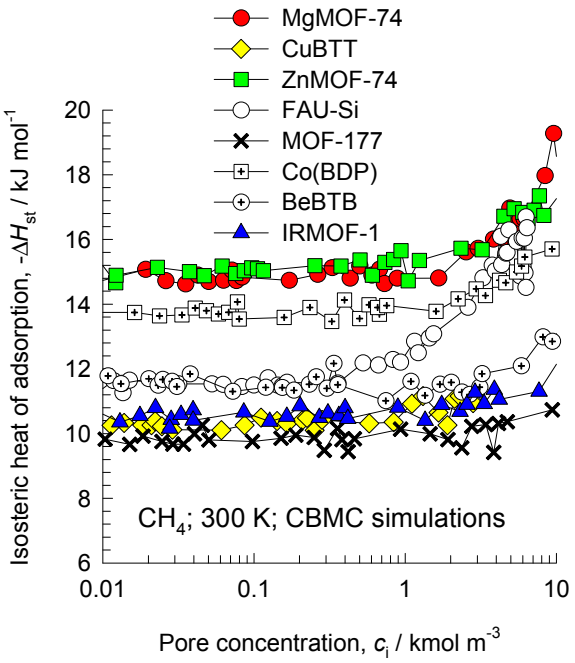

Figure A11

# Self-, and Maxwell-Stefan diffusivities

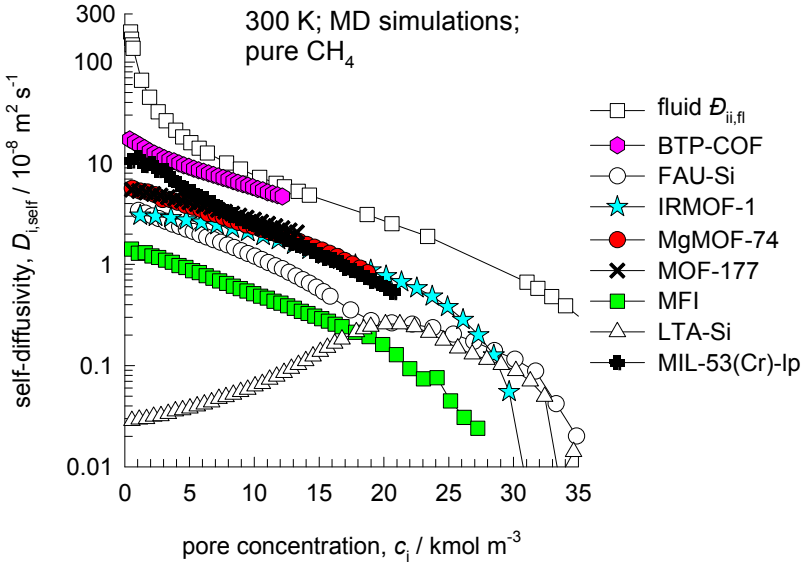


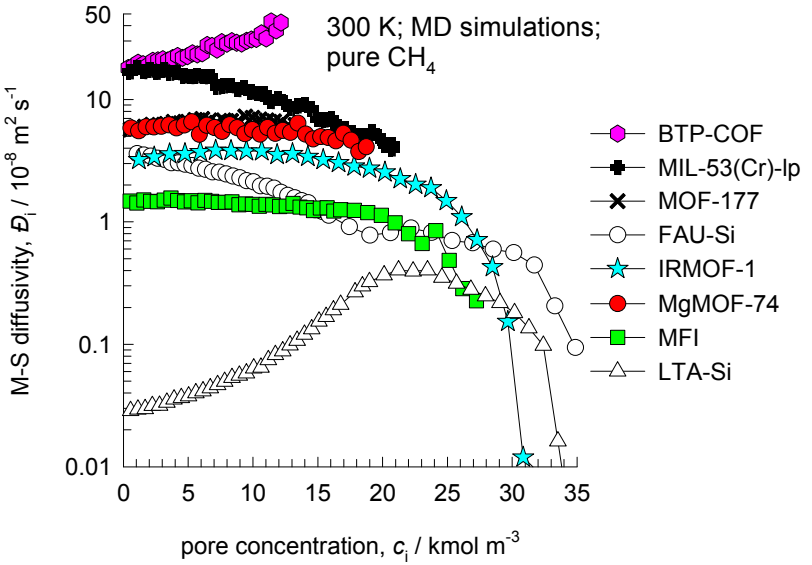


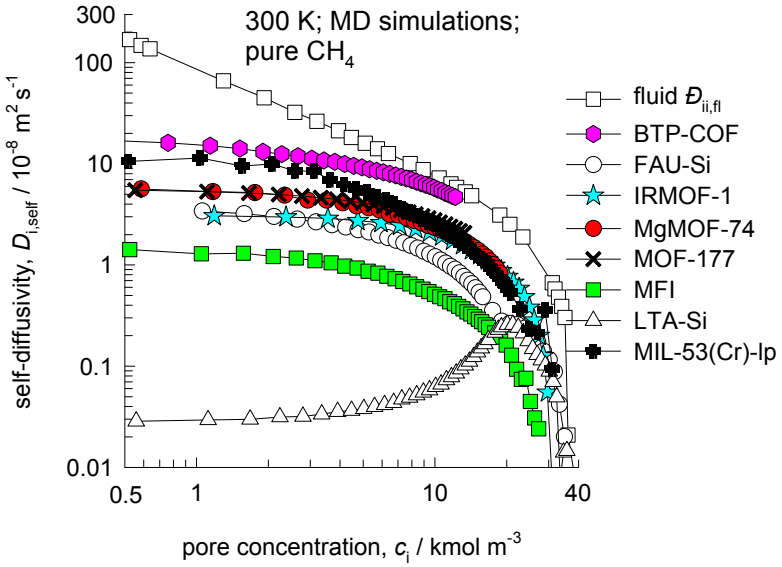


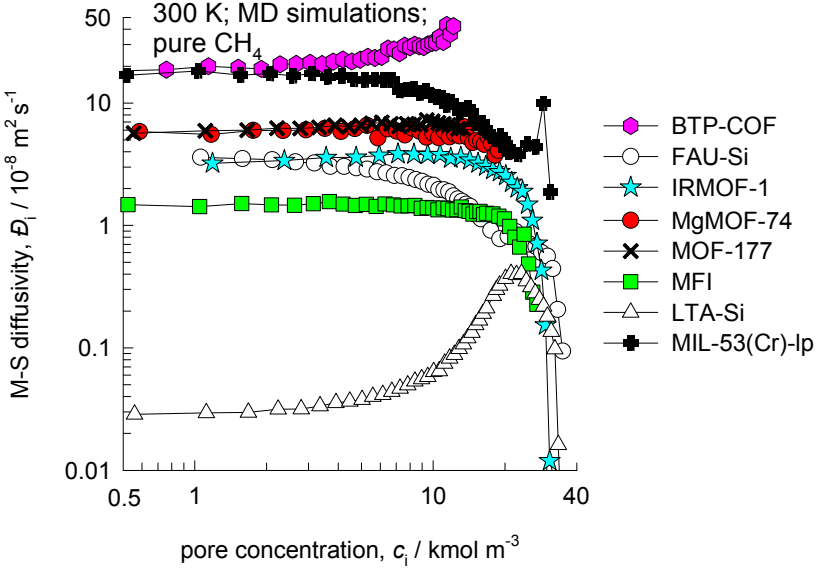

# Self-exchange coefficients and Degrees of correlations

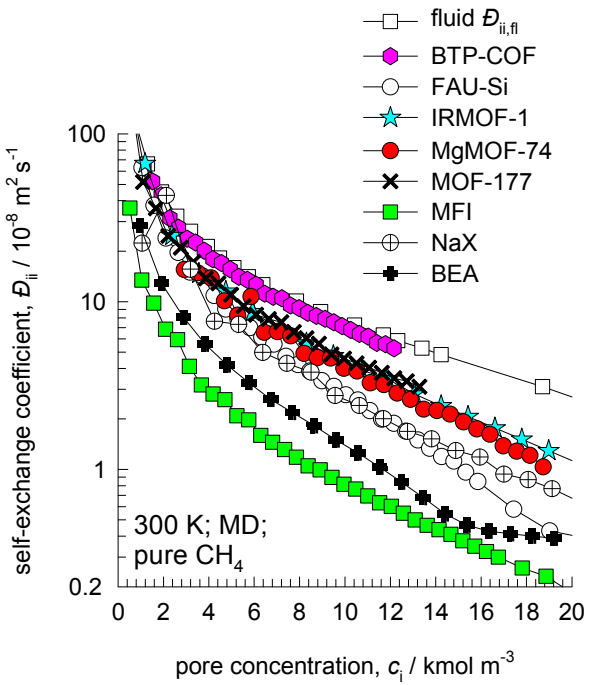


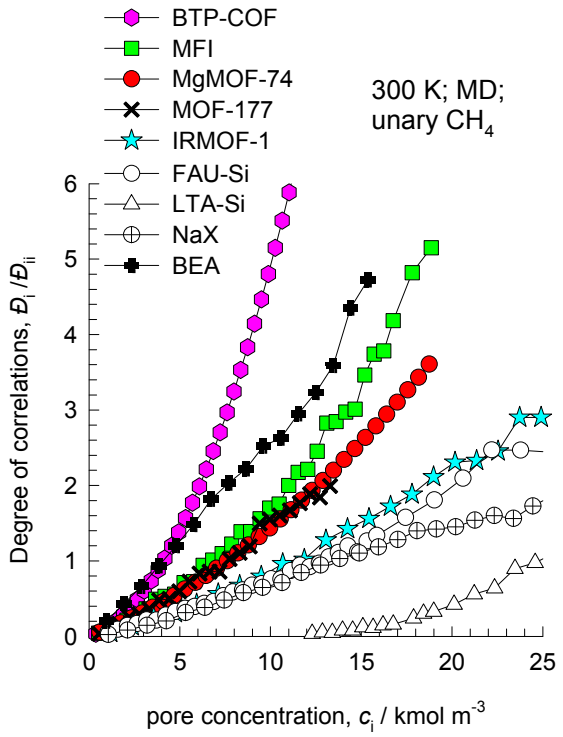


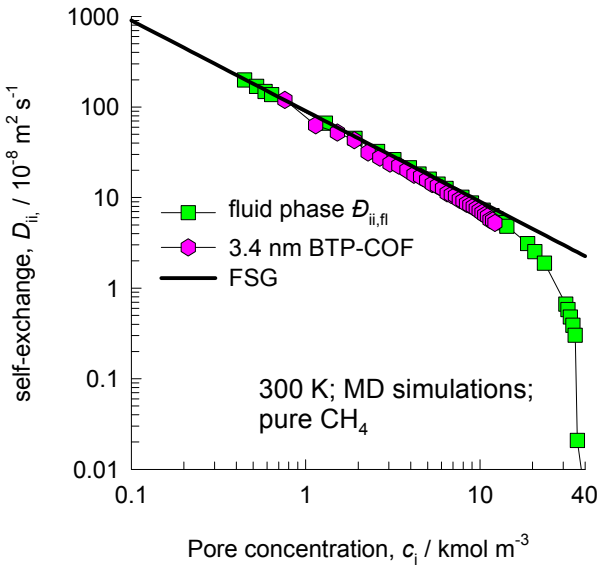


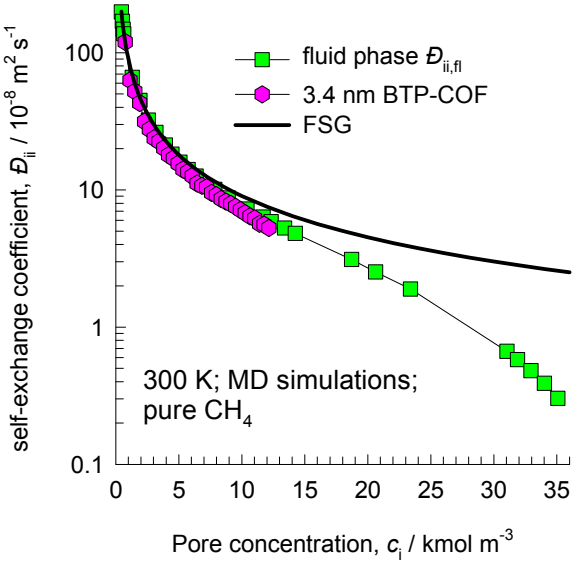

Figure A13

# Exchange coefficients as fraction of fluid phase $Đ_{ii,fl}$

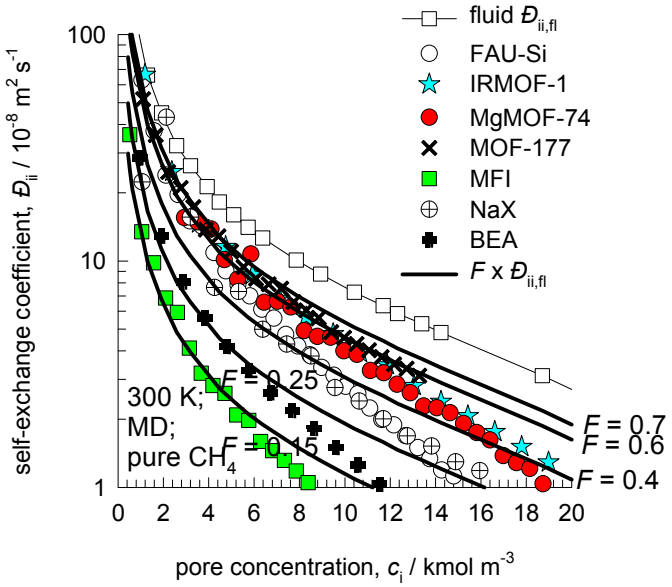


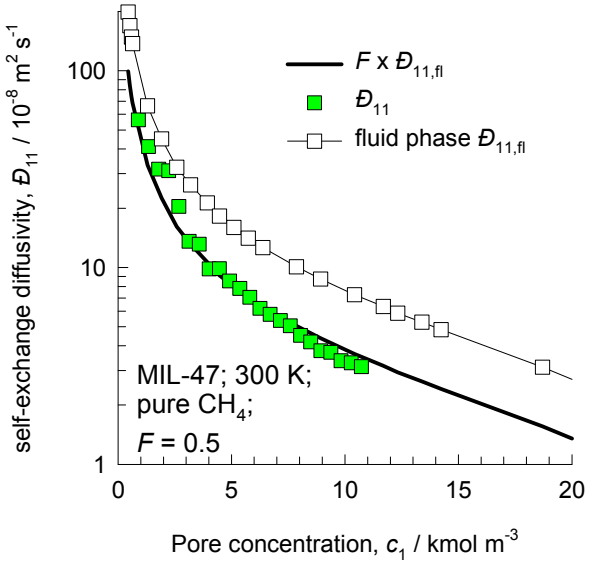

Figure A14

# Exchange coefficients as fraction of fluid phase $Đ_{ii,fl}$

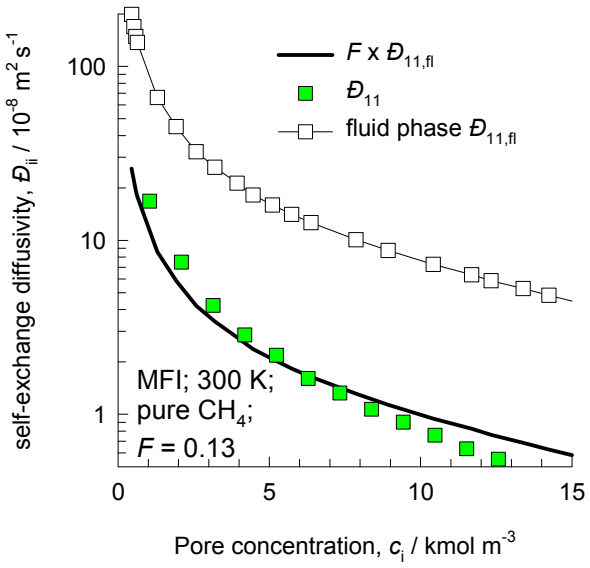


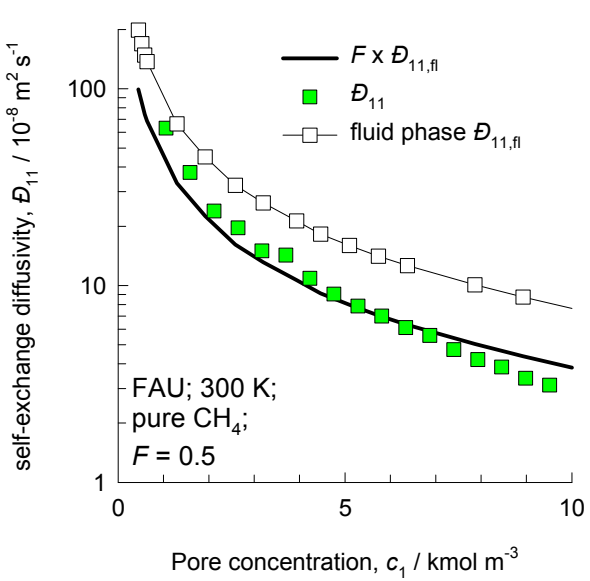


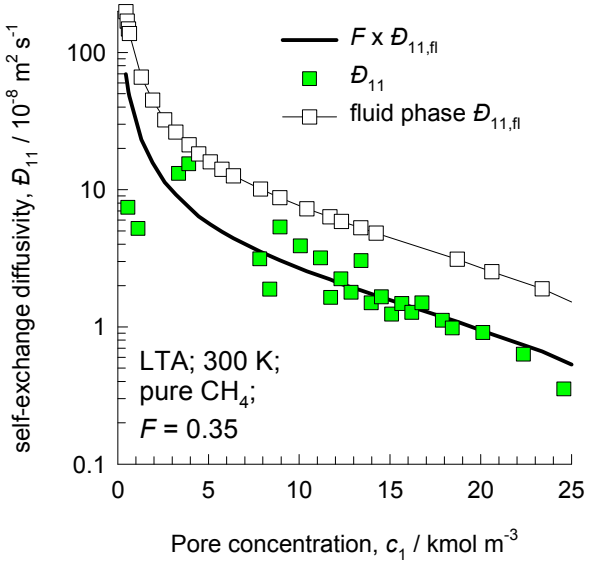


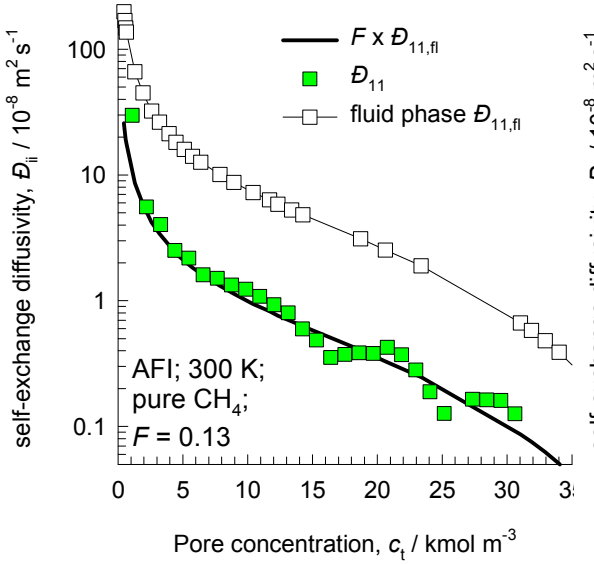


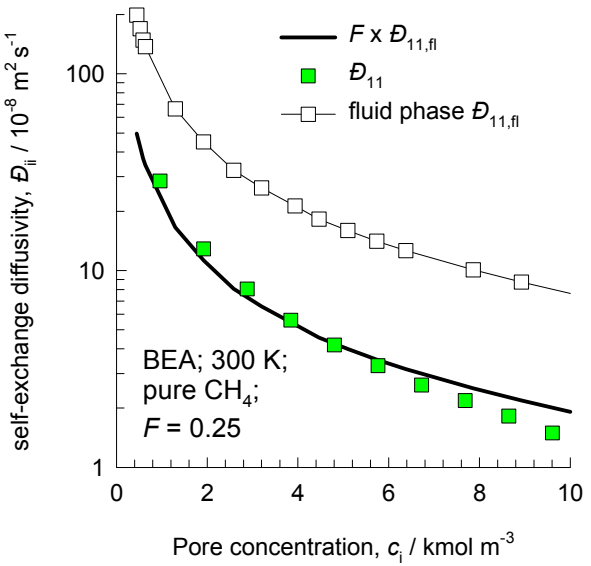


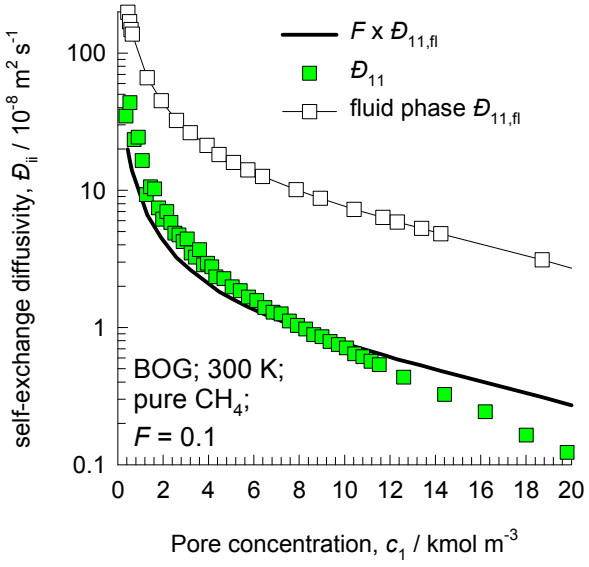

Figure A15

# Exchange coefficients as fraction of fluid phase $Đ_{ii,fl}$

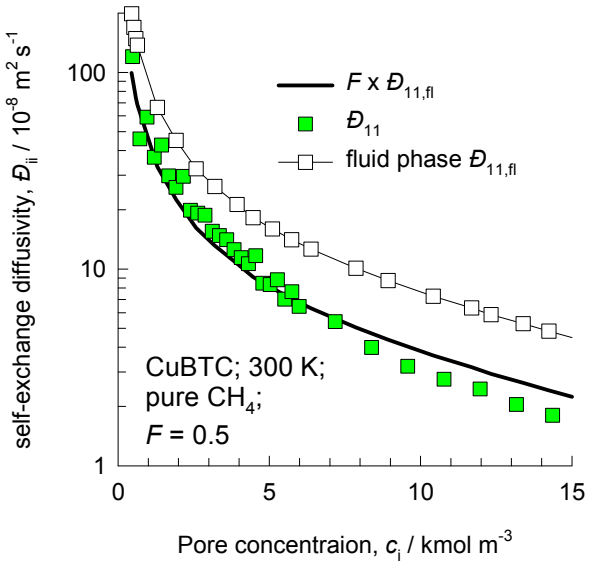


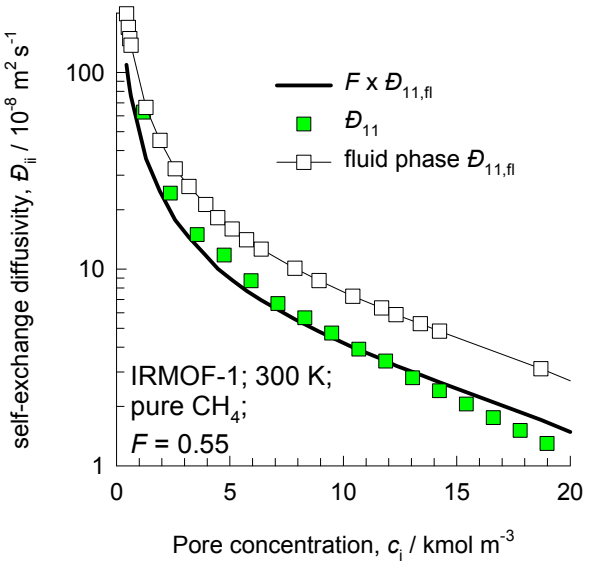


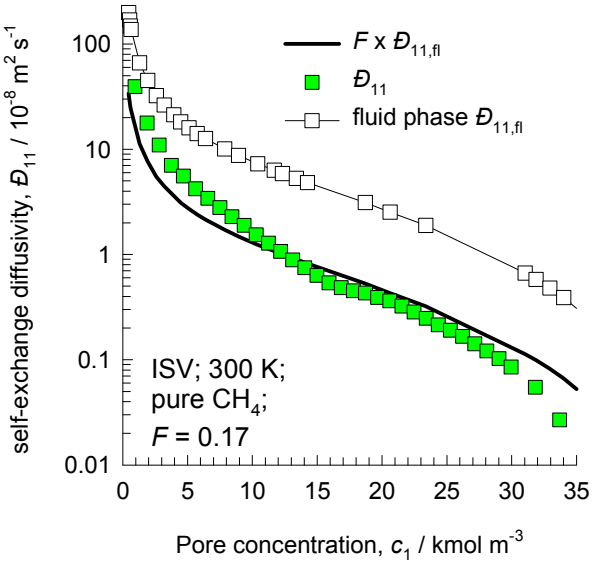


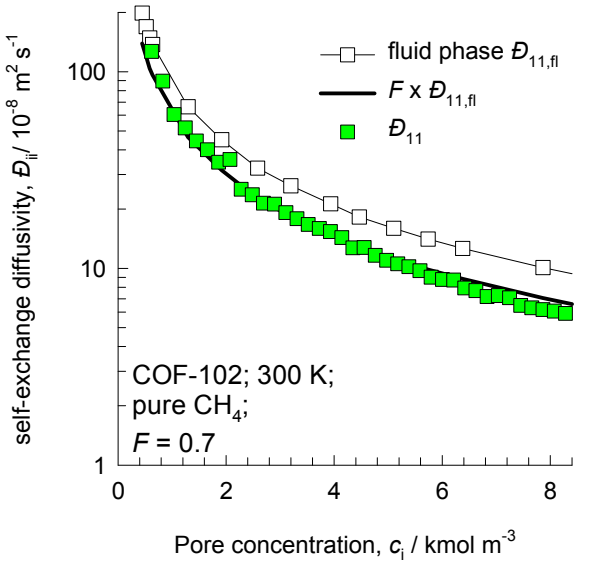


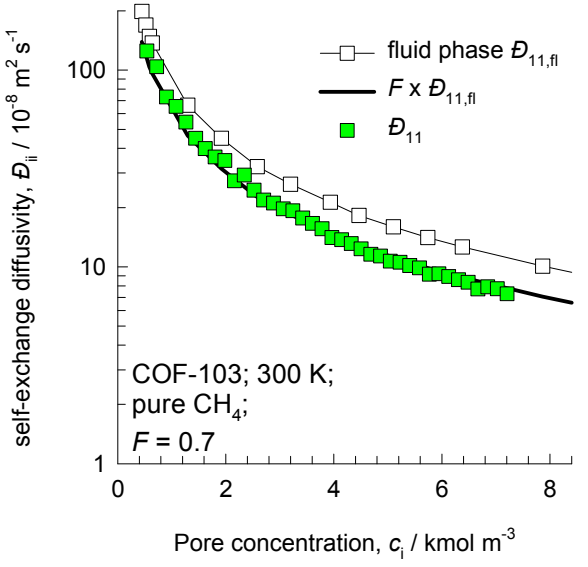


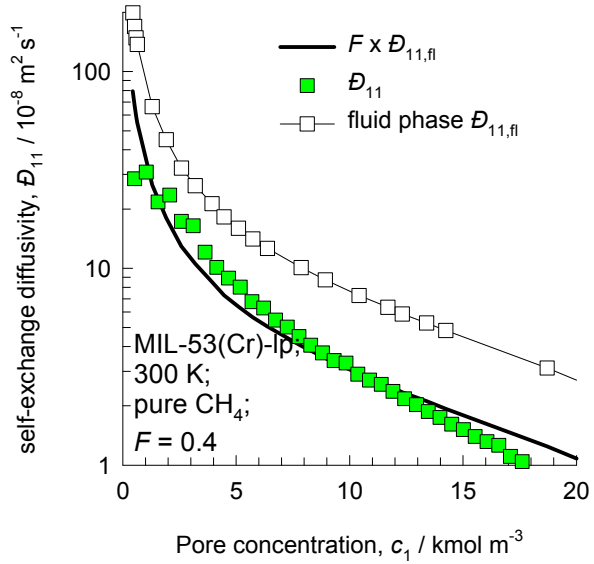

Figure A16

# Guest Molecule:
# $H_2$

Figure A17

# Self-, and Maxwell-Stefan diffusivities

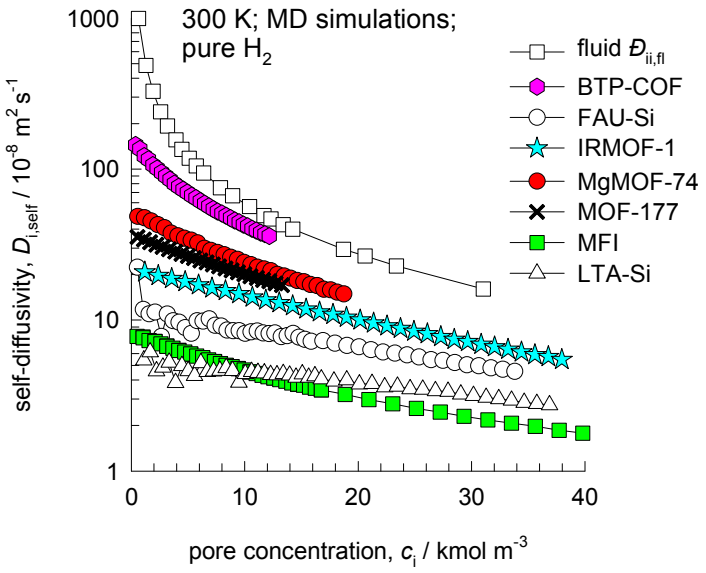


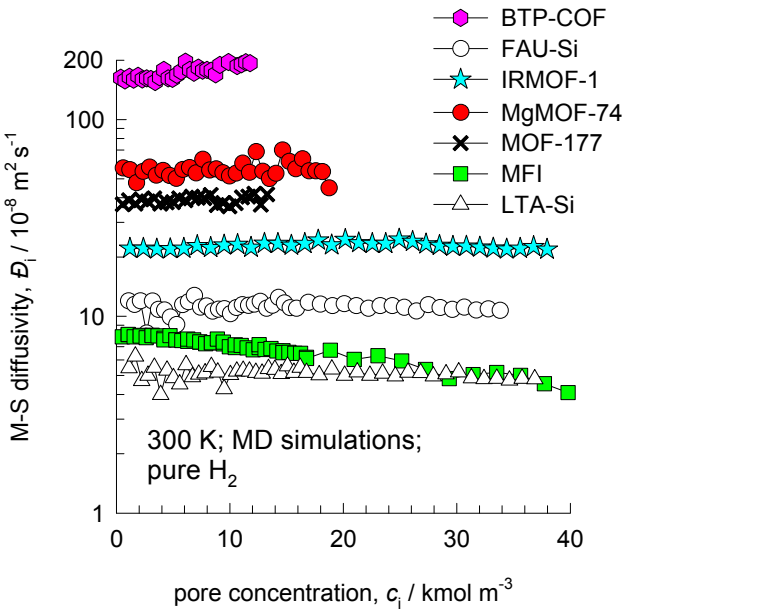


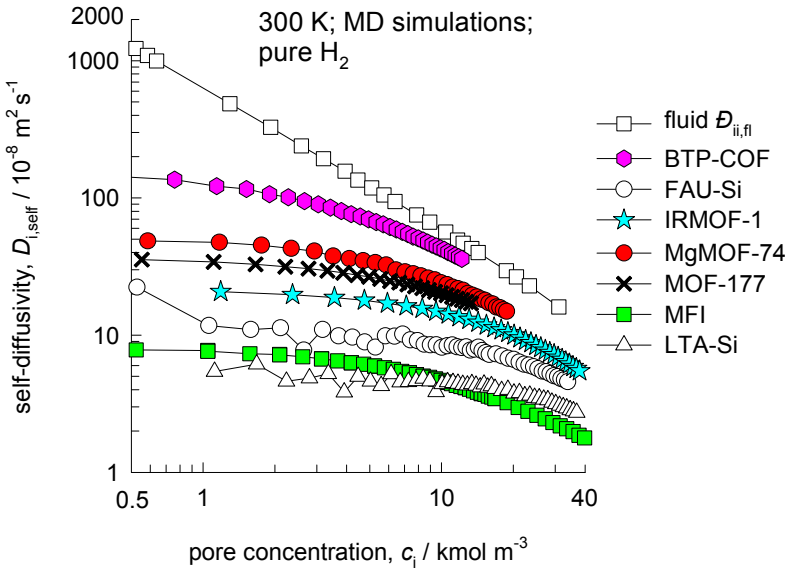


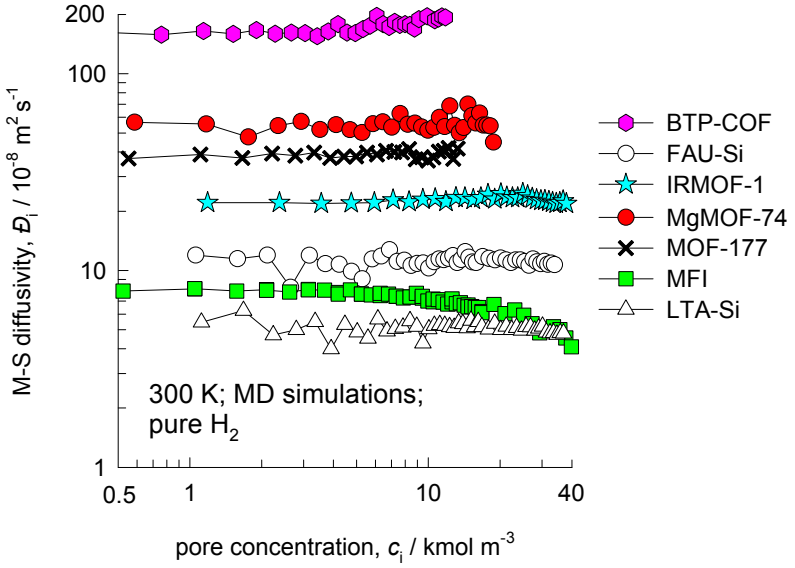

Figure A18

# Self-exchange coefficients and Degrees of correlations

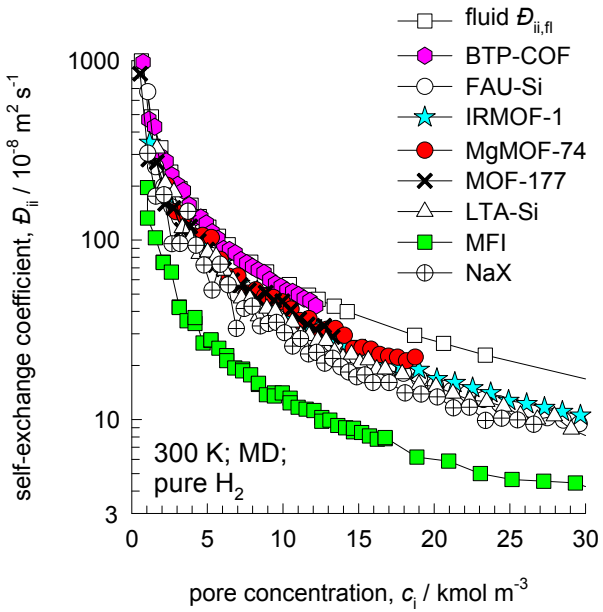


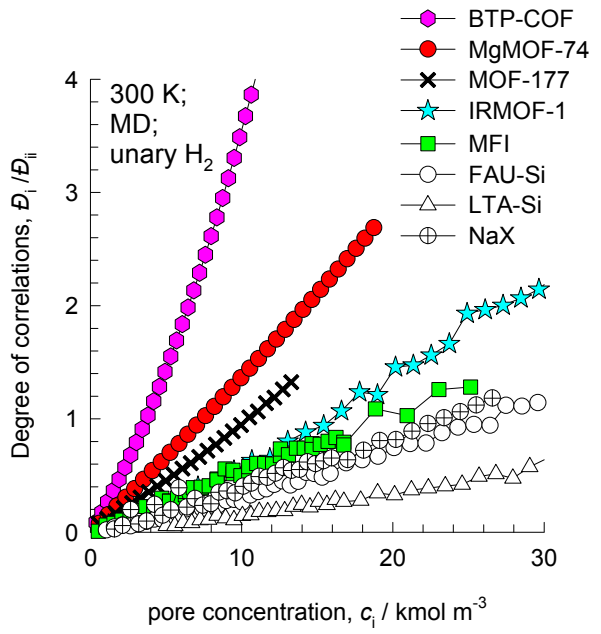


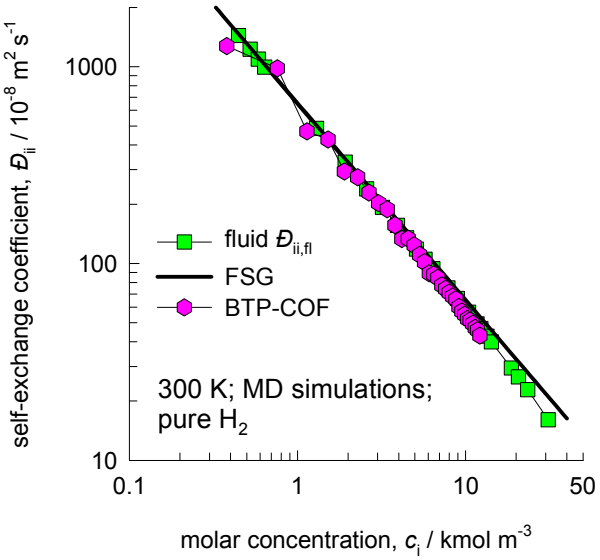


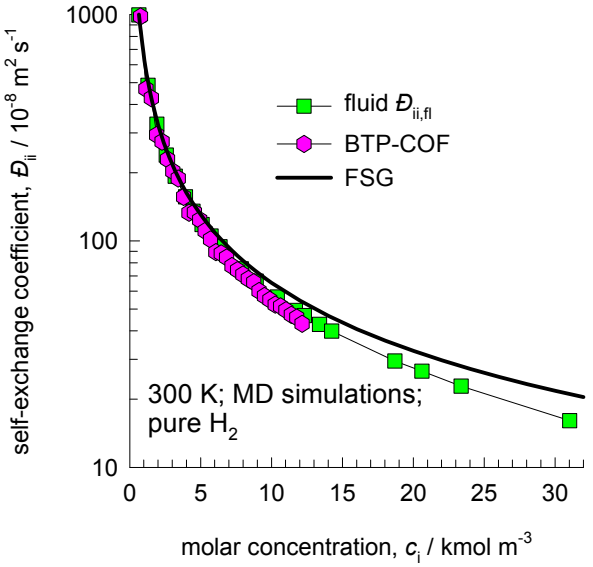

Figure A19

# Exchange coefficients as fraction of fluid phase $Đ_{ii,fl}$

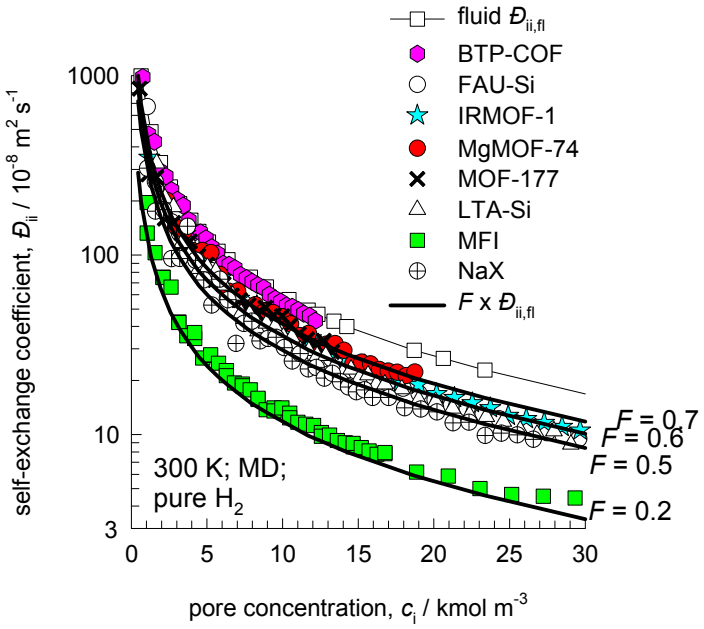


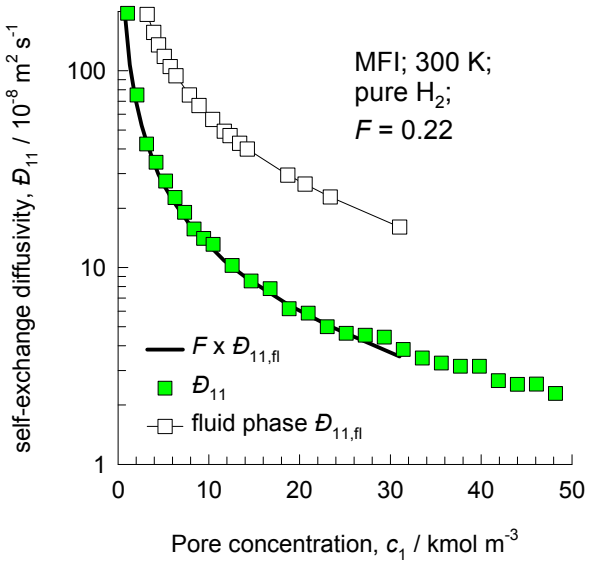

Figure A20

# Guest Molecule:
# Ar

Figure A21

# Self-, and Maxwell-Stefan diffusivities

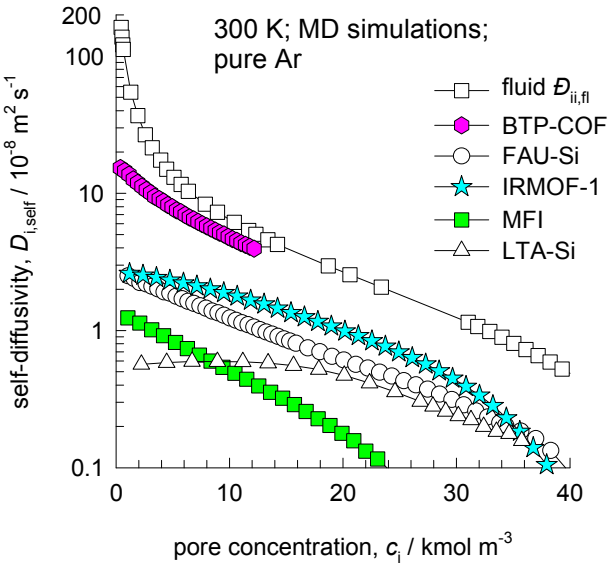


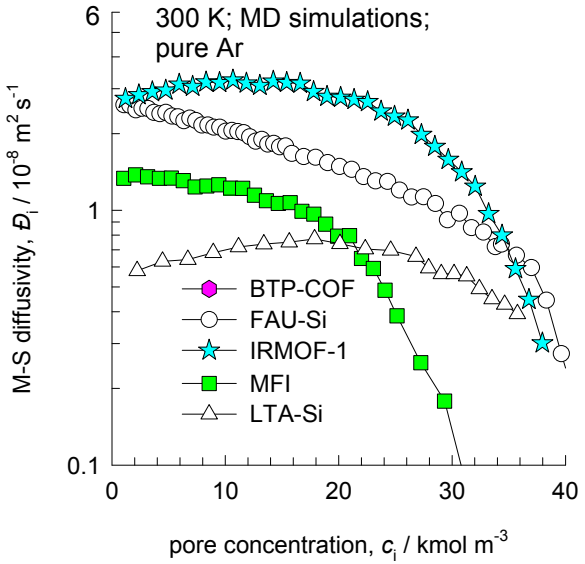

Figure A22

# Self-exchange coefficients and Degrees of correlations

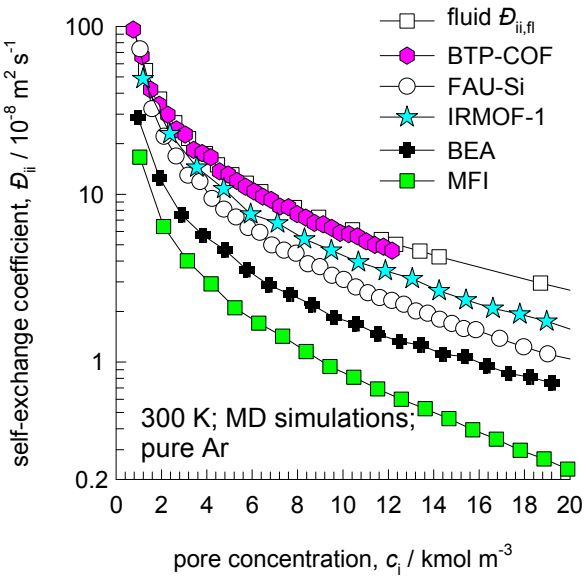


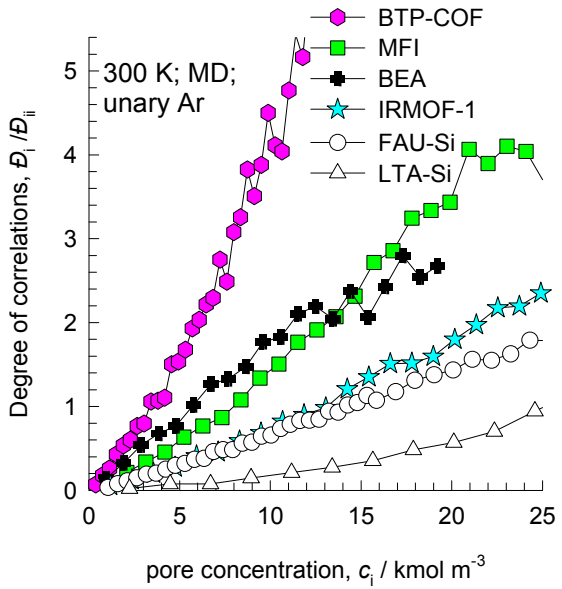


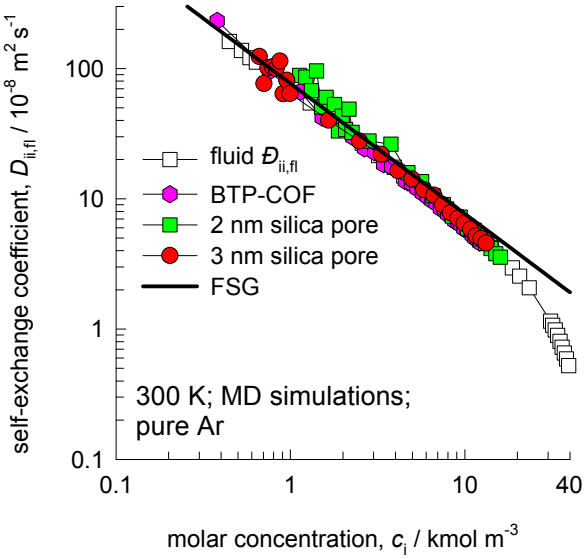


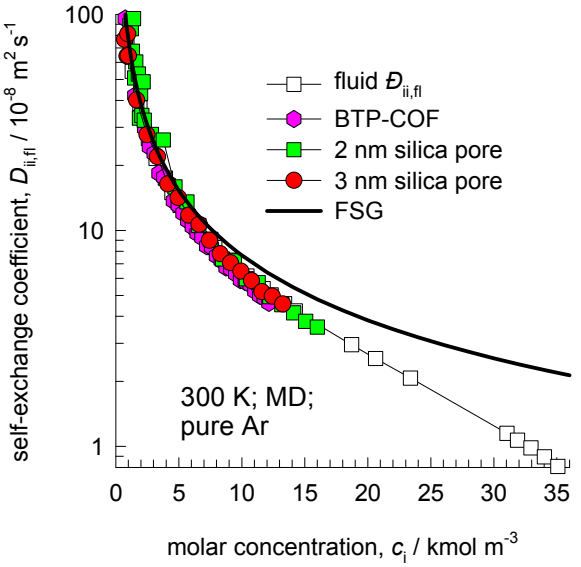

Figure A23

# Exchange coefficients as fraction of fluid phase $Đ_{ii,fl}$

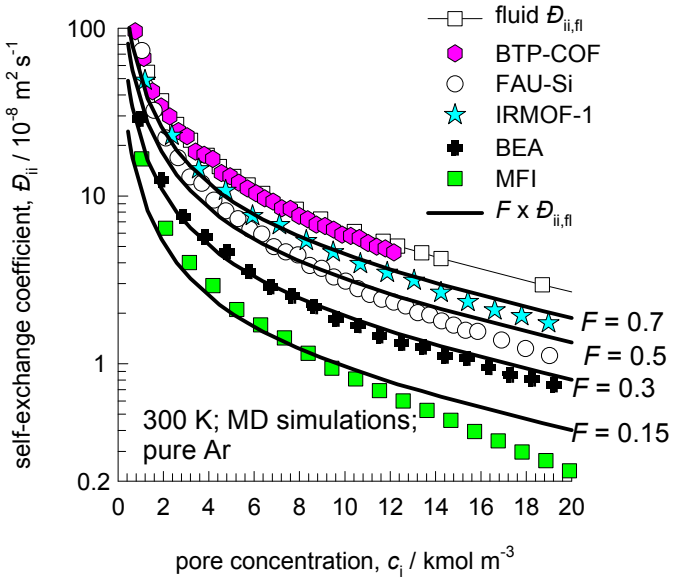


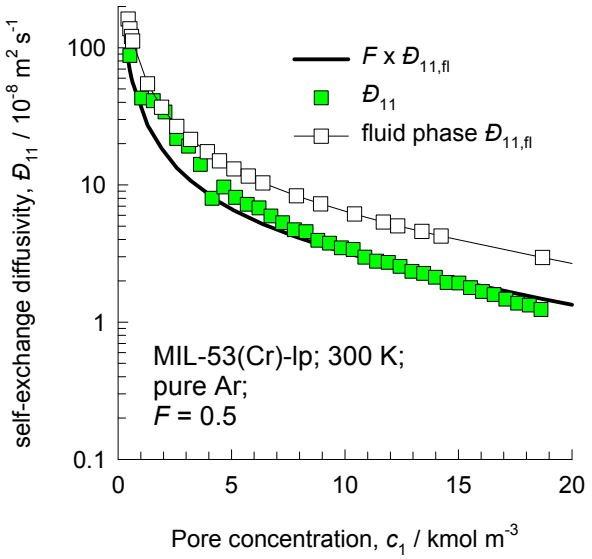


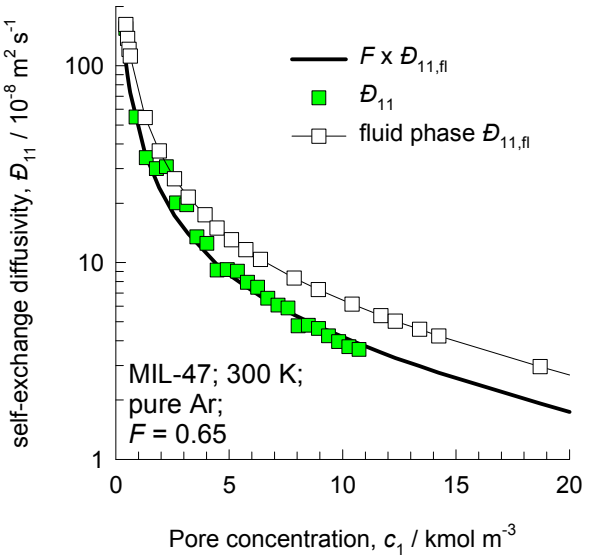

Figure A24

# Exchange coefficients as fraction of fluid phase $Đ_{ii,fl}$

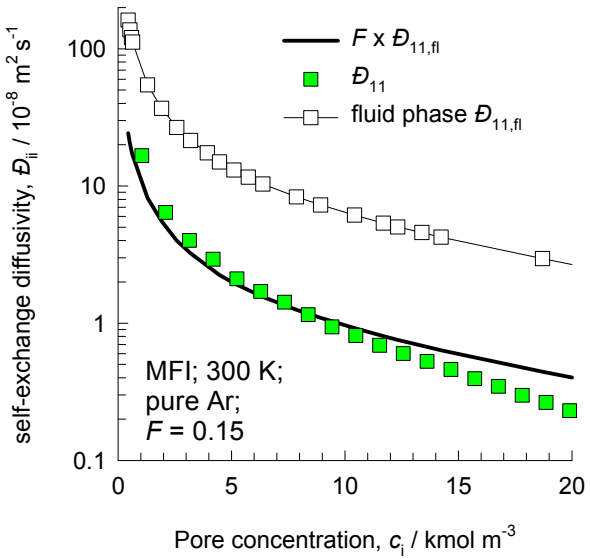


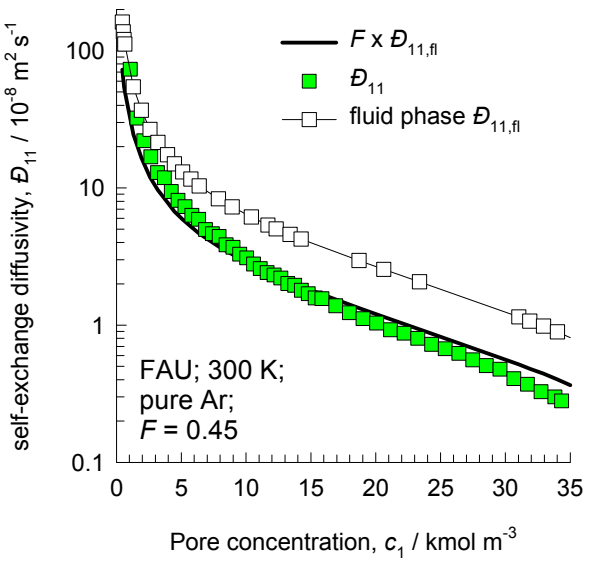


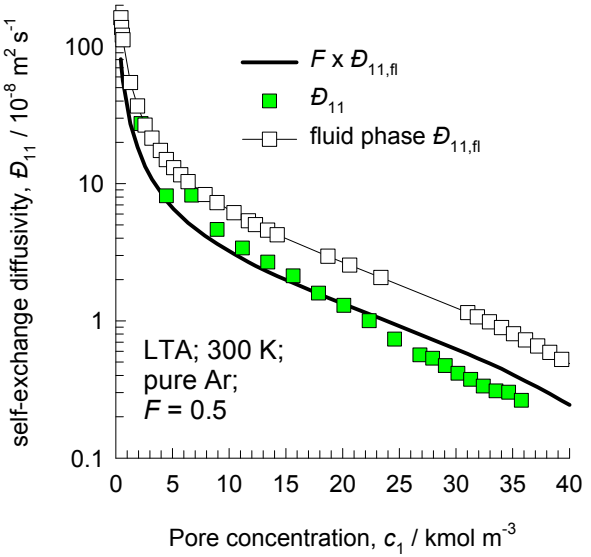


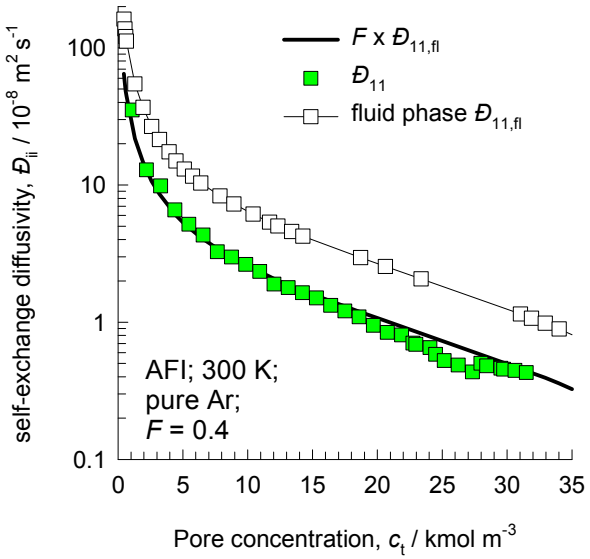


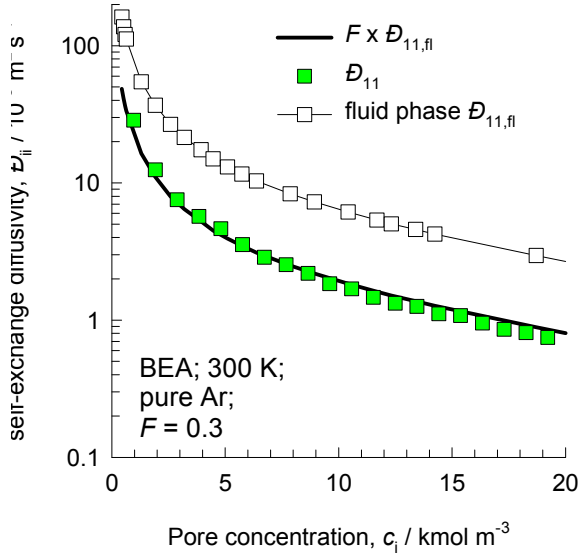


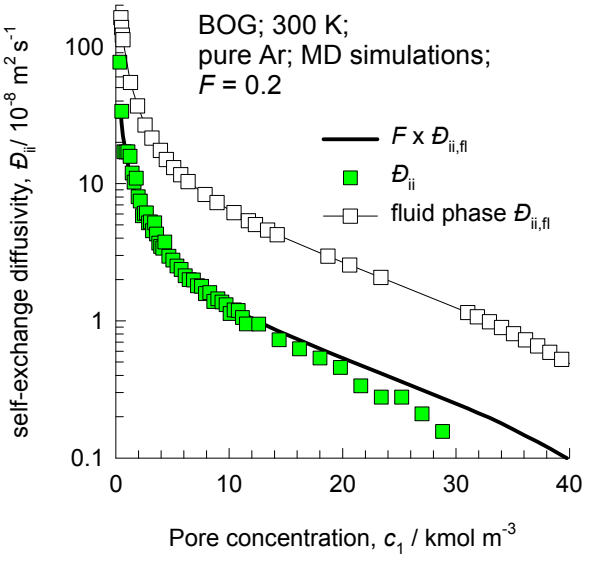

Figure A25

# Exchange coefficients as fraction of fluid phase $Đ_{ii,fl}$

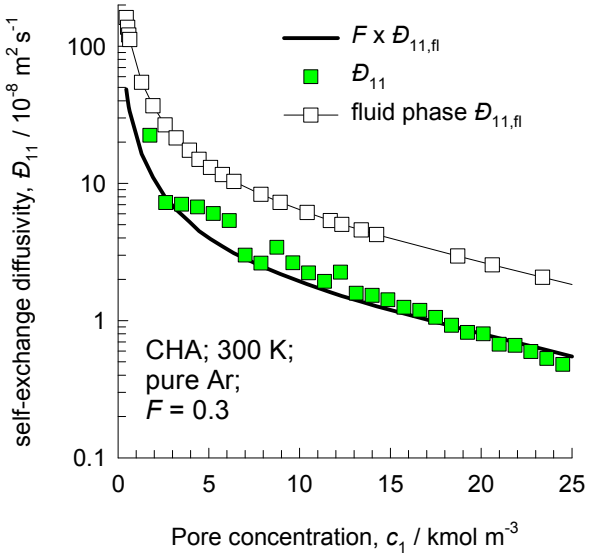


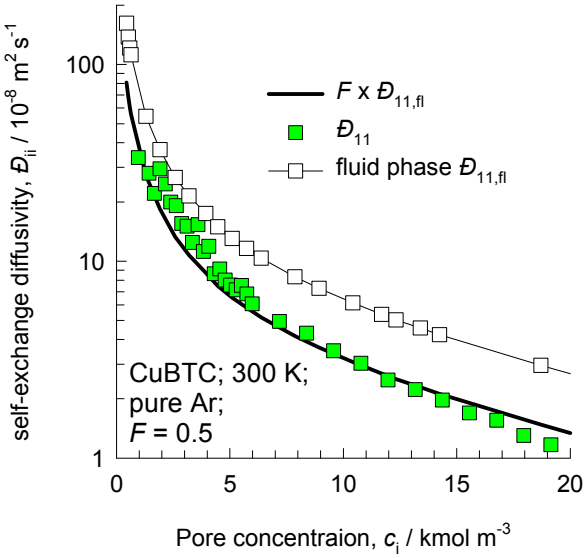


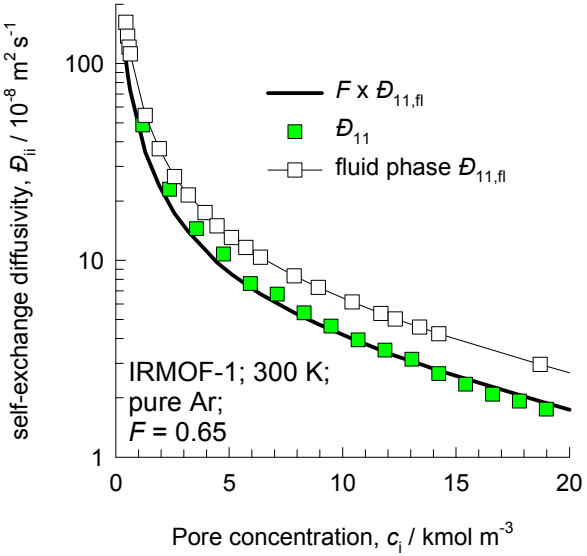


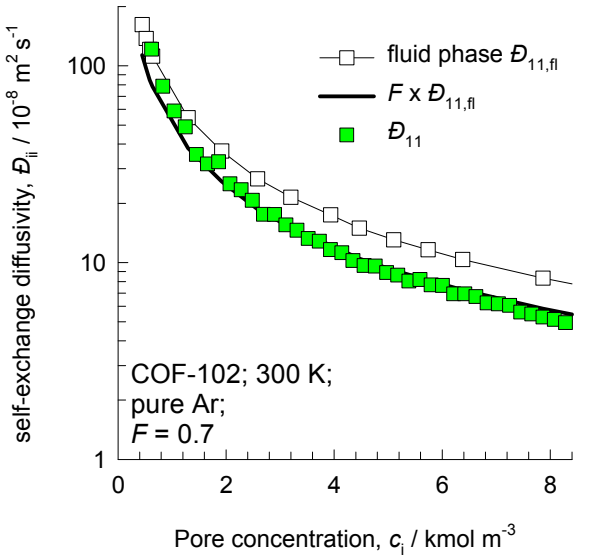


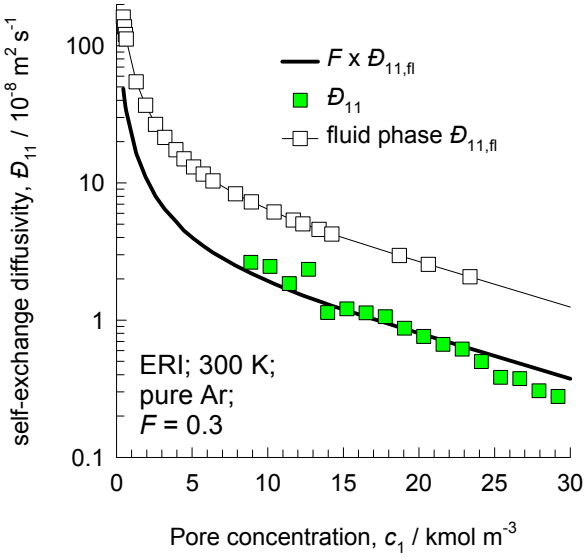


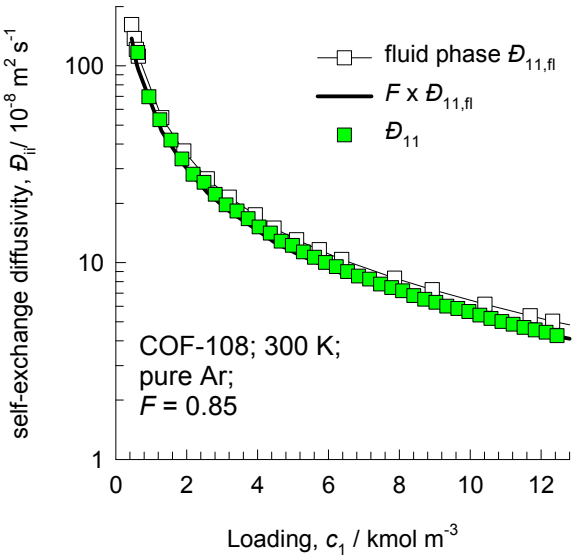

Figure A26

# Guest Molecule: Ne

Figure A27

# Self-, and Maxwell-Stefan diffusivities

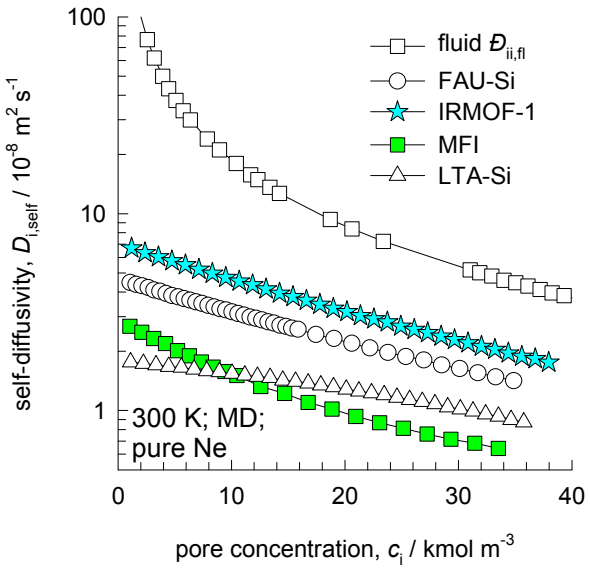


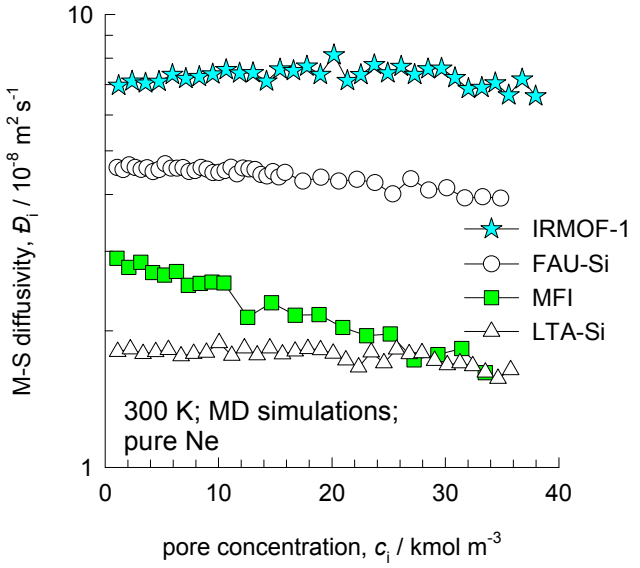

Figure A28

# Self-exchange coefficients and Degrees of correlations

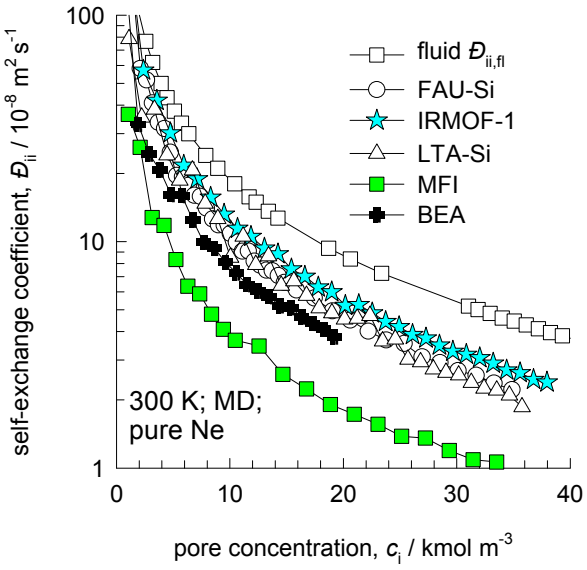


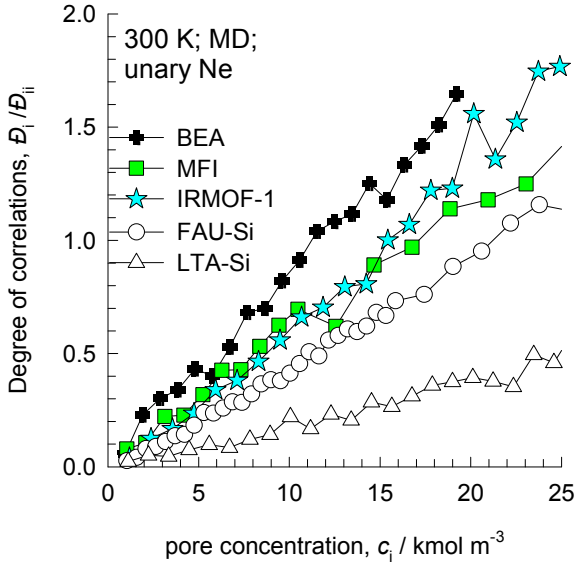


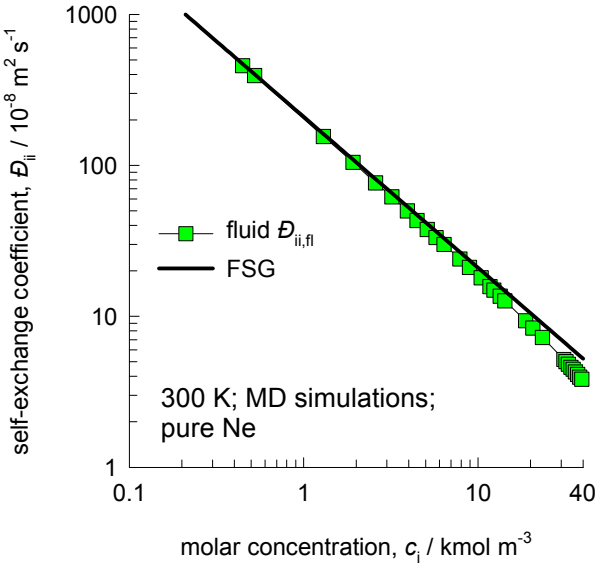

Figure A29

# Exchange coefficients as fraction of fluid phase $Đ_{ii,fl}$

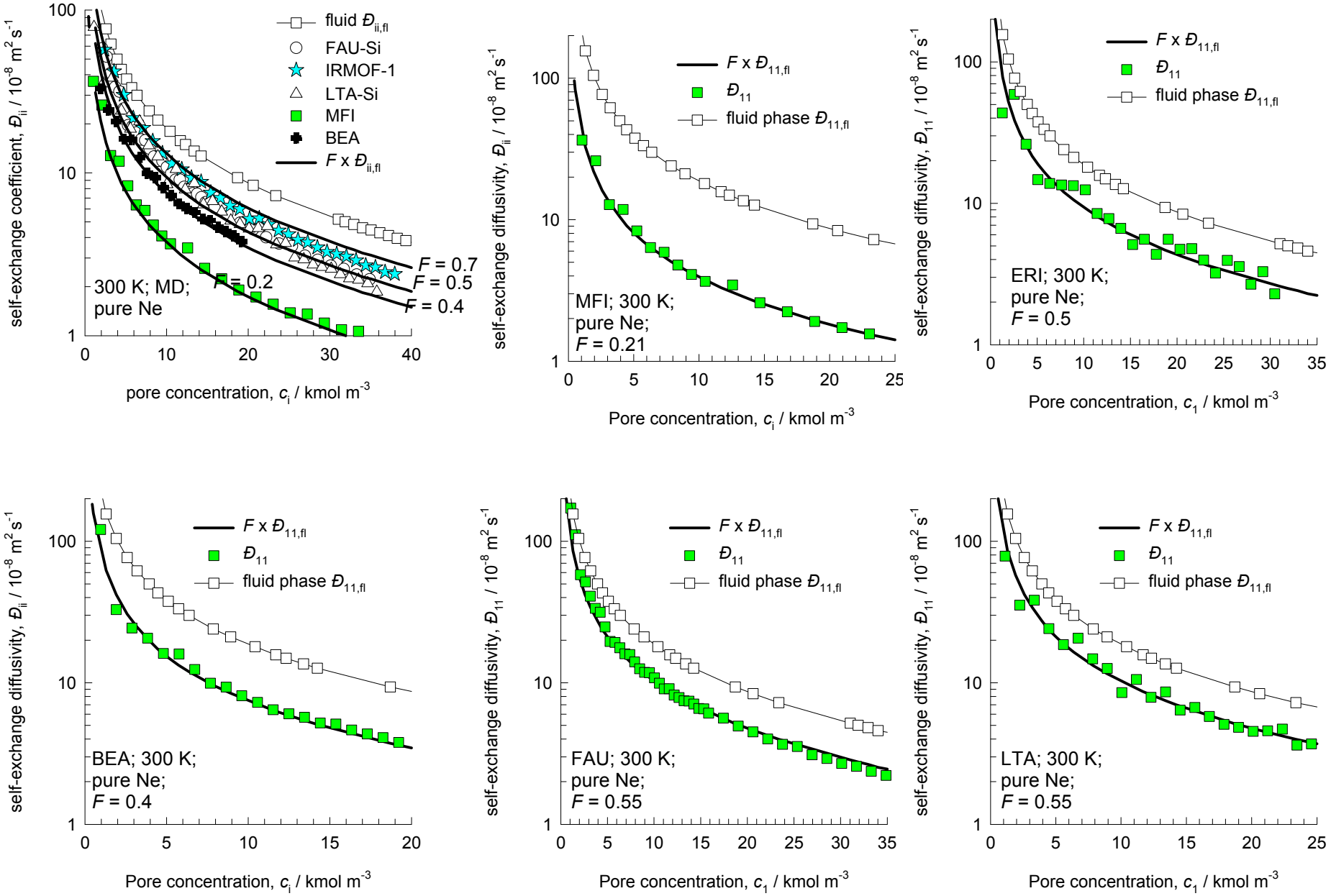

Figure A30

# Exchange coefficients as fraction of fluid phase $Đ_{ii,fl}$

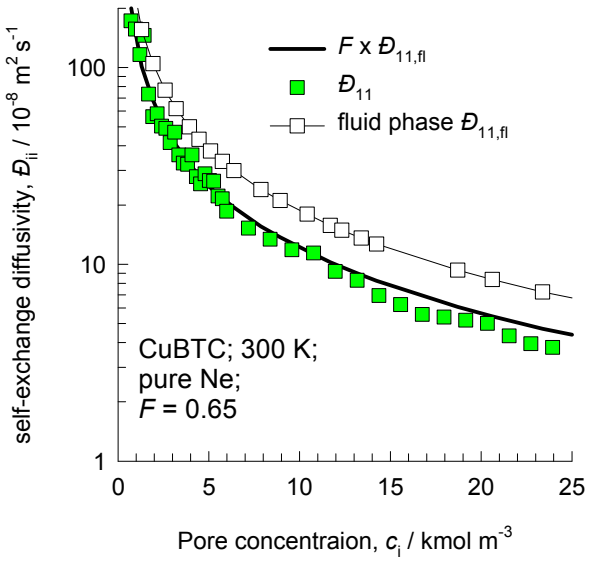


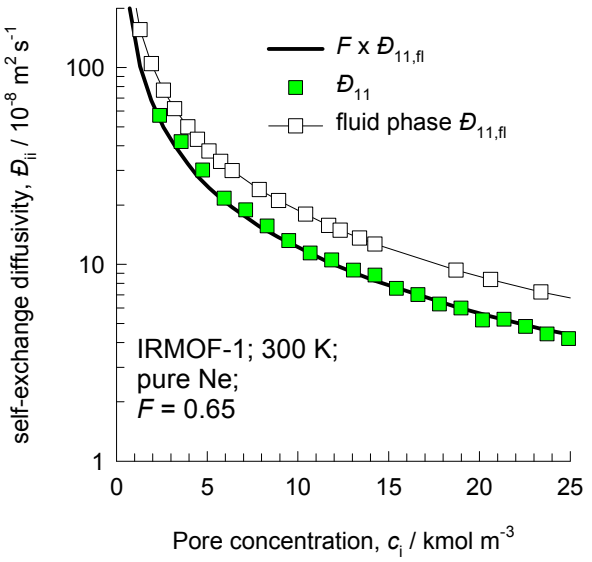


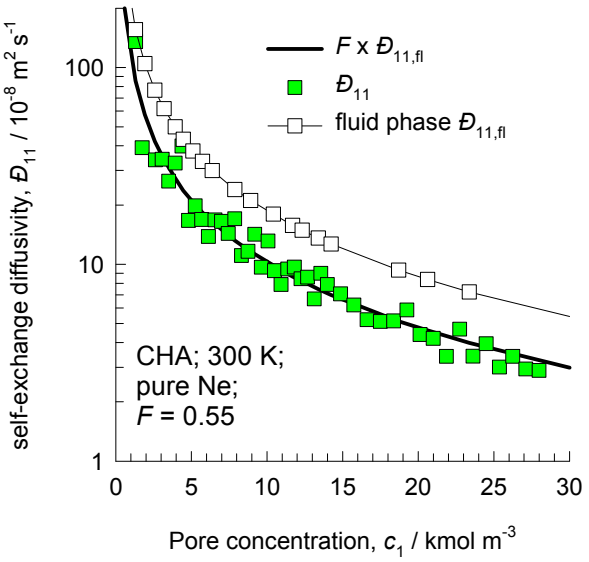


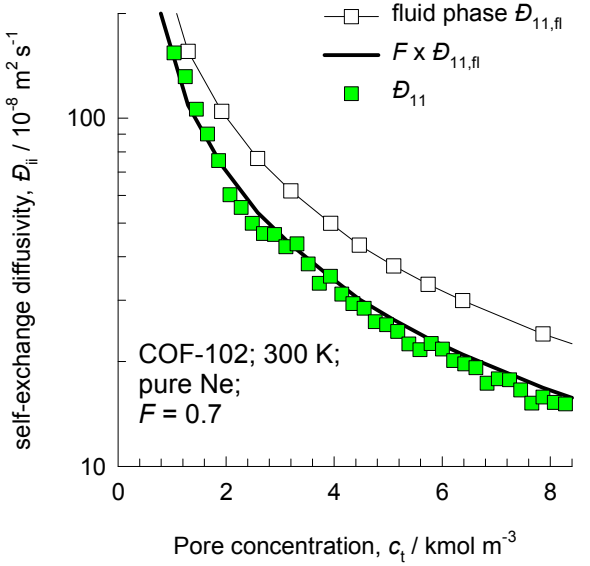


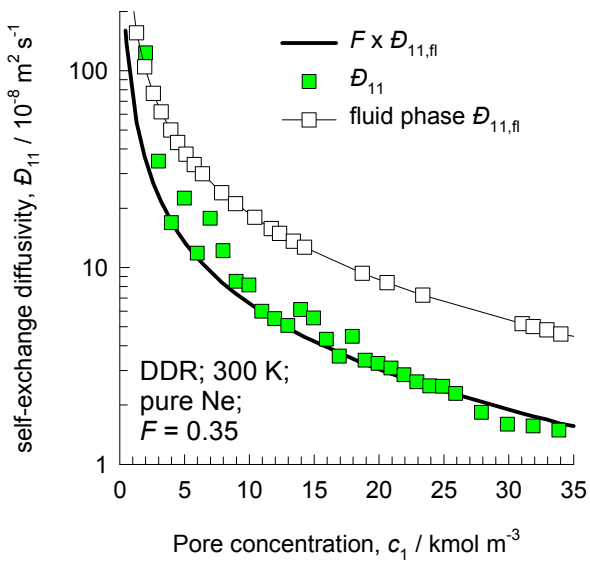


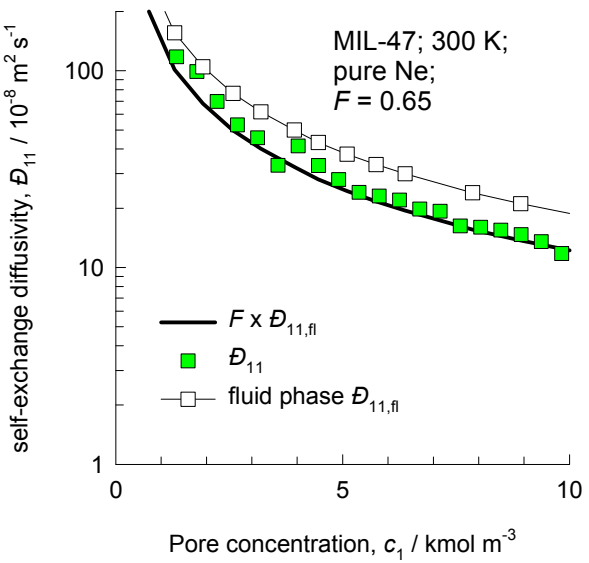

Figure A31

# Guest Molecule: Kr

Figure A32

# Self-, and Maxwell-Stefan diffusivities

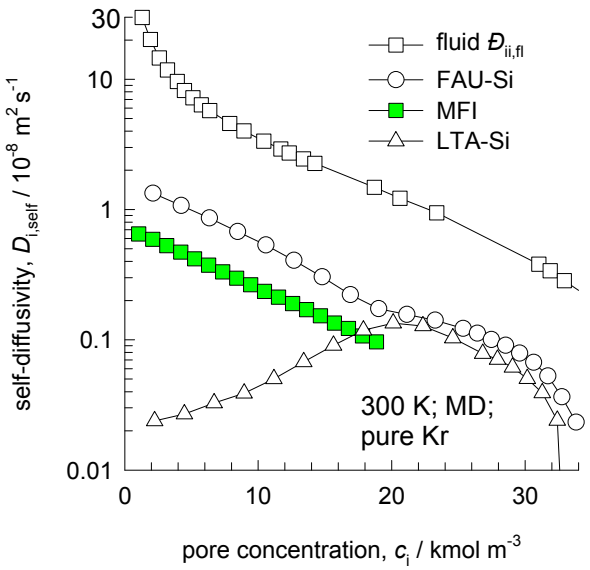


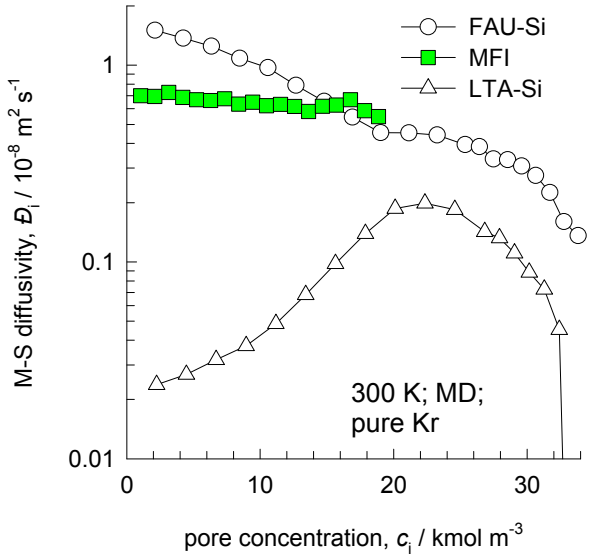

Figure A33

# Self-exchange coefficients and Degrees of correlations

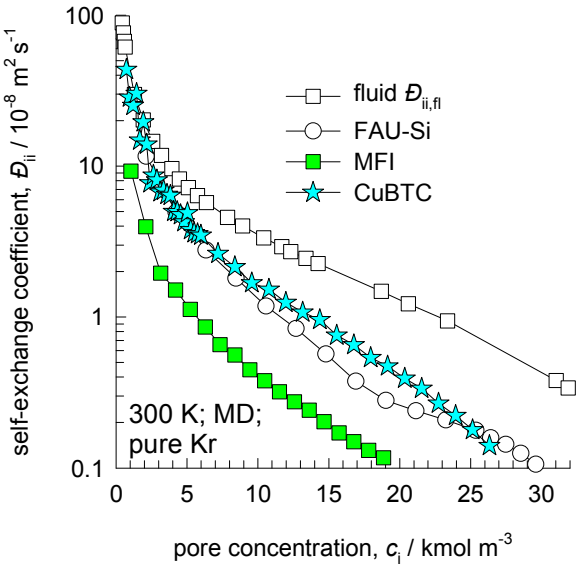


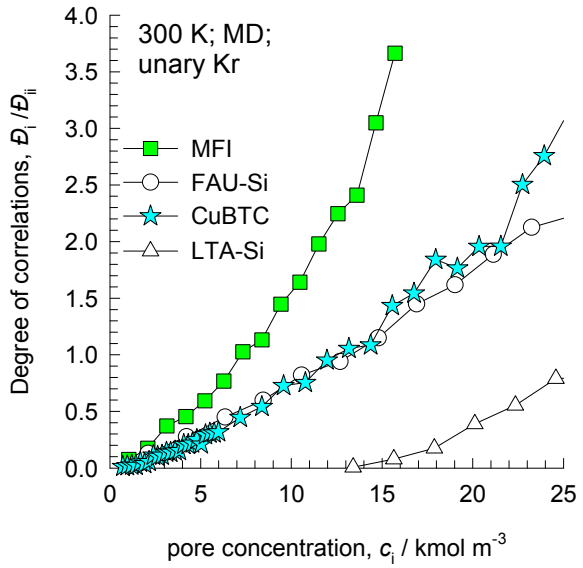


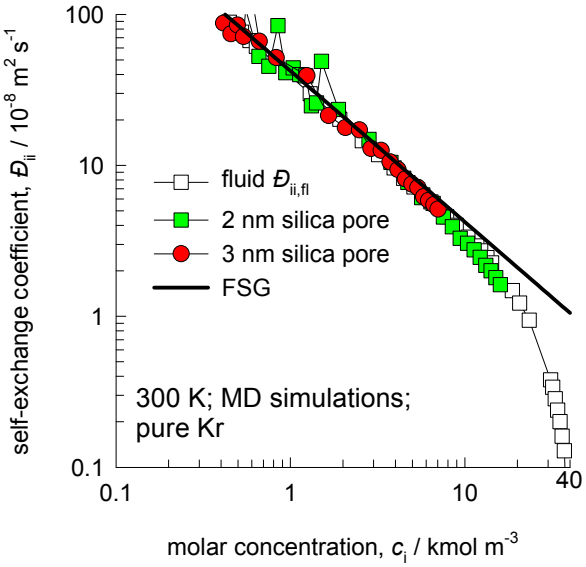


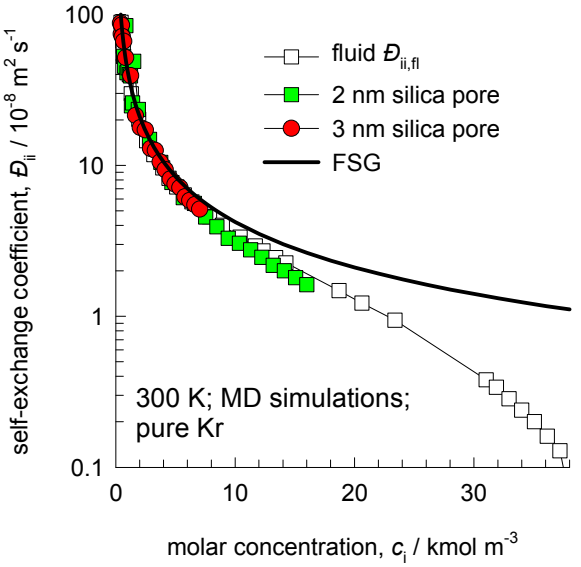

Figure A34

# Exchange coefficients as fraction of fluid phase $Đ_{ii,fl}$

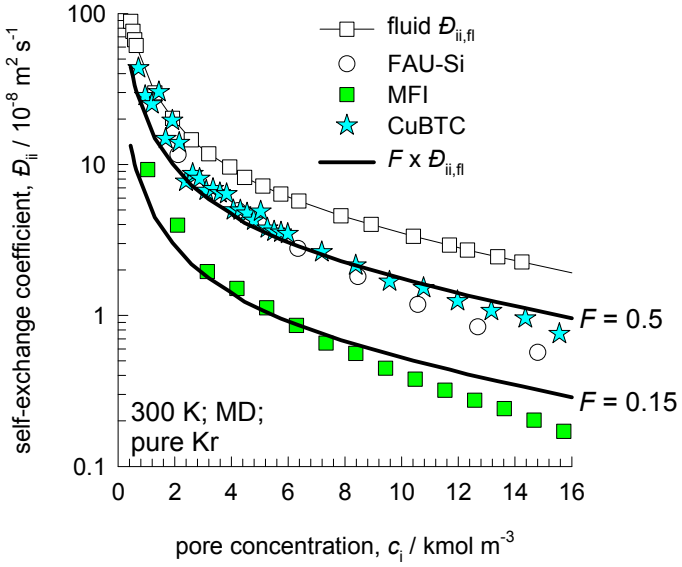


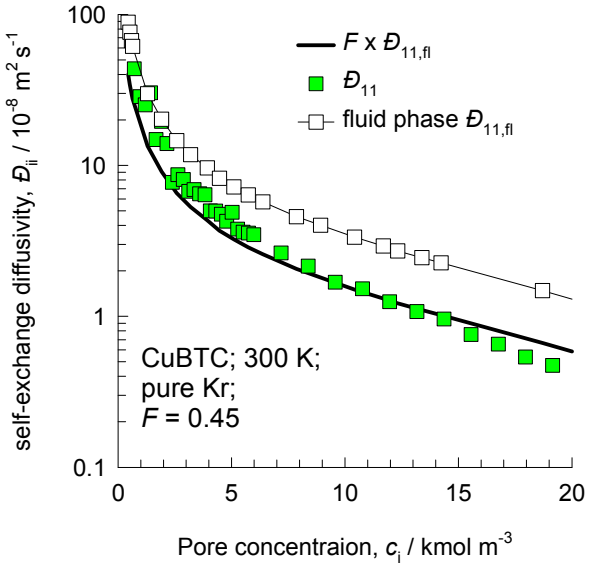


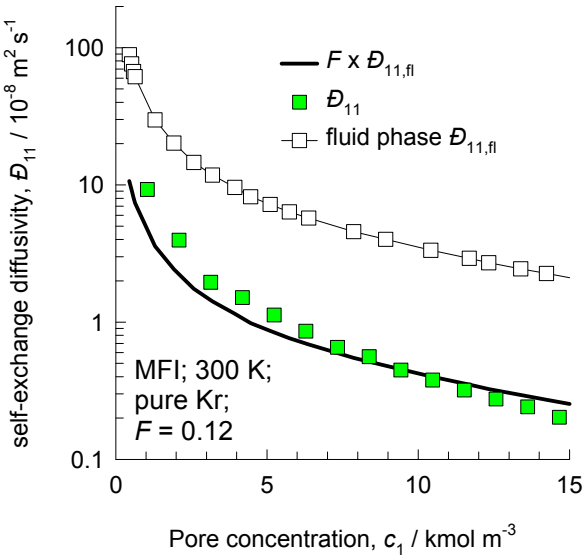


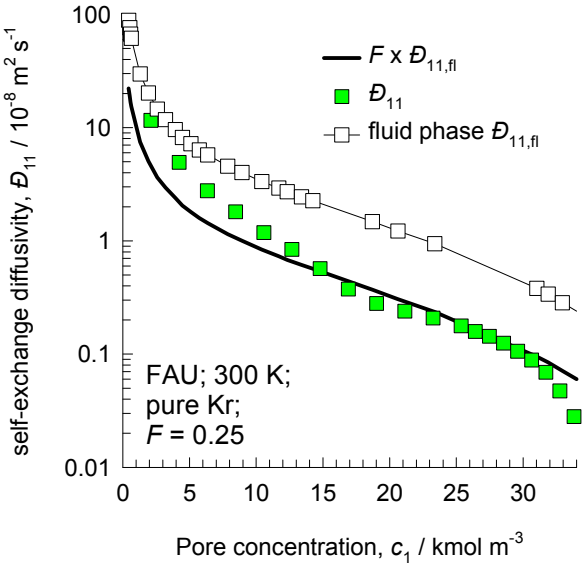

Figure A35

# Guest Molecule:
# $N_2$

Figure A36

# Self-, and Maxwell-Stefan diffusivities

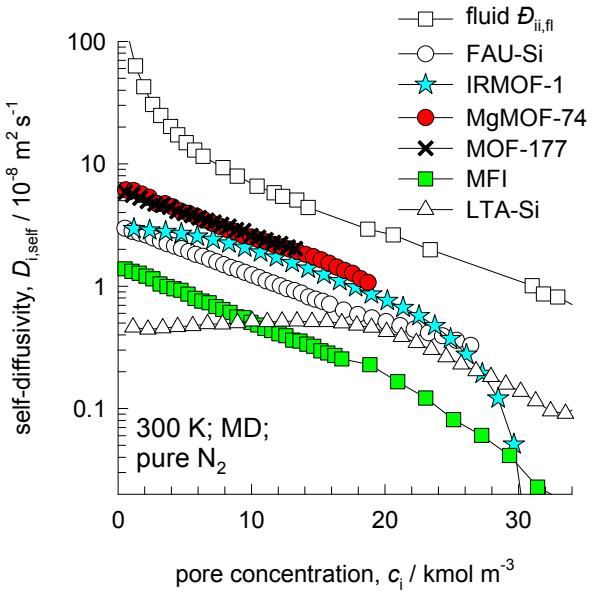


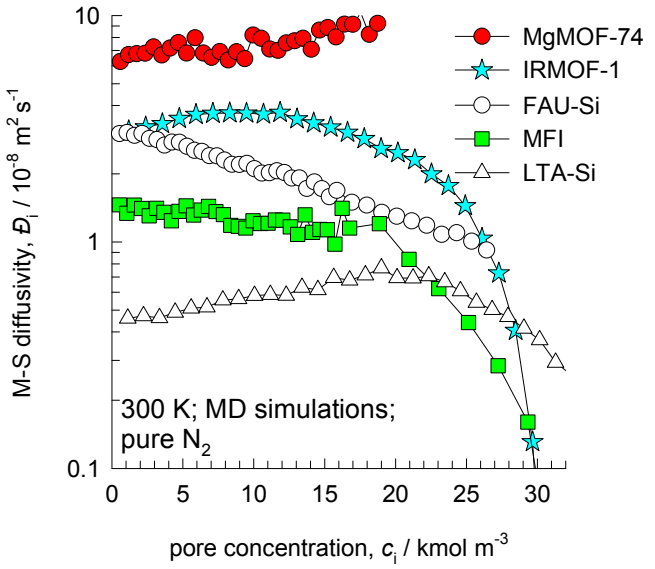

Figure A37

# Self-exchange coefficients and Degrees of correlations

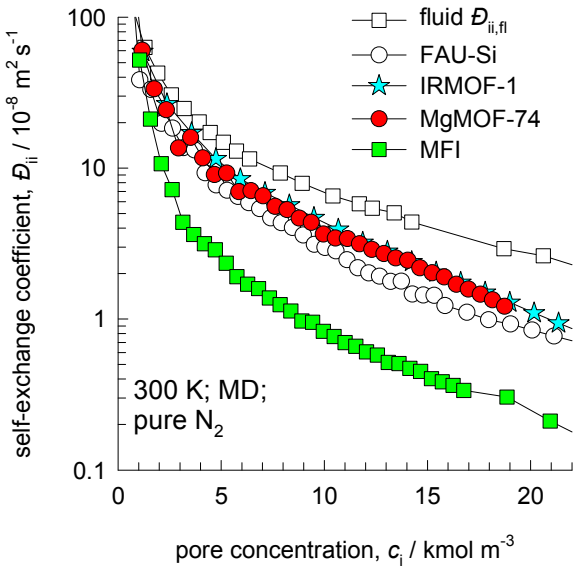


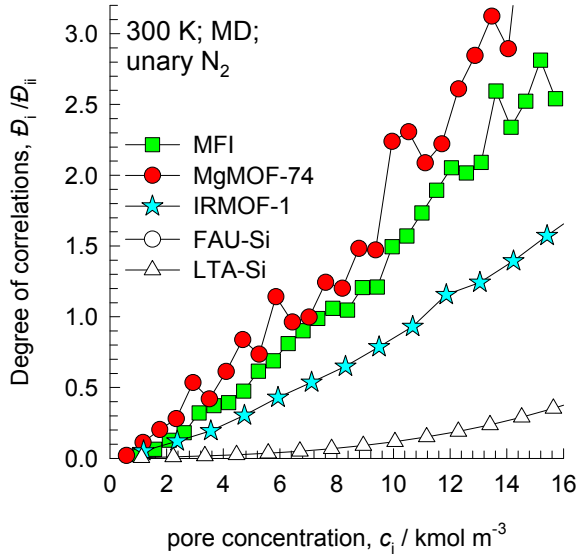


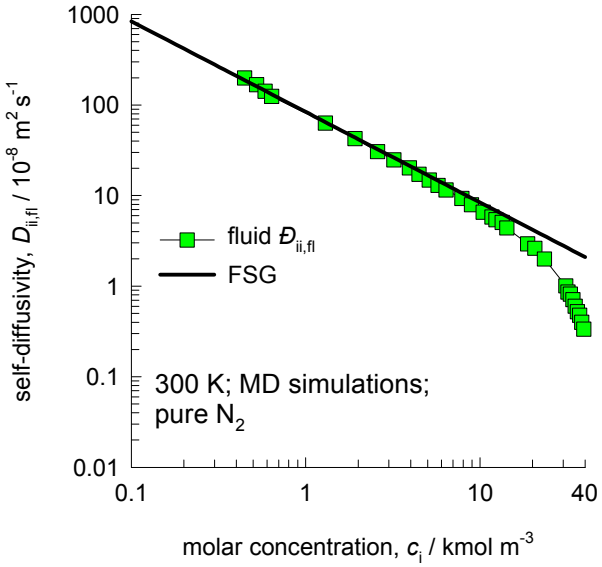

Figure A38

# Exchange coefficients as fraction of fluid phase $Đ_{ii,fl}$

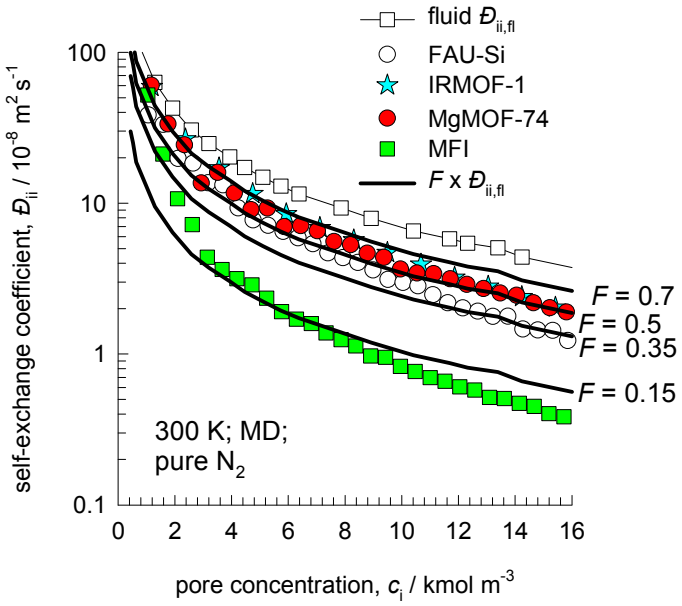


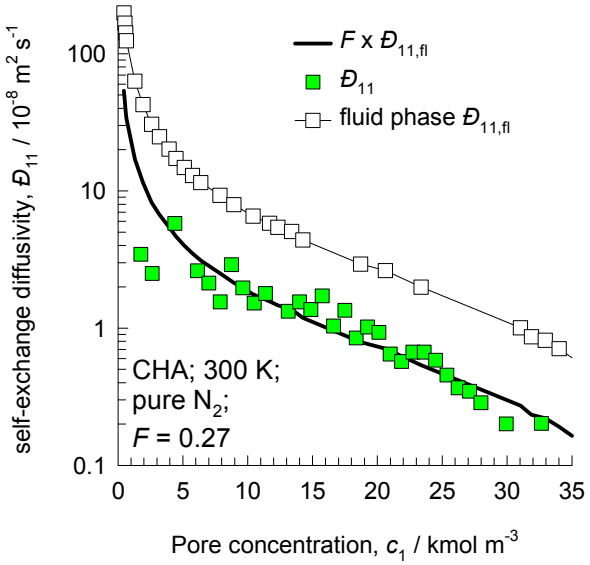


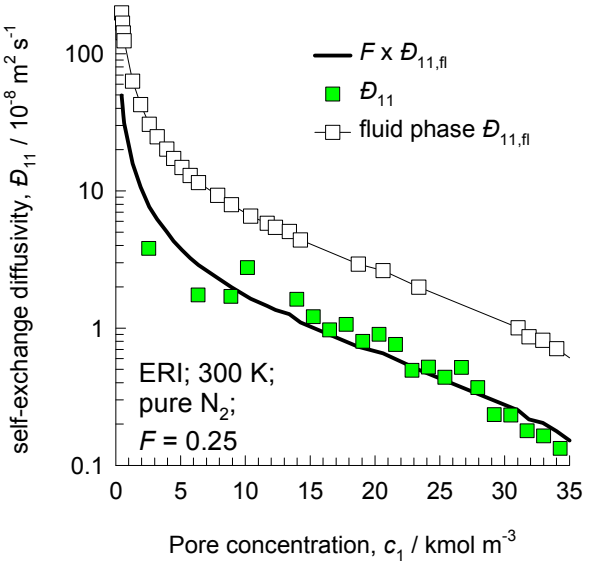

Figure A39

# Guest Molecule:
# $C_2H_6$

Figure A40

# Self-, and Maxwell-Stefan diffusivities

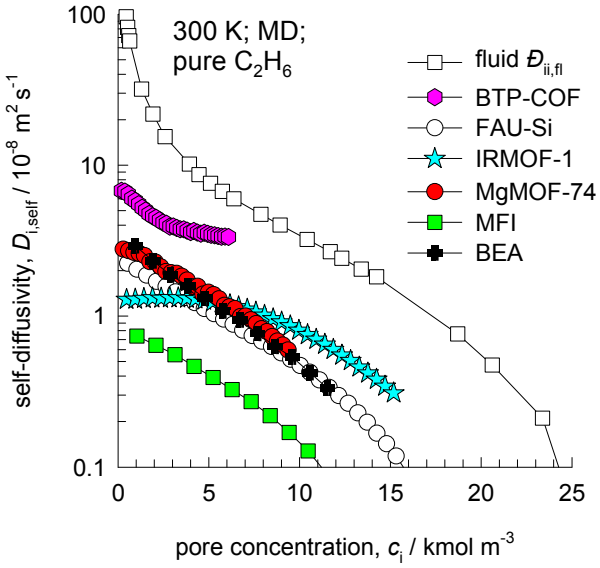


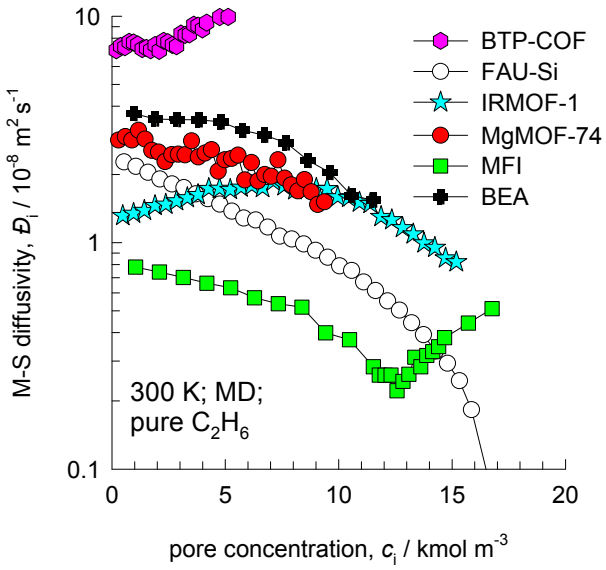

Figure A41

# Self-exchange coefficients and Degrees of correlations

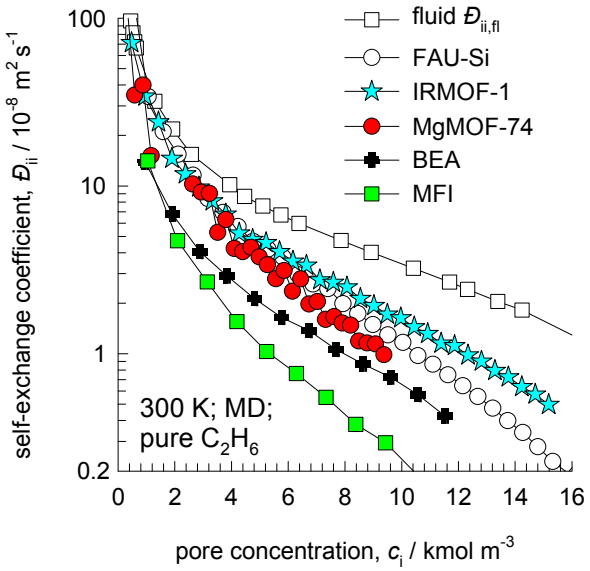


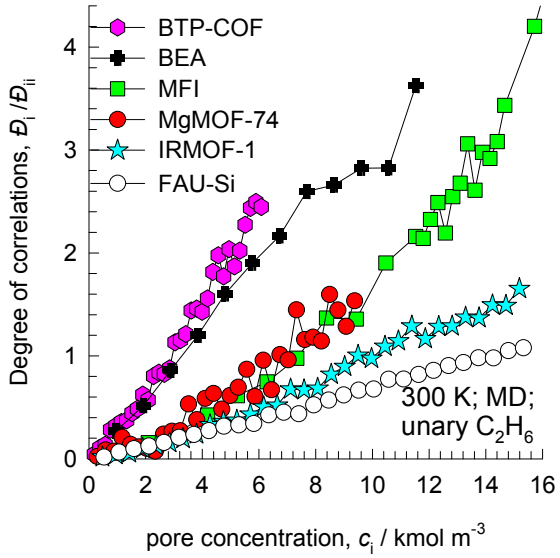


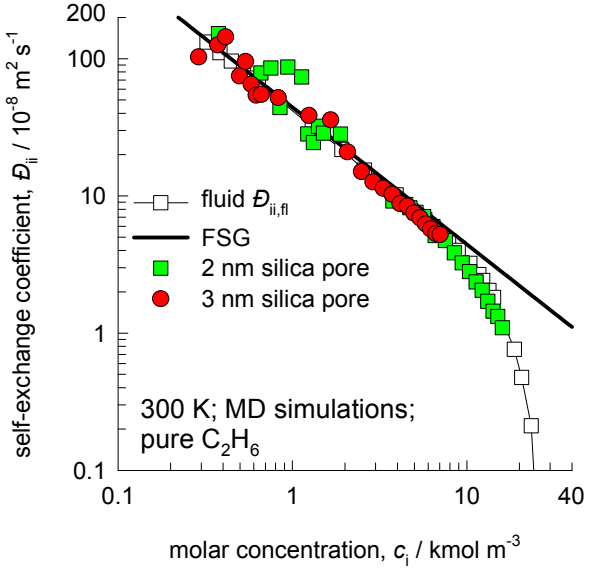


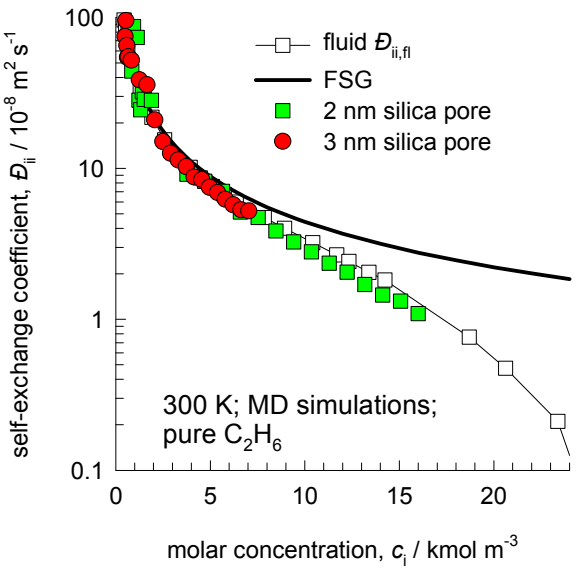

Figure A42

# Exchange coefficients as fraction of fluid phase $Đ_{ii,fl}$

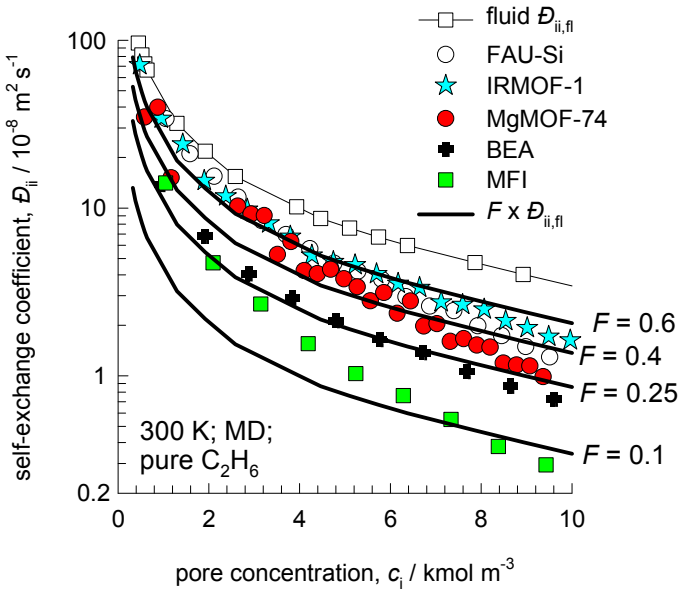


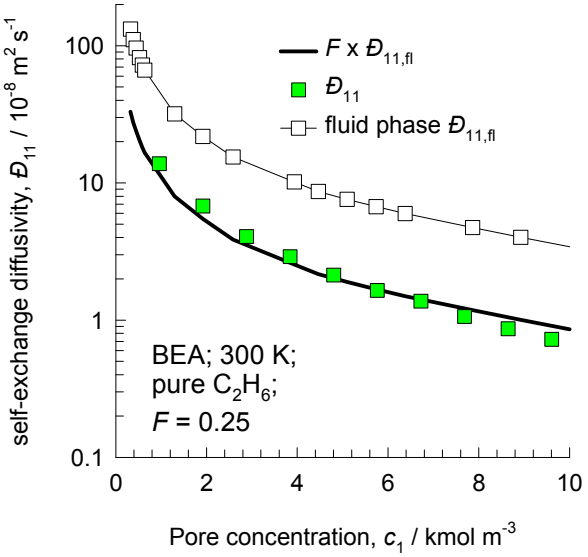

Figure A43

# Guest Molecule:
# $C_3H_8$

Figure A44

# Self-, and Maxwell-Stefan diffusivities

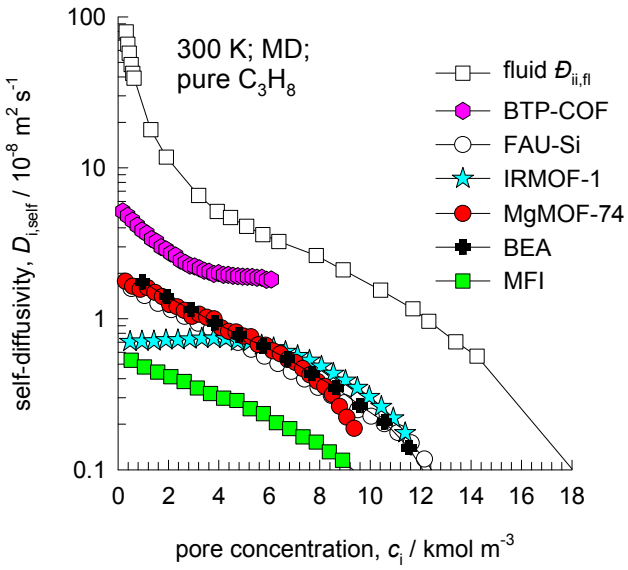


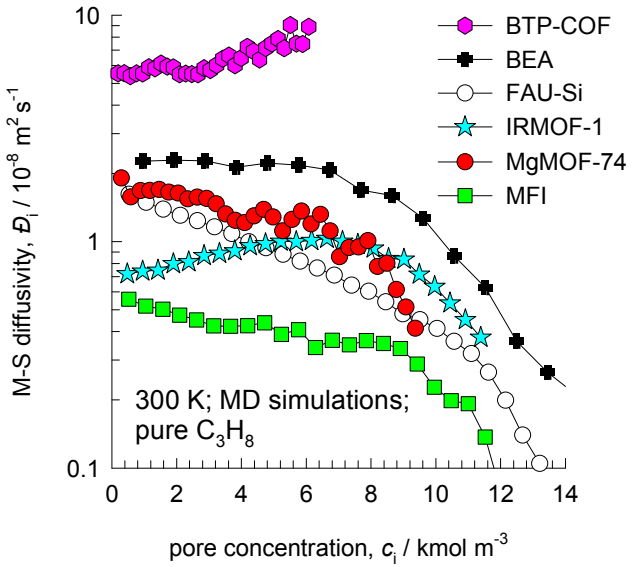

Figure A45

# Self-exchange coefficients and Degrees of correlations

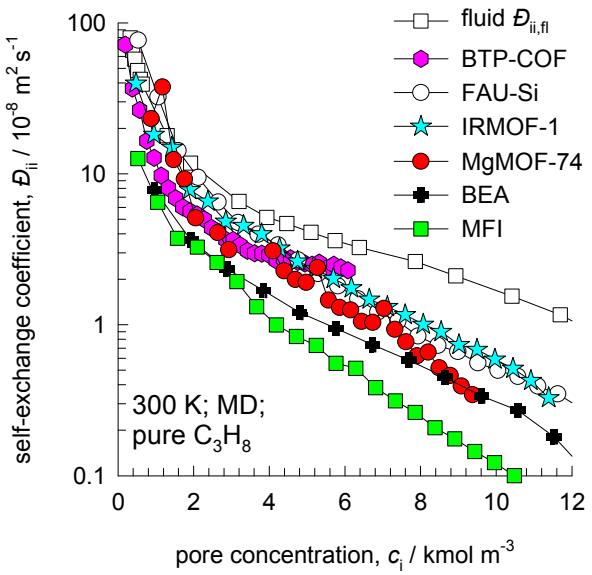


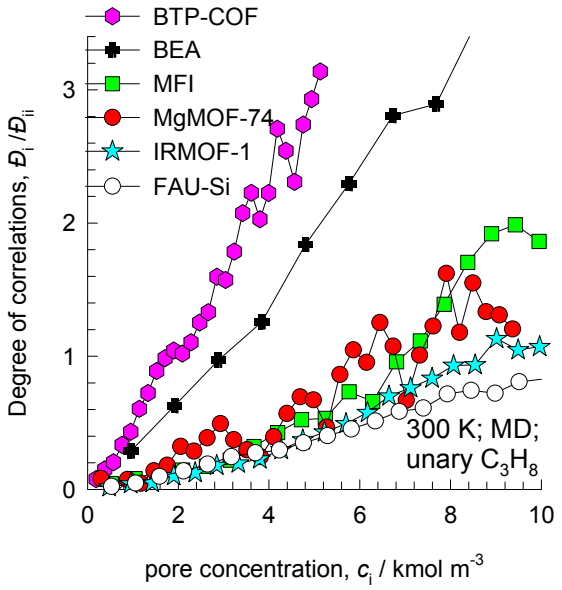


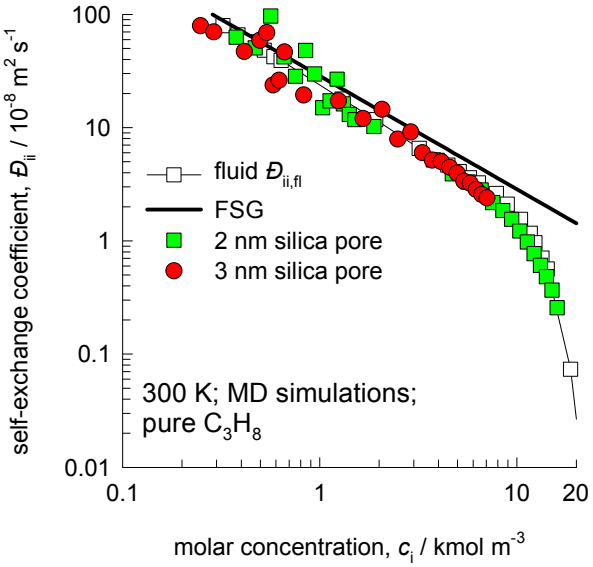


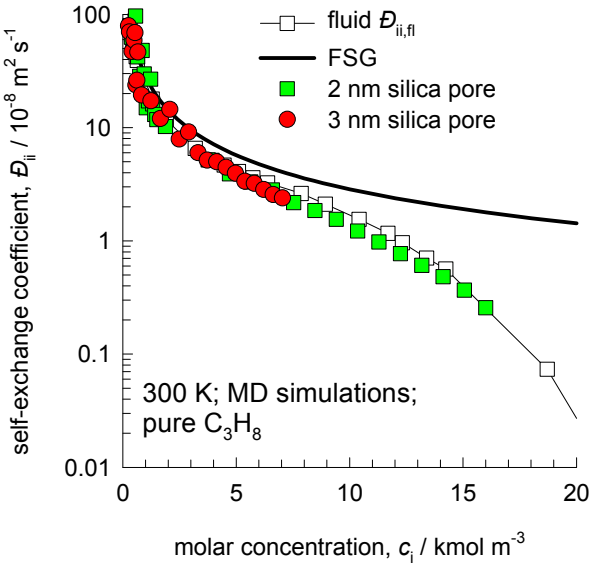

Figure A46

# Exchange coefficients as fraction of fluid phase $Đ_{ii,fl}$

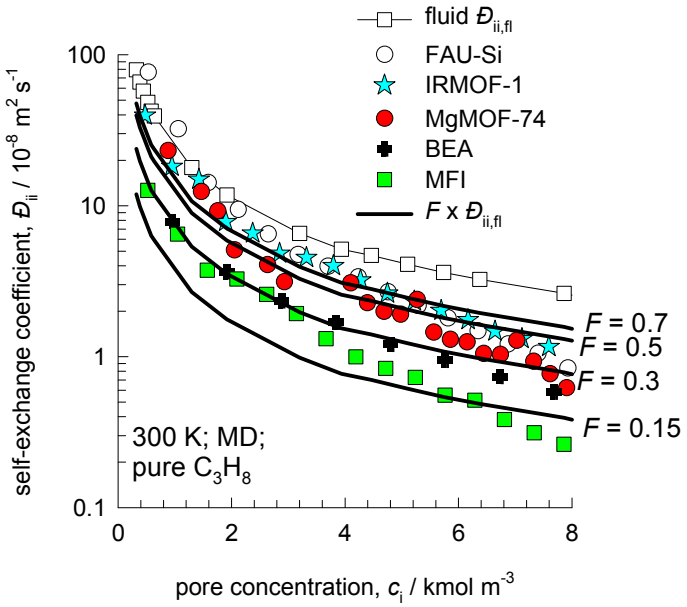


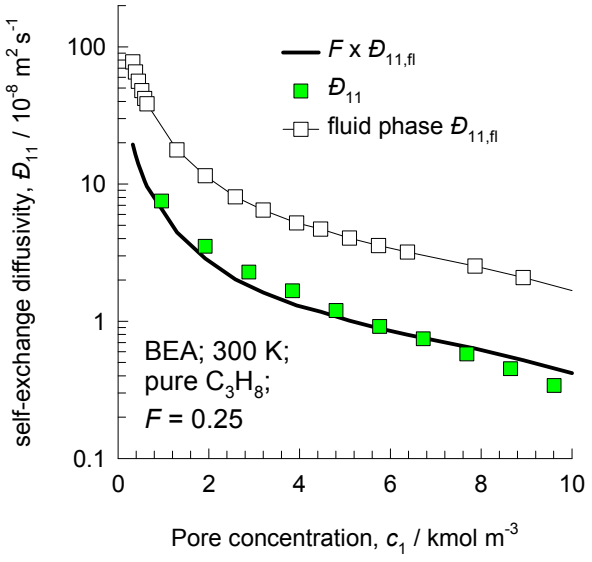

# Guest Molecule: $nC_4H_{10}$

Figure A48

# Self-, and Maxwell-Stefan diffusivities

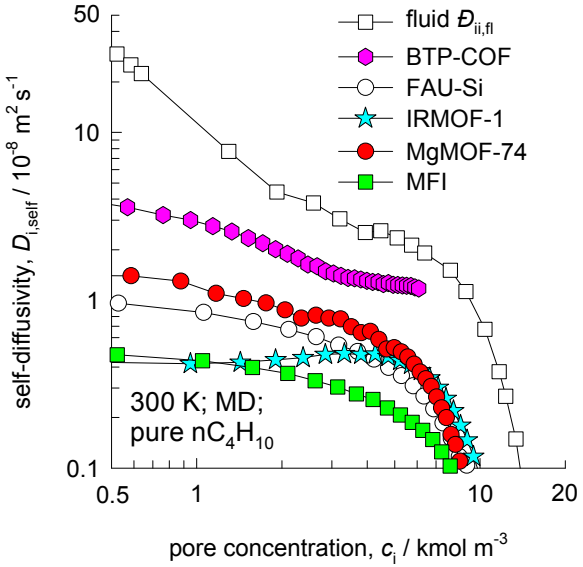


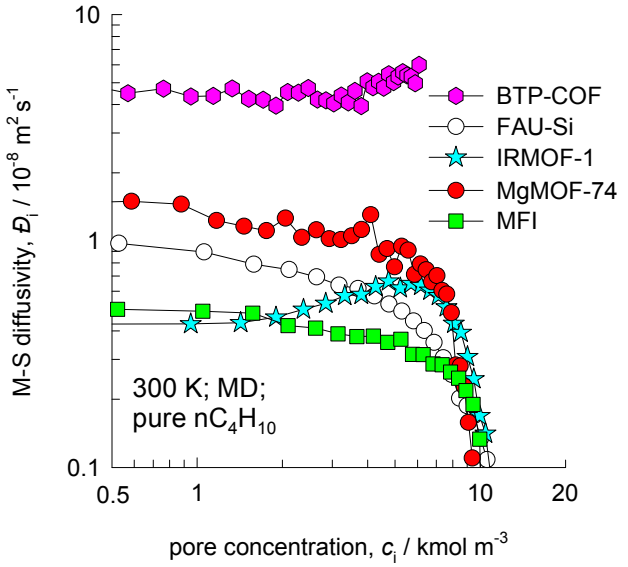

Figure A49

# Self-exchange coefficients and Degrees of correlations

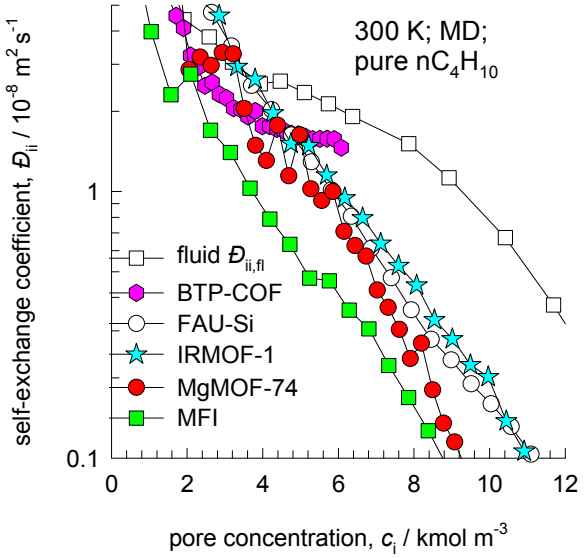


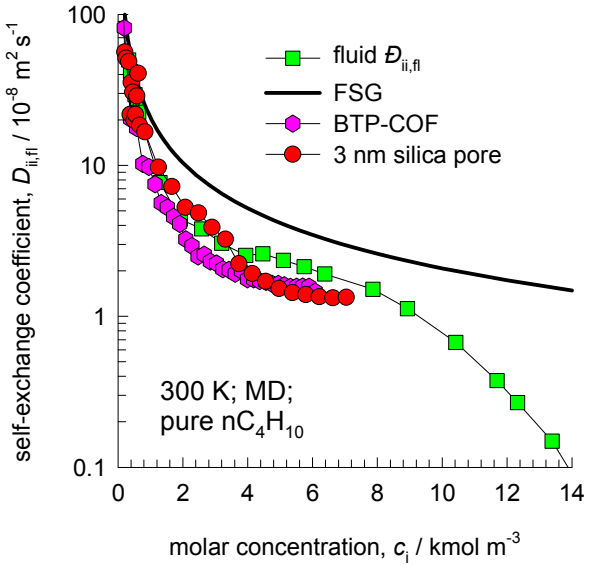

Figure A50

# Snapshots showing the location of nC4 molecules within MFI

Linear, chain, alkanes can locate anywhere along the channels of MFI

## nC4: 4 molecules/uc

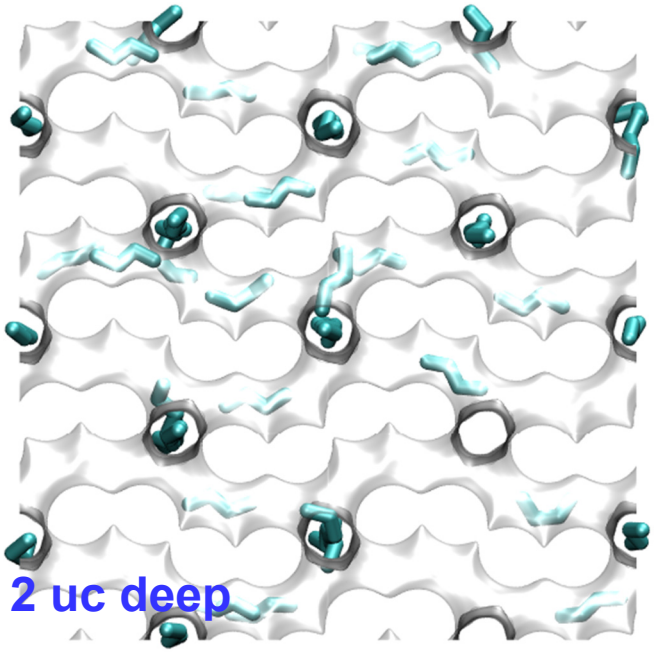

2 uc deep

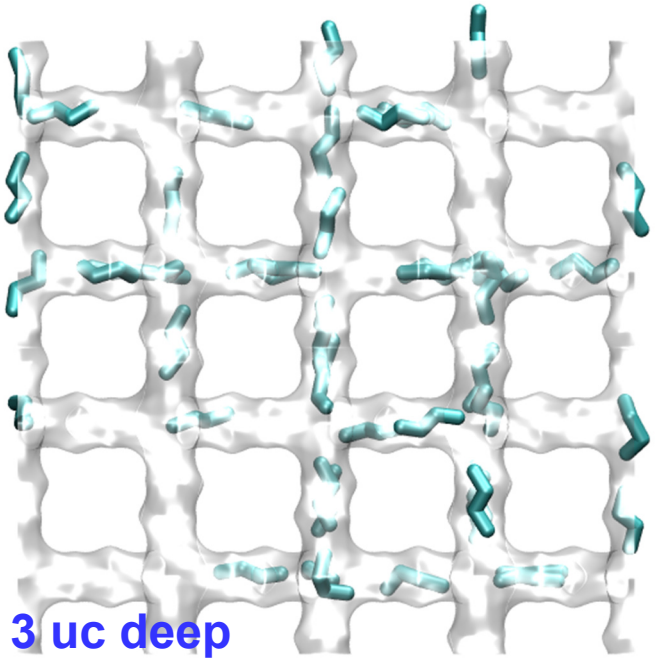

3 uc deep

Figure A51

# Snapshots showing the location of nC4 molecules within MFI

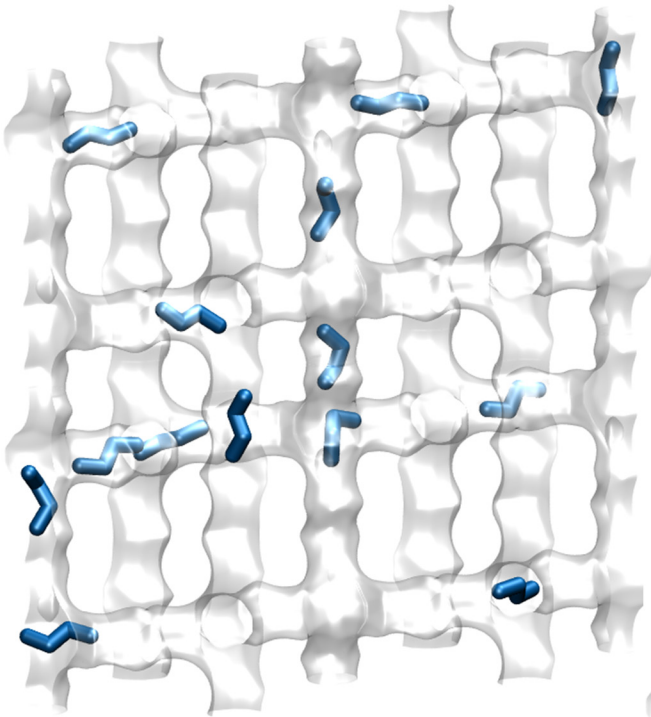

Linear, chain, alkanes can locate anywhere along the channels of MFI

**nC4: 4 molecules/uc**

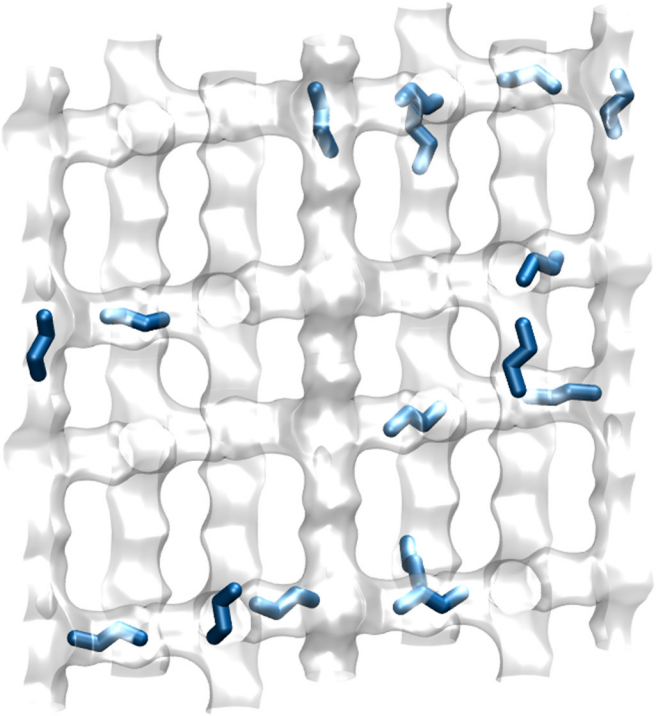

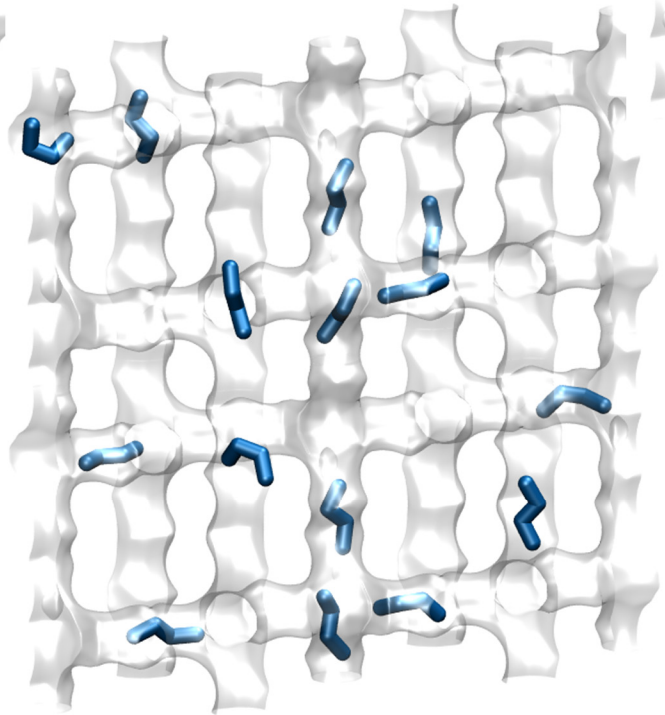

Figure A52

# Guest Molecule:
# $H_2O$

# **MFI** snapshot of water molecules

Figure A53

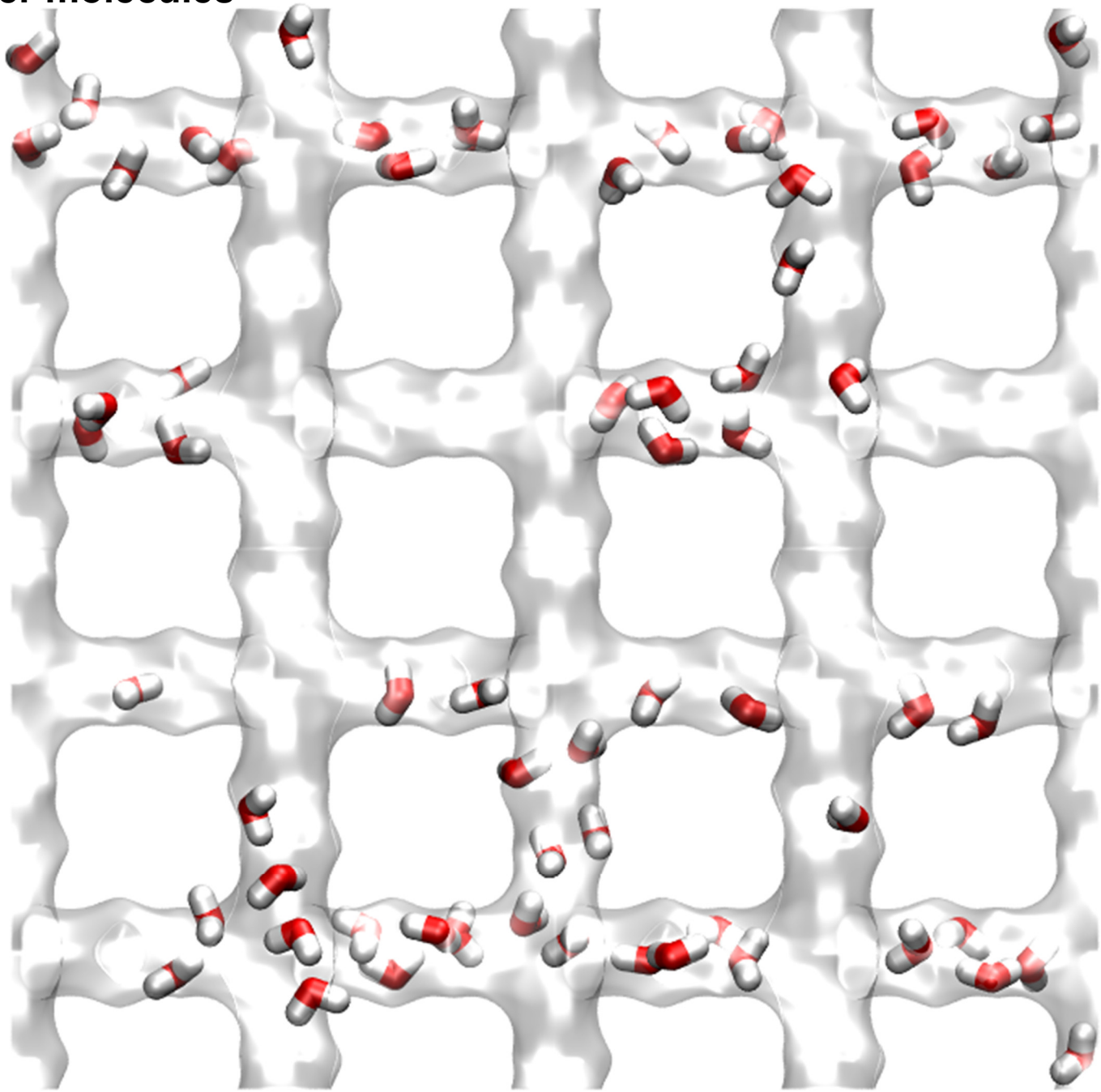

The snapshot shows some qualitative indication of clustering of water molecules caused by hydrogen bonding.

# **LTA** water snapshot showing clustering

Figure A54

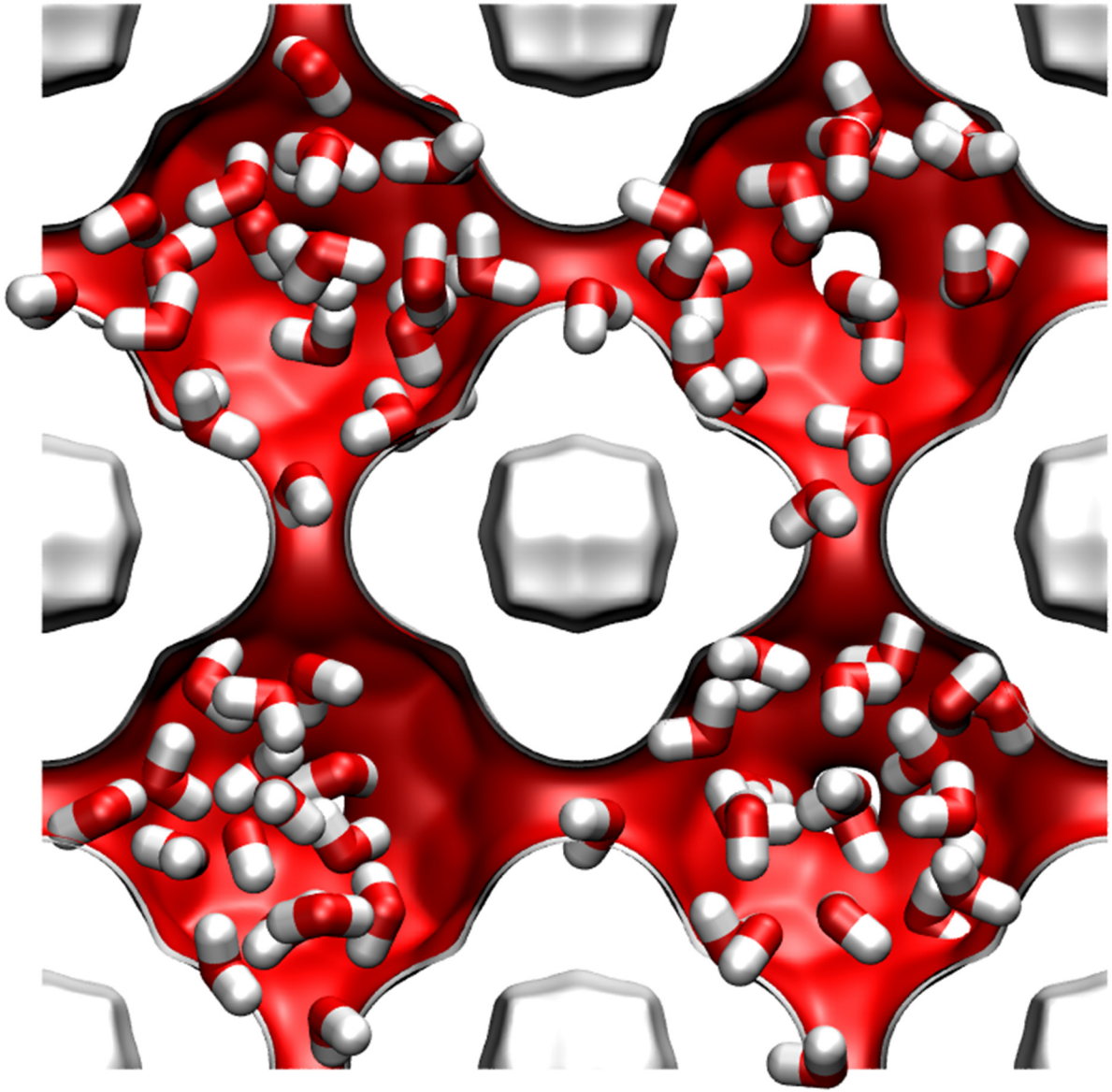

# DDR snapshot of water molecules

Figure A55

The snapshot shows some qualitative indication of clustering of water molecules caused by hydrogen bonding.

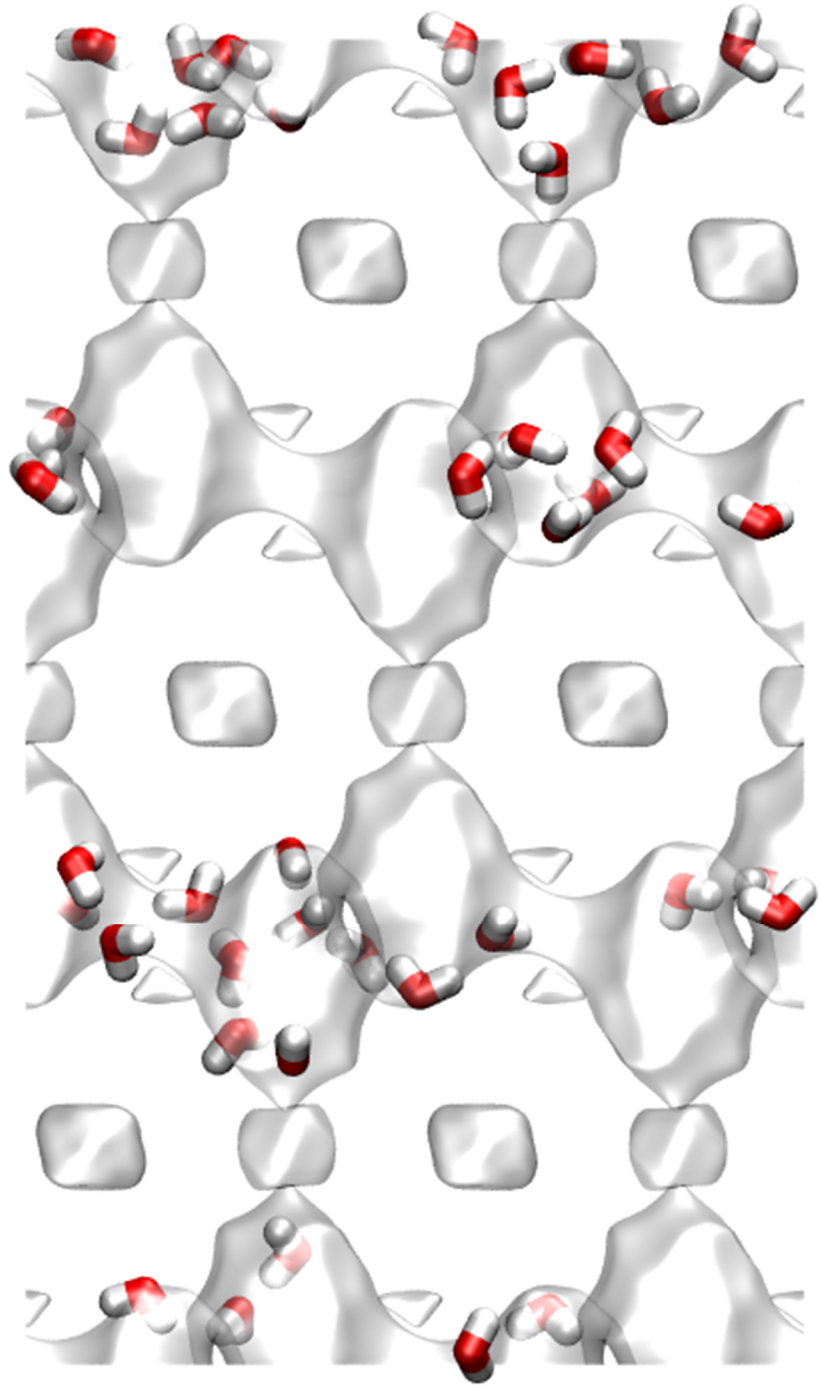

# Guest Molecule: $CH_3OH$

# **MFI** snapshot of methanol molecules

Figure A57

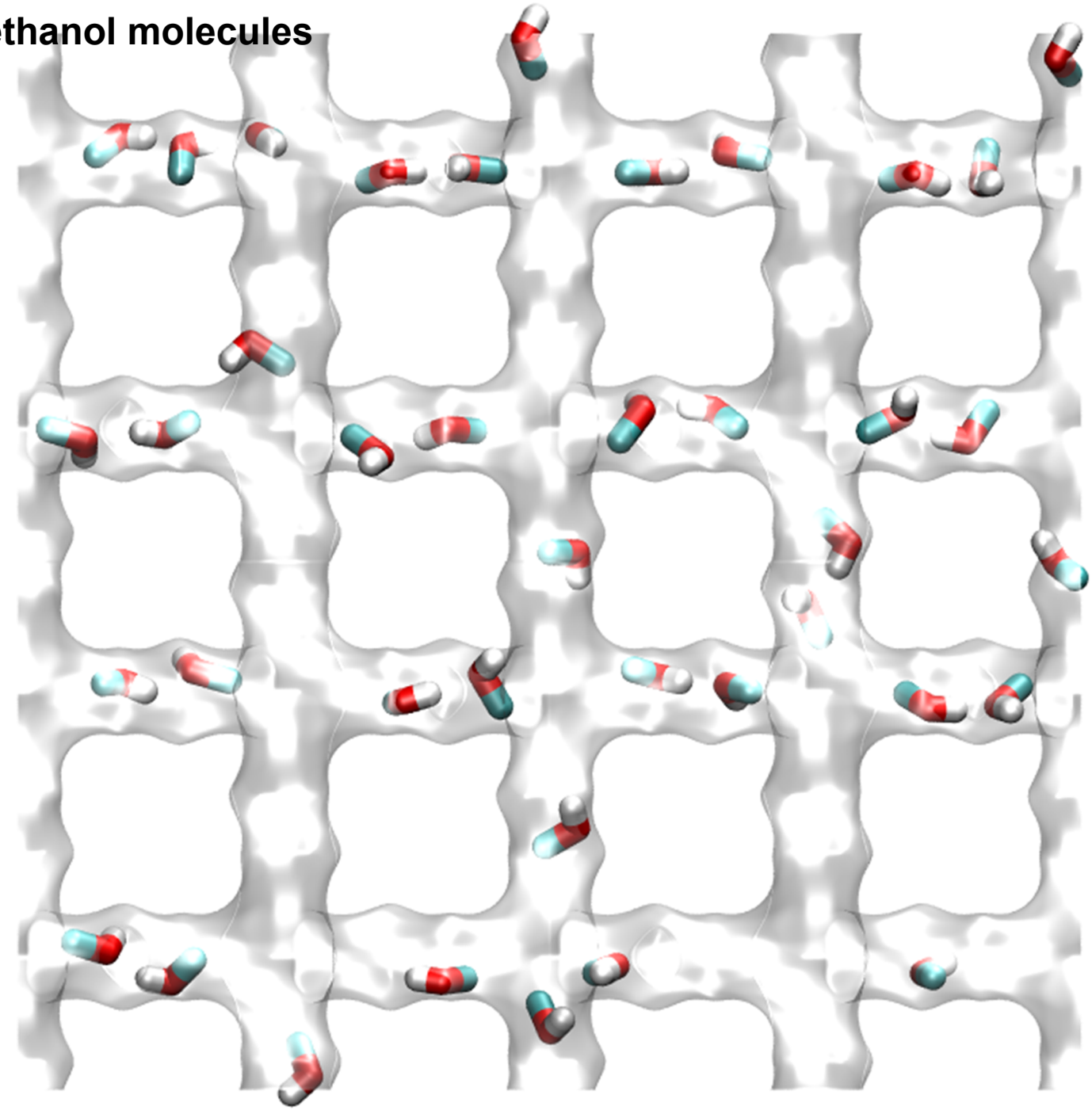

The snapshot shows some qualitative indication of clustering of methanol molecules caused by hydrogen bonding.

# **LTA** methanol snapshot showing clustering

Figure A58

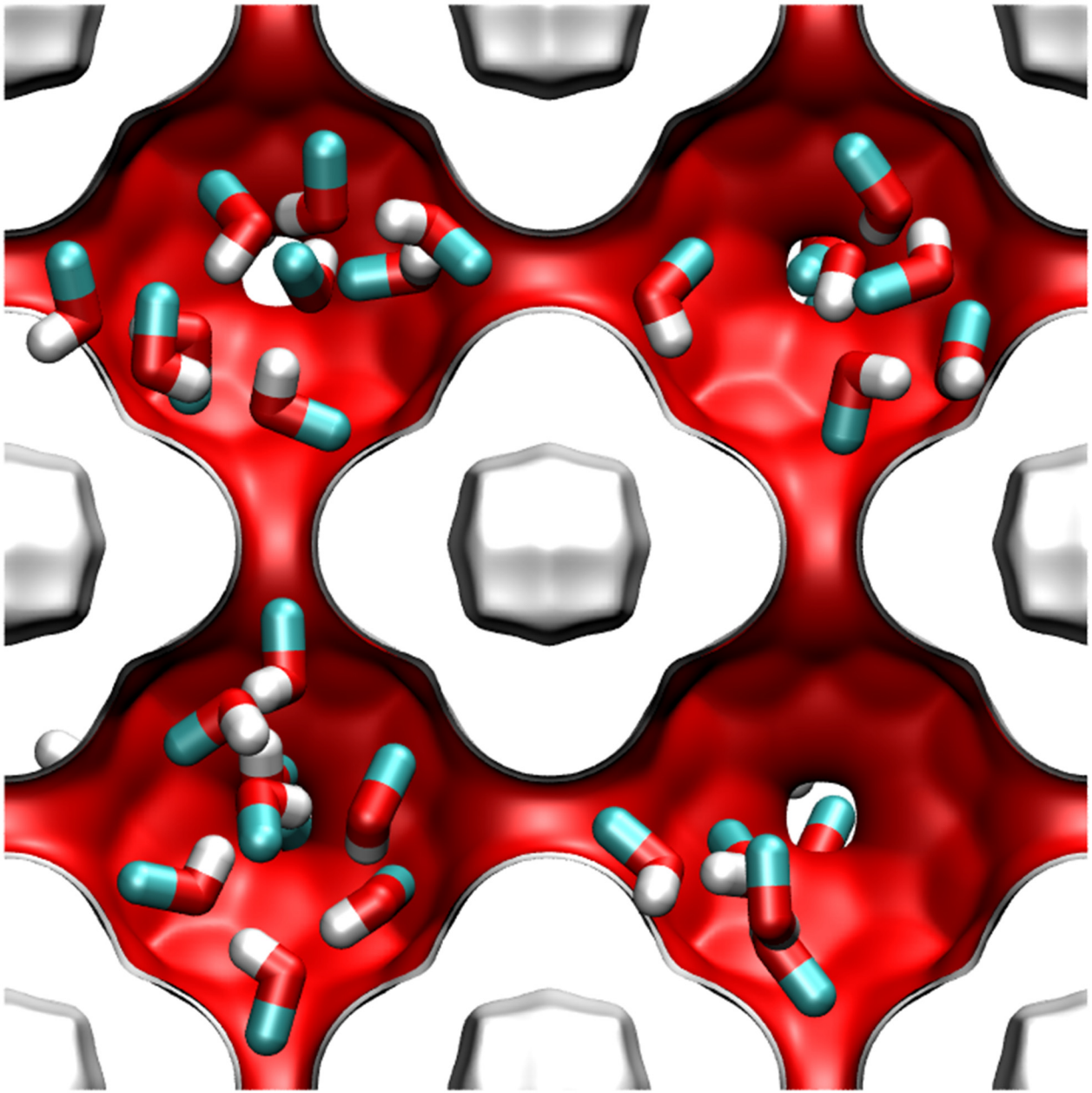

# **CHA** methanol snapshot showing clustering

Figure A59

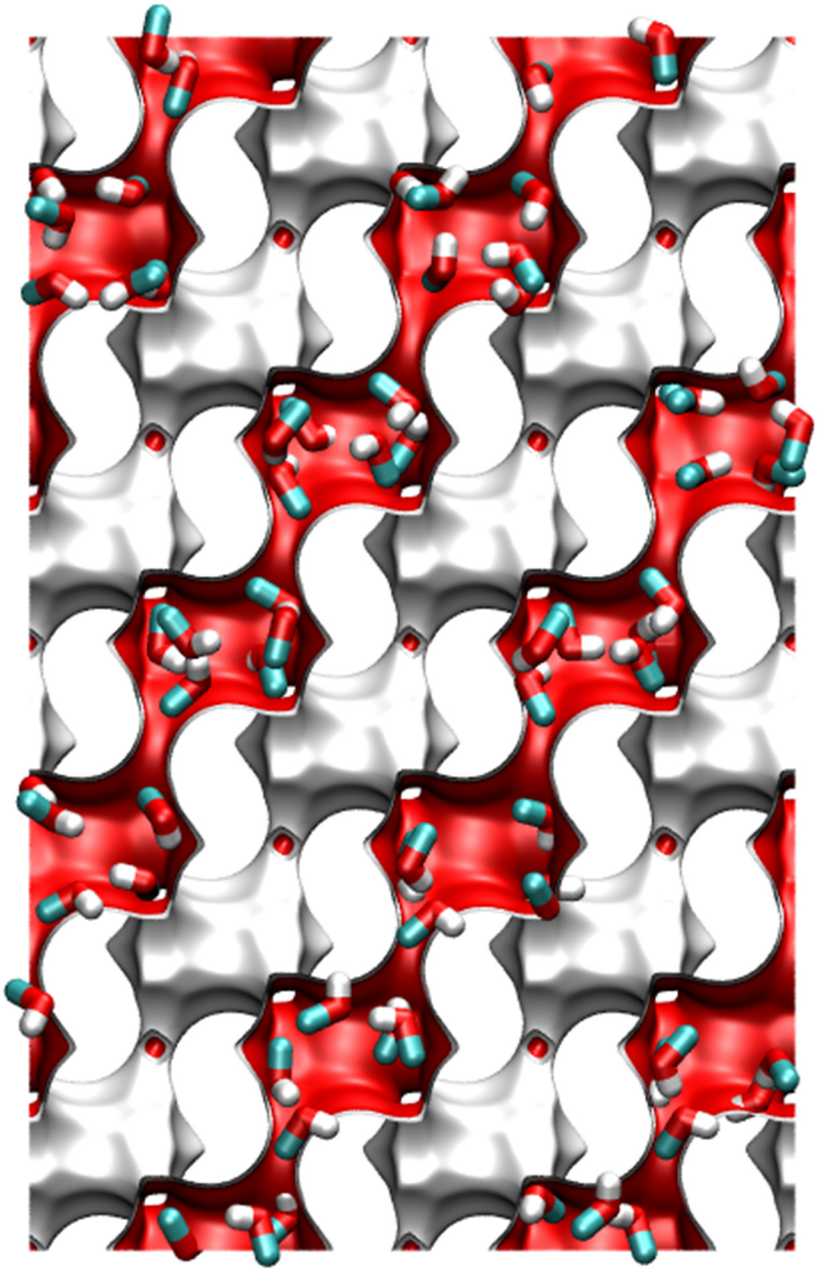

# Guest Molecule:
# $C_2H_5OH$

Figure A61

# **MFI** snapshot of ethanol molecules

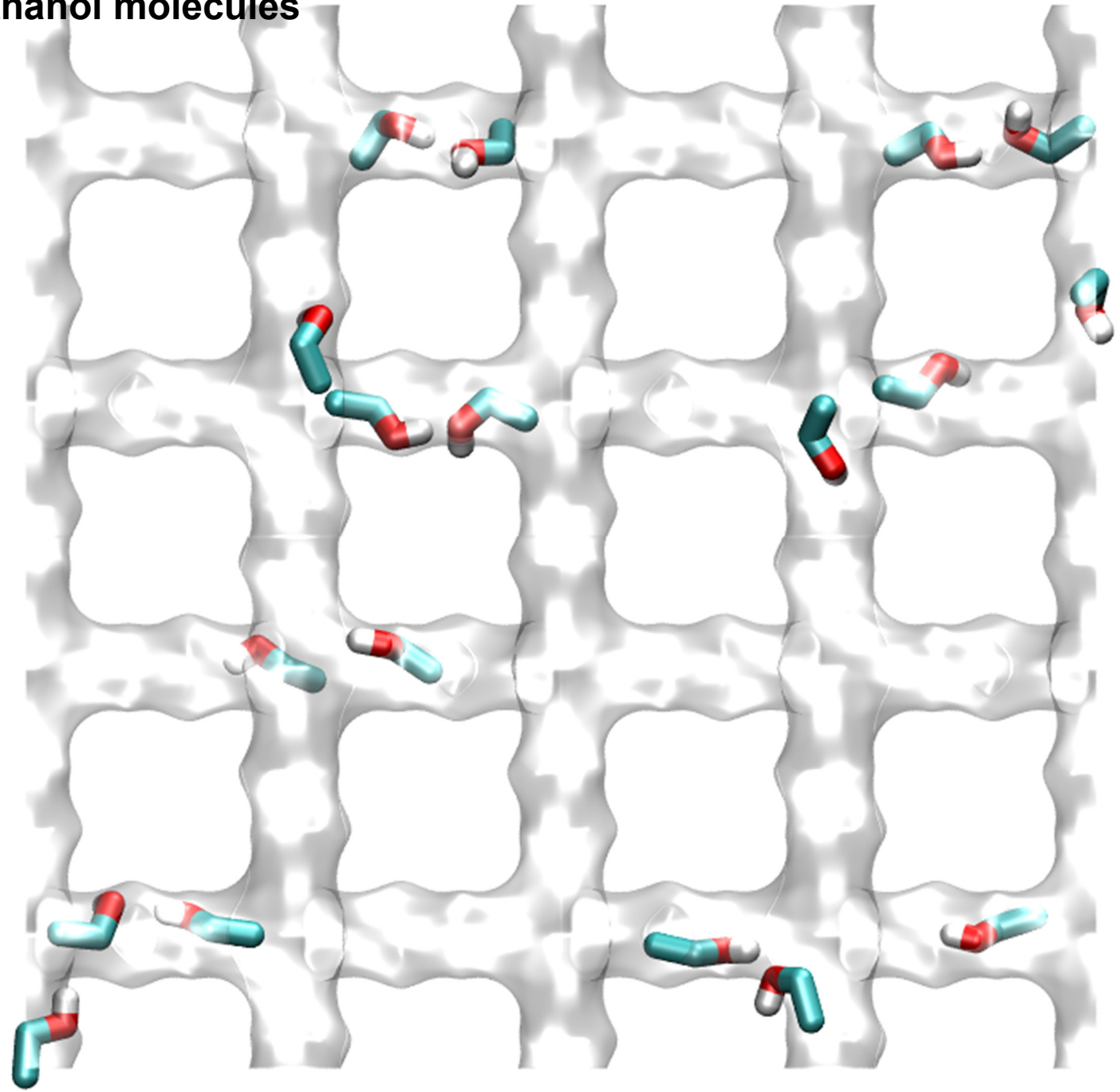

The snapshot shows some qualitative indication of clustering of ethanol molecules caused by hydrogen bonding.

# **LTA** ethanol snapshot showing clustering

Figure A62

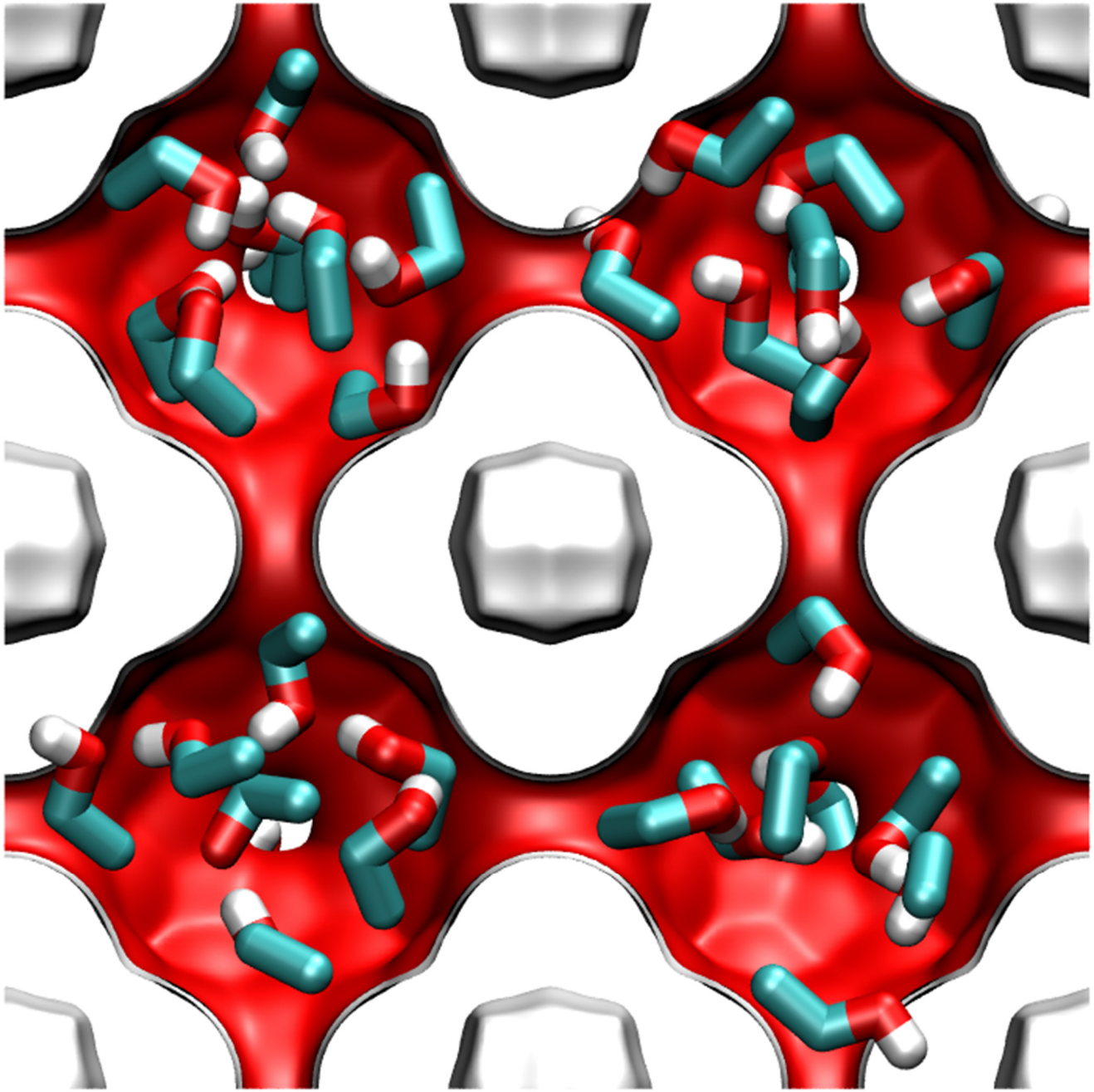

# **CHA** ethanol snapshot showing clustering

Figure A63

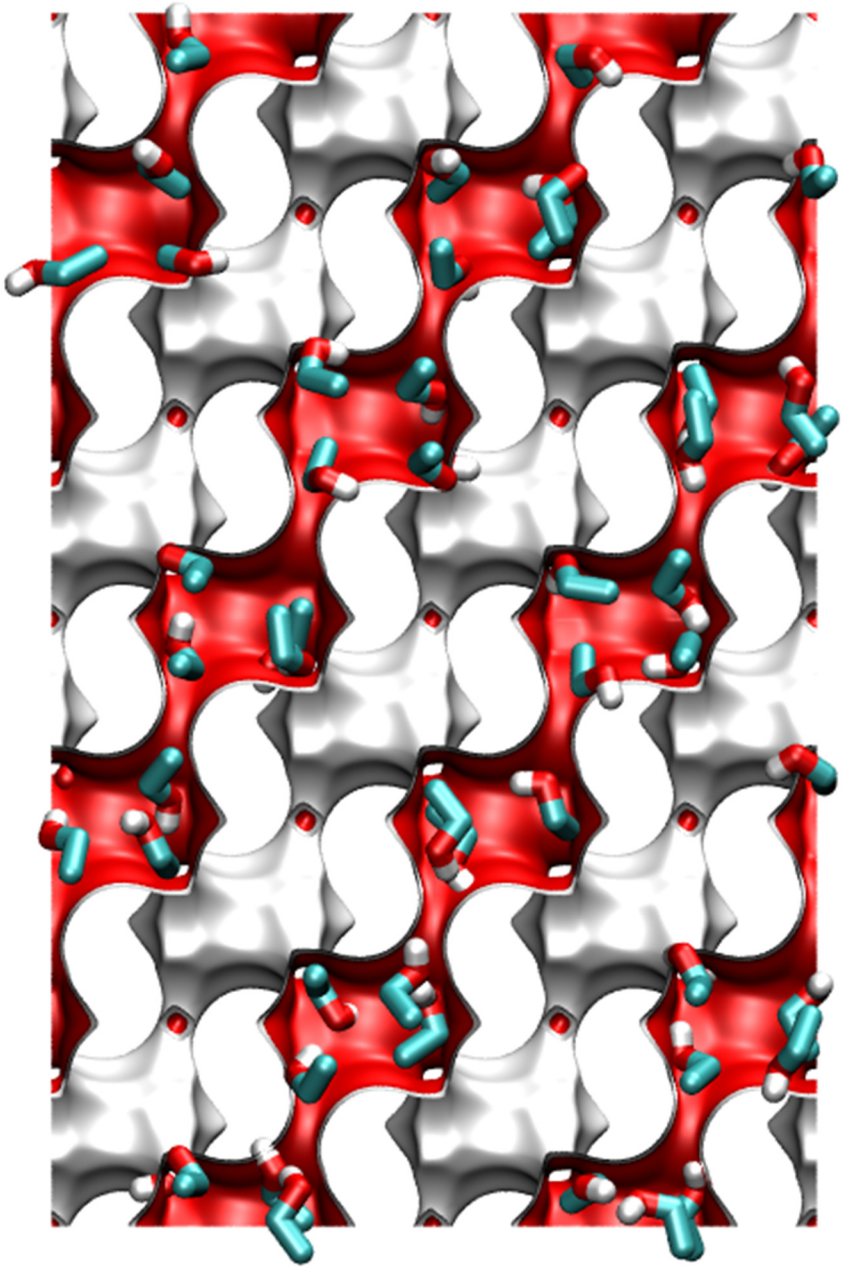

Figure A64

# Guest Molecule in MFI:
# $iC_4H_{10}$ = iC4

Figure A65

# CBMC simulation of iC4 isotherms in MFI; Experimental validation

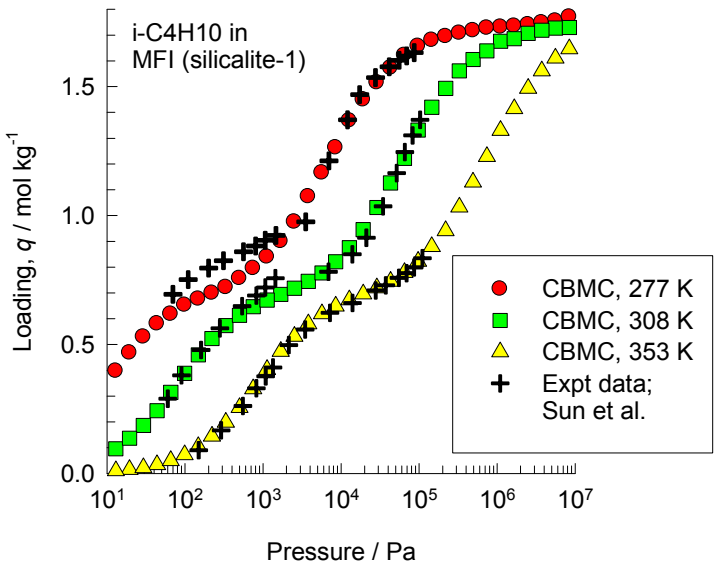


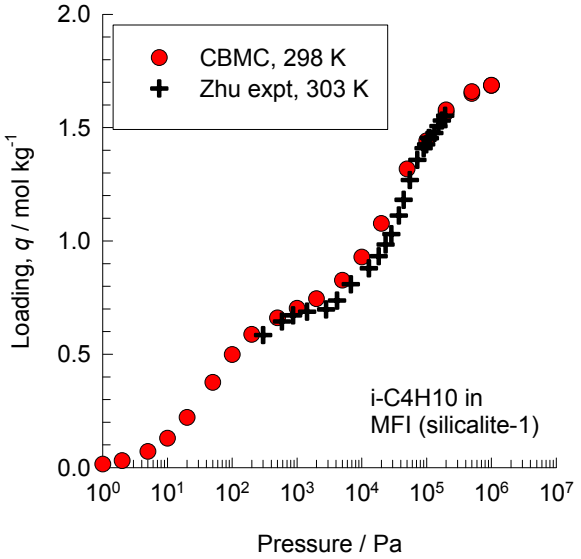


The inflection in the isotherm is caused due to preferential location of iC4 at the intersections. There are 4 intersections per unit cell.

The inflection occurs at a loading of 4 molecules per unit cell, corresponding to 0.693 mol $kg^{-1}$

# **MFI** iso-butane (iC4) diffusion in MFI: IR microscopy data

Figure A66

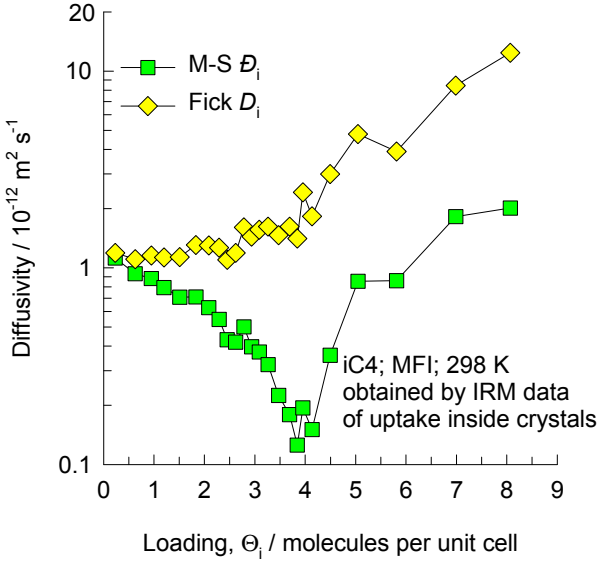


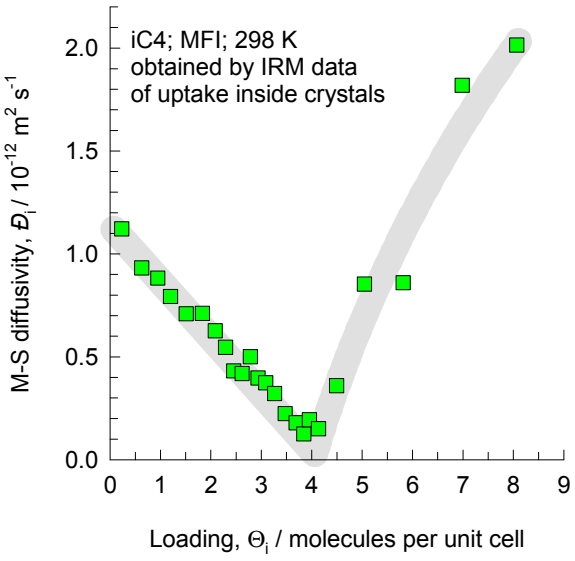


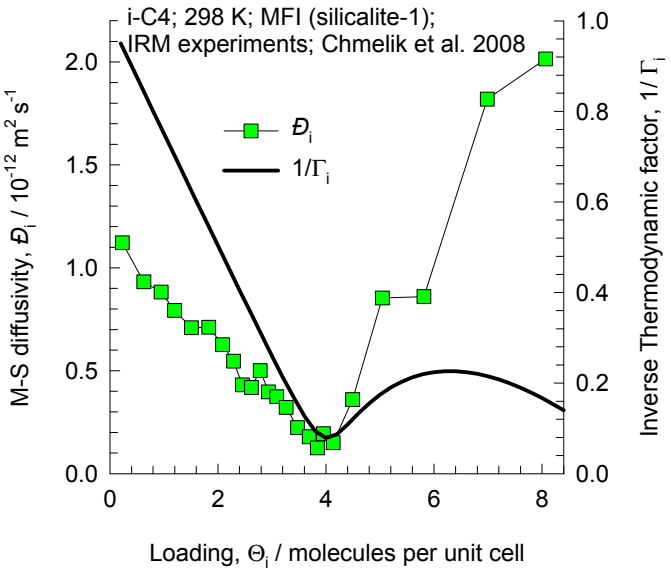


The inflection in the isotherm has a profound influence on the diffusivity of iC4.

The data are re-plotted using the information in:
C. Chmelik, L. Heinke, J. Kärger, D.B. Shah, W. Schmidt, J.M. van Baten, R. Krishna, Inflection in the loading dependence of the Maxwell-Stefan diffusivity of iso-butane in MFI zeolite, Chem. Phys. Lett. 459 (2008) 141-145.

# MFI iso-butane (iC4) diffusivity in MFI from membrane permeation

Figure A67

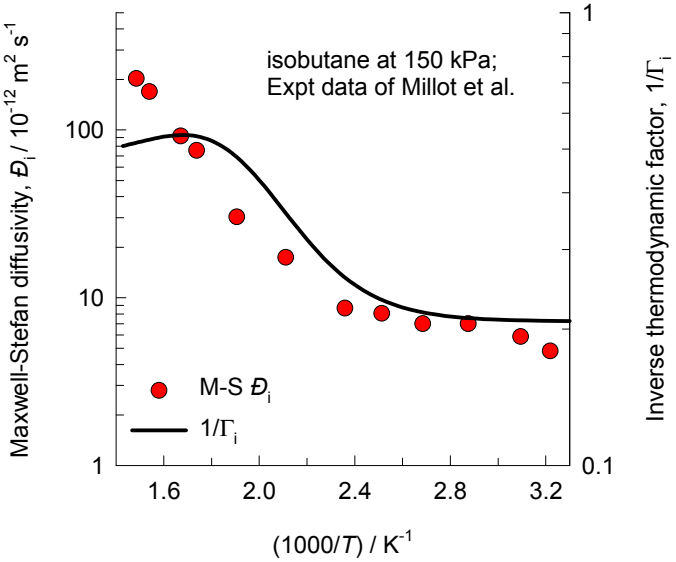


The experimental data are re-plotted using the information in:
B. Millot, A. Méthivier, H. Jobic, H. Moueddeb, M. Bee, Diffusion of isobutane in ZSM-5 zeolite: A comparison of quasi-elastic neutron scattering and supported membrane results, J. Phys. Chem. B 103 (1999) 1096-1101.
B. Millot, A. Méthivier, H. Jobic, H. Moueddeb, J.A. Dalmon, Permeation of linear and branched alkanes in ZSM-5 supported membranes, Microporous Mesoporous Mat. 38 (2000) 85-95.

The interpretation of the non-Arrhenius temperature dependence of the M-S diffusivity is discussed in our earlier works
R. Krishna, R. Baur, Modelling issues in zeolite based separation processes, Sep. Purif. Technol. 33 (2003) 213-254.
R. Krishna, Describing the diffusion of guest molecules inside porous structures, J. Phys. Chem. C 113 (2009) 19756-19781.

Figure A68

# Snapshots showing the location of molecules within MFI

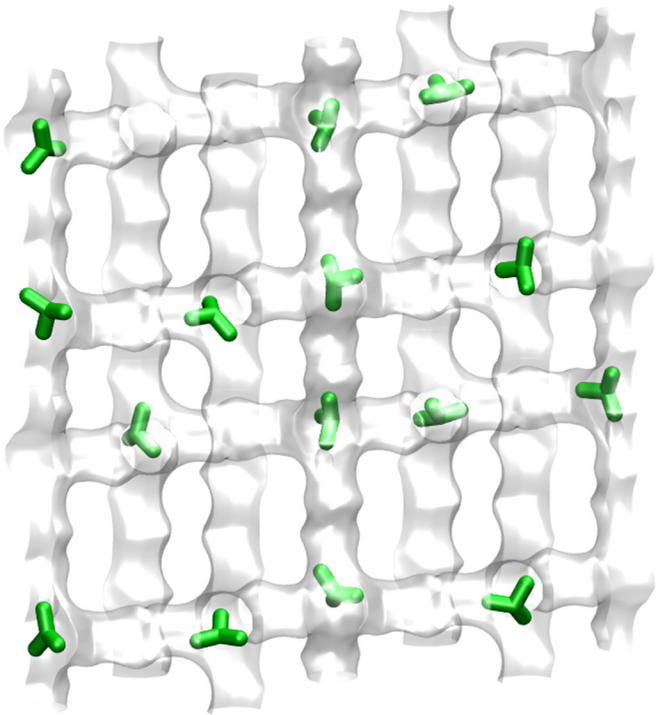

iC4 locates preferentially at the intersections

**iC4: 4 molecules/uc**

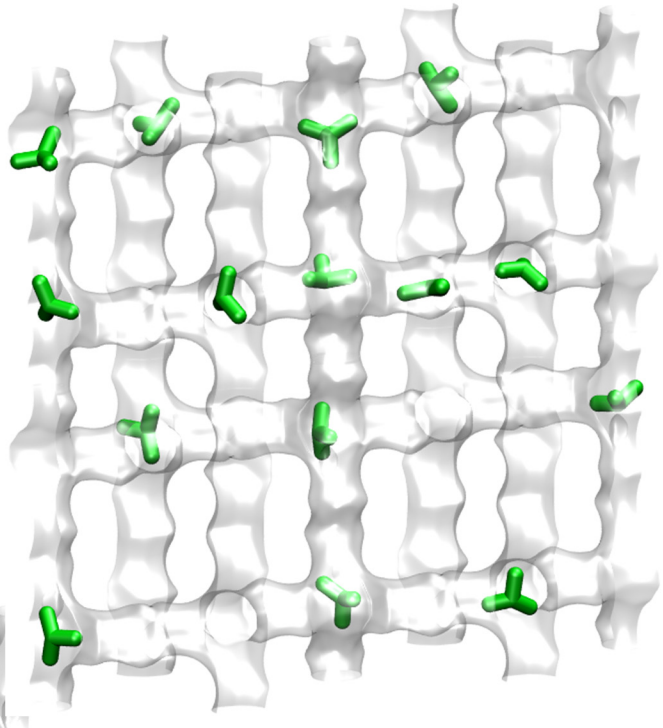

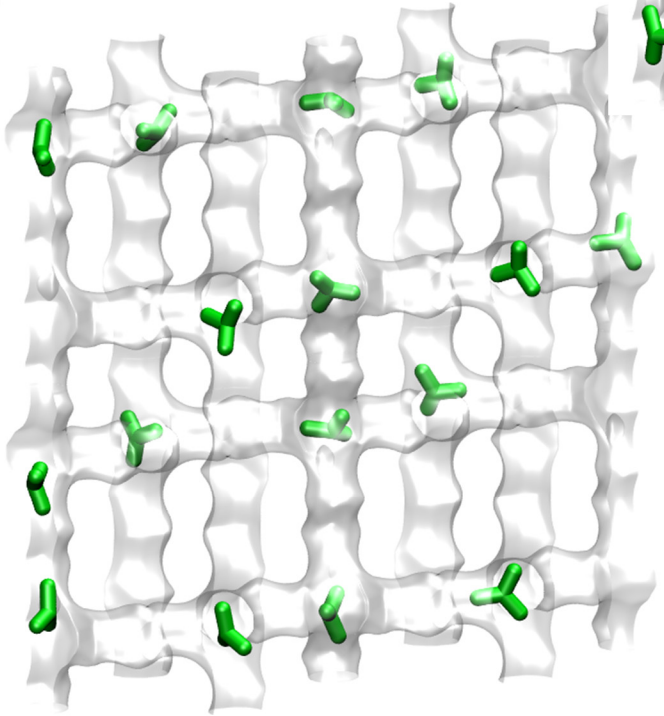

**Snapshots showing the location of molecules**

**within MFI**

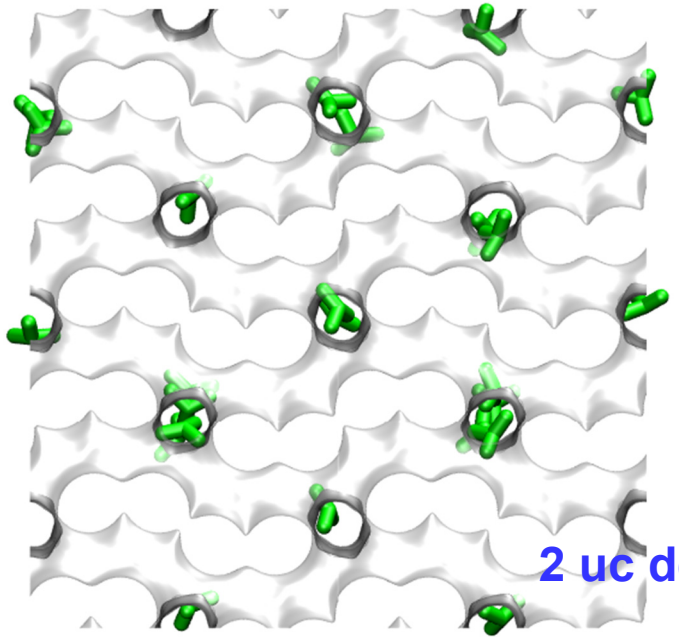

2 uc deep

2 uc deep

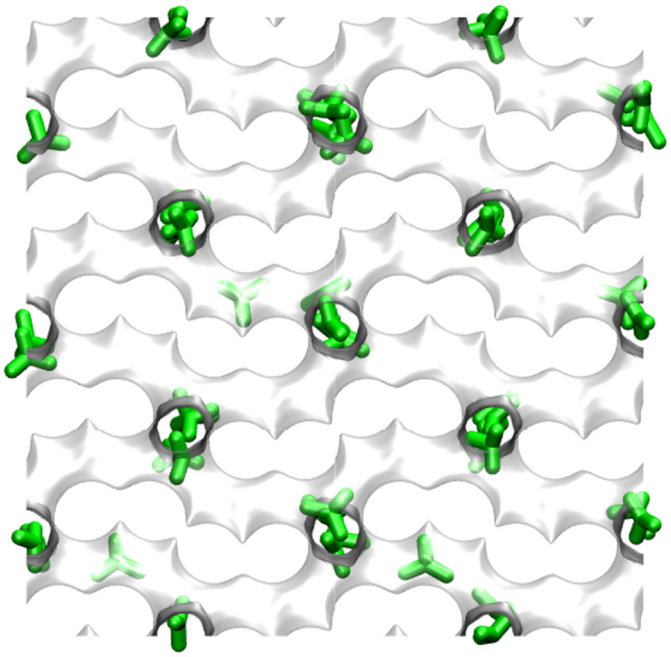

**iC4: 2 molecules/uc**

iC4 locates preferentially at the intersections

**iC4: 4 molecules/uc**

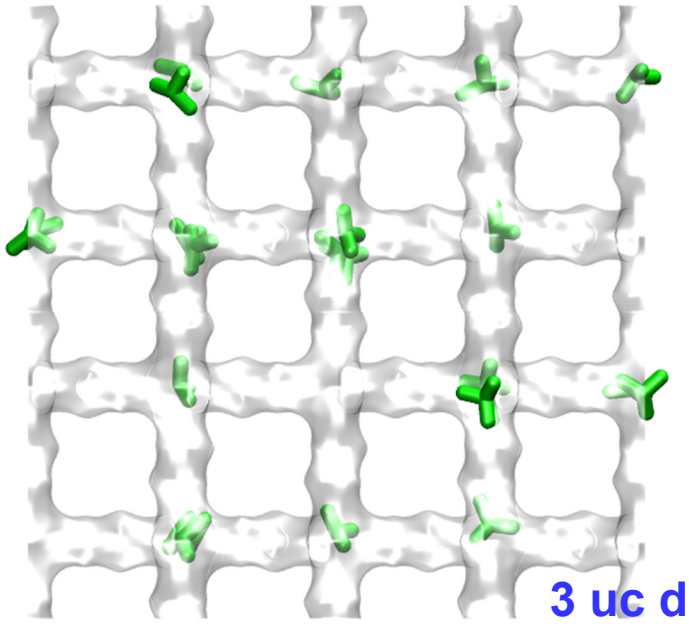

3 uc deep

3 uc deep

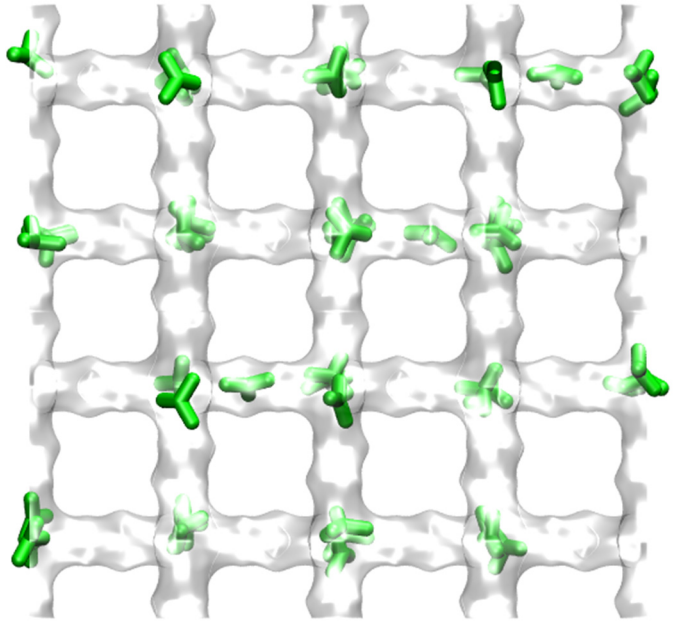

Figure A70

# Snapshots showing the location of molecules within MFI

Very high pressures are required to locate the iC4 within the channels.

**iC4: 6 molecules/uc**

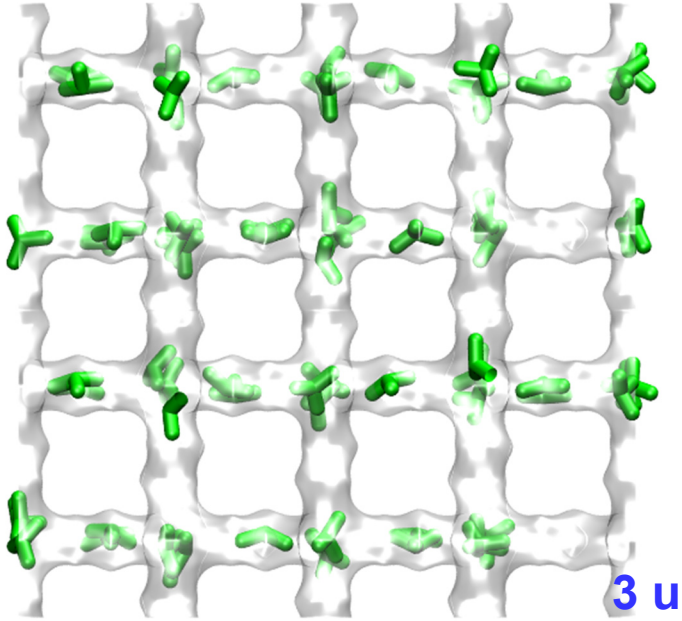

**3 uc deep**

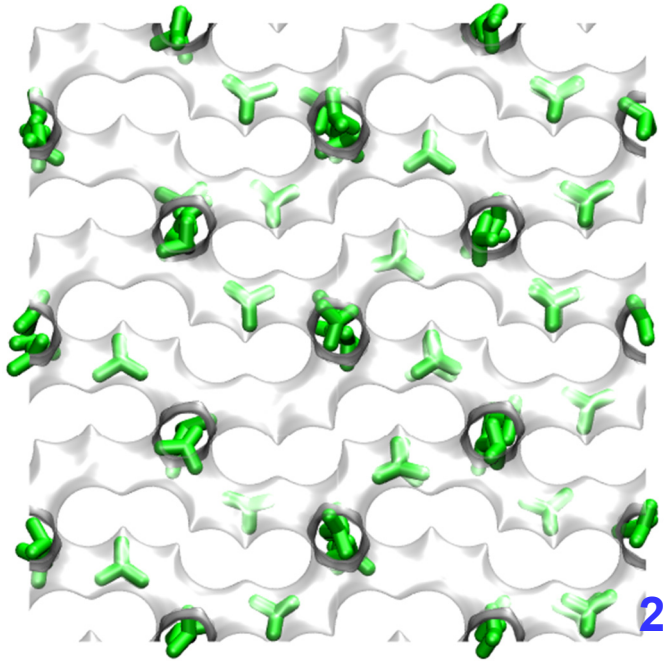

**2 uc deep**

Figure A71

# Guest Molecule in MFI: $nC_5H_{12}$ = nC5

Figure A72

# MD simulations of diffusivities in MFI zeolite

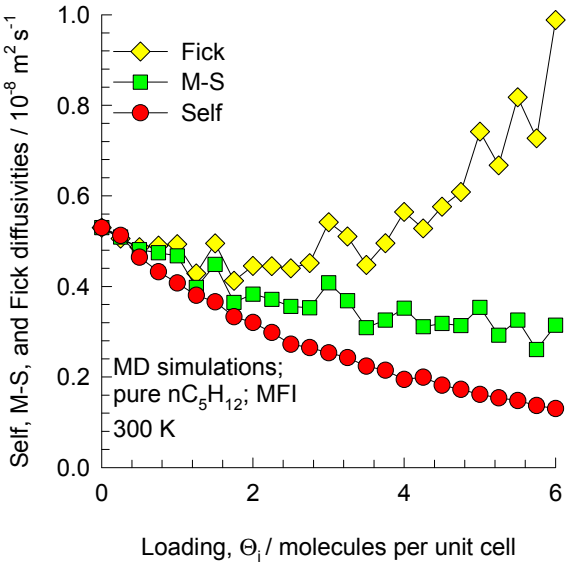

# Guest Molecule in MFI: $nC_6H_{14}$ = nC6

Figure A74

# CBMC simulation of nC6 isotherms in MFI; Experimental validation

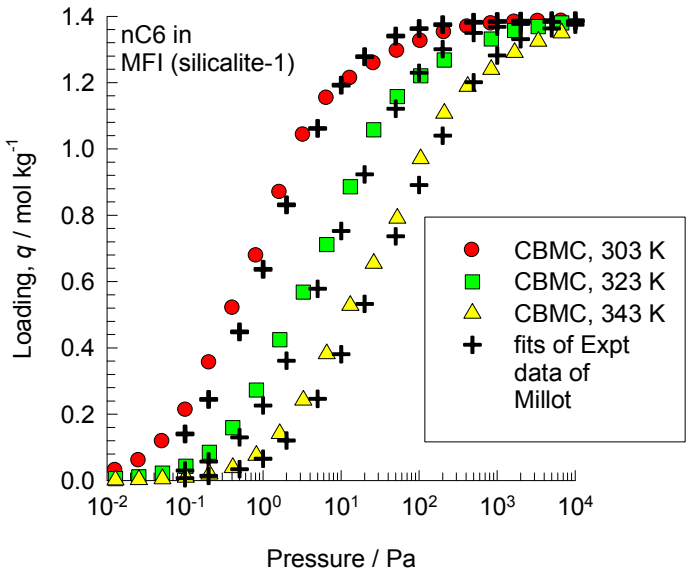


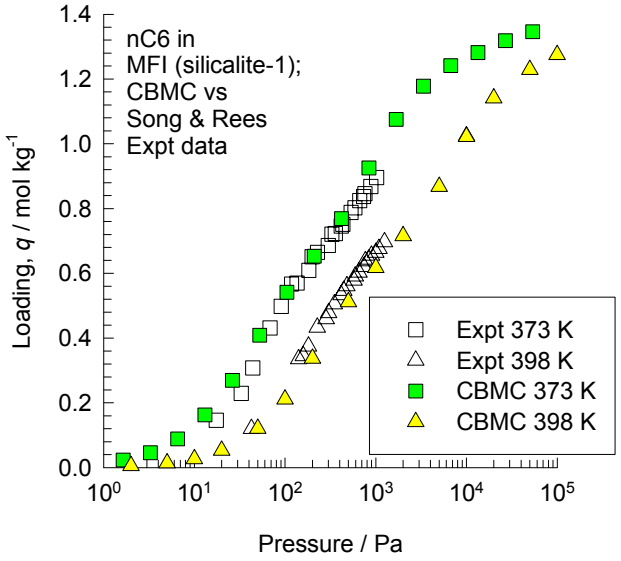


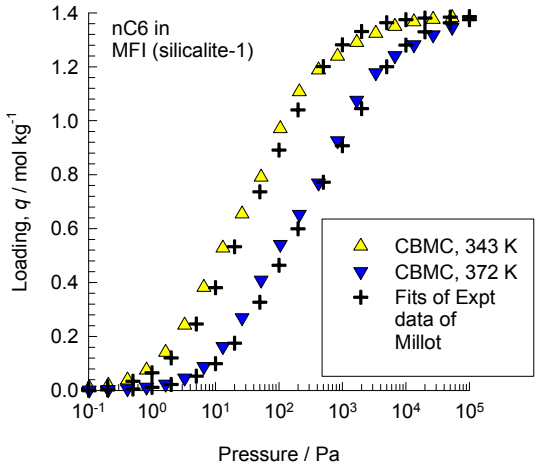

Figure A75

# Snapshots showing the location of molecules within MFI

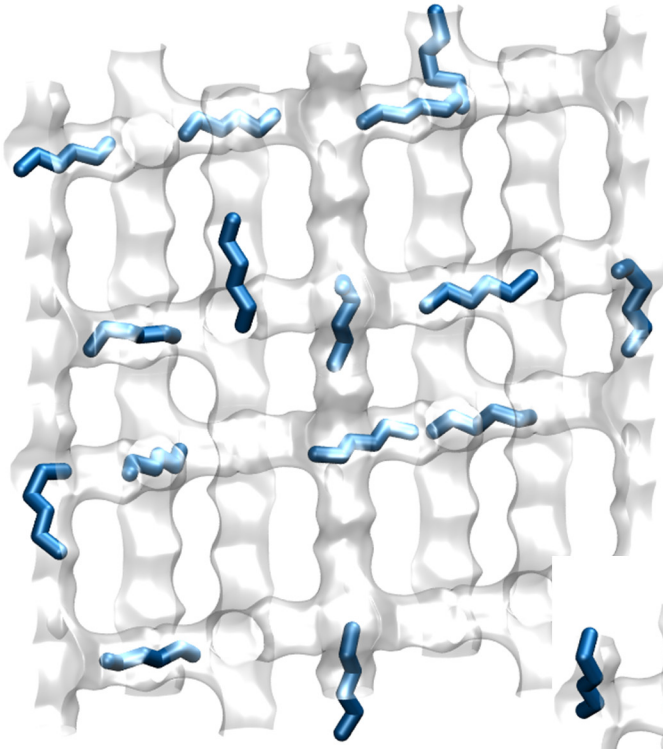

Linear, chain, alkanes can locate anywhere along the channels of MFI. The length of nC6 is commensurate with the distance between two intersections

**nC6: 4 molecules/uc**

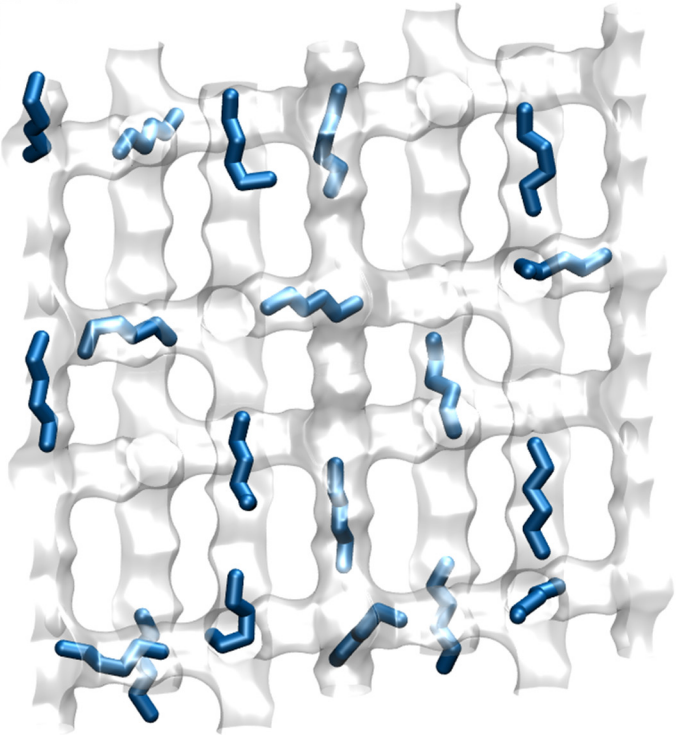

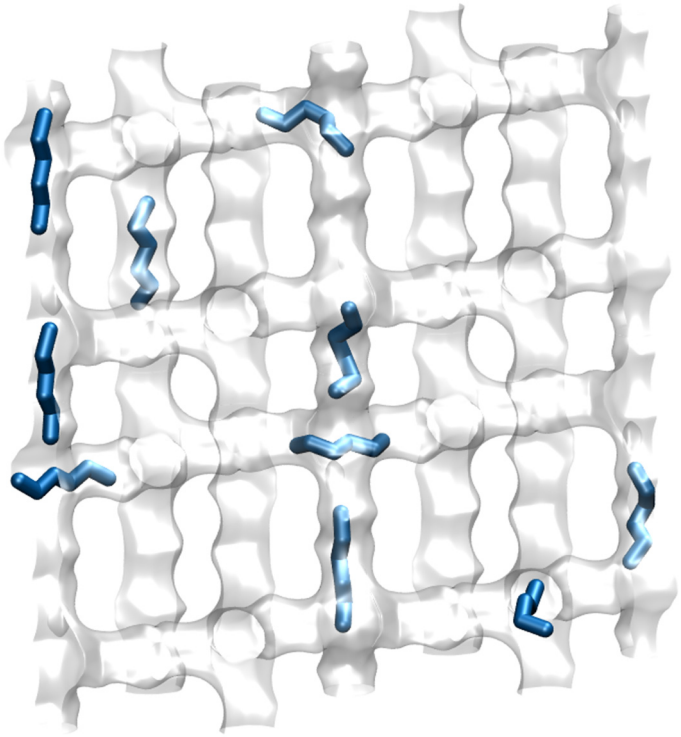

Figure A76

# MD simulations of diffusivities in MFI zeolite

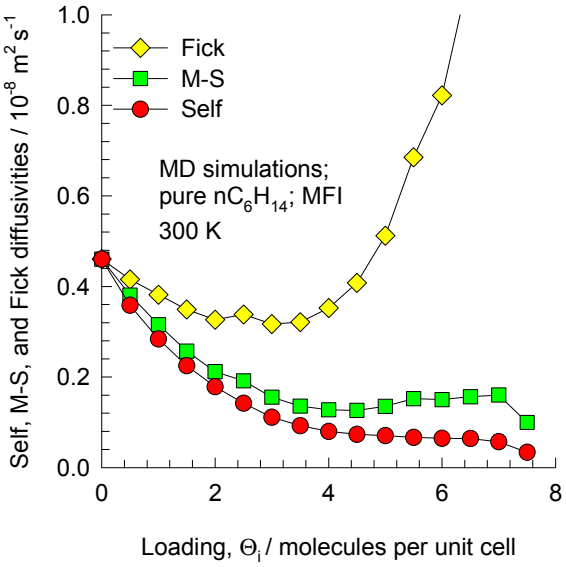


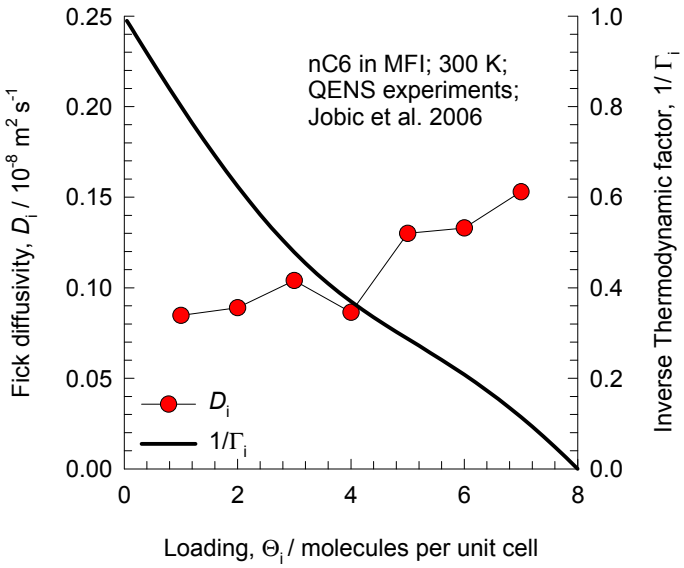


The QENS experimental data are re-plotted using the information in:

H. Jobic, C. Laloué, C. Laroche, J.M. van Baten, R. Krishna, Influence of isotherm inflection on the loading dependence of the diffusivities of n-hexane and n-heptane in MFI zeolite. Quasi-Elastic Neutron Scattering experiments supplemented by molecular simulations, J. Phys. Chem. B 110 (2006) 2195-2201.

# Guest Molecule in MFI:
# $nC_7H_{18}$ = nC7

Figure A78

# MD simulations of nC7 diffusivities in MFI zeolite

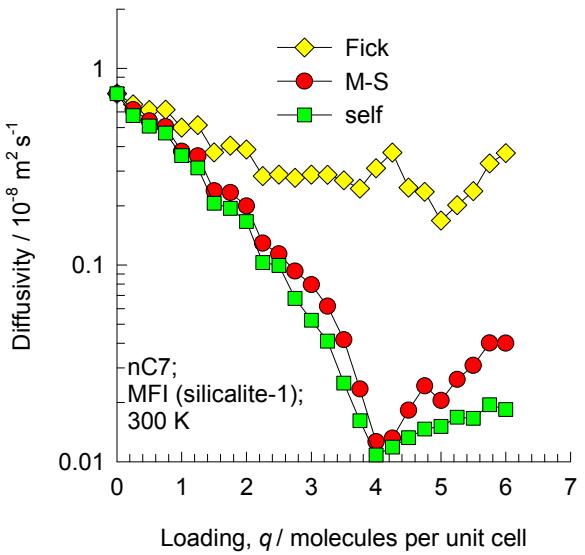


The inflection in the isotherm of nC7 has a significant influence on the loading dependence of the diffusivities in MFI

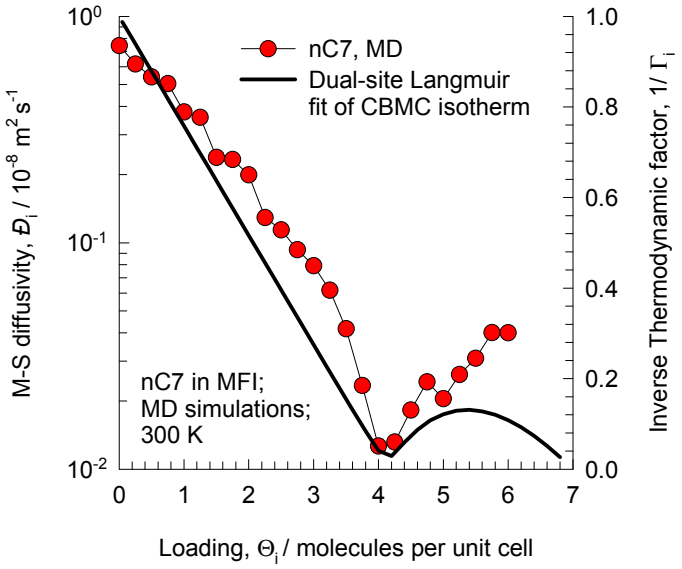


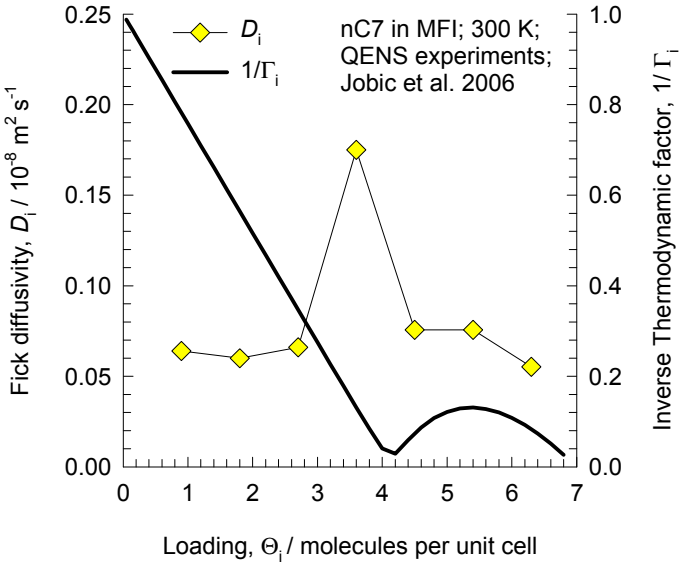


The QENS experimental data are re-plotted using the information in:

H. Jobic, C. Laloué, C. Laroche, J.M. van Baten, R. Krishna, Influence of isotherm inflection on the loading dependence of the diffusivities of n-hexane and n-heptane in MFI zeolite. Quasi-Elastic Neutron Scattering experiments supplemented by molecular simulations, J. Phys. Chem. B 110 (2006) 2195-2201.

Figure A79

# Snapshots showing the location of molecules within MFI

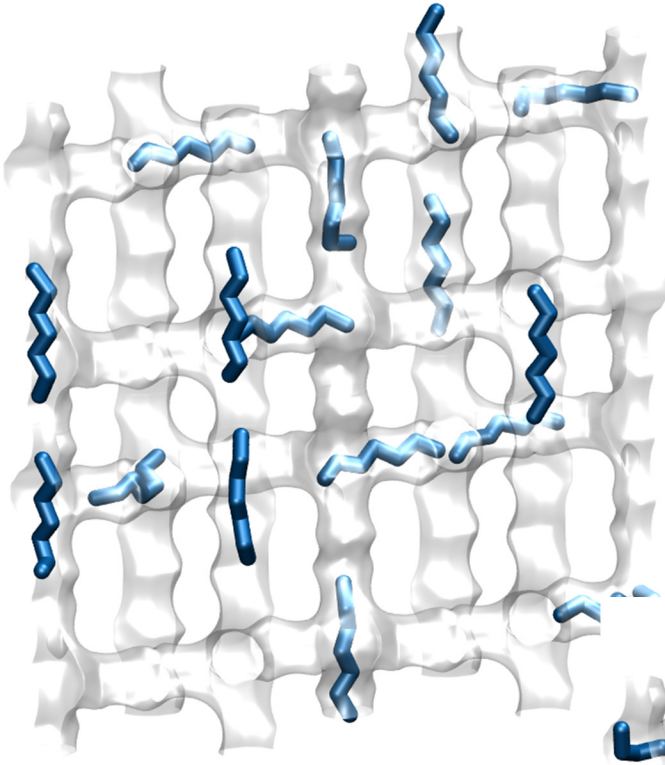

nC7 can locate anywhere along the channels of MFI.

**nC7: 4 molecules/uc**

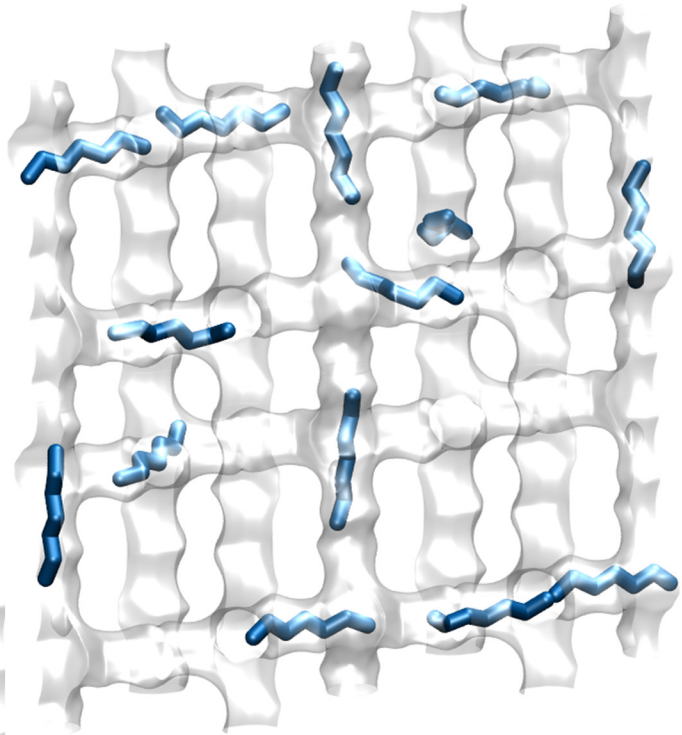

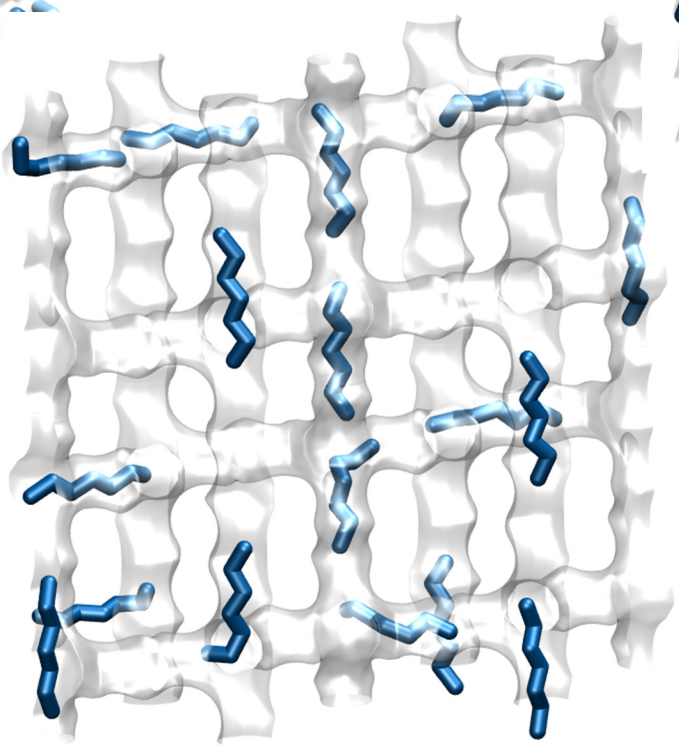

# Guest Molecule in MFI: 2,2dimethylbutane = 22DMB

Figure A81

# CBMC simulation of isotherms; Experimental validation

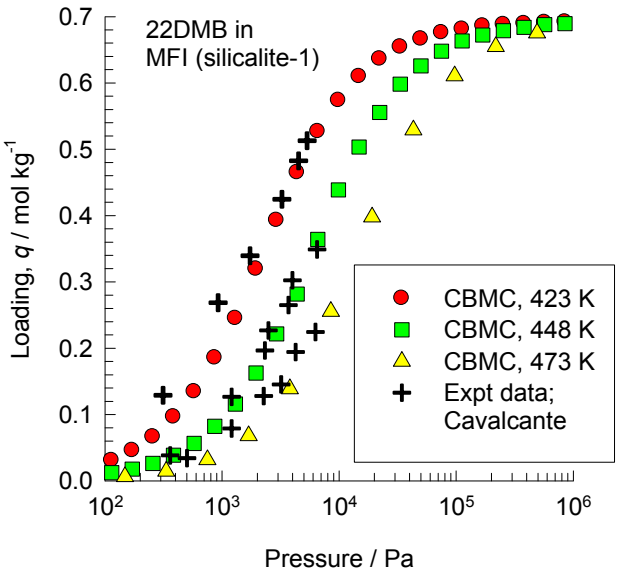


The saturation capacity is dictated by the fact that 22DMB locates at the intersections only. There are 4 intersections per unit cell.

The saturation loading is therefore = 4 molecules per unit cell, corresponding to 0.693 mol $kg^{-1}$

Figure A82

# Snapshots showing the location of molecules within MFI

22DMB molecules can only locate at the intersections of MFI

**22DMB: 4 molecules/uc**

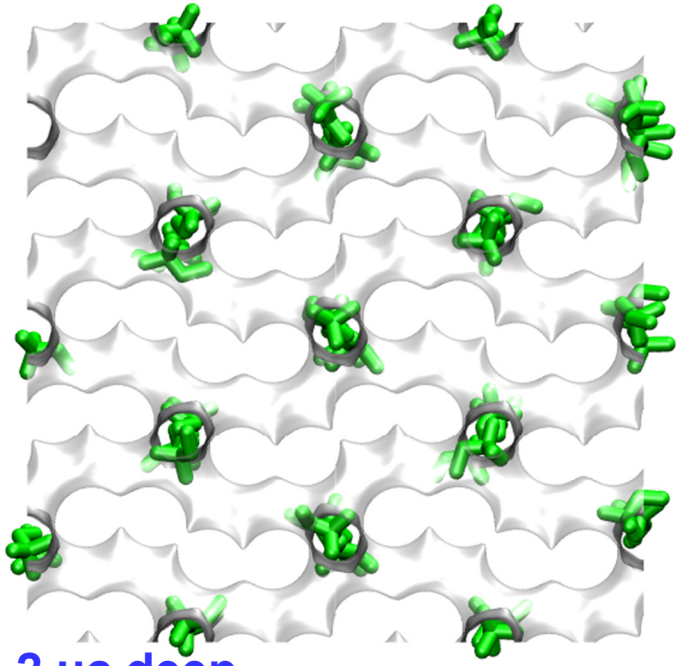

**2 uc deep**

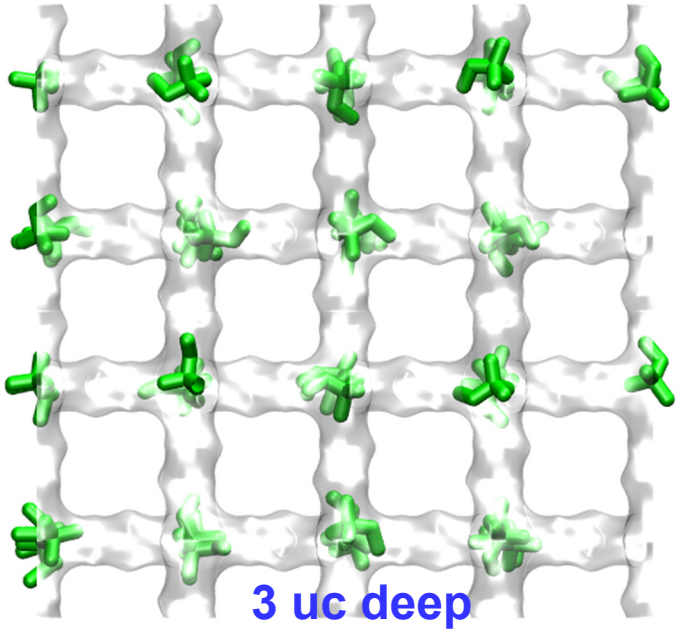

**3 uc deep**

# Guest Molecule in MFI: 2-methylpentane = 2MP

Figure A84

# CBMC simulation of isotherms; Experimental validation

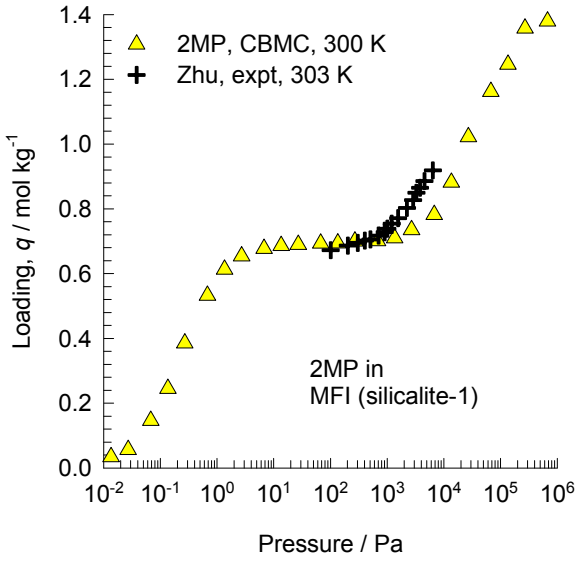


The inflection in the isotherm is caused due to preferential location of 2MP at the intersections. There are 4 intersections per unit cell.

The inflection occurs at a loading of 4 molecules per unit cell, corresponding to 0.693 mol $kg^{-1}$

Figure A85

# Snapshots showing the location of molecules within MFI

2MP molecules locates preferentially at
the intersections of MFI

**2MP: 4 molecules/uc**

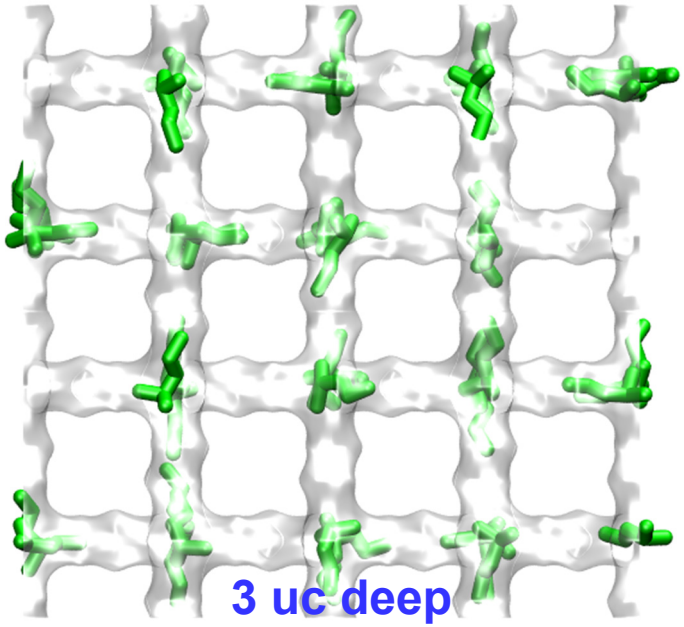


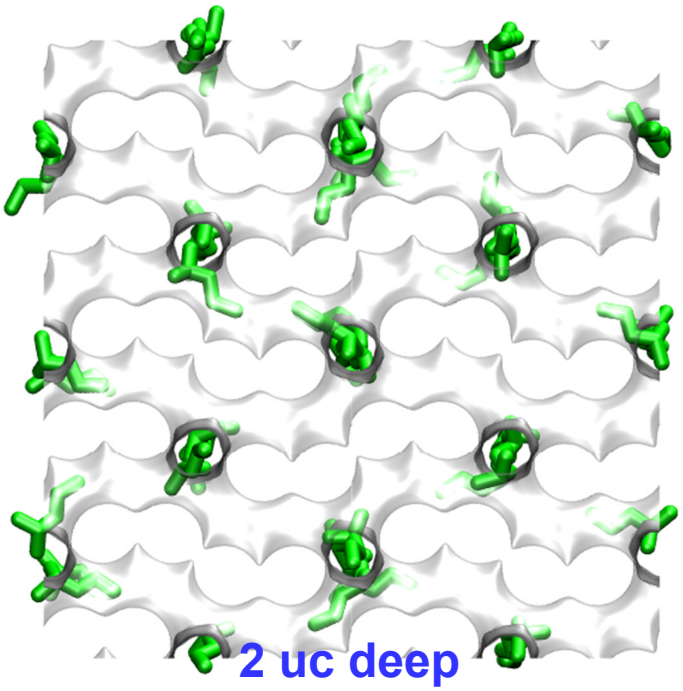

# Guest Molecule in MFI: 3-methylpentane = 3MP

Figure A87

# CBMC simulation of isotherms; Experimental validation

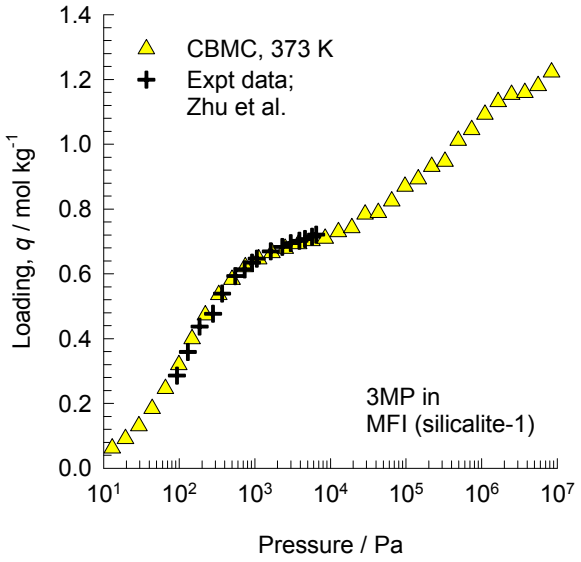


The inflection in the isotherm is caused due to preferential location of 3MP at the intersections. There are 4 intersections per unit cell.

The inflection occurs at a loading of 4 molecules per unit cell, corresponding to 0.693 mol $kg^{-1}$

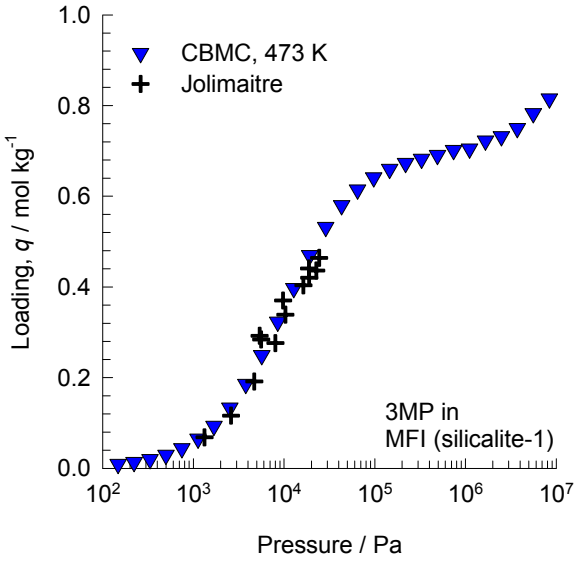

# MFI 3-methylpentane (3MP) diffusivity in MFI from membrane permeation

Figure A88

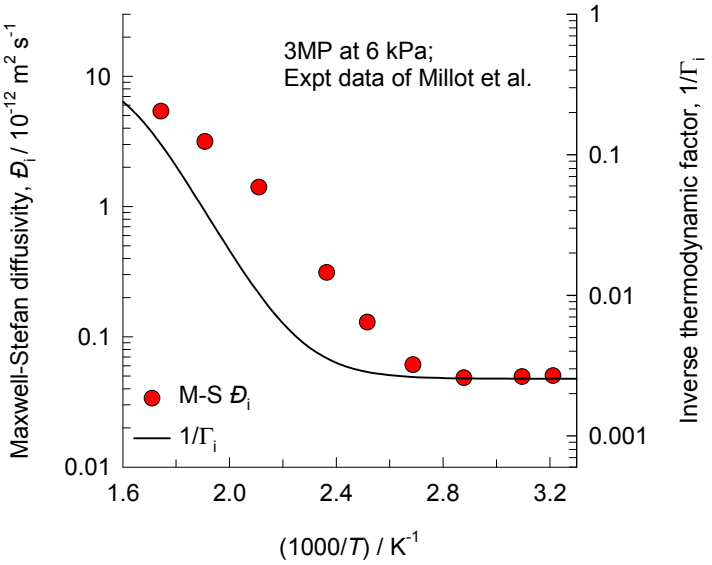


The experimental data are re-plotted using the information in:
B. Millot, A. Méthivier, H. Jobic, H. Moueddeb, M. Bee, Diffusion of isobutane in ZSM-5 zeolite: A comparison of quasi-elastic neutron scattering and supported membrane results, J. Phys. Chem. B 103 (1999) 1096-1101.
B. Millot, A. Méthivier, H. Jobic, H. Moueddeb, J.A. Dalmon, Permeation of linear and branched alkanes in ZSM-5 supported membranes, Microporous Mesoporous Mat. 38 (2000) 85-95.

The interpretation of the non-Arrhenius temperature dependence of the M-S diffusivity is discussed in our earlier works
R. Krishna, R. Baur, Modelling issues in zeolite based separation processes, Sep. Purif. Technol. 33 (2003) 213-254.
R. Krishna, Describing the diffusion of guest molecules inside porous structures, J. Phys. Chem. C 113 (2009) 19756-19781.

Figure A89

# Snapshots showing the location of molecules within MFI

3MP molecules locates preferentially at
the intersections of MFI

**3MP: 4 molecules/uc**

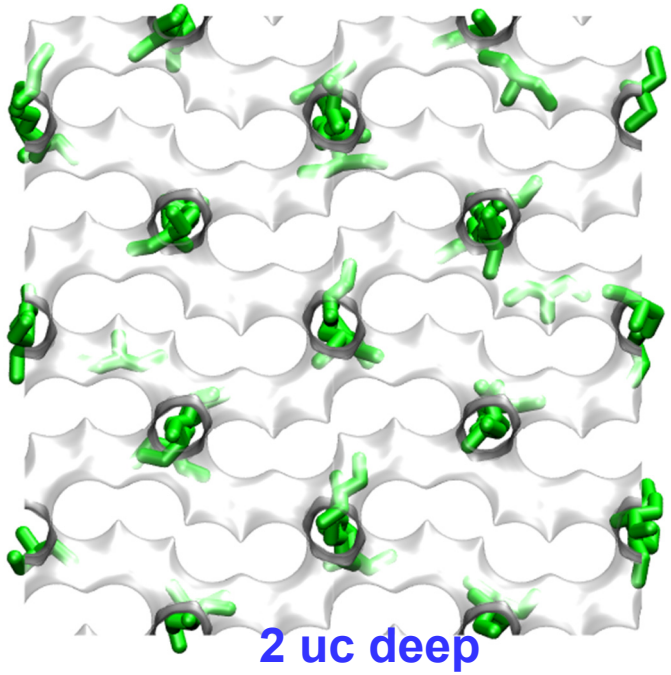

**2 uc deep**

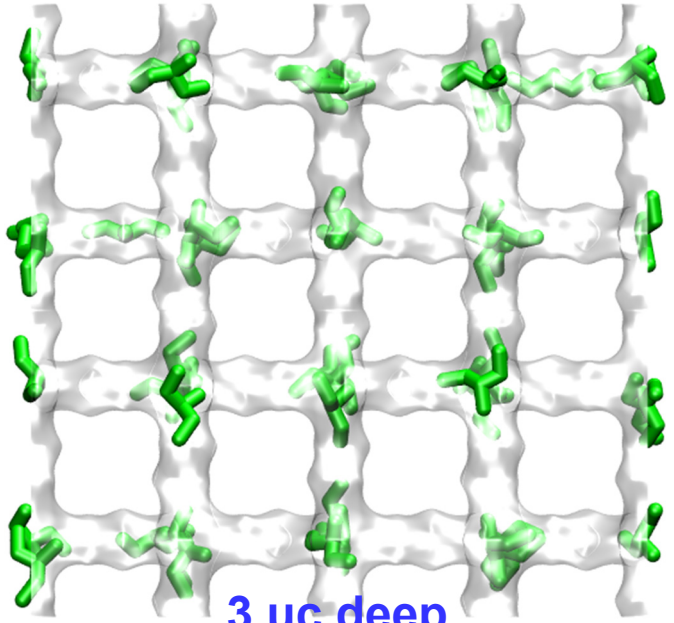

**3 uc deep**

# Guest Molecule in MFI: Benzene = Bz

**Snapshots showing the location of Bz molecules within**

**MFI**

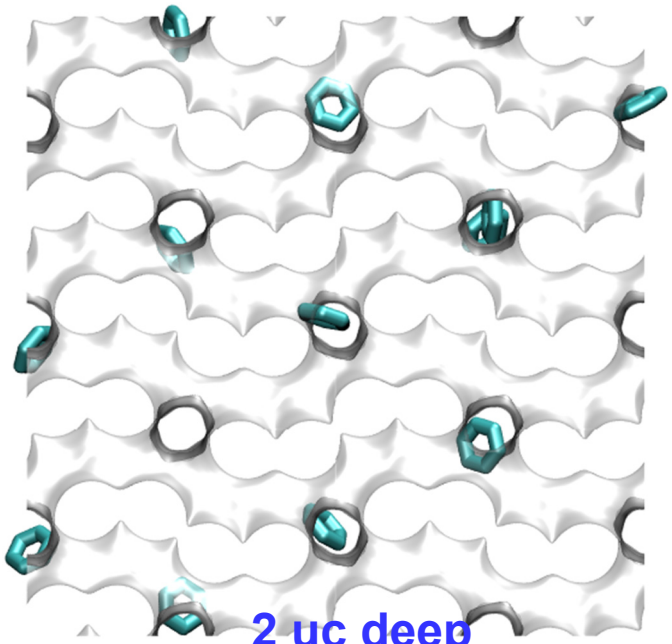

2 uc deep

Benzene: 1 molecules/uc

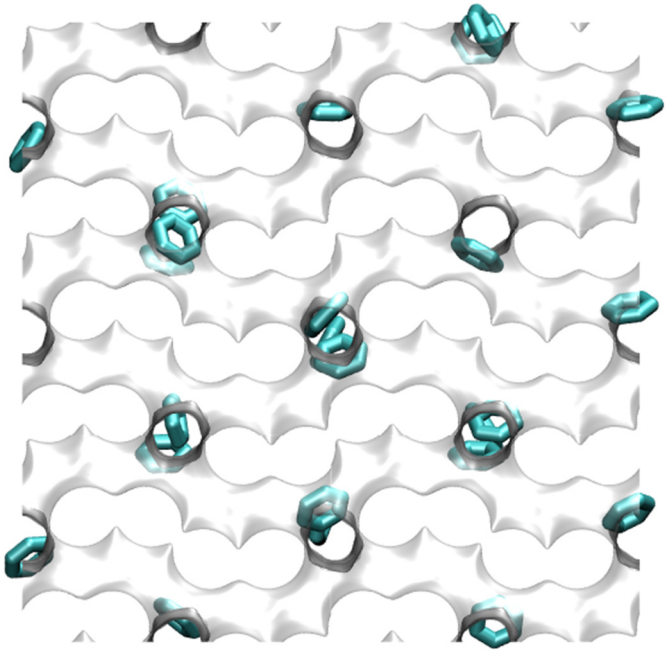

Benzene: 2 molecules/uc

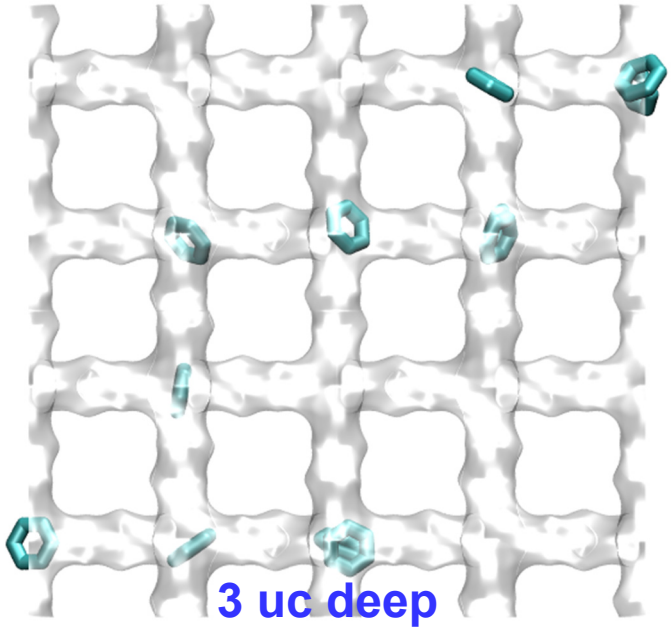

3 uc deep

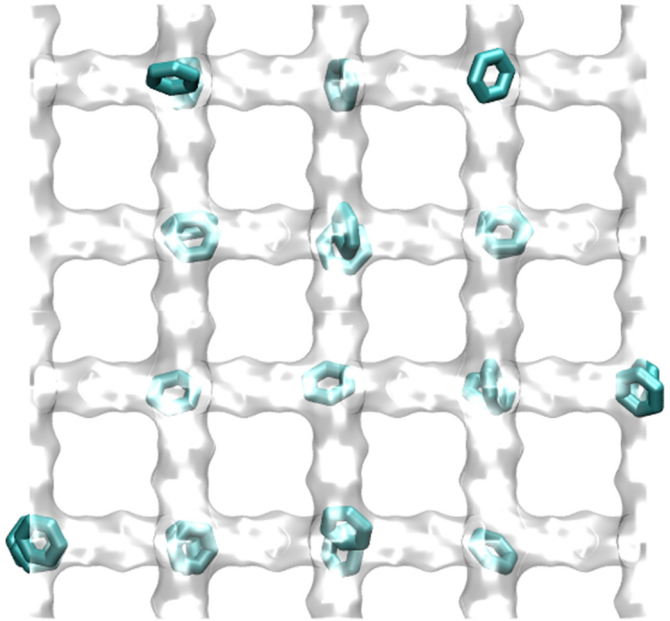

**Snapshots showing the location of Bz molecules**

**within MFI**

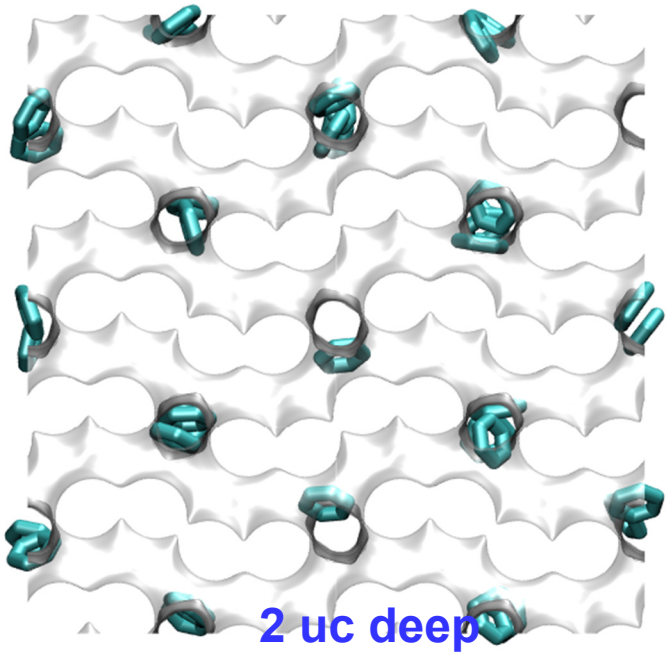

2 uc deep

Benzene: 3 molecules/uc

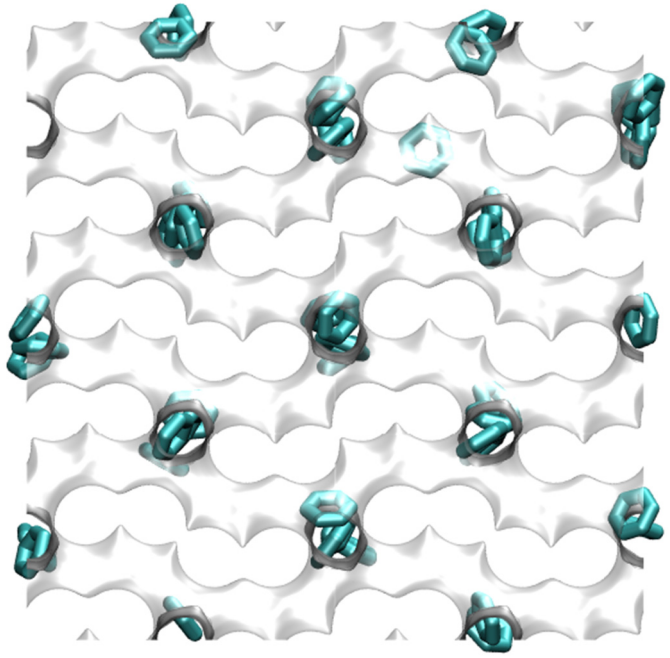

Benzene: 4 molecules/uc

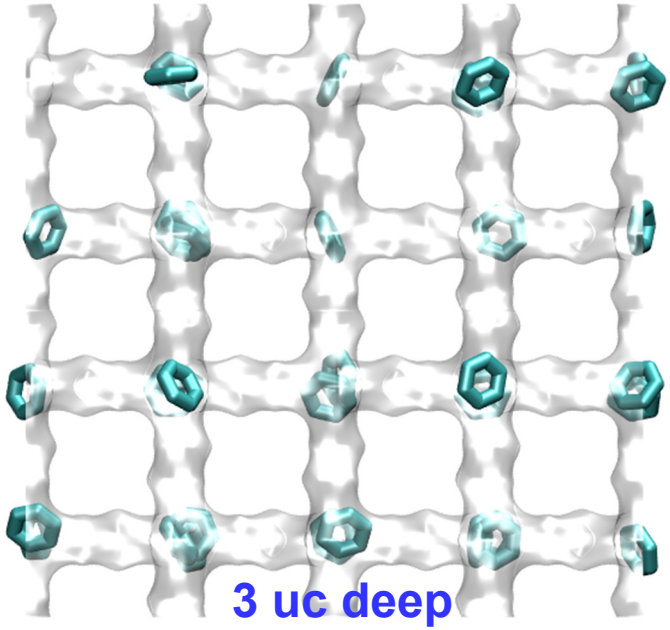

3 uc deep

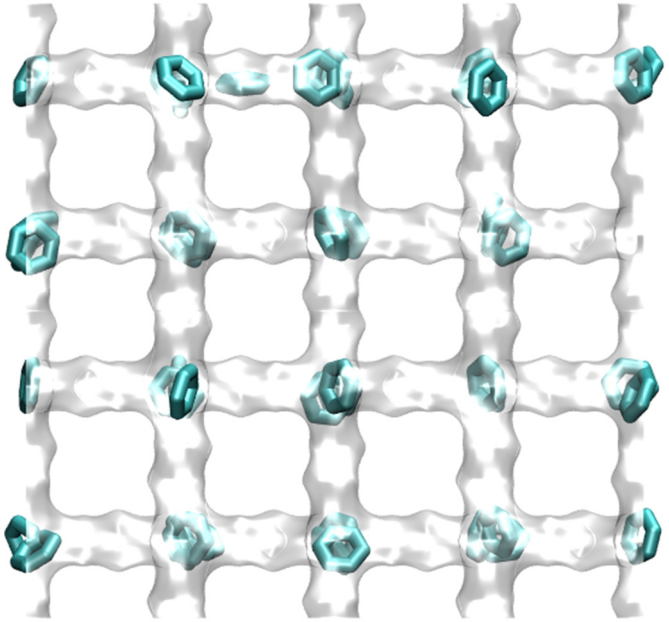

# Figure B1

Figures B1-B118:
Binary mixture MD data, including validation of Vignes interpolation formula, arranged according to guest mixtures in the following order:
$H_2/CO_2$
$CH_4/CO_2$
$CO_2/N_2$
$CH_4/C_2H_6$
$CH_4/C_3H_8$
$CH_4/nC_4H_{10}$
$H_2/CH_4$
$N_2/CH_4$
Ne/Ar
$H_2$/Ar
$CH_4$/Ar
Ne/$CO_2$
Ar/Kr
water/methanol, and water/ethanol
$CH_4/iC_4H_{10}$ in MFI zeolite
$C_2H_6/iC_4H_{10}$ in MFI zeolite
$C_3H_8/iC_4H_{10}$ in MFI zeolite
$nC_4H_{10}/iC_4H_{10}$ in MFI zeolite
$CH_4$/Benzene in MFI zeolite
$CH_4$/22MB in MFI zeolite
$C_3H_8$/Benzene in MFI zeolite
nC6/22MB in MFI zeolite
nC6/2MP in MFI zeolite
nC6/3MP in MFI zeolite
nC6/Benzene in MFI zeolite
$C_2H_4$/Benzene in MFI zeolite
nC6/3MP/22MB in MFI zeolite
$C_2H_4$/Benzene/Ethylbenzene in MFI zeolite

Figure B2

# Guest Mixture: $H_2/CO_2$

Figure B3

# Exchange coefficients and Degree of correlations

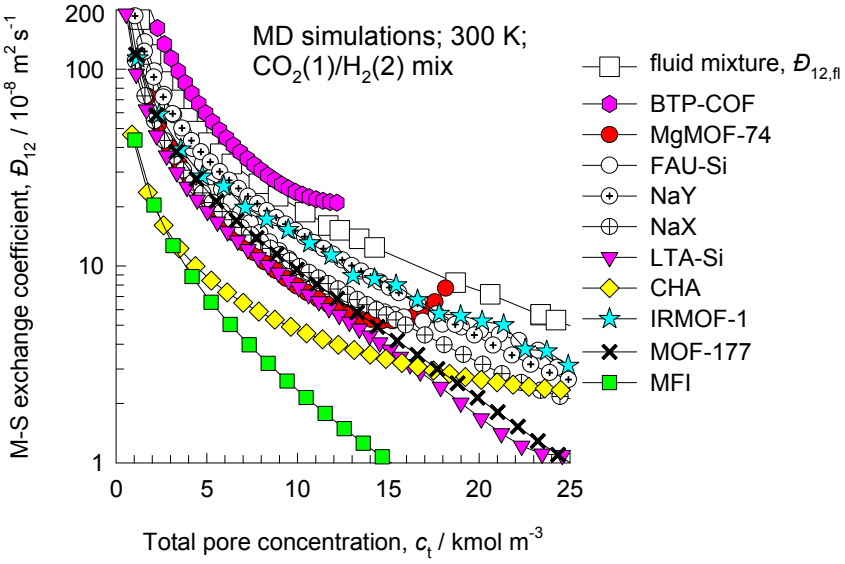


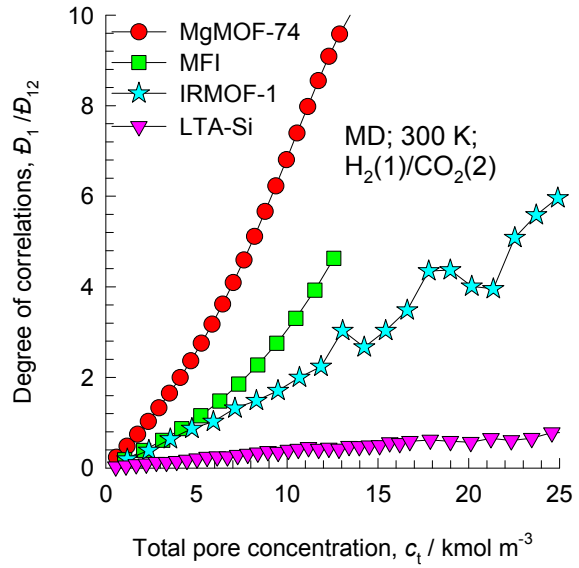


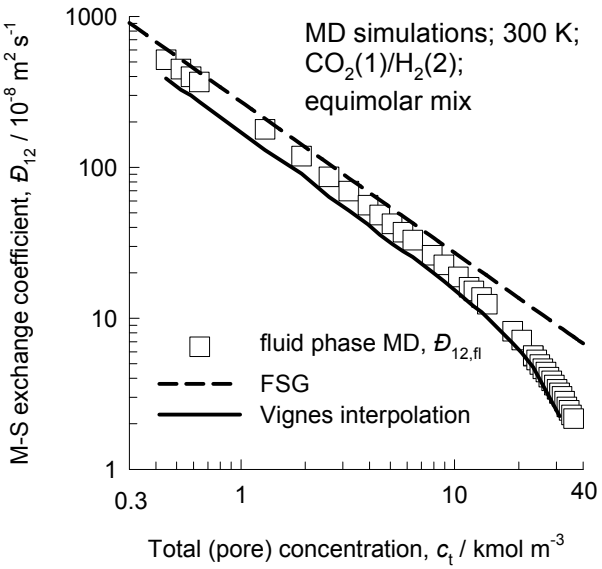


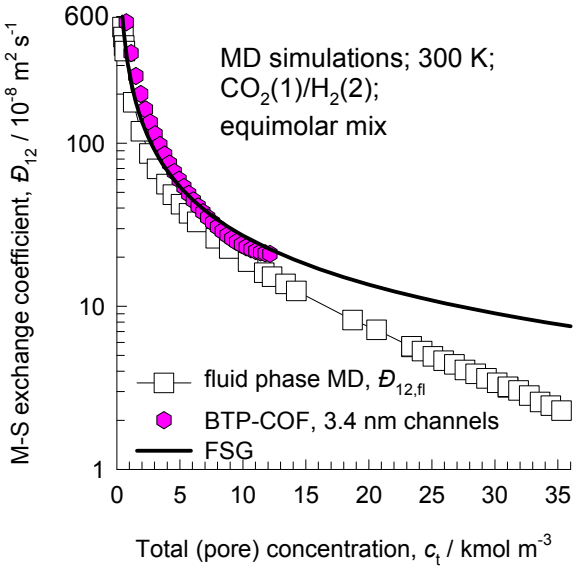

Figure B4

# Exchange coefficients as fraction of fluid phase $Đ_{12,fl}$

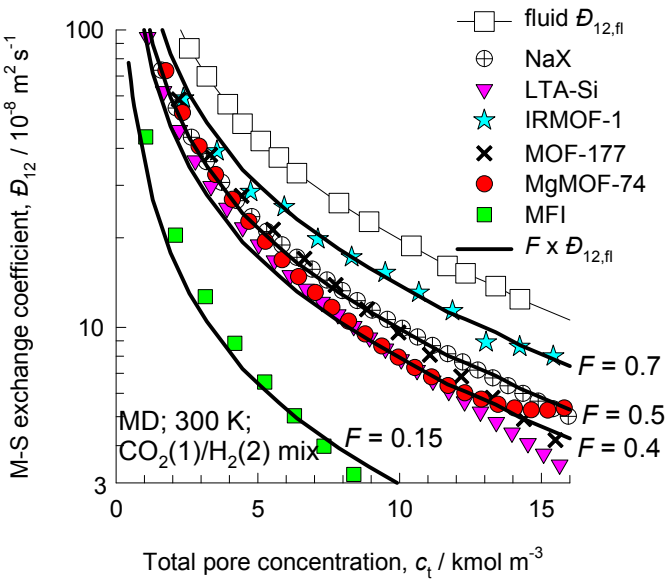


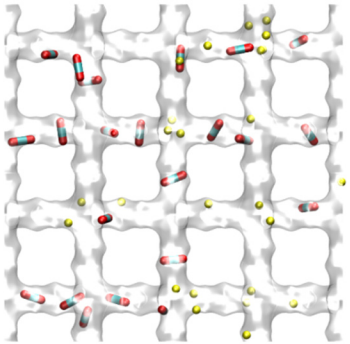

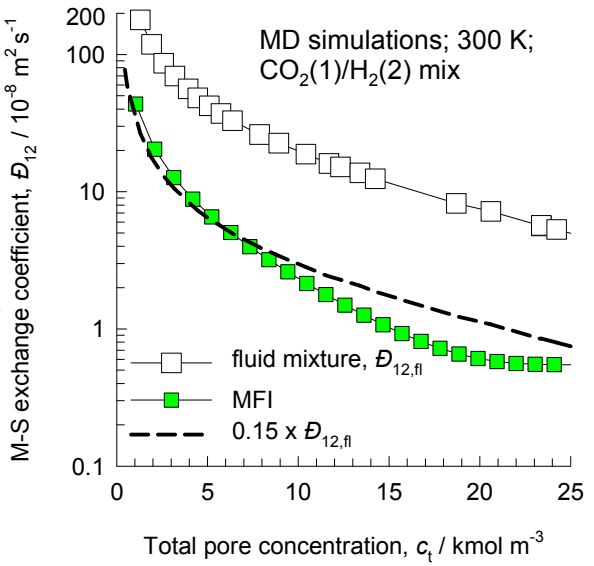


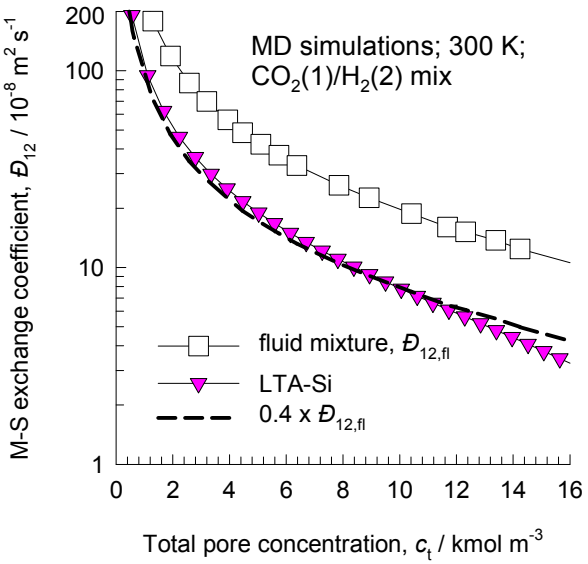


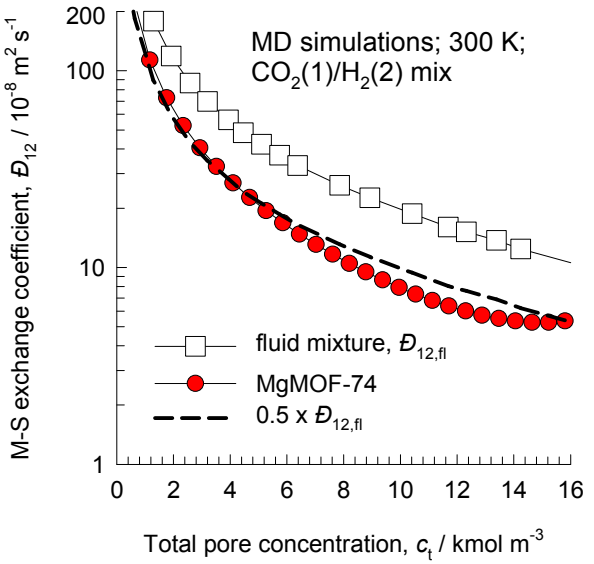

Figure B5

# Exchange coefficients as fraction of fluid phase $Đ_{12,fl}$

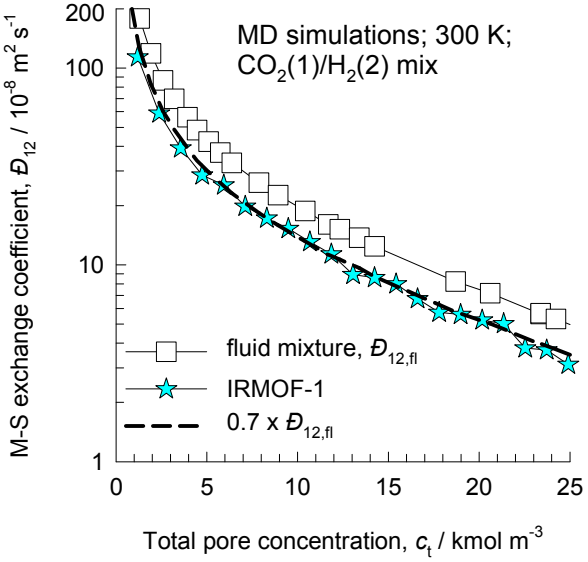


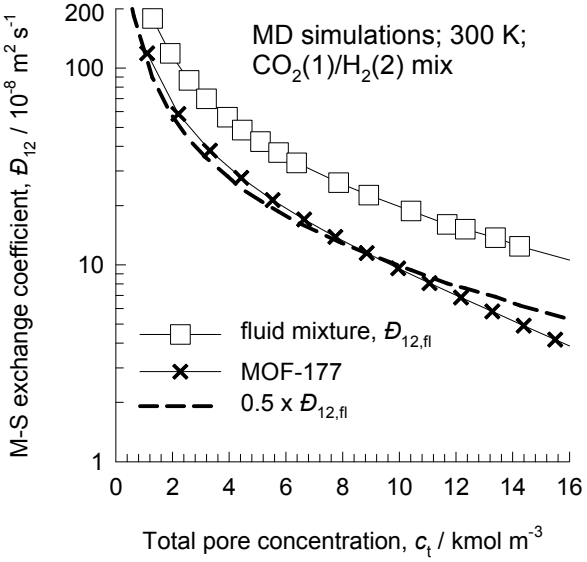


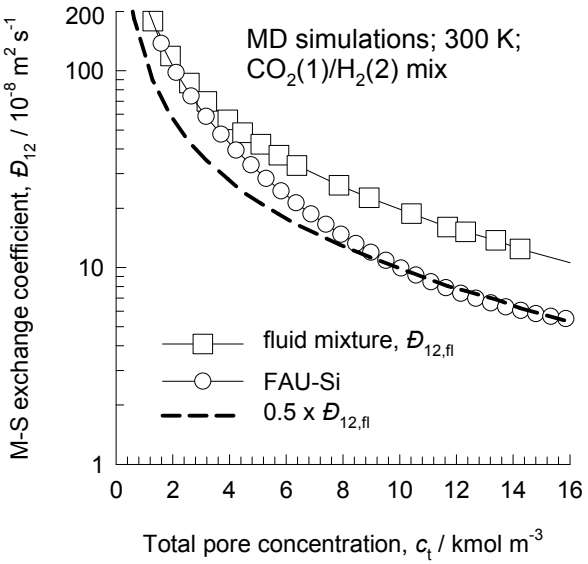


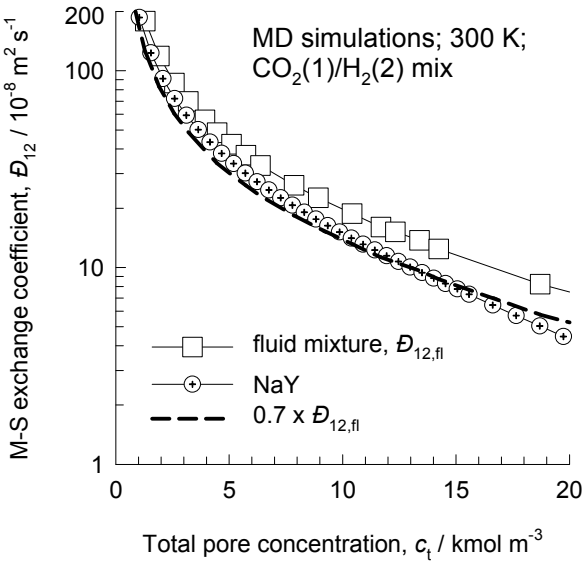


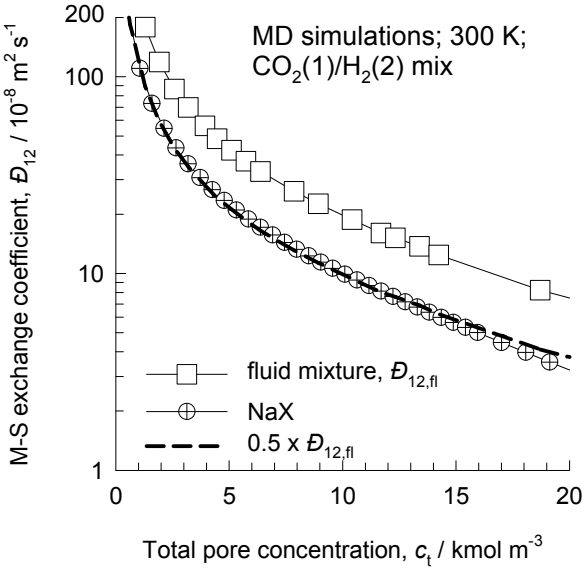

# Validation of the Vignes interpolation formula for $Đ_{12}$

Figure B6

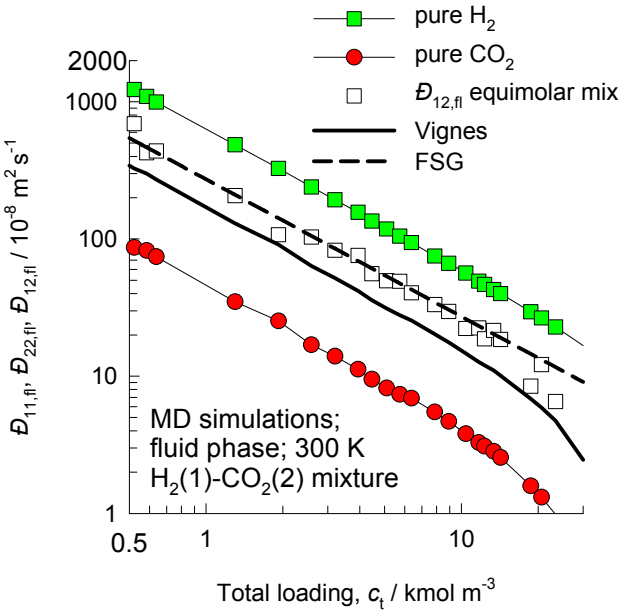


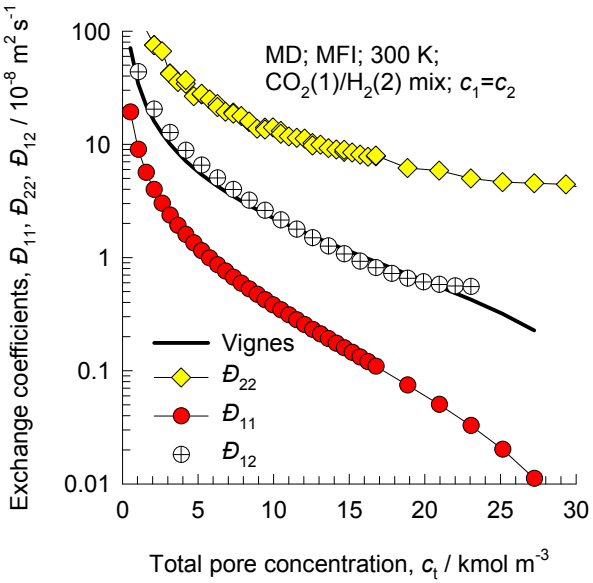


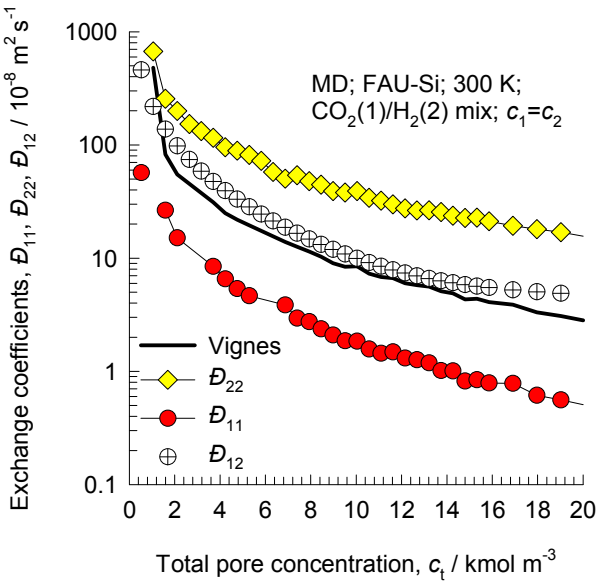


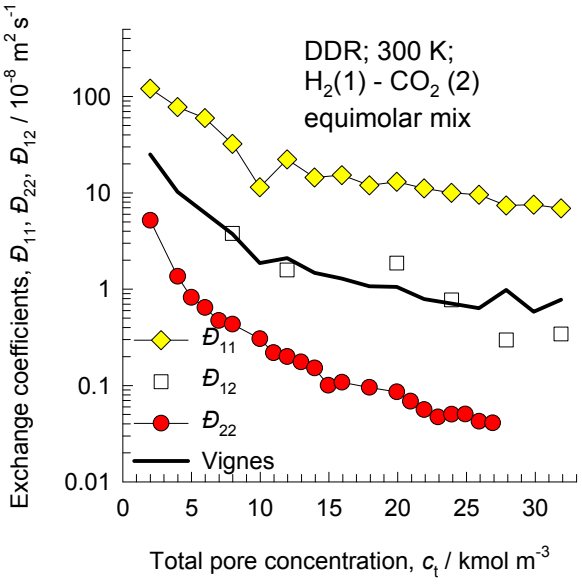

Figure B7

# Guest Mixture: $CH_4/CO_2$

Figure B8

# Exchange coefficients and Degree of correlations

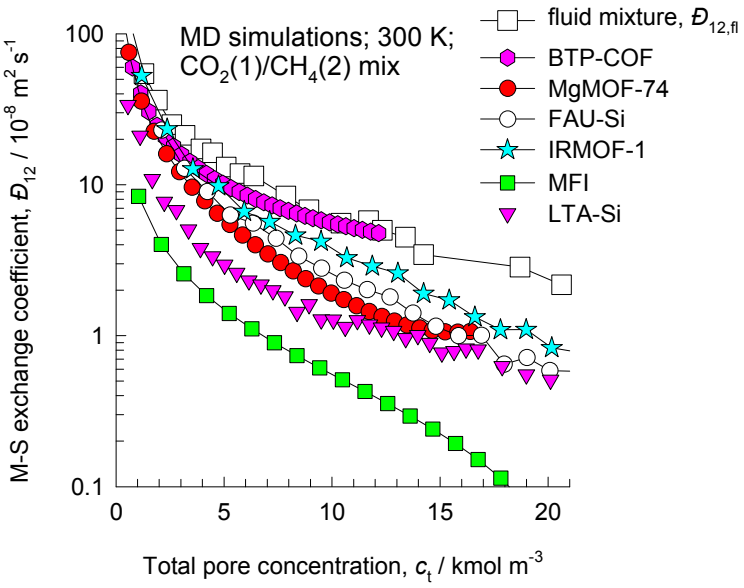


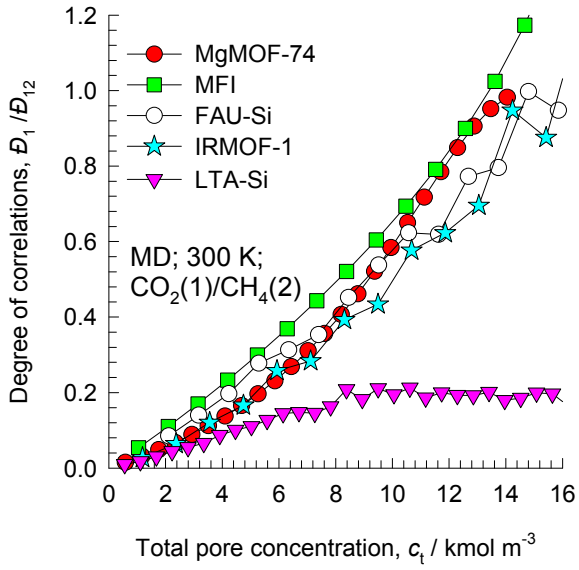


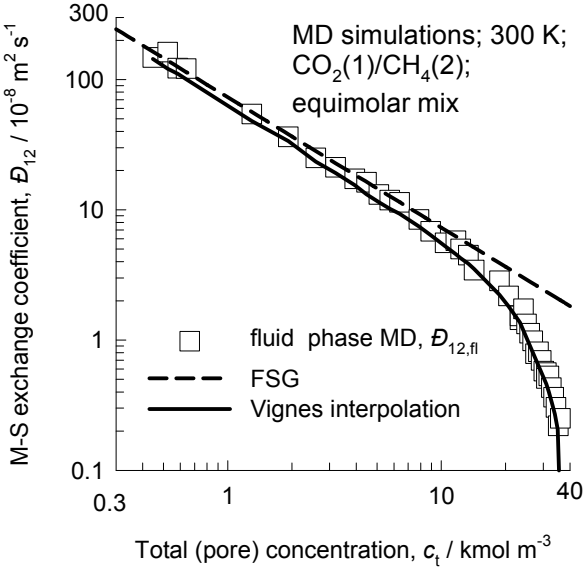


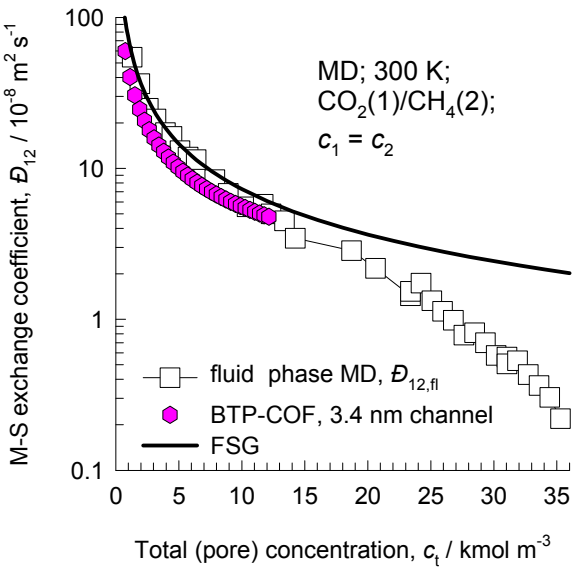

Figure B9

# Exchange coefficients as fraction of fluid phase $Đ_{12,fl}$

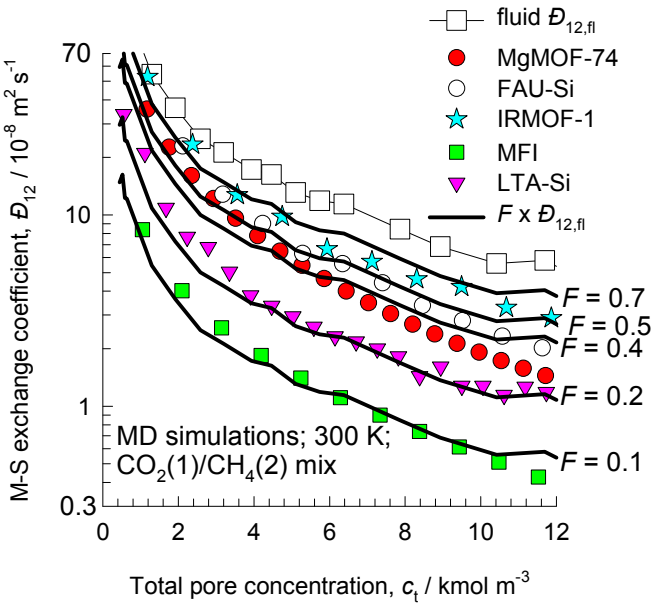


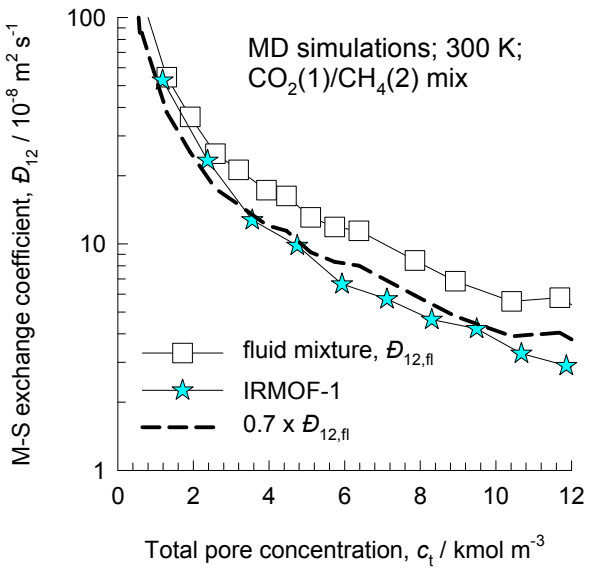

Figure B10

# Exchange coefficients as fraction of fluid phase $Đ_{12,fl}$

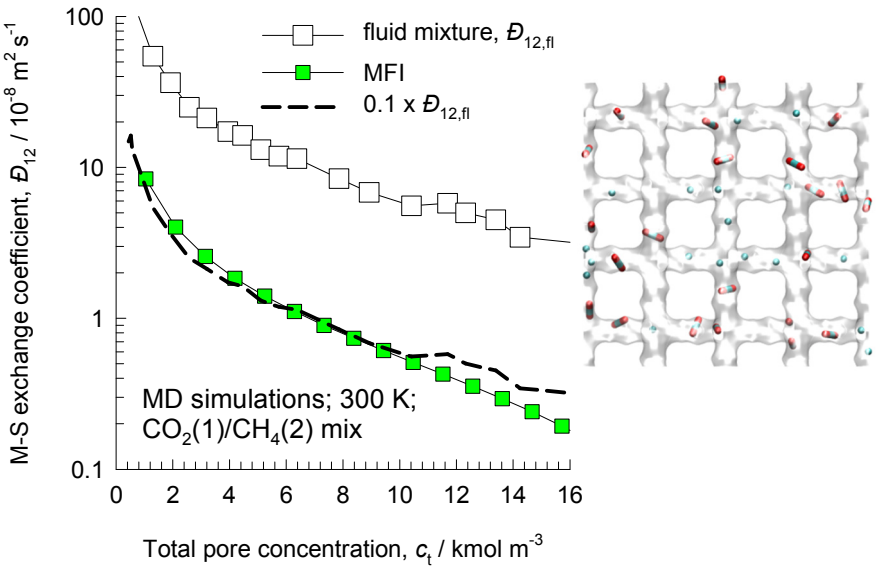


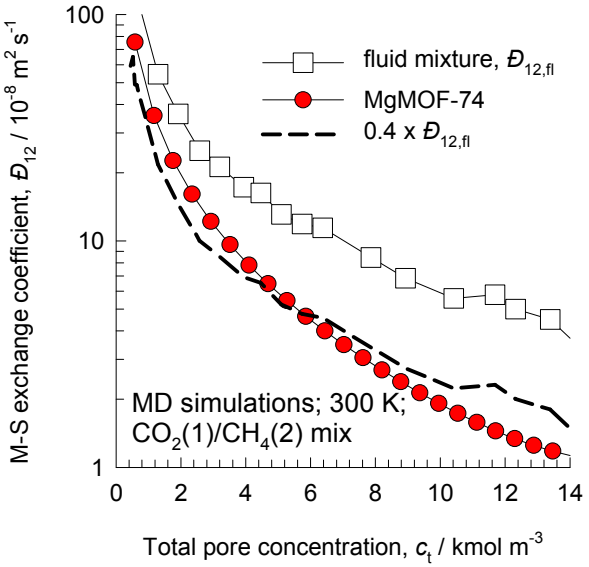


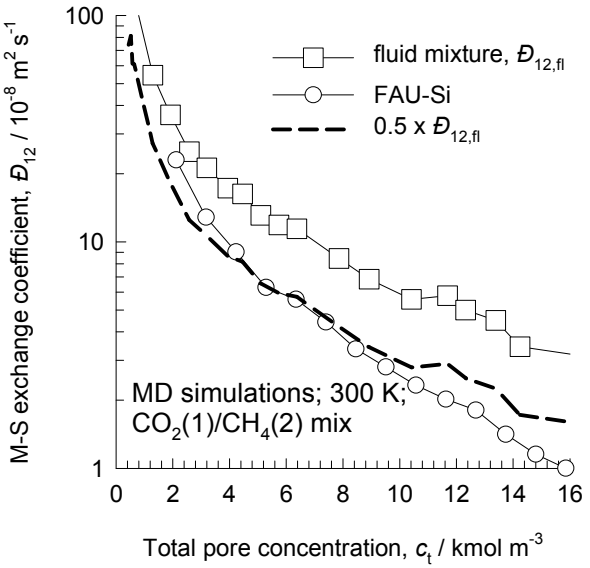


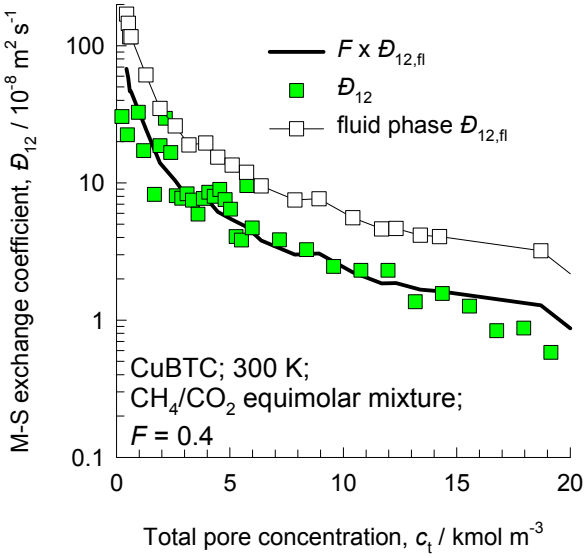


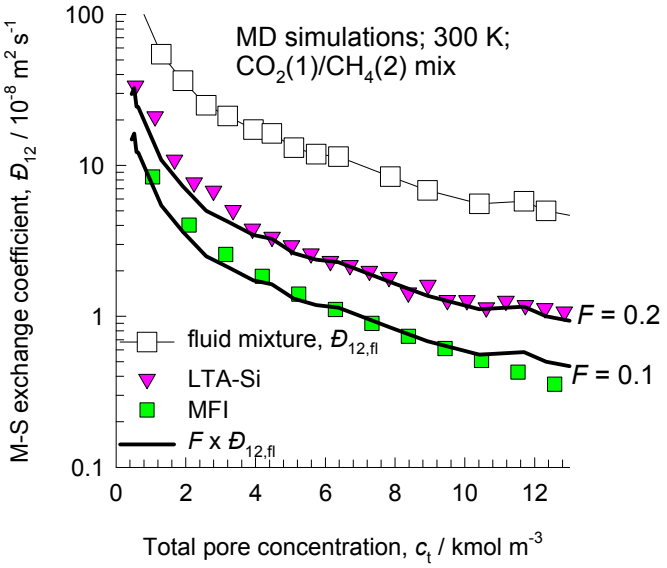

# Validation of the Vignes interpolation formula for $Đ_{12}$

Figure B11

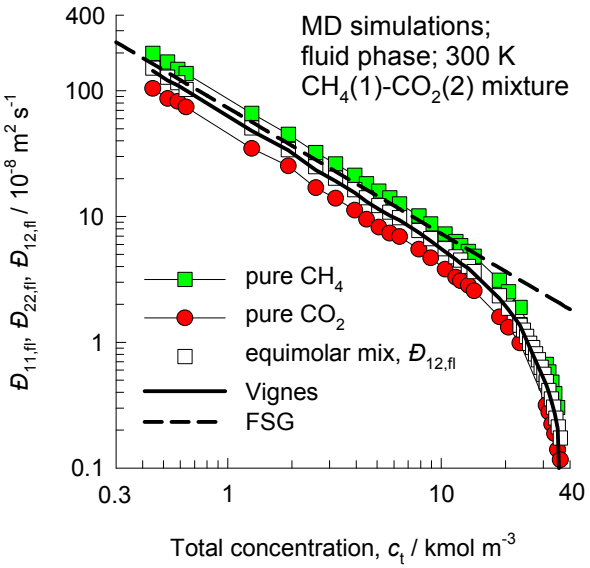


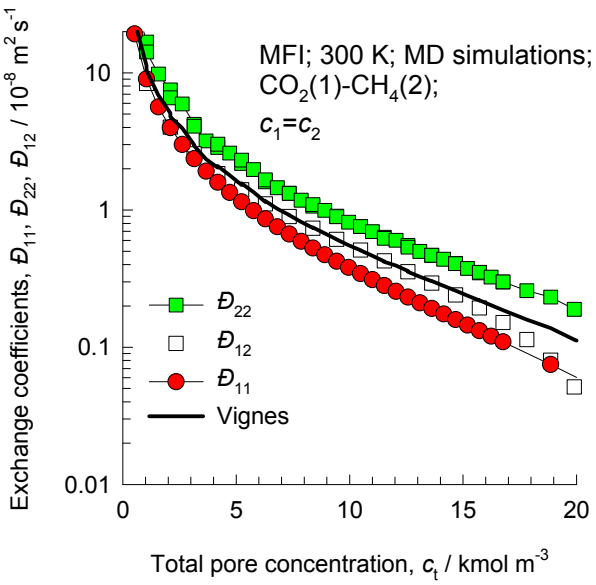


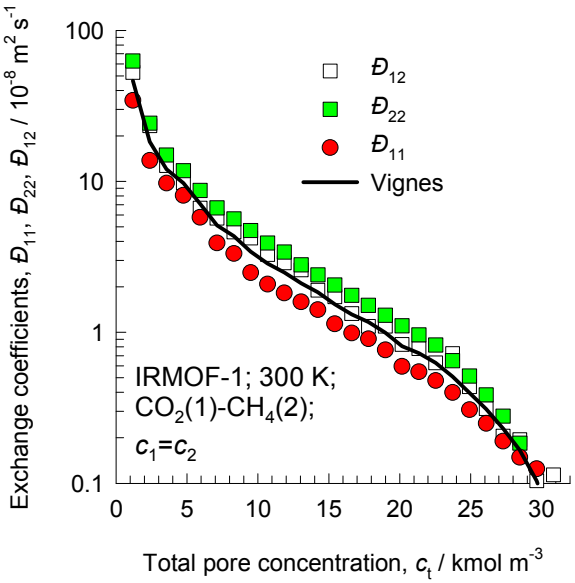


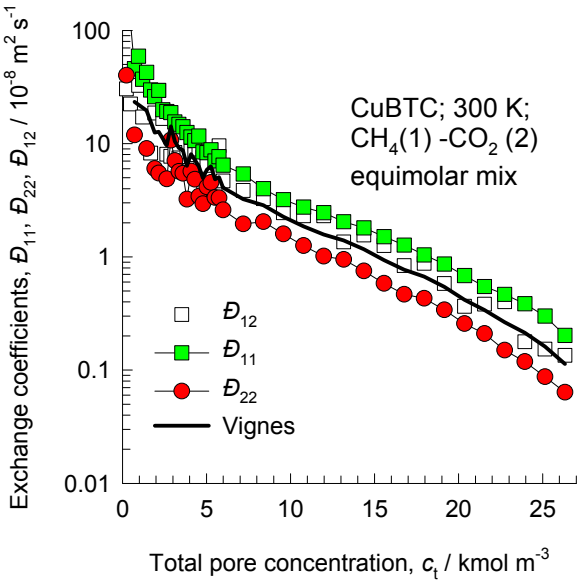


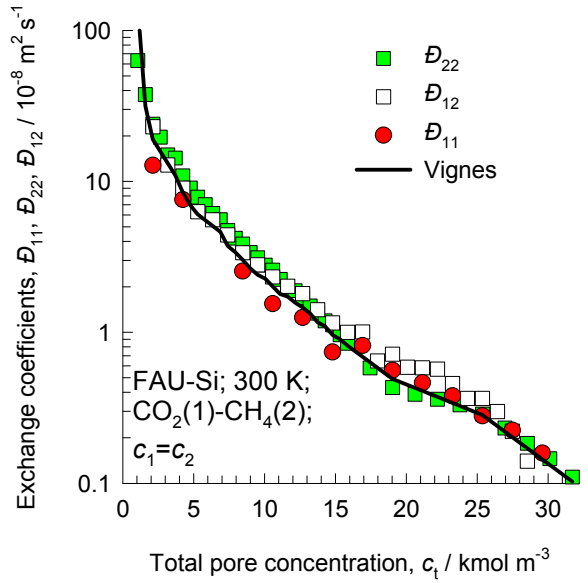

Figure B12

# Guest Mixture: $CO_2/N_2$

Figure B13

# Exchange coefficients and Degree of correlations

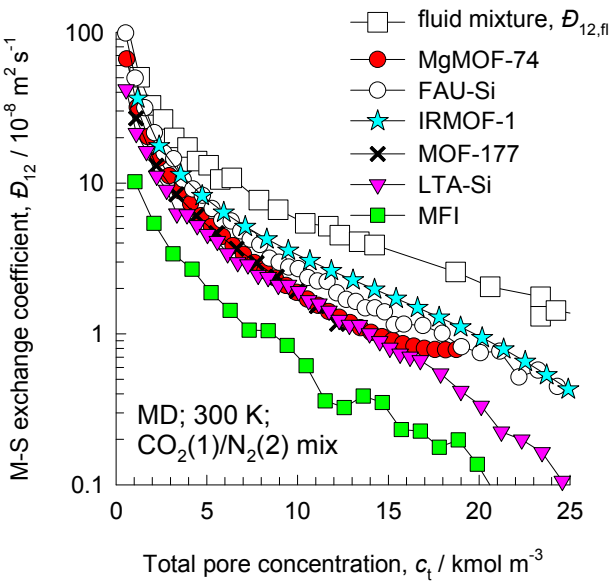


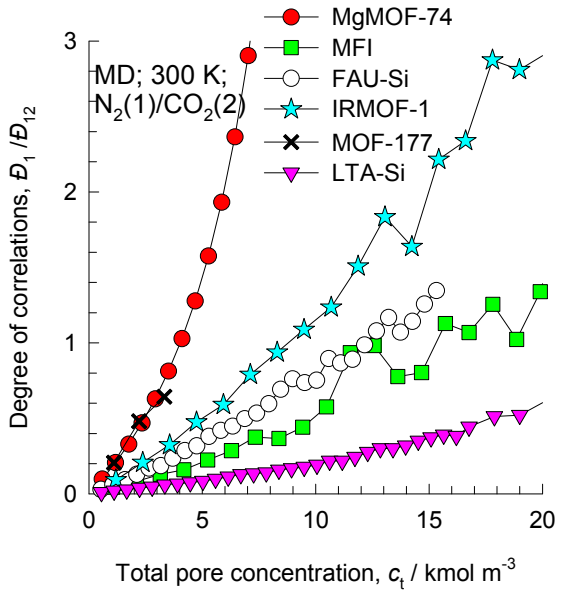


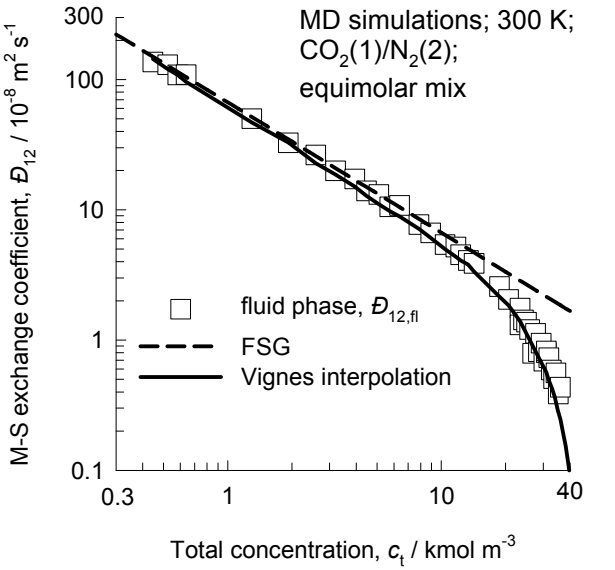

Figure B14

# Exchange coefficients as fraction of fluid phase $Đ_{12,fl}$

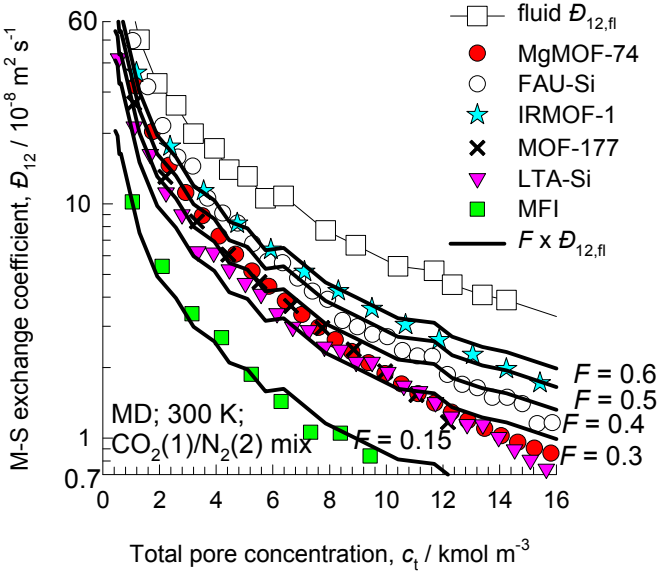


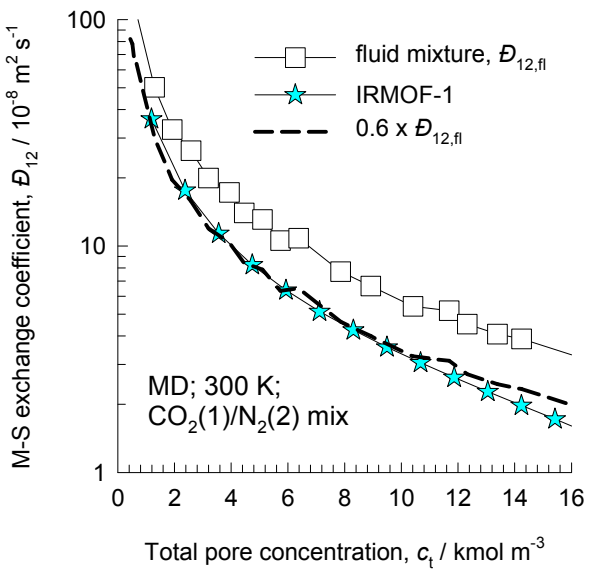

Figure B15

# Exchange coefficients as fraction of fluid phase $Đ_{12,fl}$

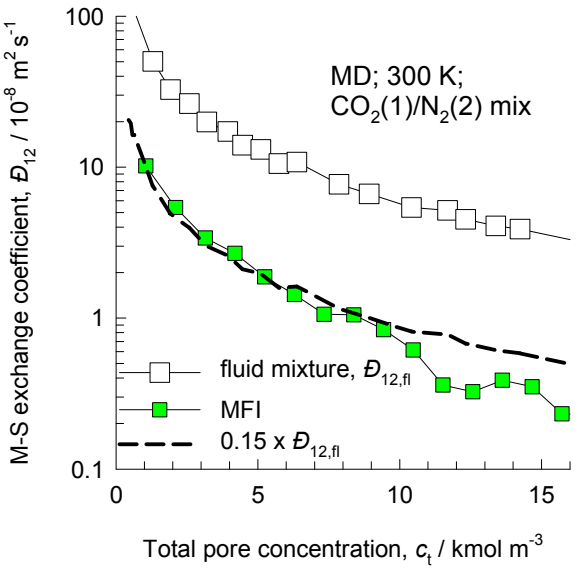


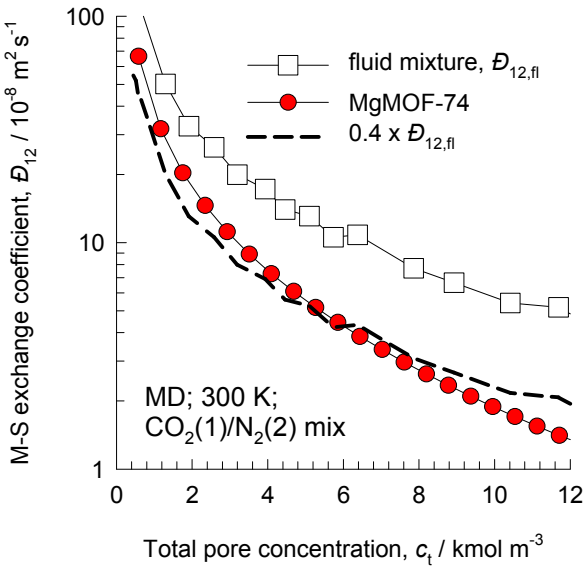


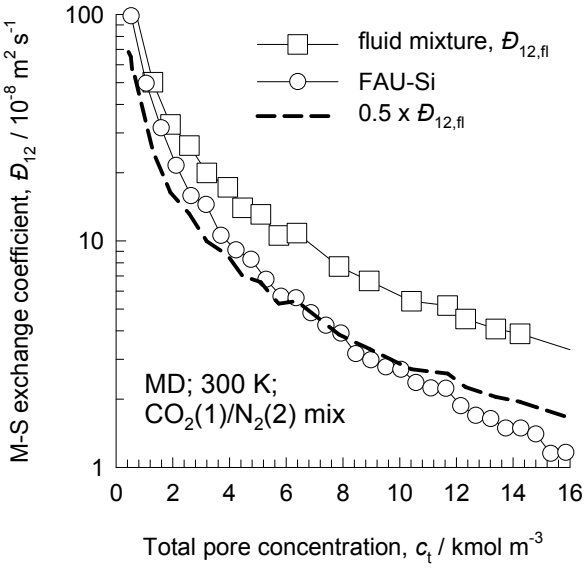


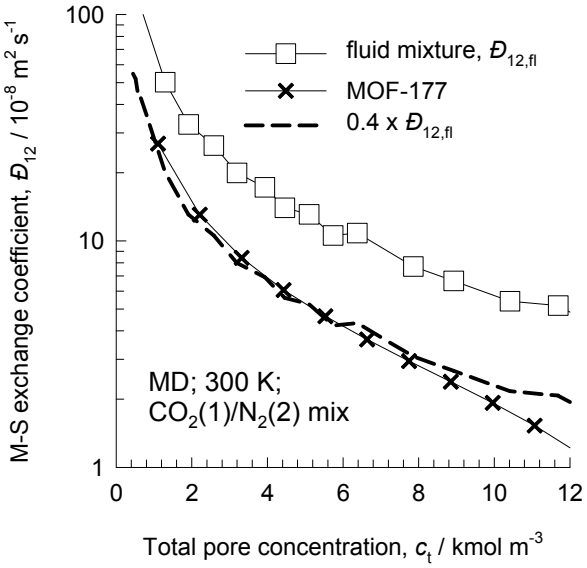


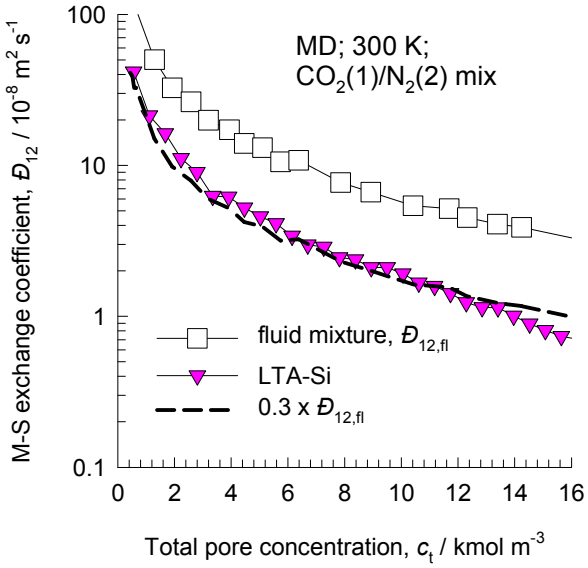

# Validation of the Vignes interpolation formula for $Đ_{12}$

Figure B16

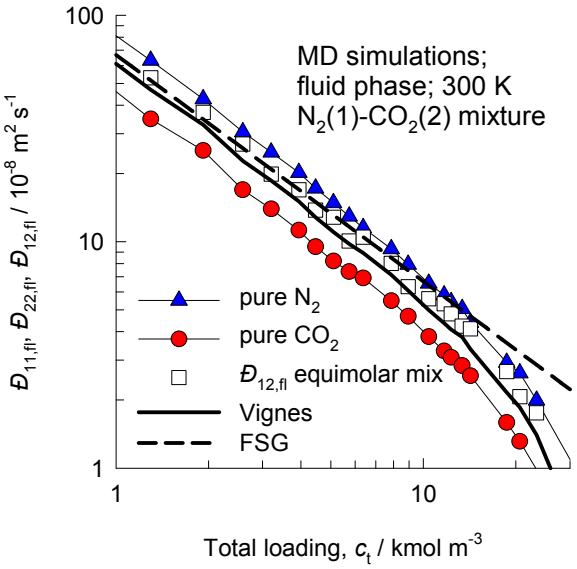


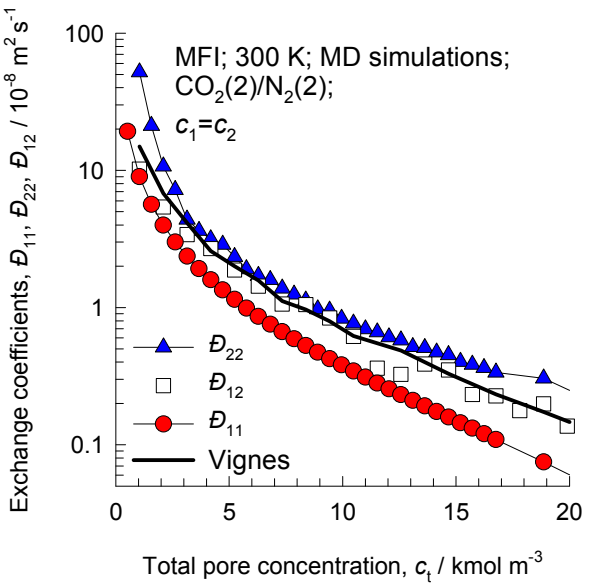

Figure B17

# Guest Mixture: $CH_4/C_2H_6$

Figure B18

# Exchange coefficients and Degree of correlations

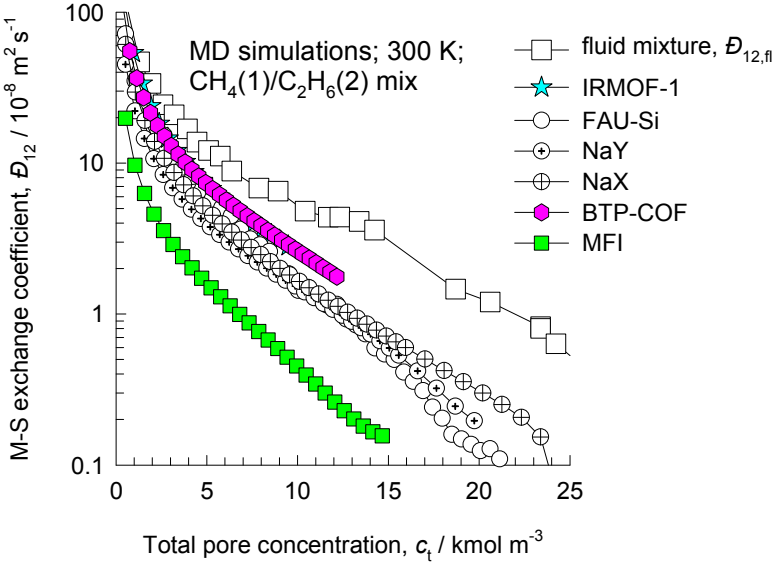


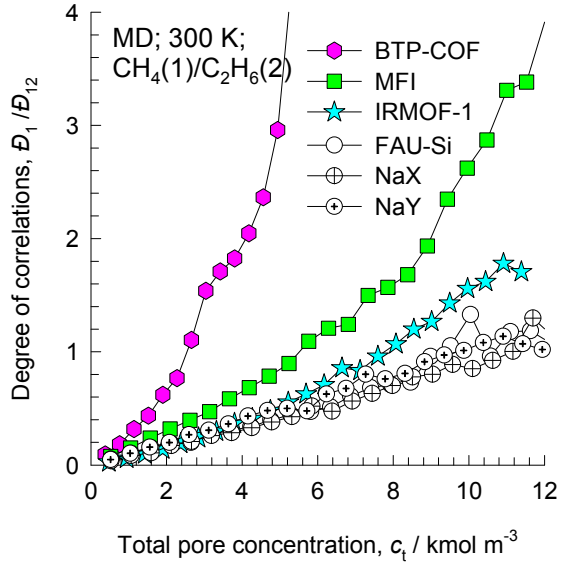


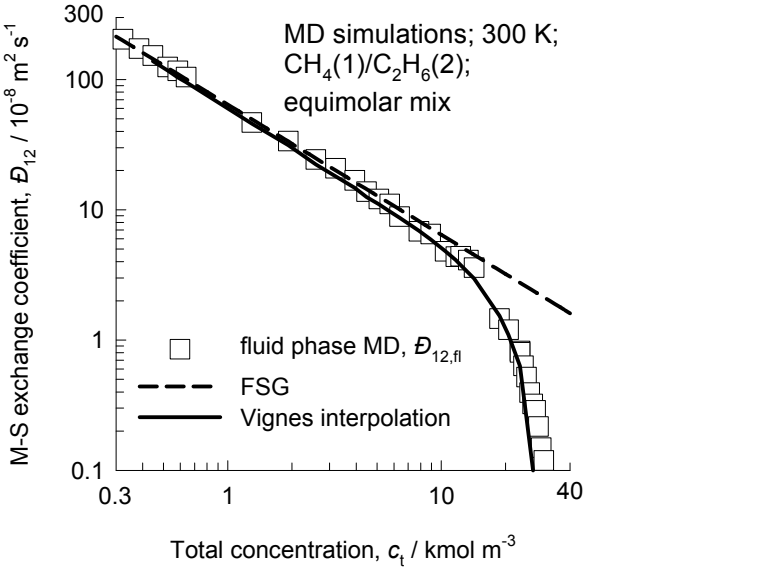


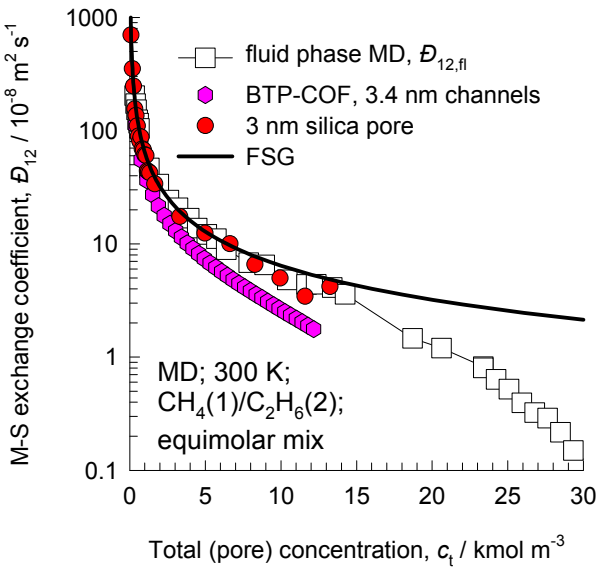

Figure B19

# Exchange coefficients as fraction of fluid phase $Đ_{12,fl}$

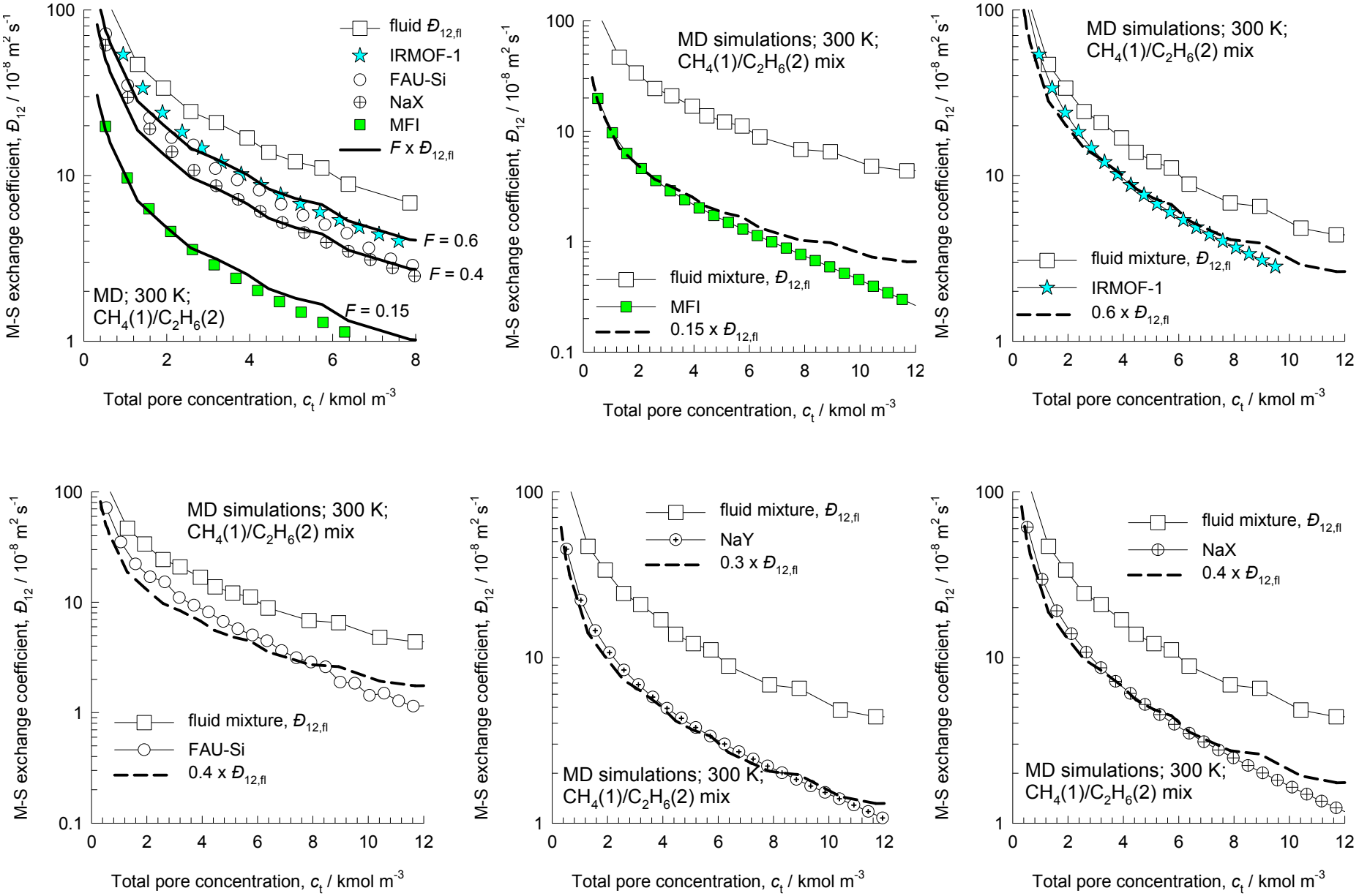

# Validation of the Vignes interpolation formula for $Đ_{12}$

Figure B20

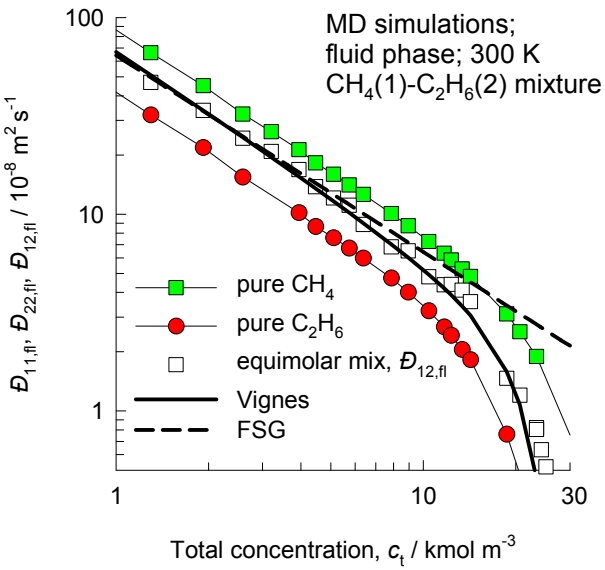


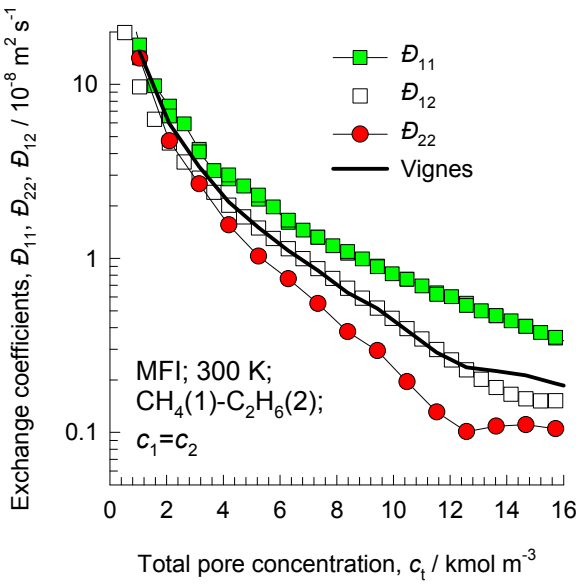


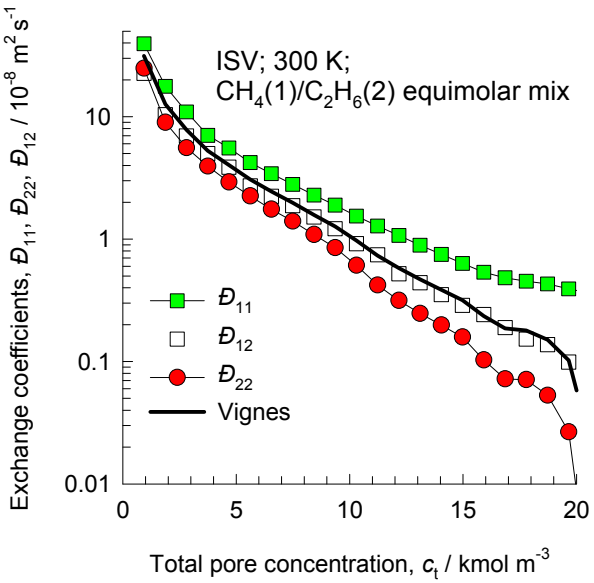


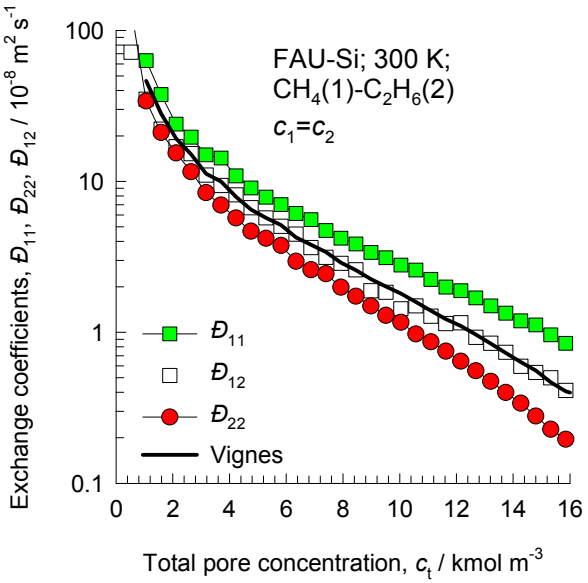


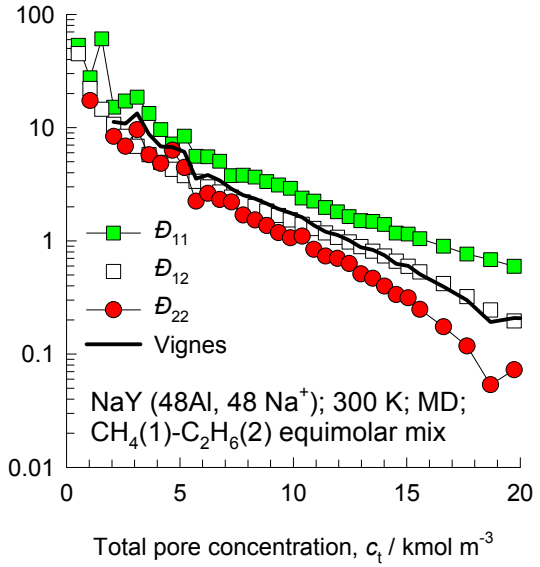


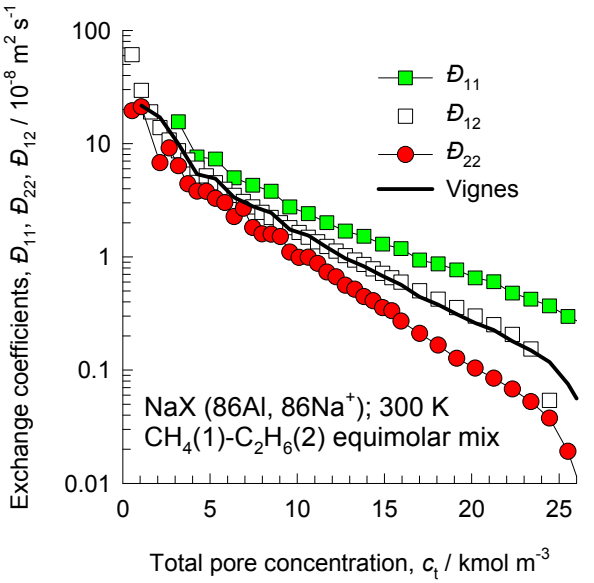

Figure B21

# Guest Mixture: $CH_4/C_3H_8$

Figure B22

# Exchange coefficients and Degree of correlations

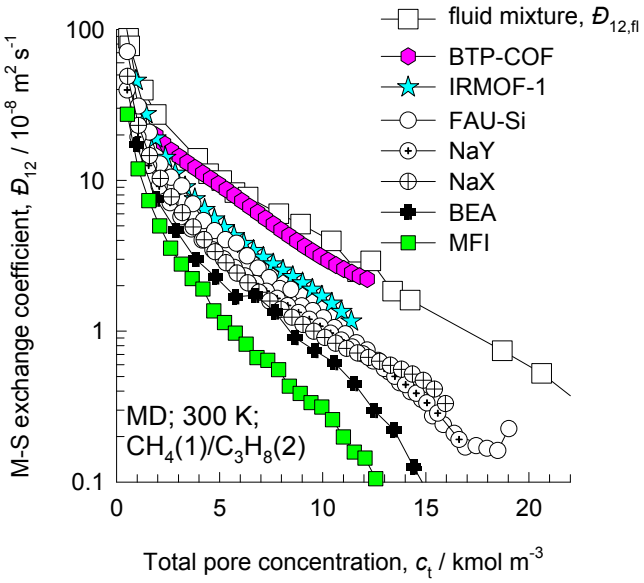


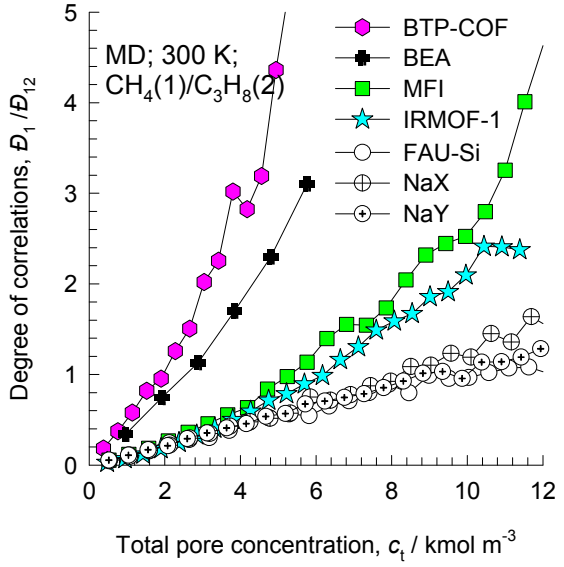


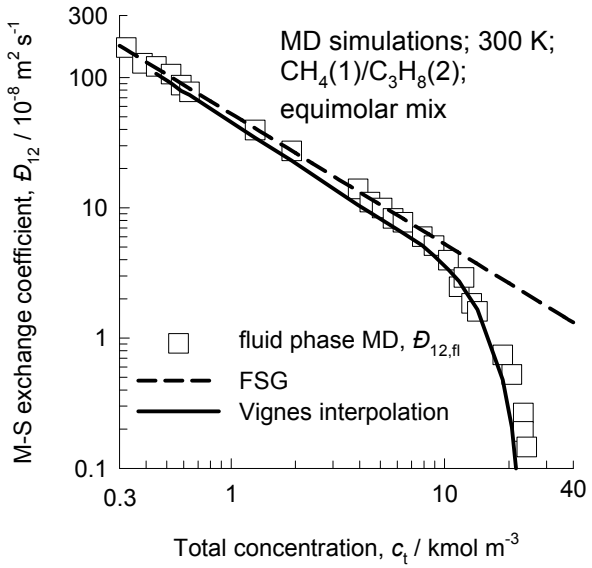


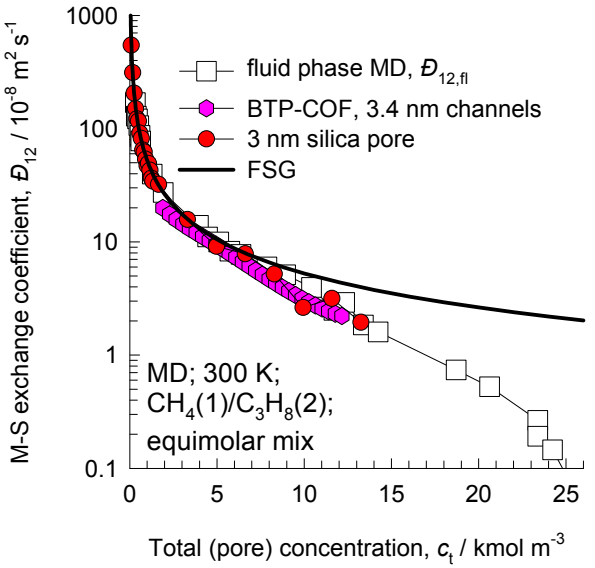

Figure B23

# Exchange coefficients as fraction of fluid phase $Đ_{12,fl}$

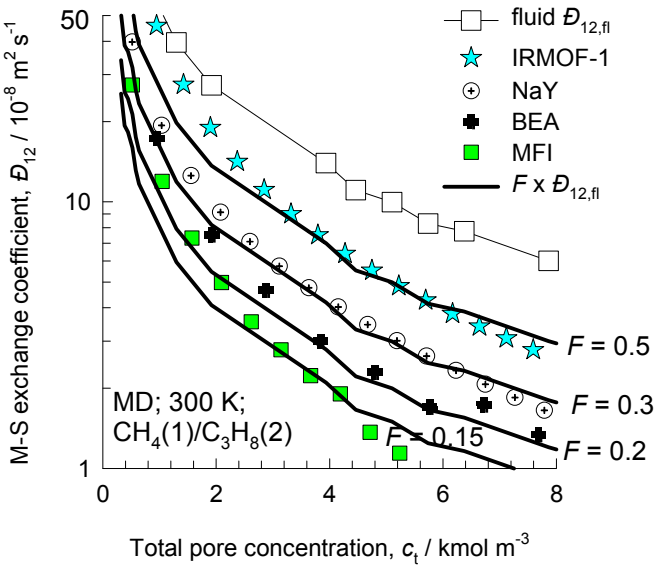


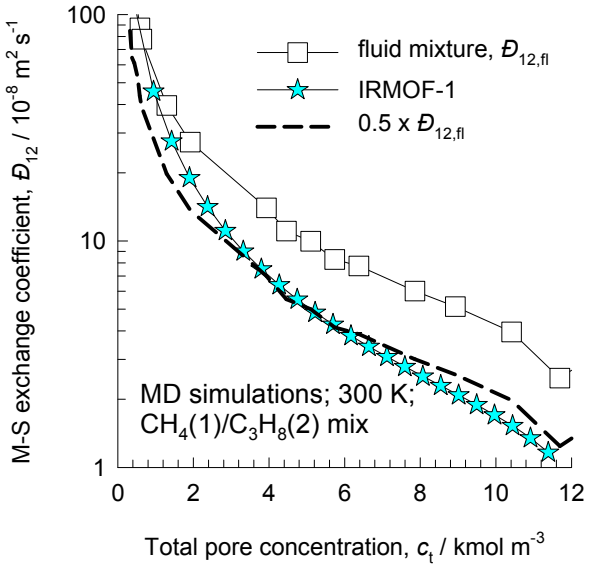

Figure B24

# Exchange coefficients as fraction of fluid phase $Đ_{12,fl}$

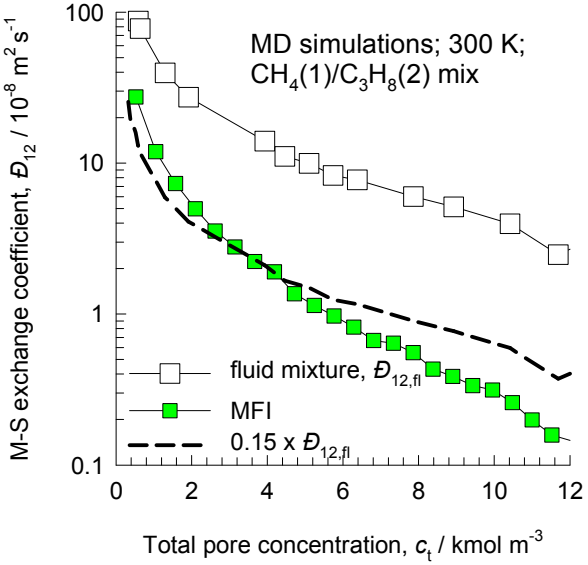


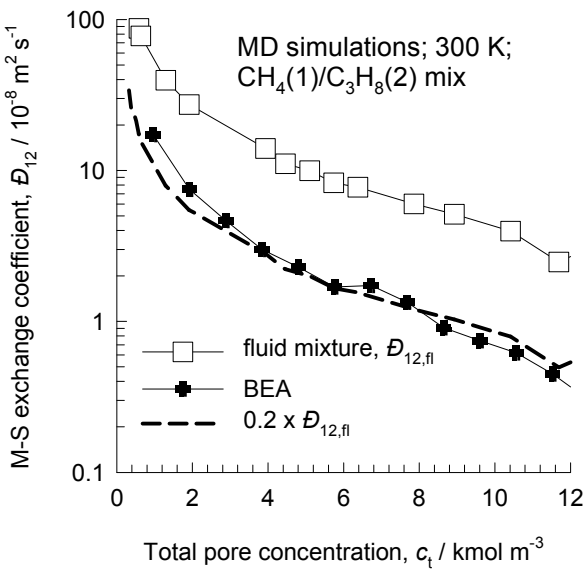


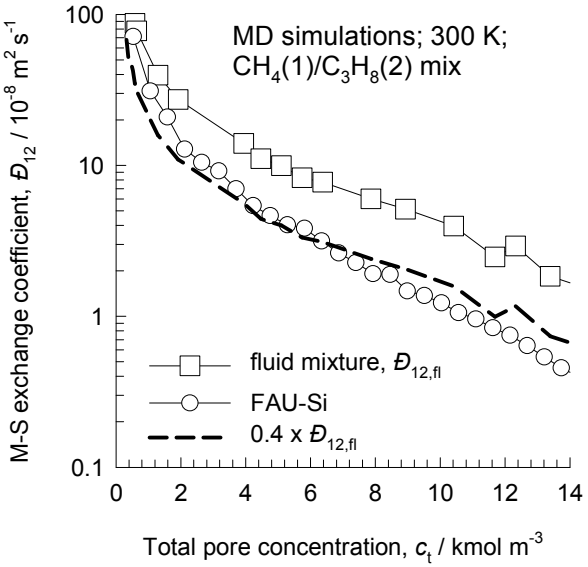


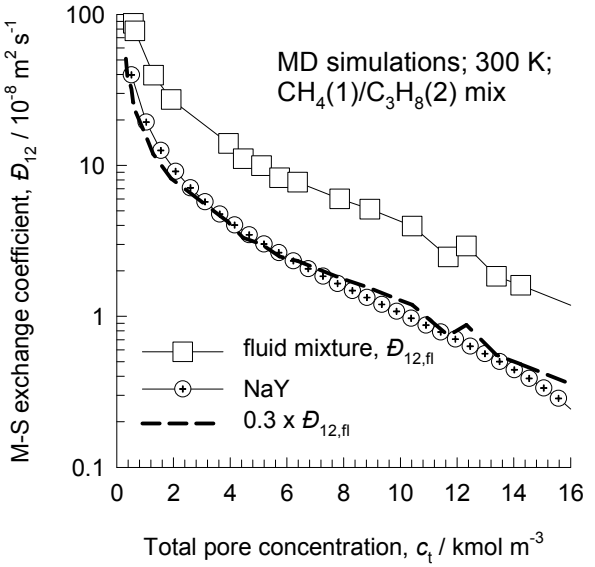


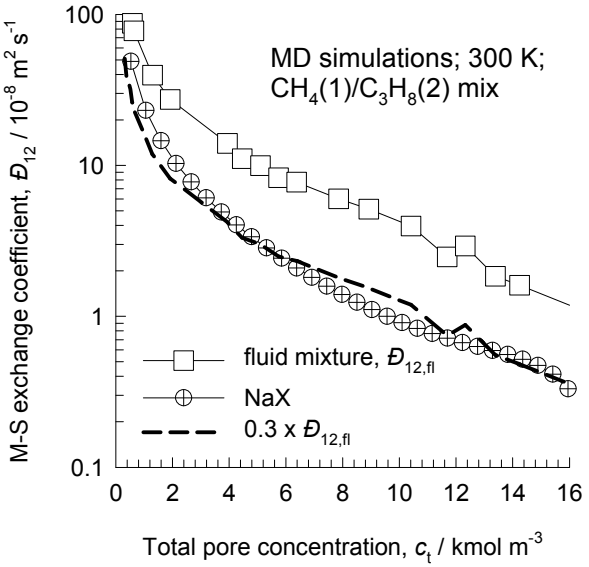

# Validation of the Vignes interpolation formula for $Đ_{12}$

Figure B25

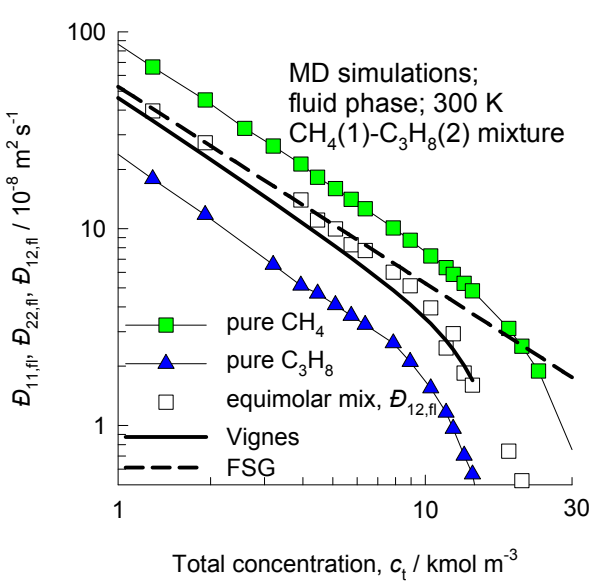


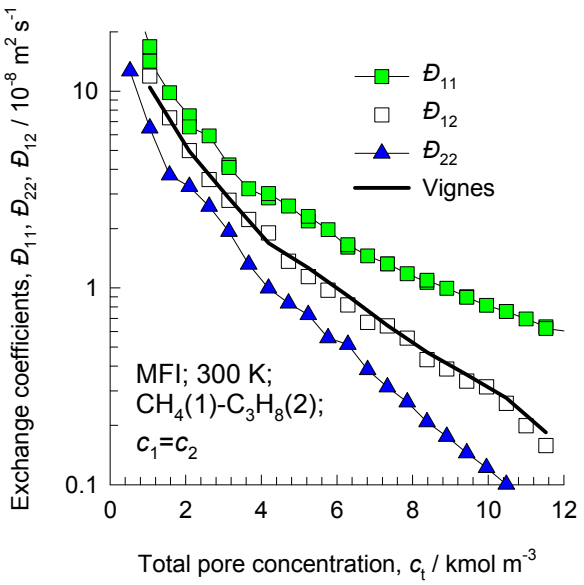


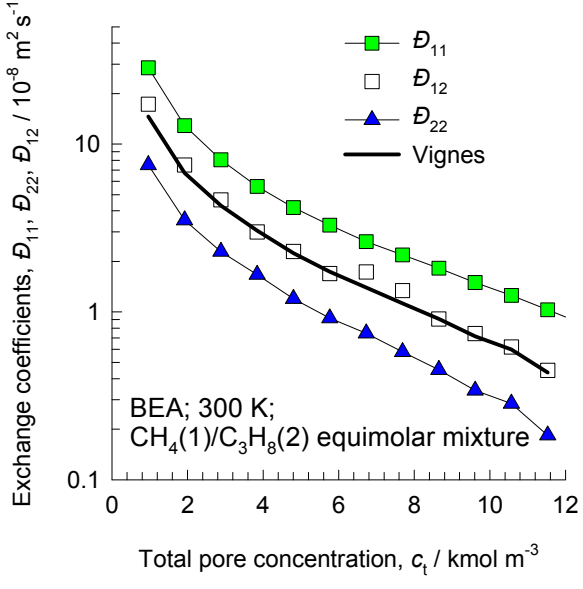


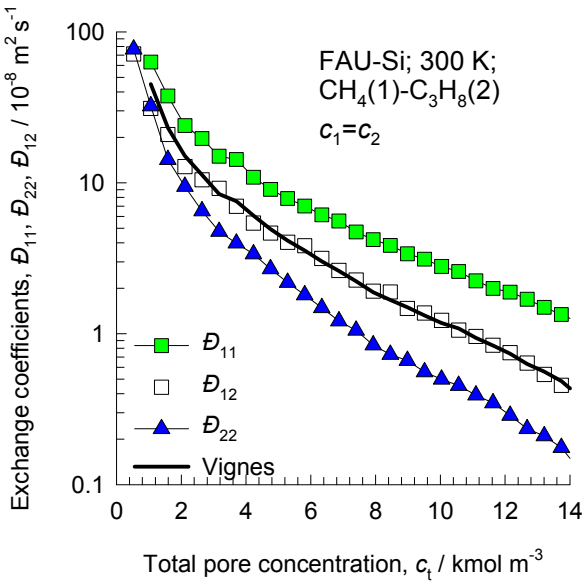


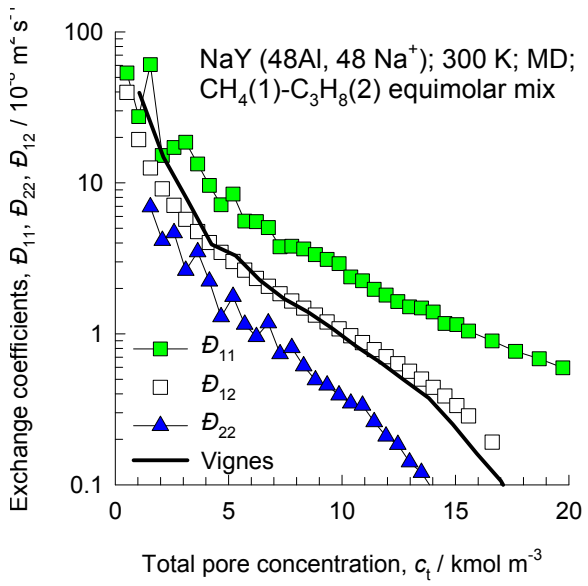


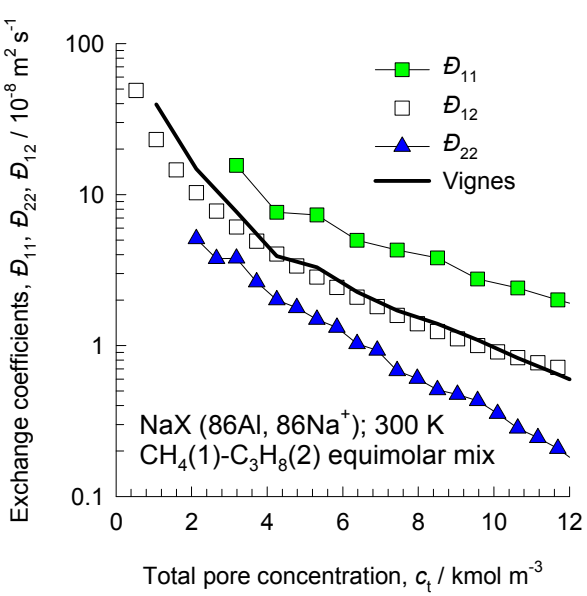

# Guest Mixture: $CH_4/nC_4H_{10}$

Figure B27

# Exchange coefficients and Degree of correlations

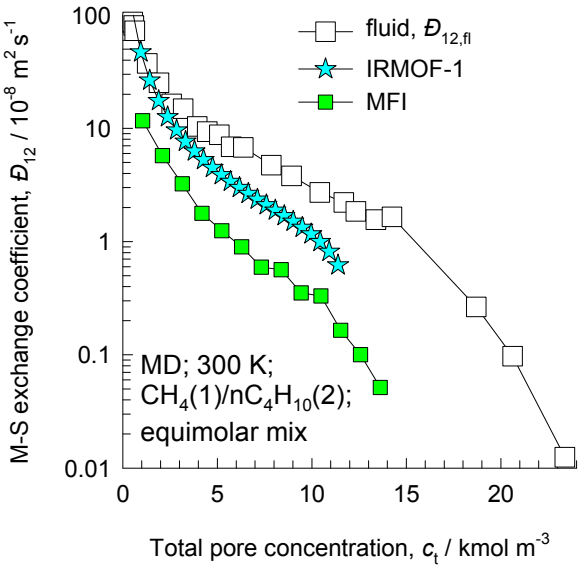


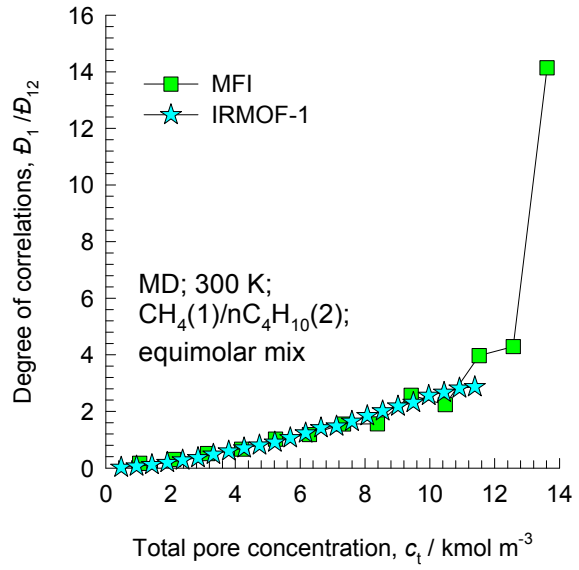


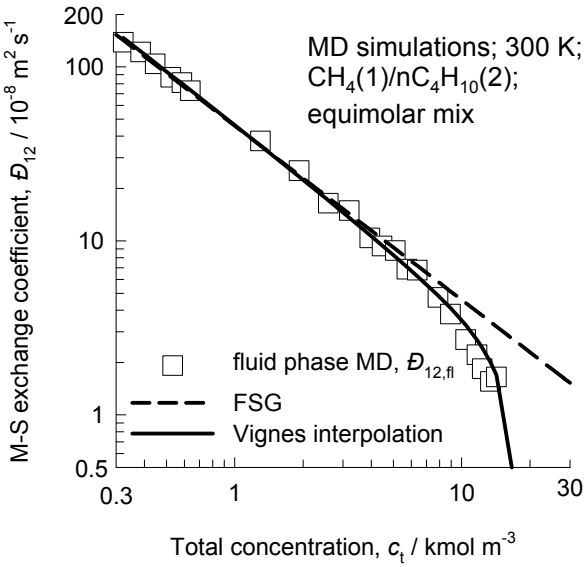


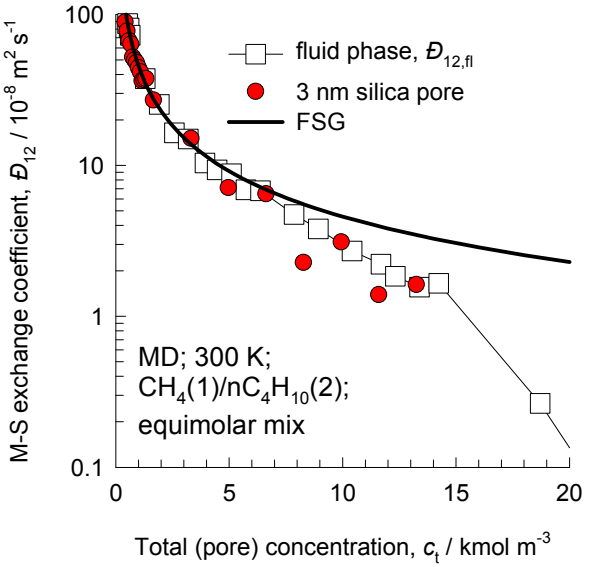

Figure B28

# Exchange coefficients as fraction of fluid phase $Đ_{12,fl}$

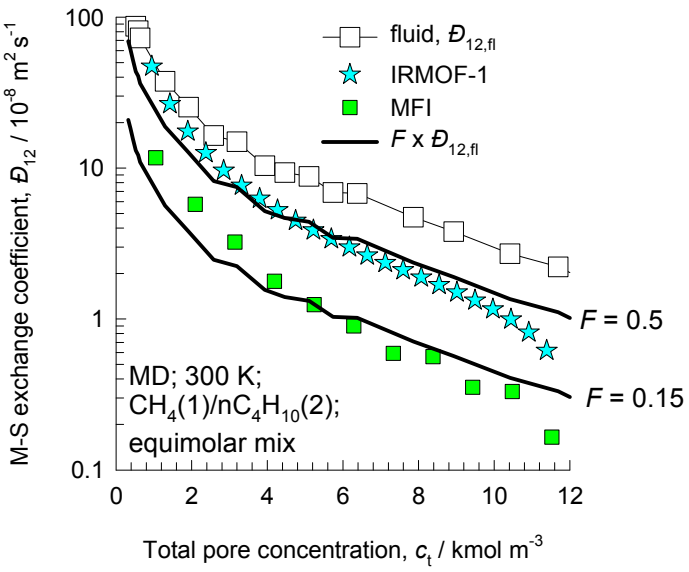

# Validation of the Vignes interpolation formula for $Đ_{12}$

Figure B29

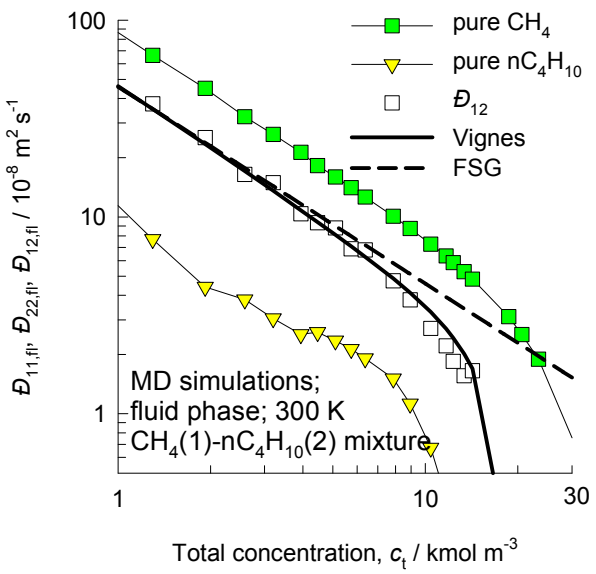

Figure B30

# Guest Mixture: $H_2/CH_4$

Figure B31

# Exchange coefficients and Degree of correlations

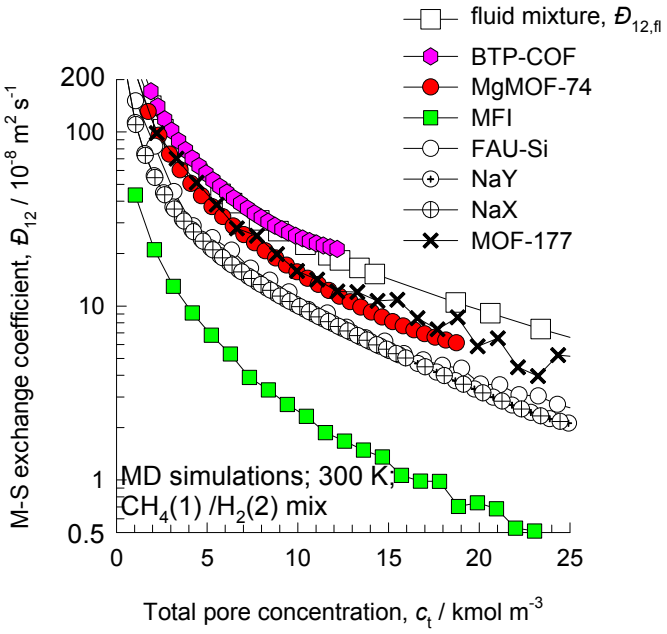


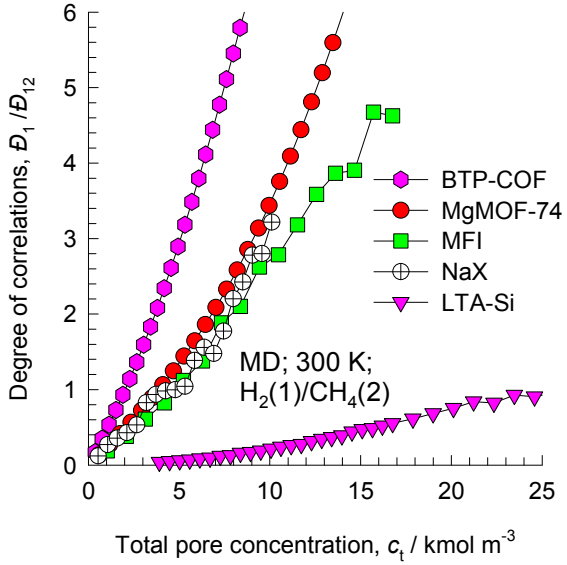


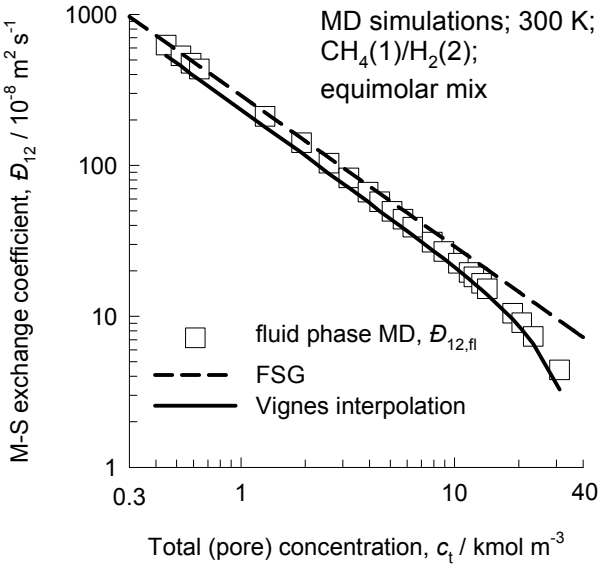


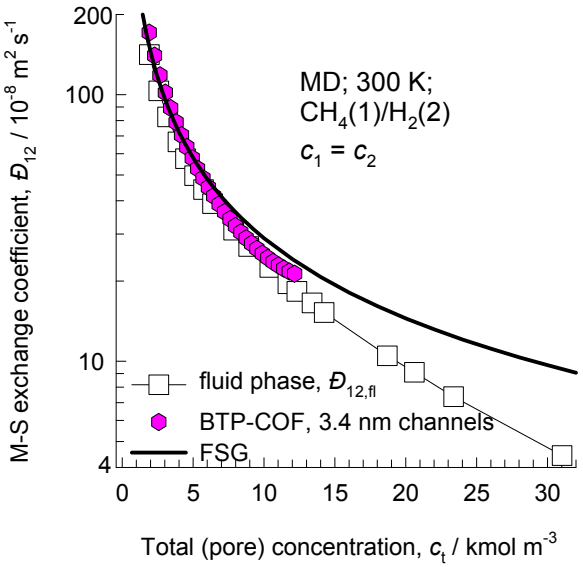

Figure B32

# Exchange coefficients as fraction of fluid phase $Đ_{12,fl}$

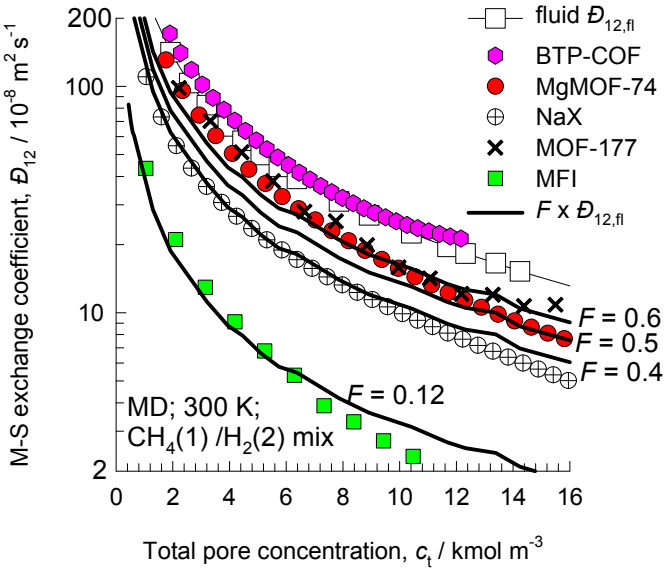


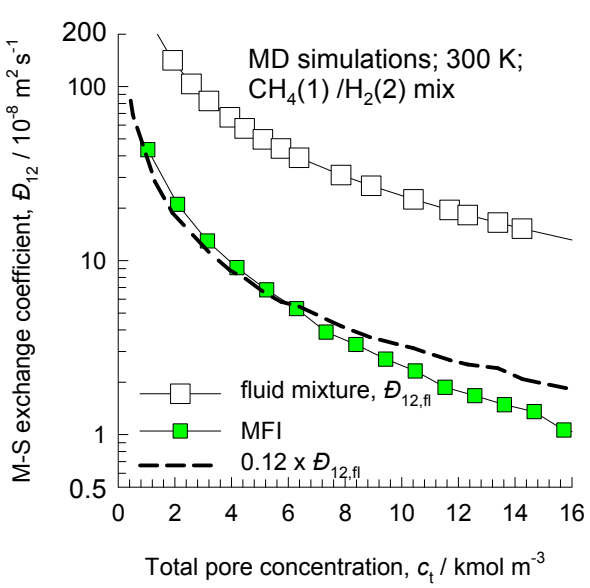


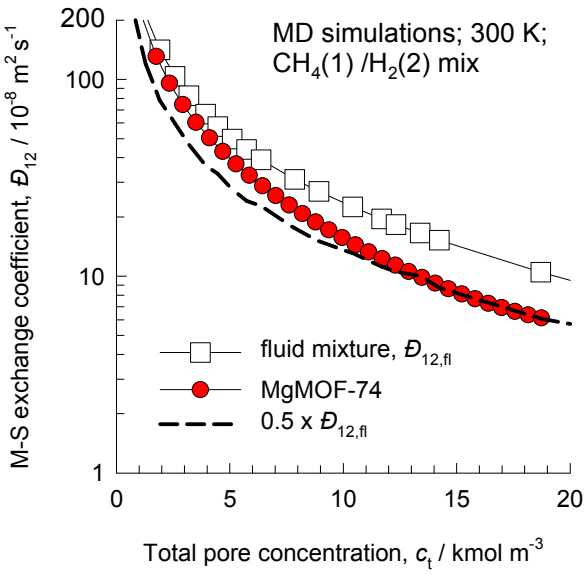


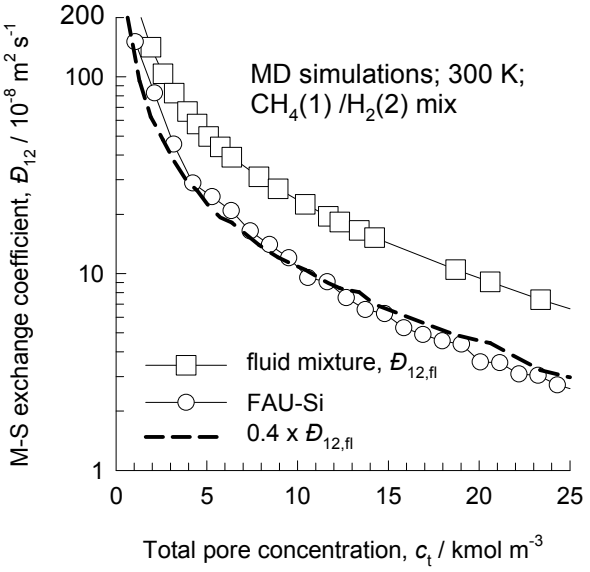


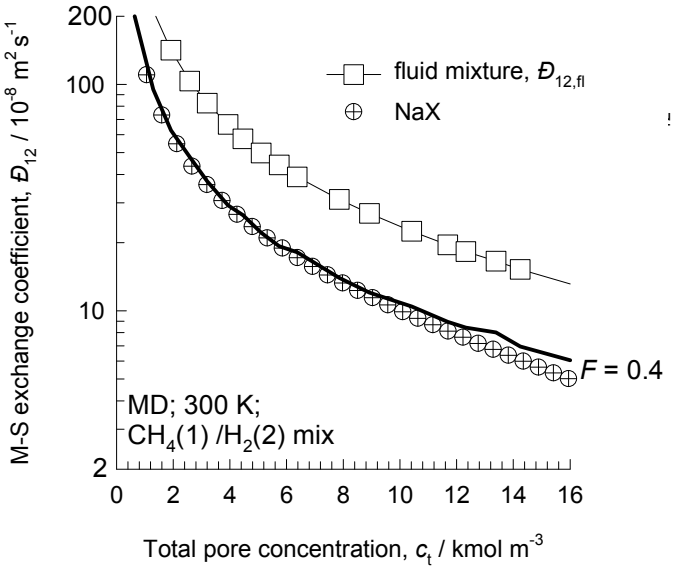


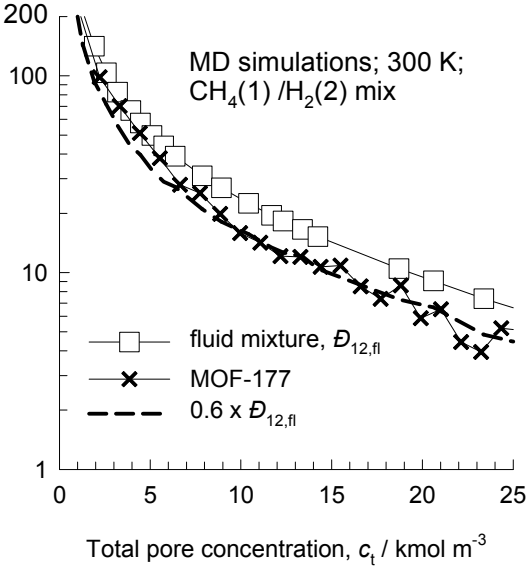

# Validation of the Vignes interpolation formula for $Đ_{12}$

Figure B33

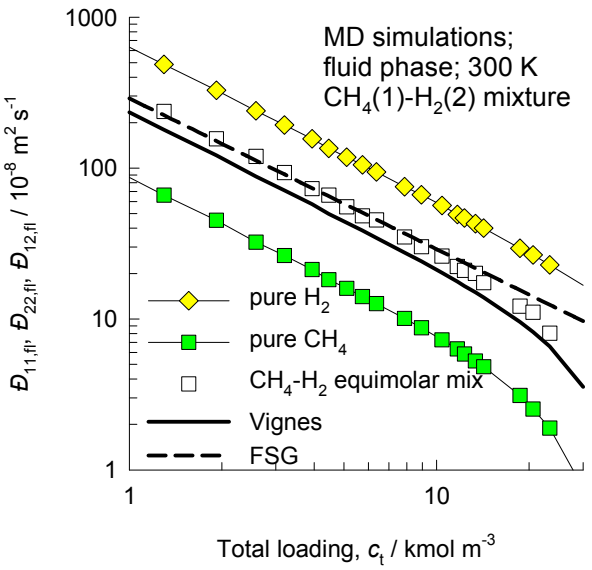


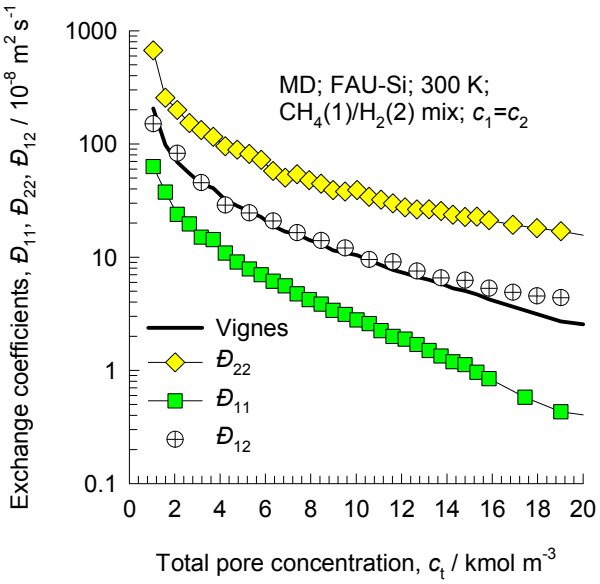

# Guest Mixture: $N_2/CH_4$

# Validation of the Vignes interpolation formula for $Đ_{12}$

Figure B35

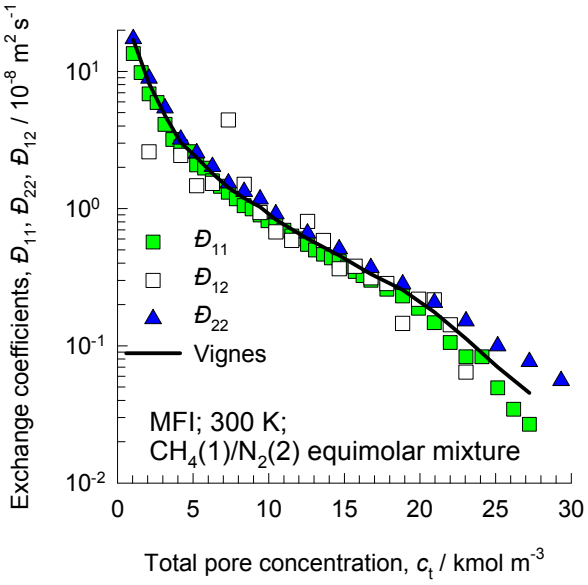


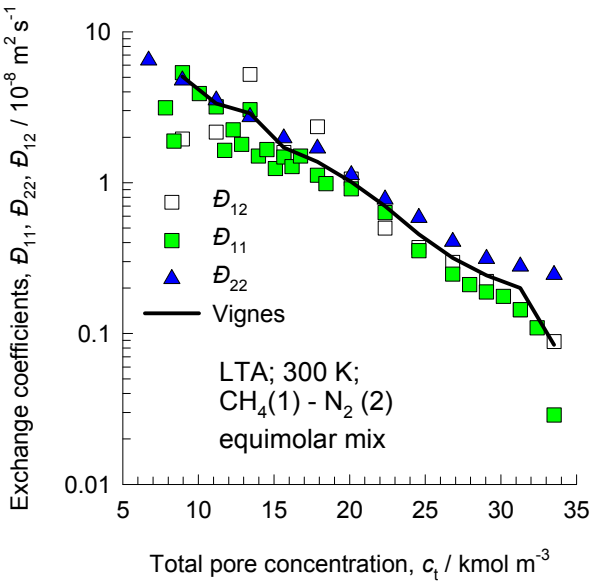

Figure B36

# Guest Mixture: Ne/Ar

Figure B37

# Exchange coefficients and Degree of correlations

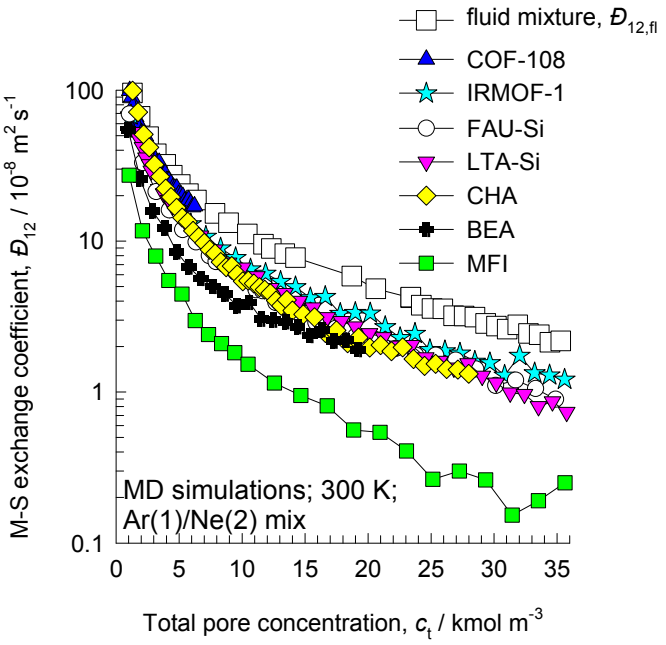


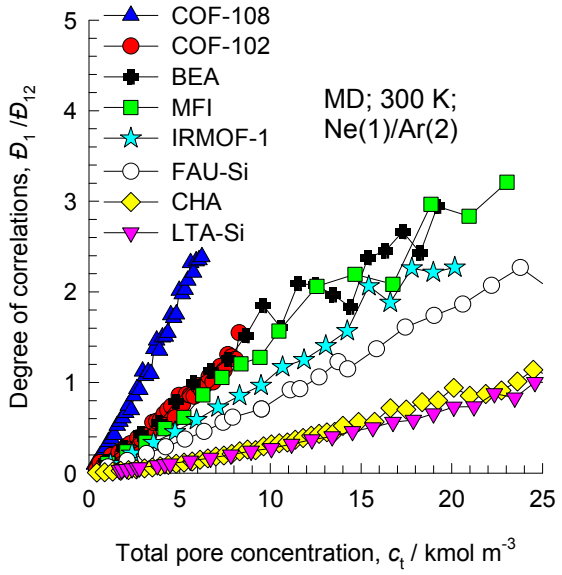


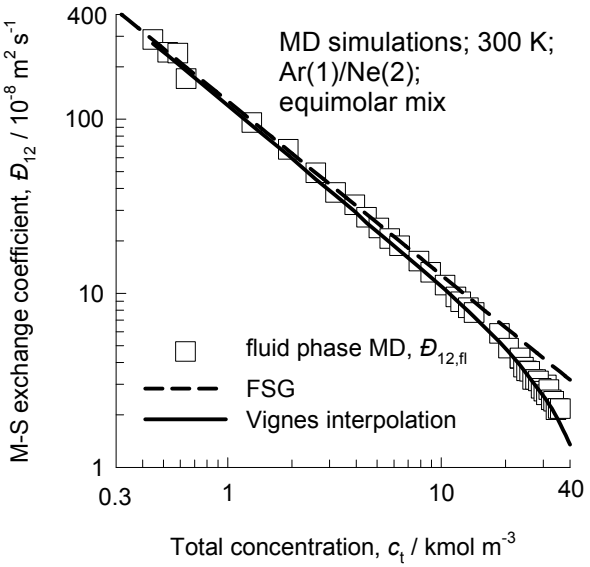

Figure B38

# Exchange coefficients as fraction of fluid phase $Đ_{12,fl}$

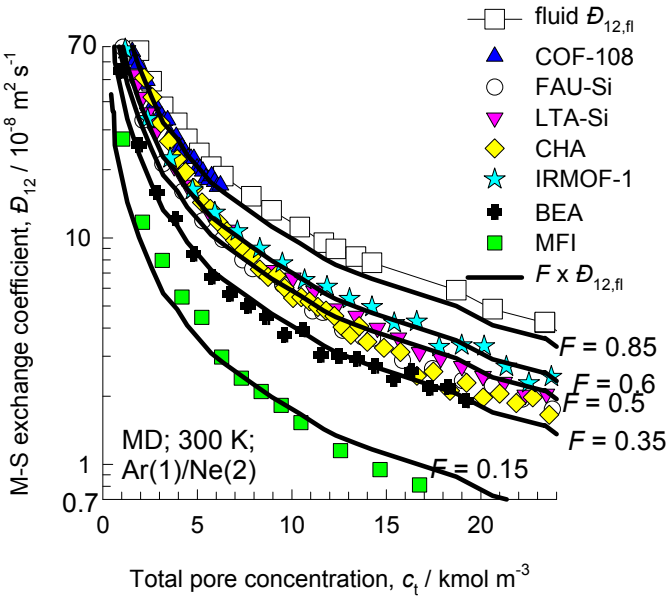


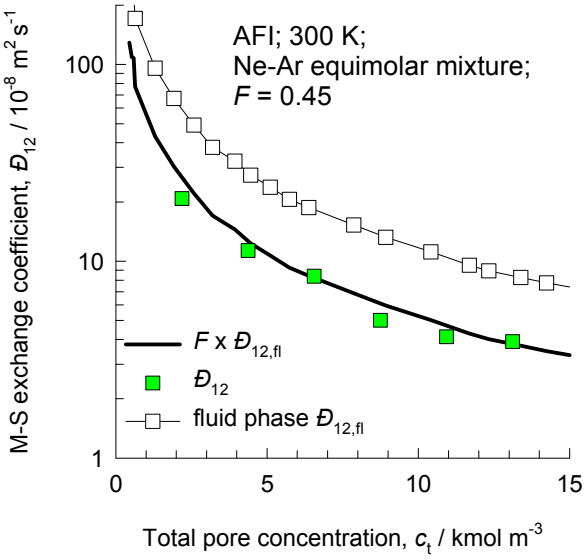


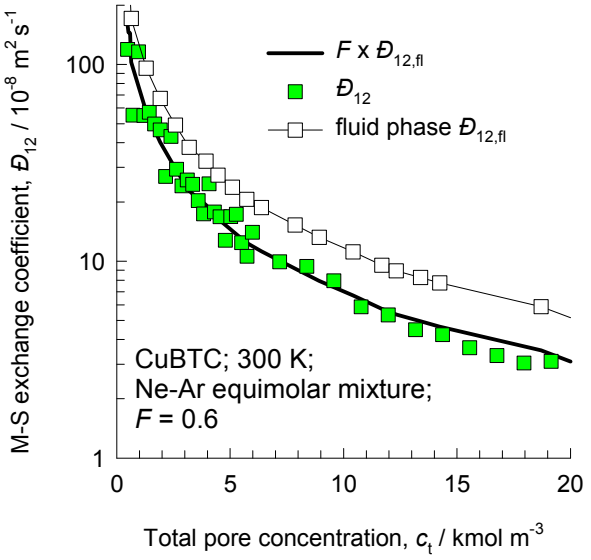


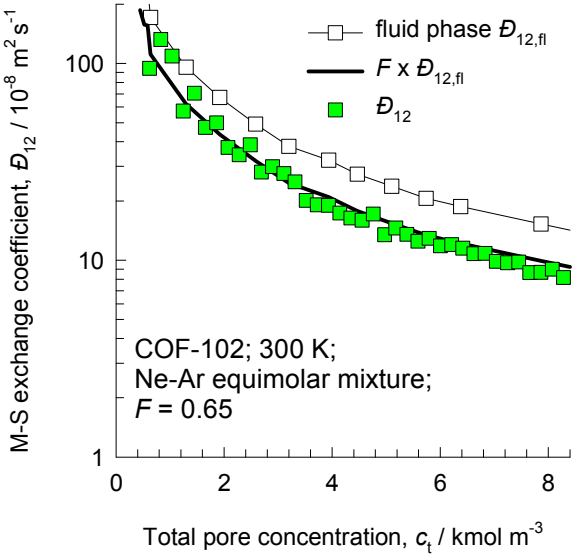


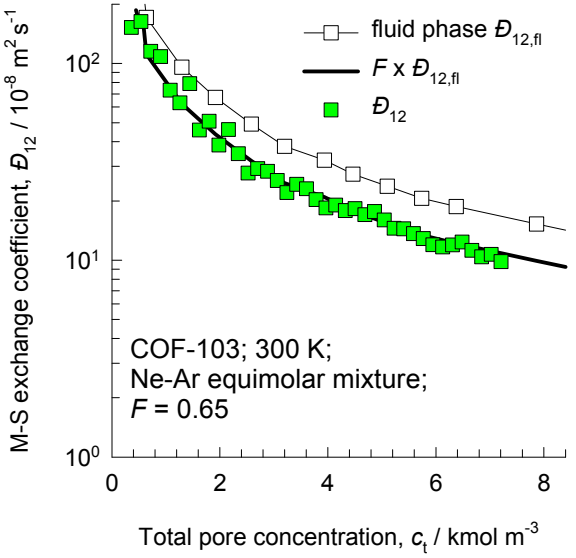


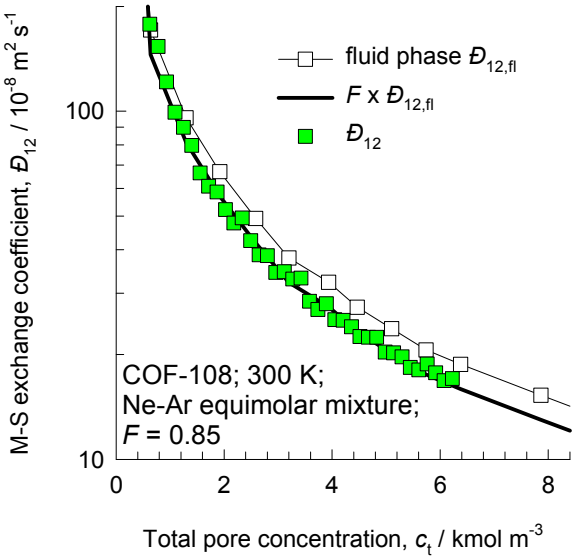

Figure B39

# Exchange coefficients as fraction of fluid phase $Đ_{12,fl}$

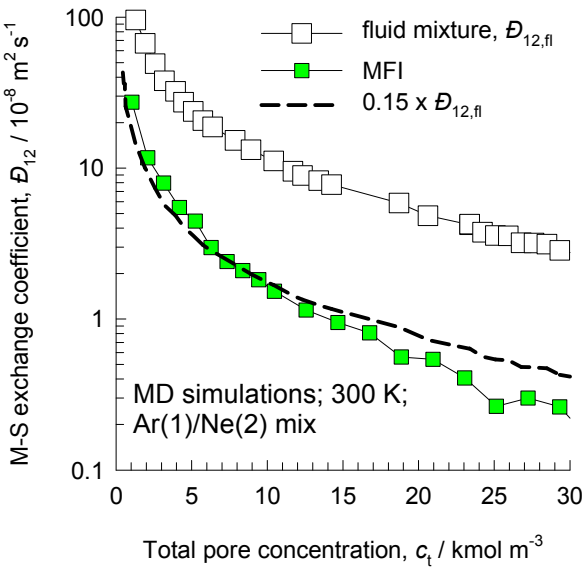


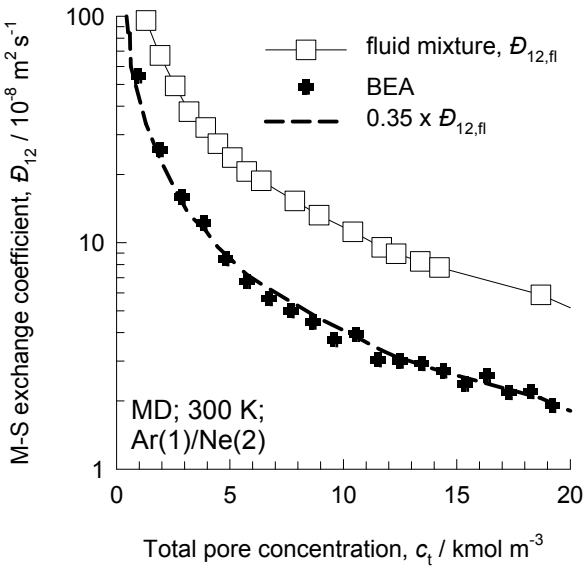


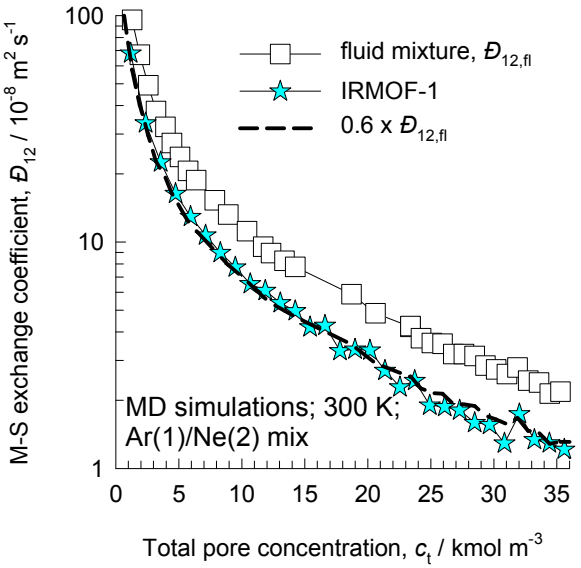


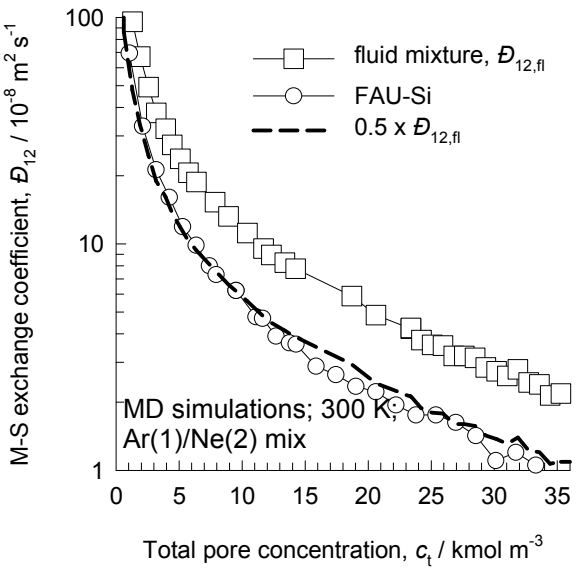


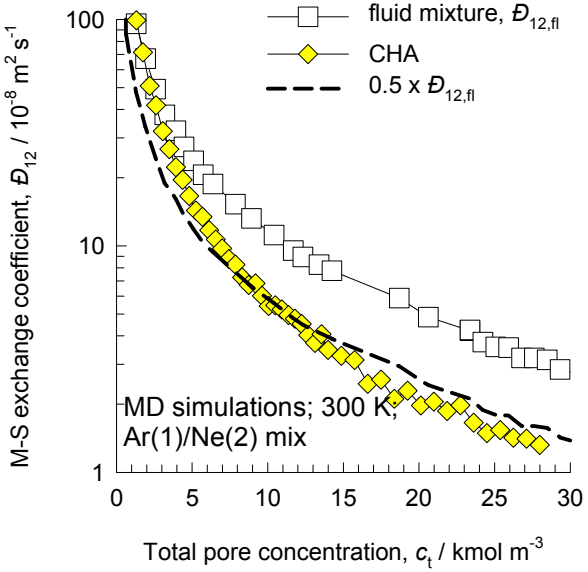


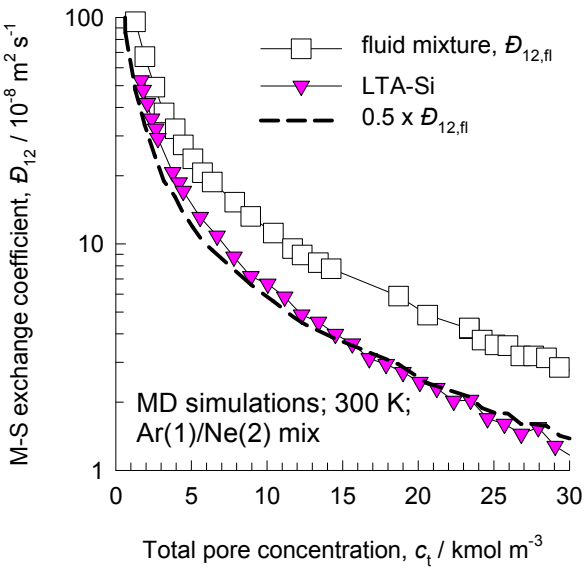

# Validation of the Vignes interpolation formula for $Đ_{12}$

Figure B40

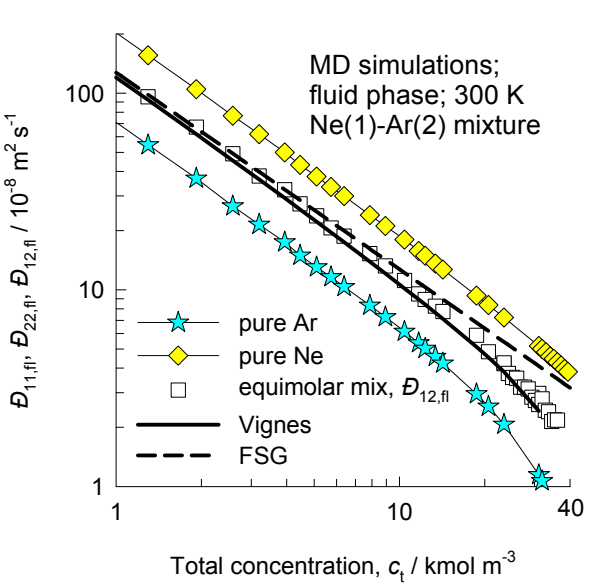


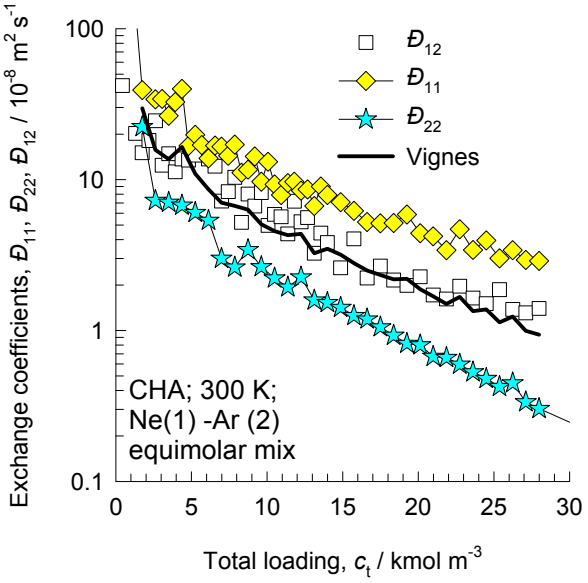


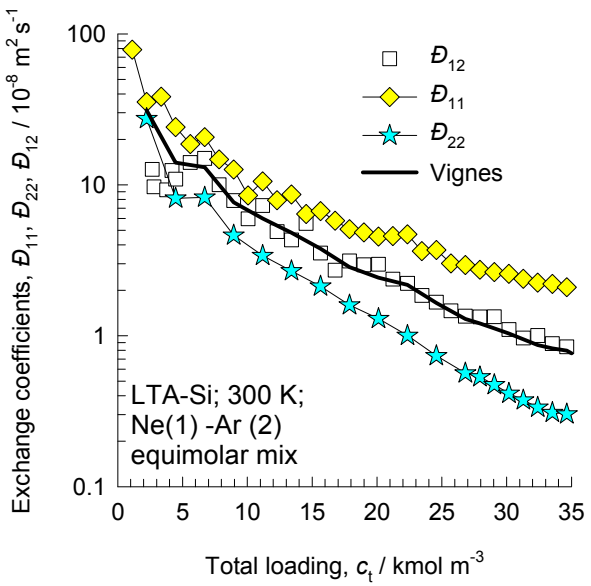


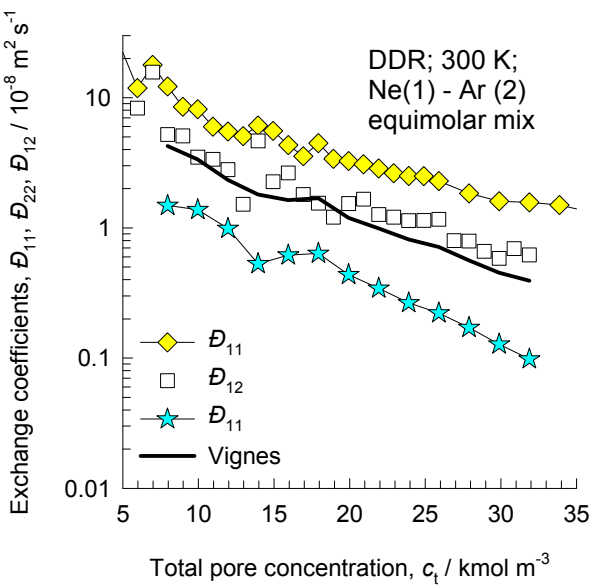


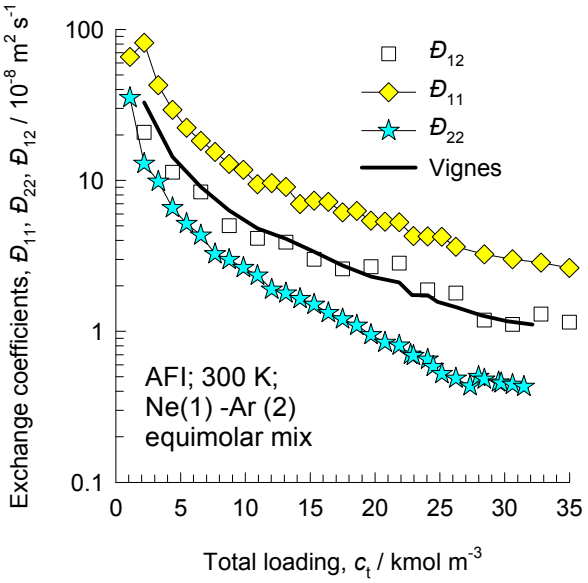


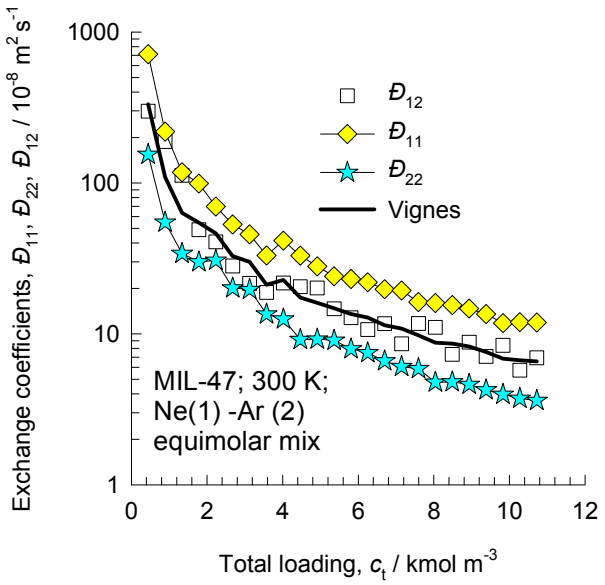

# Validation of the Vignes interpolation formula for $Đ_{12}$

Figure B41

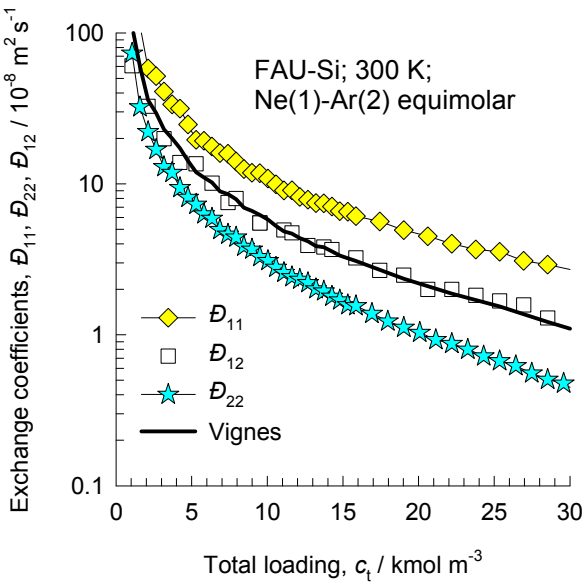


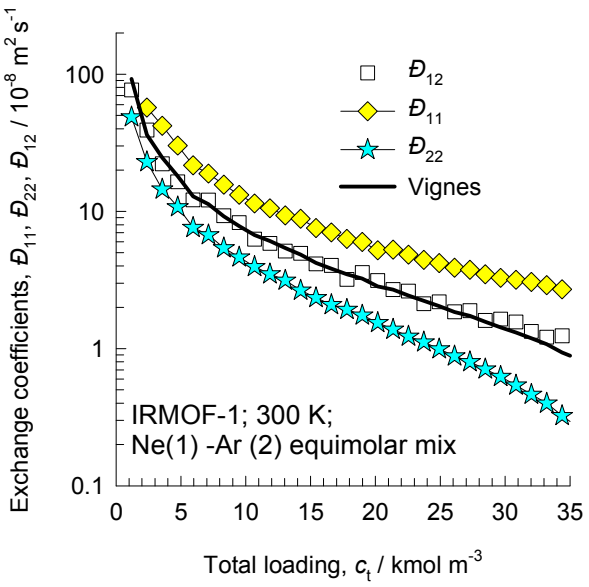


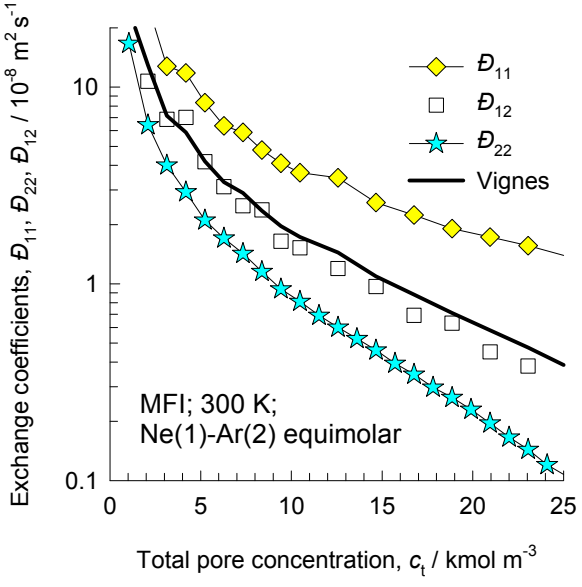


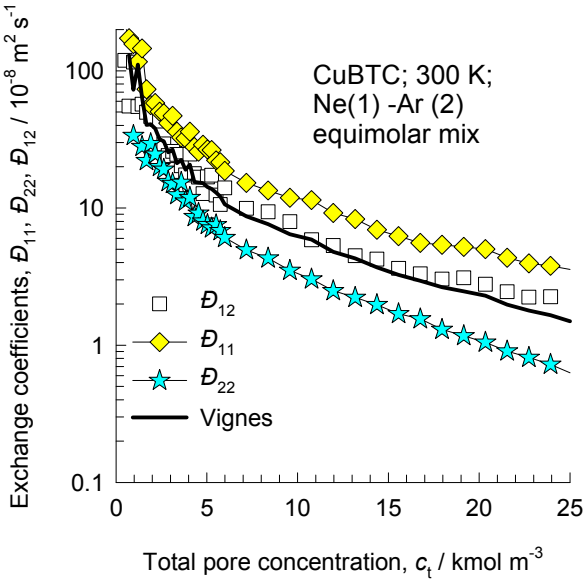


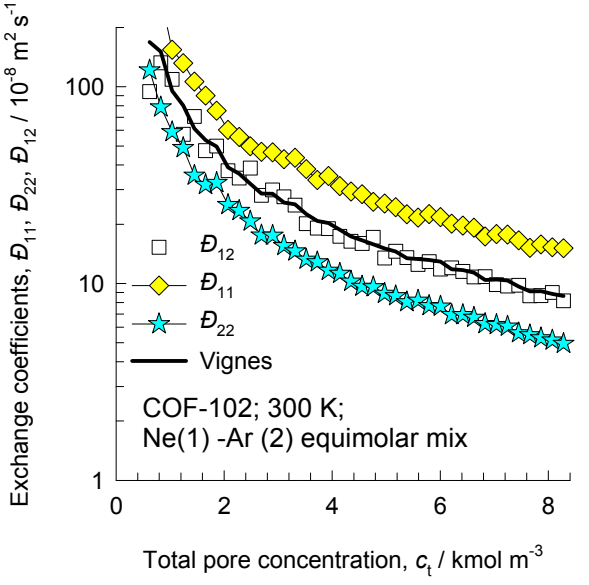


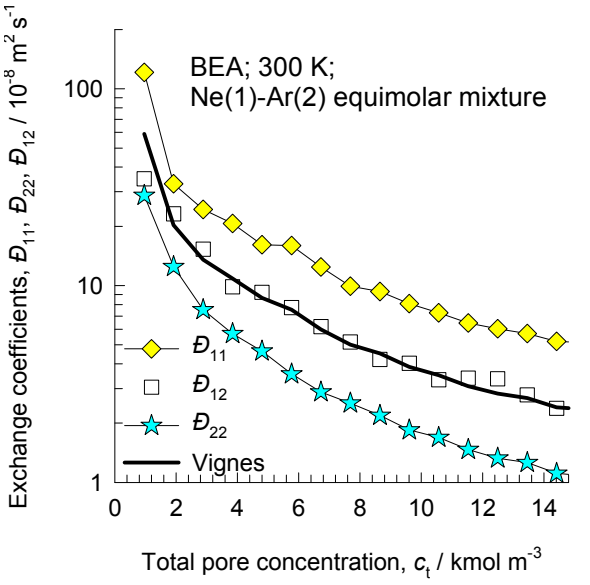

# Validation of the Vignes interpolation formula for $Đ_{12}$

Figure B42

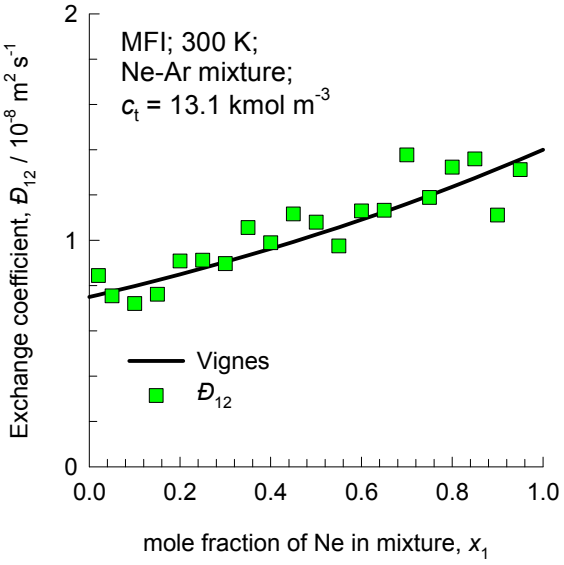


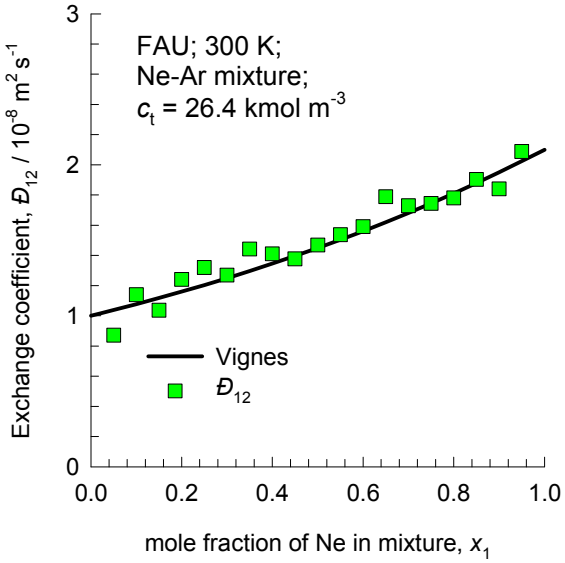

Figure B43

# Guest Mixture: $H_2$/Ar

Figure B44

# Exchange coefficients and Degree of correlations

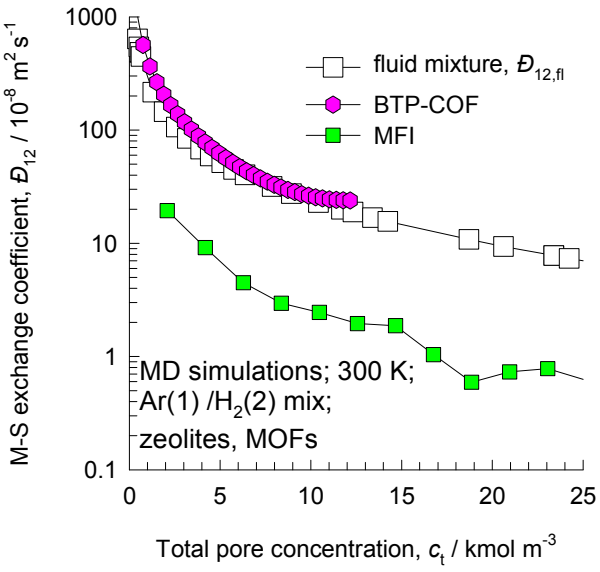


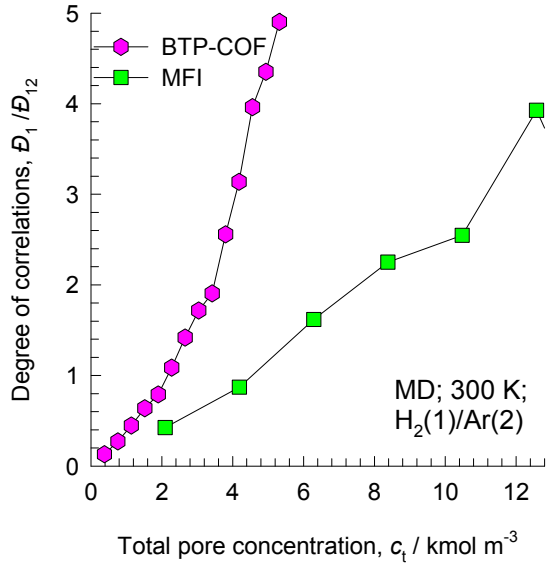


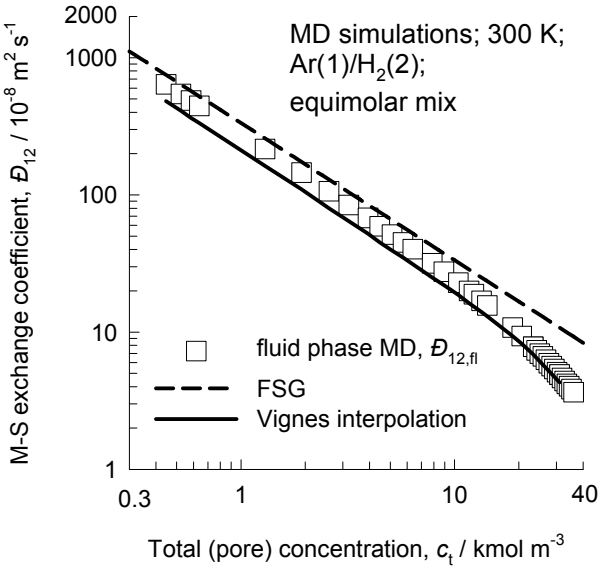


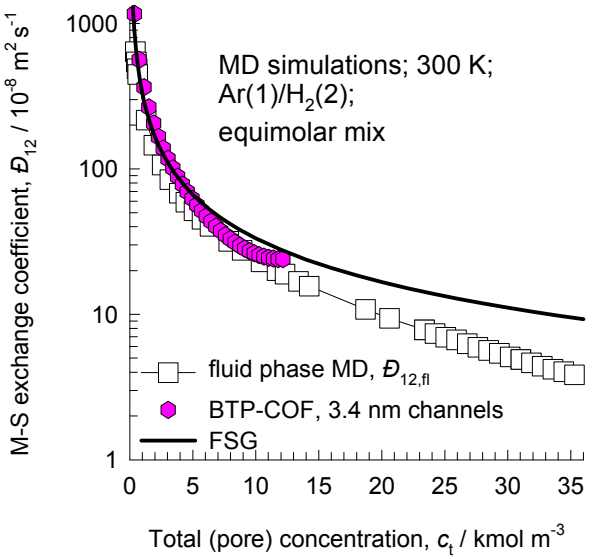

Figure B45

# Exchange coefficients as fraction of fluid phase $Đ_{12,fl}$

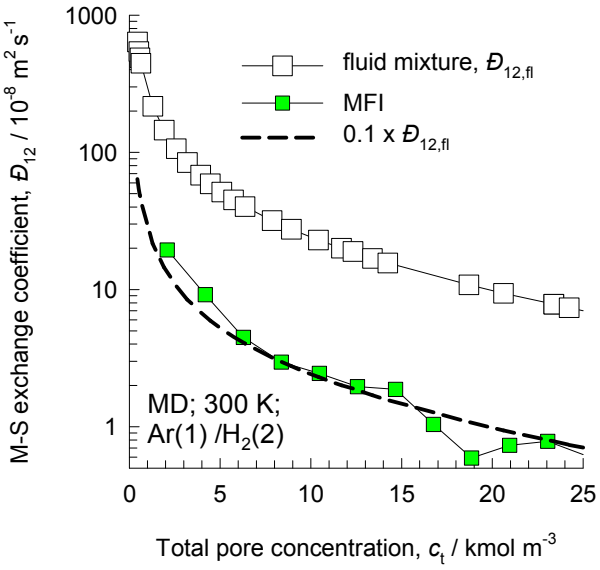

# Guest Mixture: $CH_4$/Ar

Figure B47

# Exchange coefficients and Degree of correlations

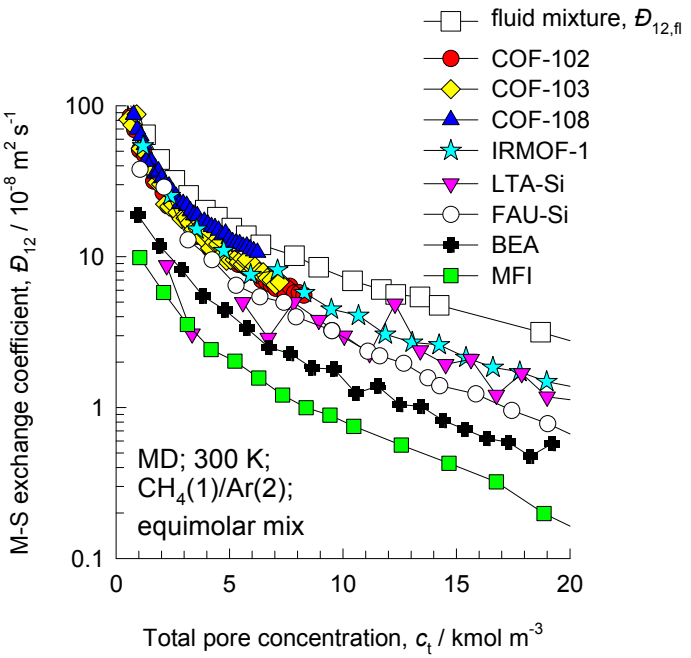


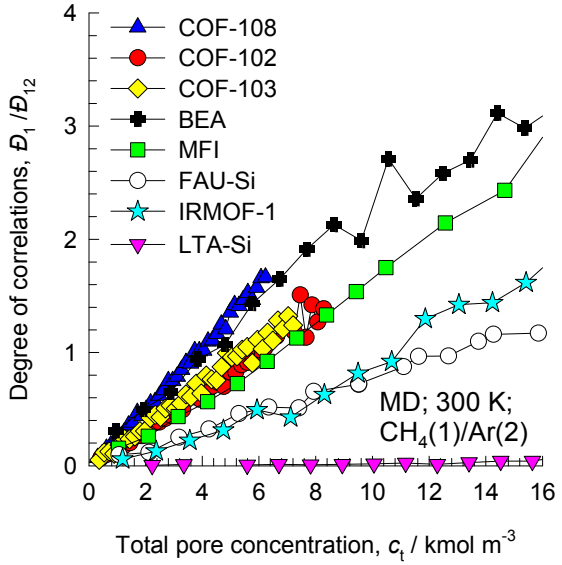


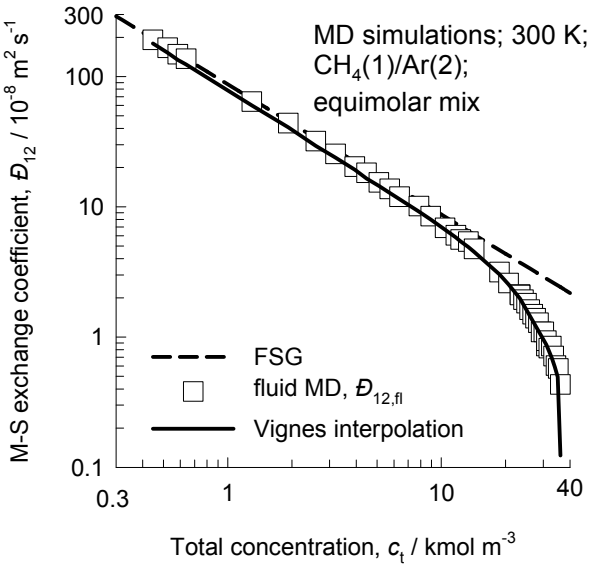


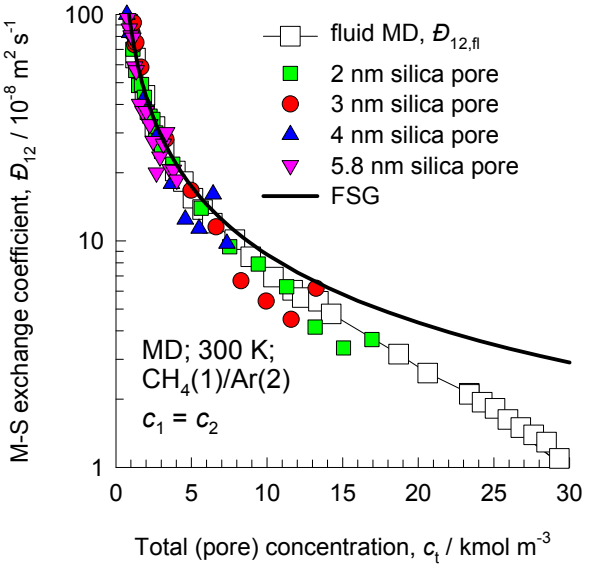

Figure B48

# Exchange coefficients as fraction of fluid phase $Đ_{12,fl}$

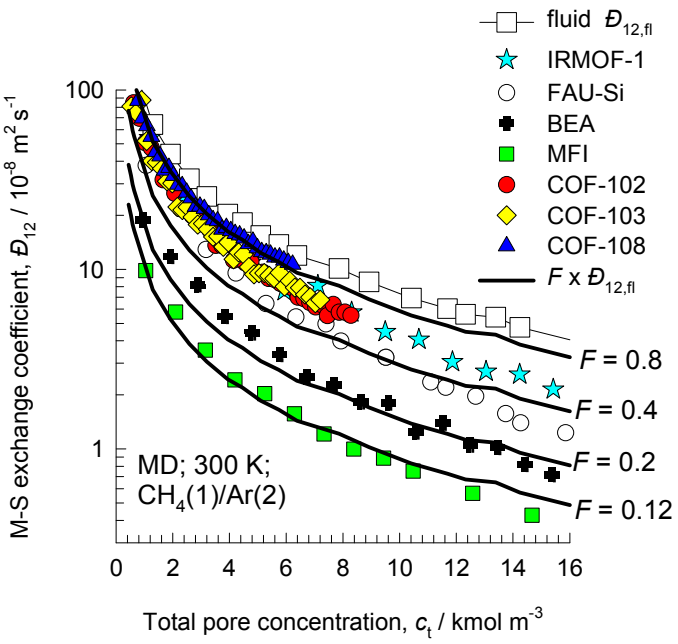


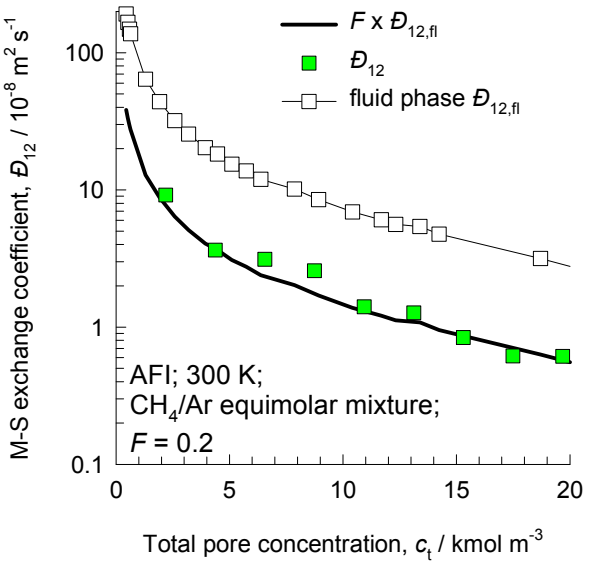

Figure B49

# Exchange coefficients as fraction of fluid phase $Đ_{12,fl}$

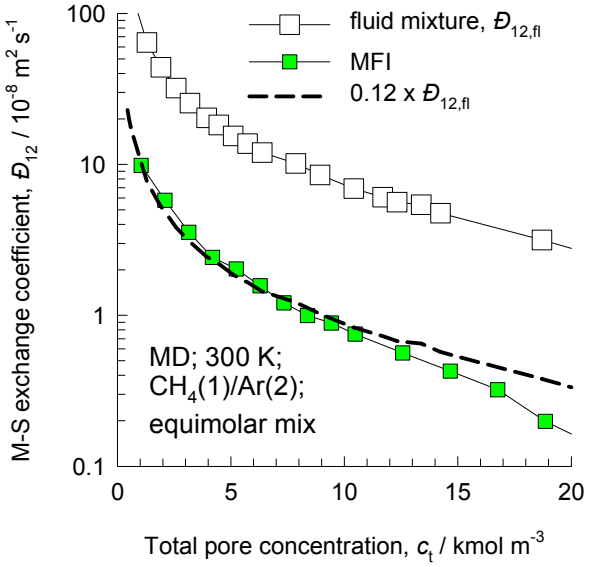


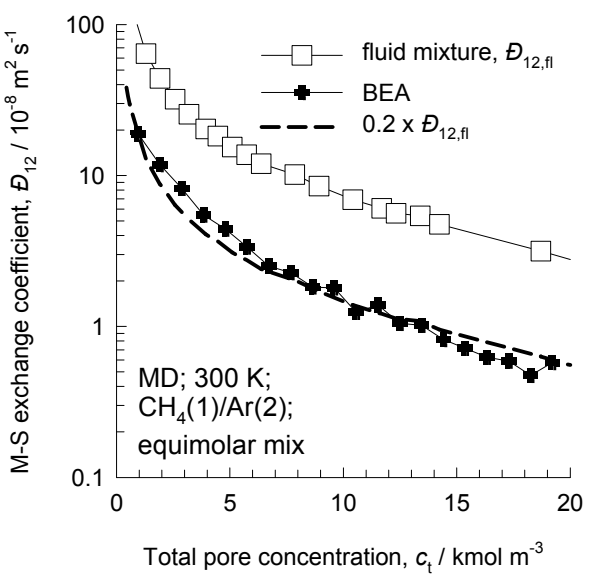


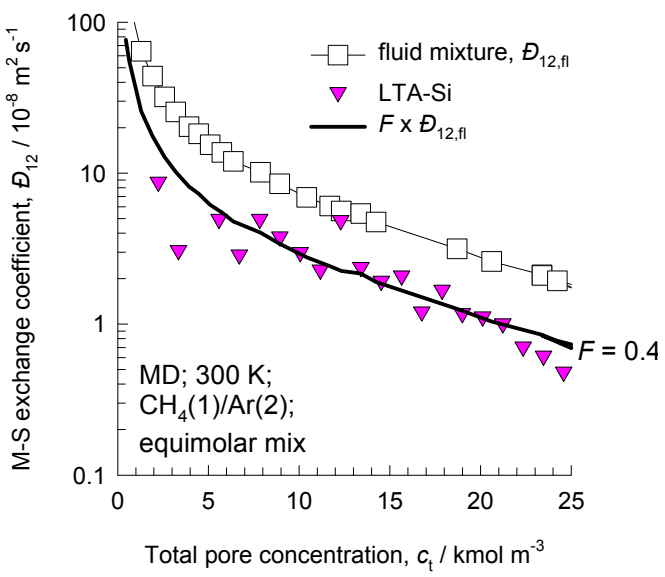


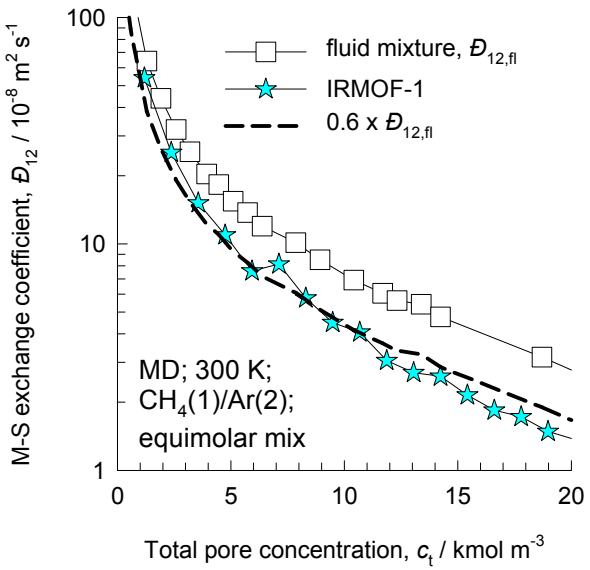


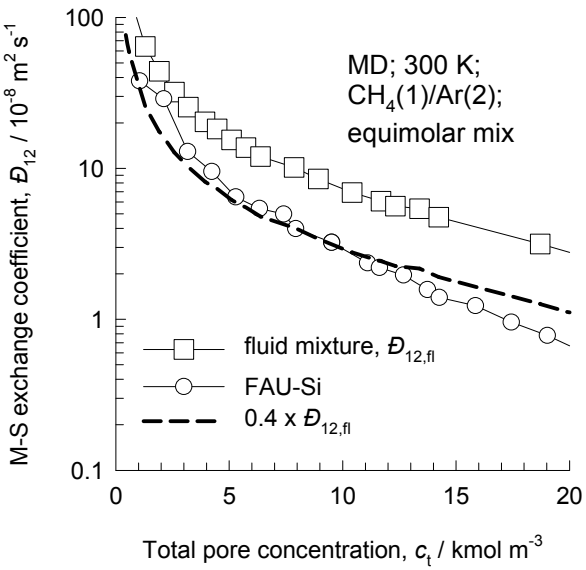


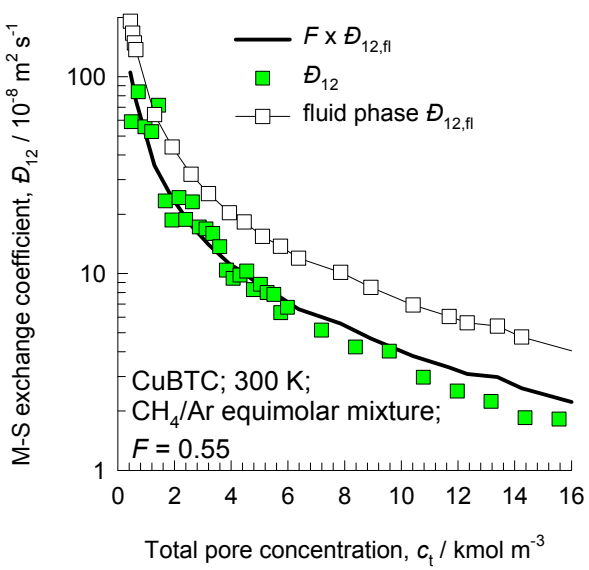

Figure B50

# Exchange coefficients as fraction of fluid phase $Đ_{12,fl}$

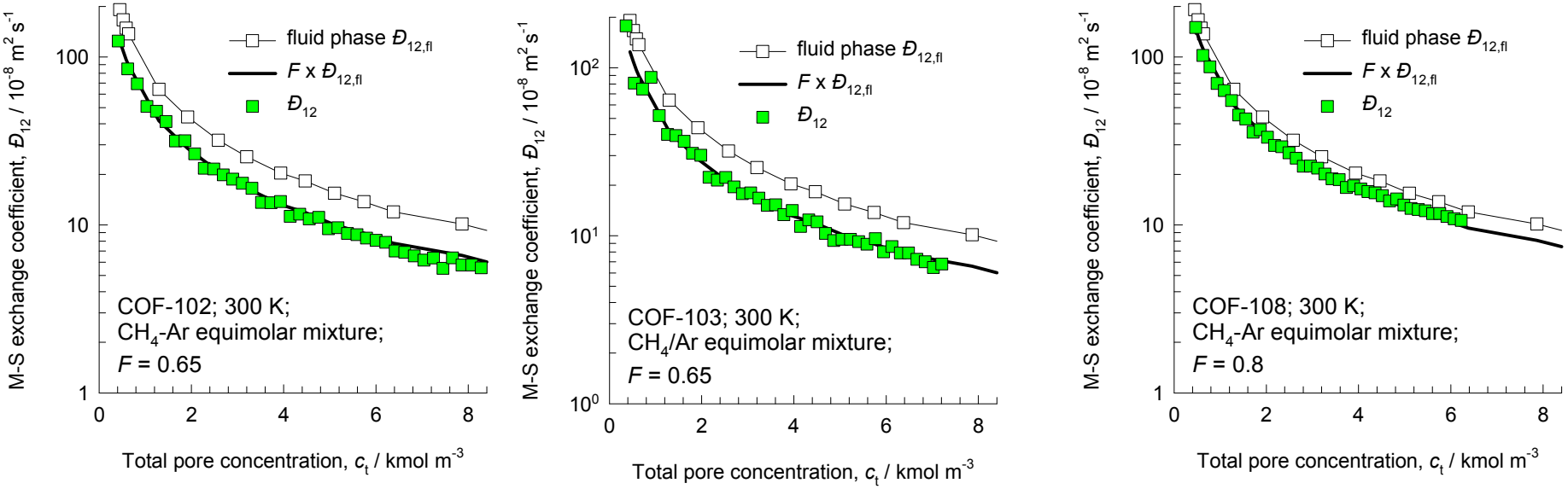

# Validation of the Vignes interpolation formula for $Đ_{12}$

Figure B51

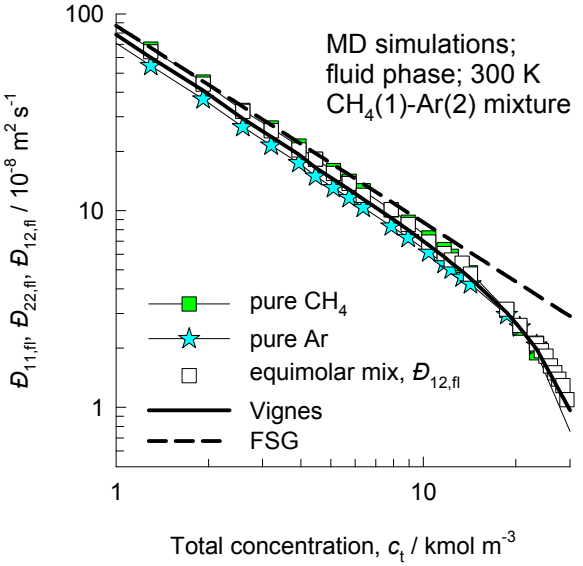


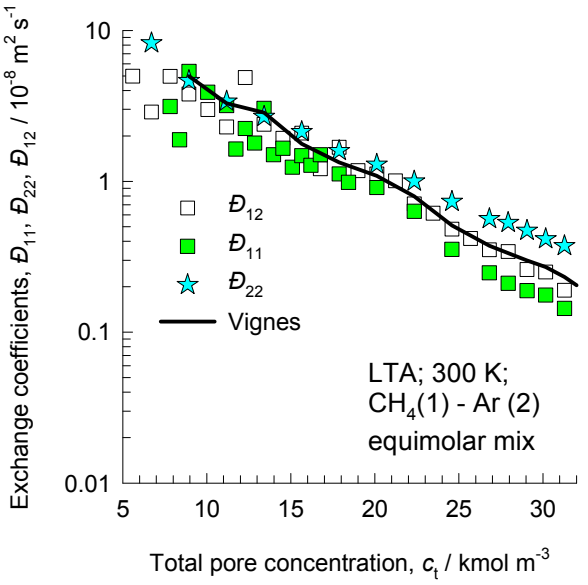


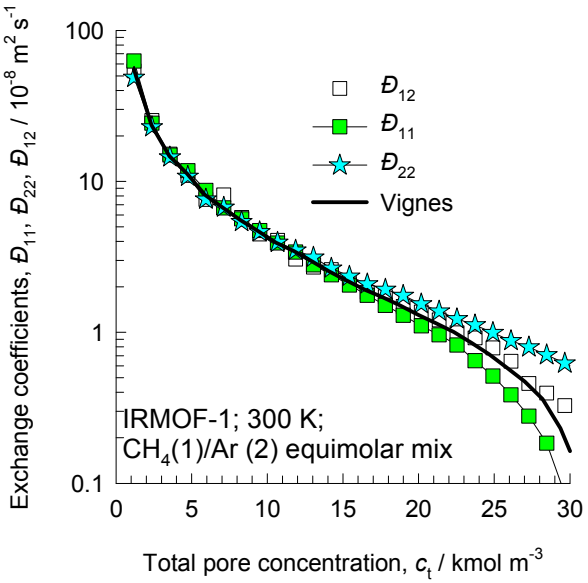


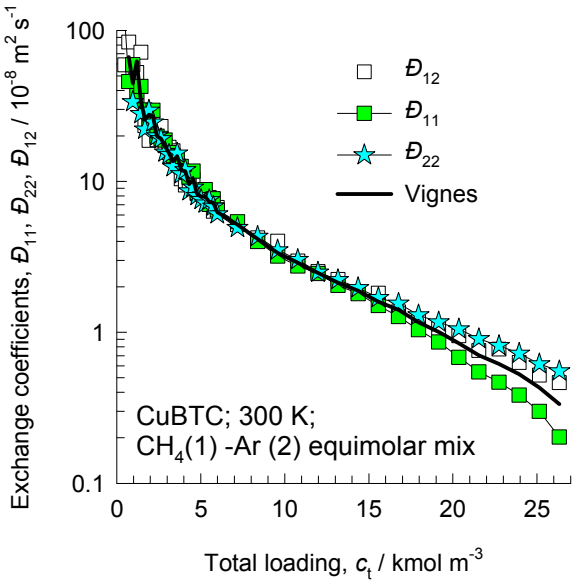


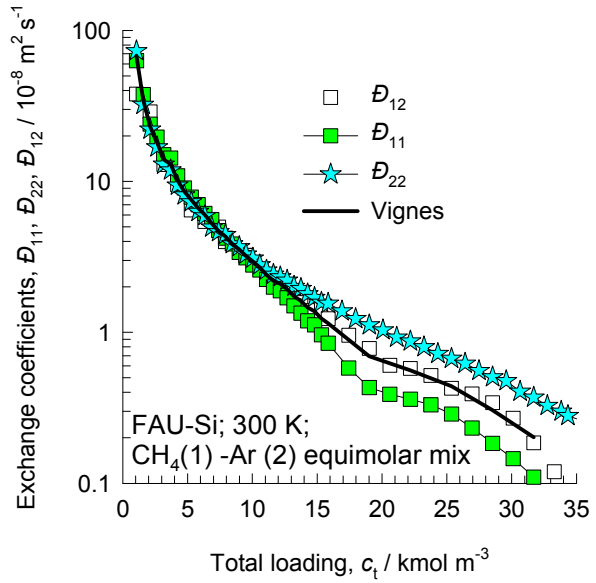

# Validation of the Vignes interpolation formula for $Đ_{12}$

Figure B52

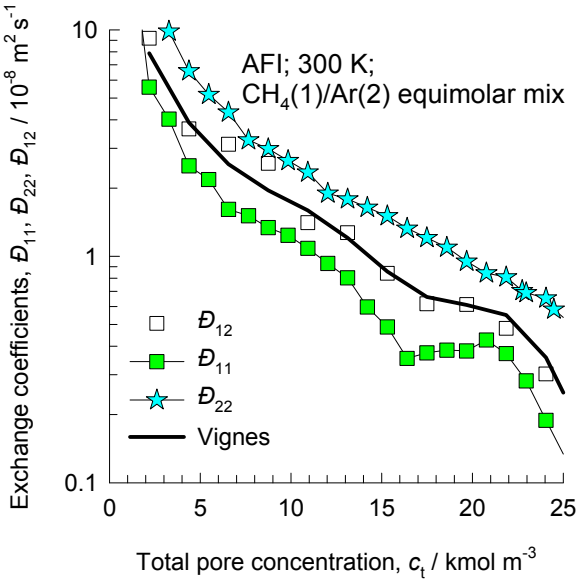


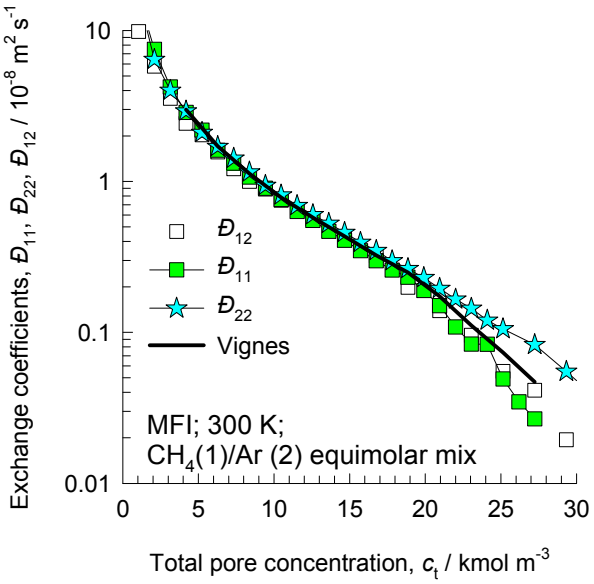


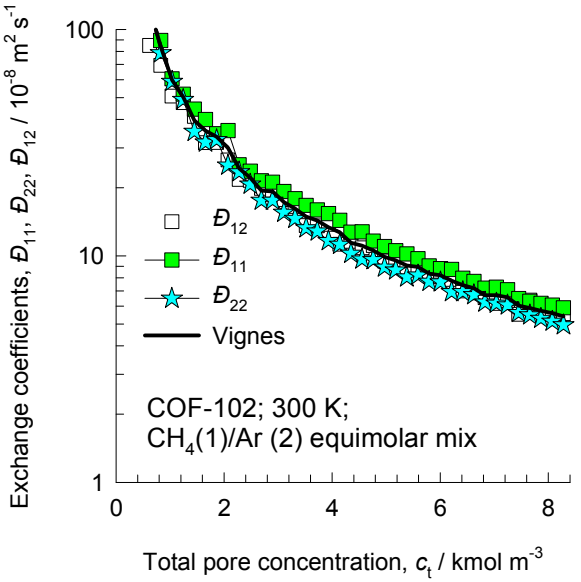


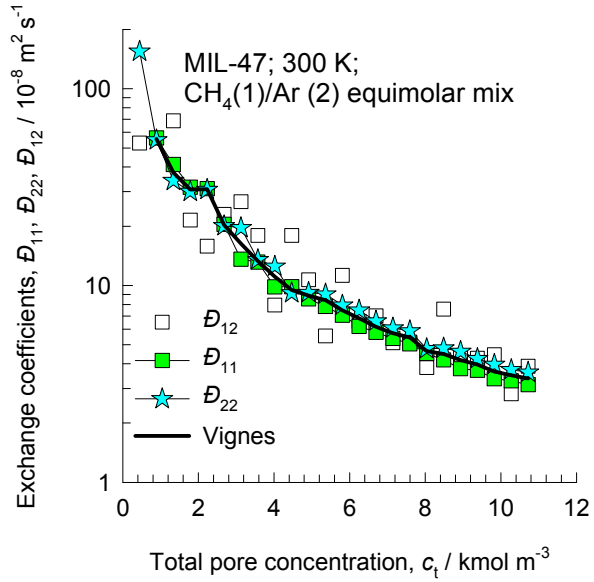

Figure B53

# Guest Mixture: $Ne/CO_2$

Figure B54

# Exchange coefficients and Degree of correlations

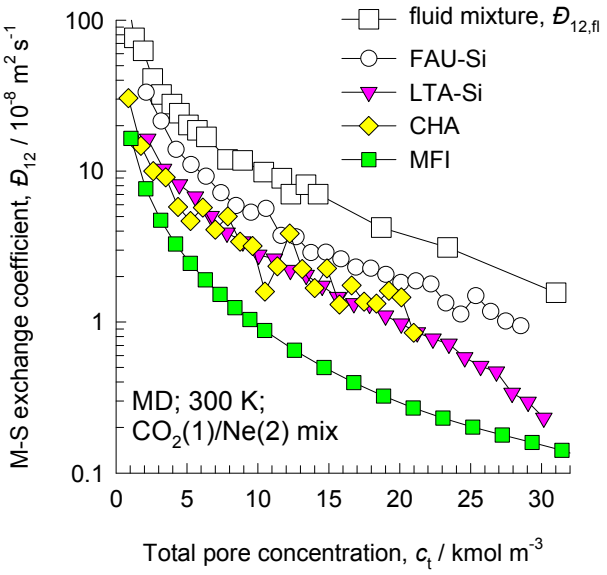


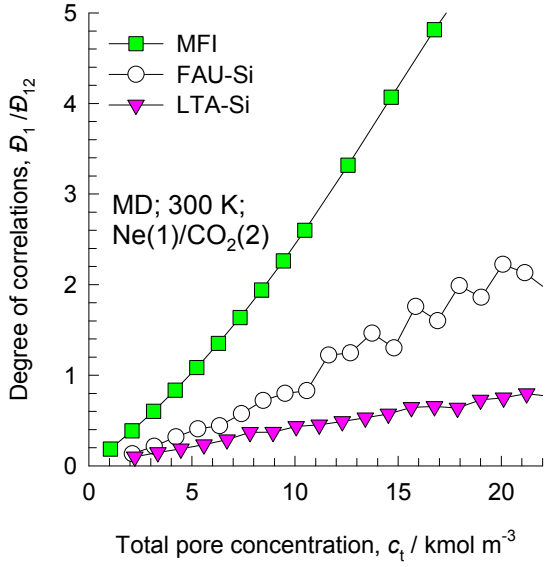


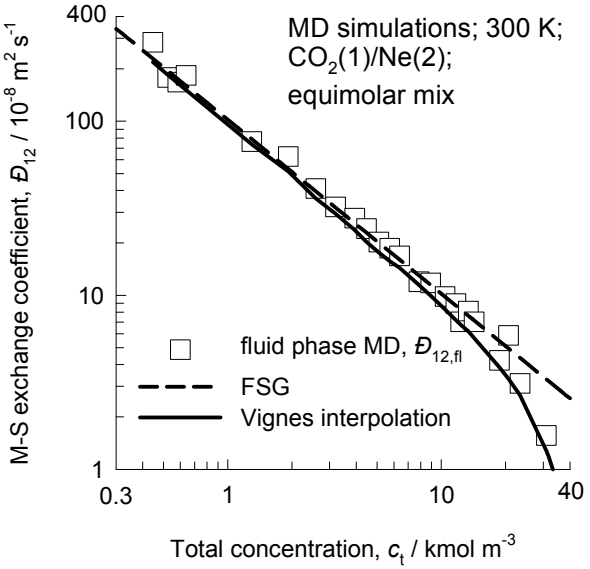

Figure B55

# Exchange coefficients as fraction of fluid phase $Đ_{12,fl}$

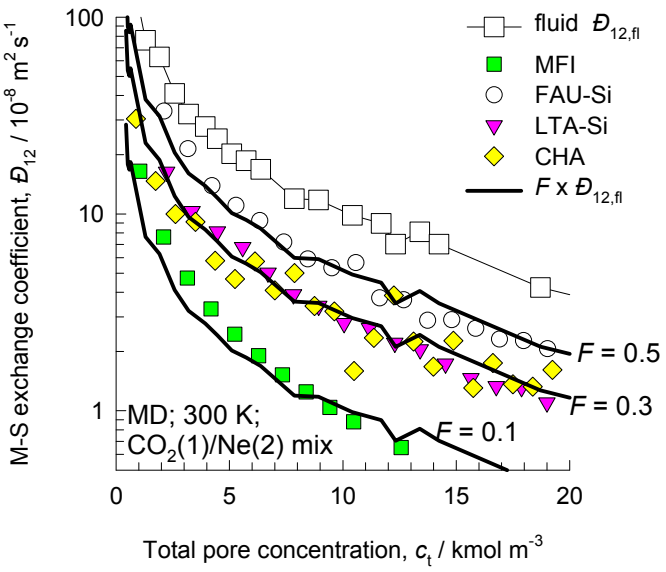


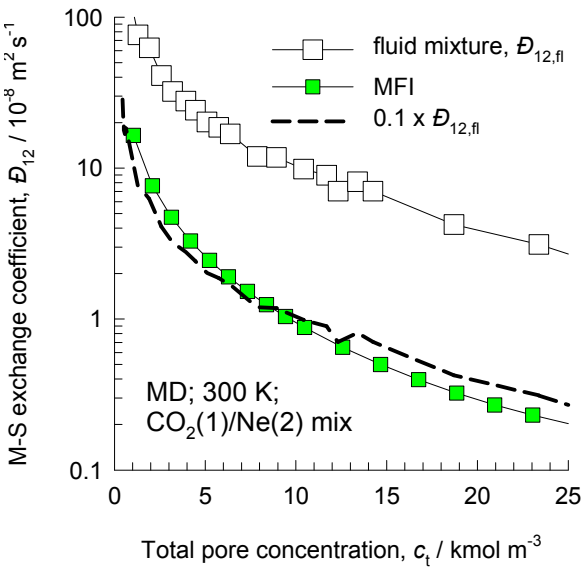


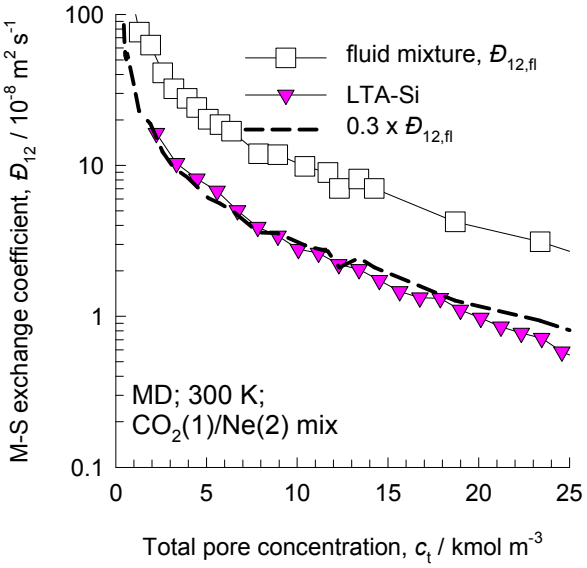


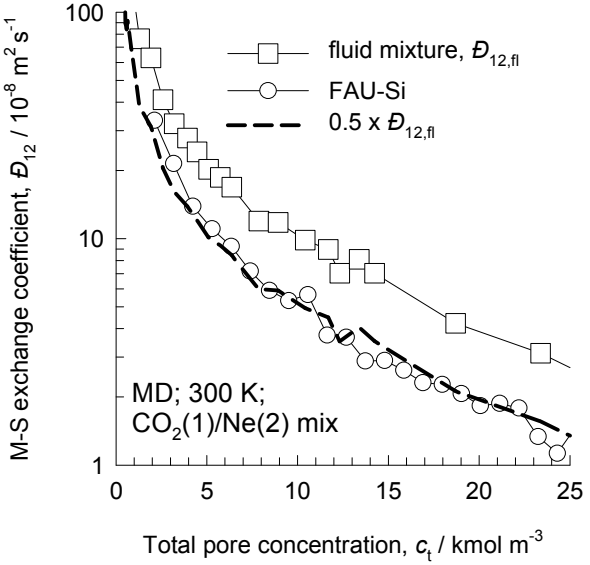


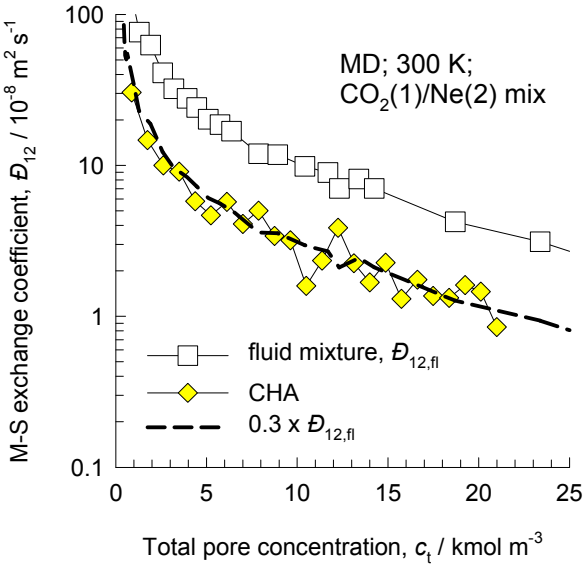

# Validation of the Vignes interpolation formula for $Đ_{12}$

Figure B56

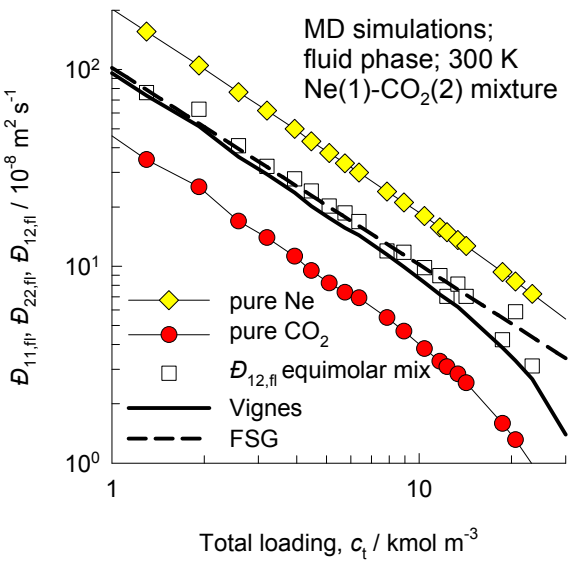


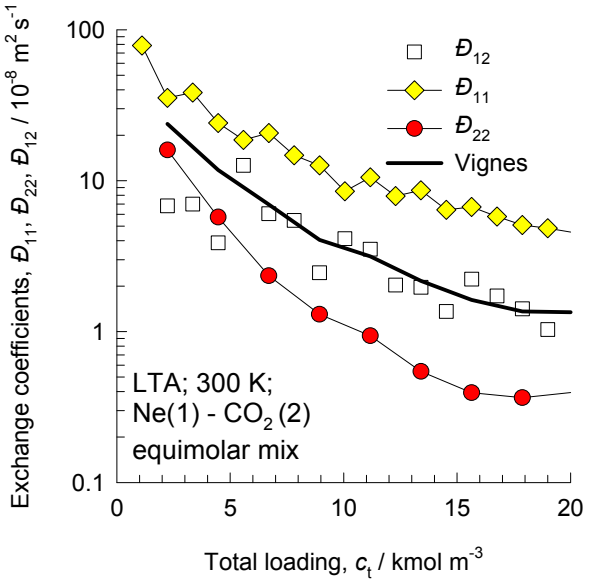


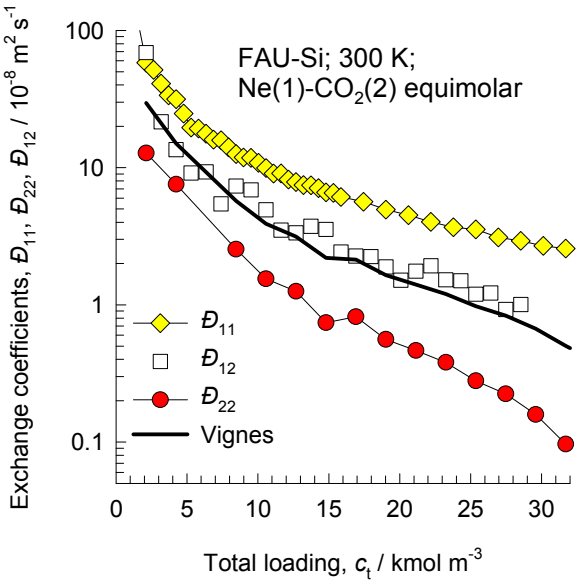


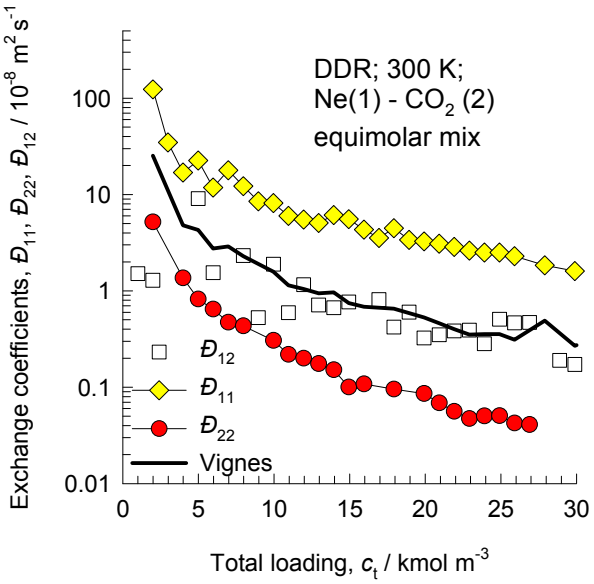

Figure B57

# Guest Mixture: Ar/Kr

Figure B58

# Exchange coefficients and Degree of correlations

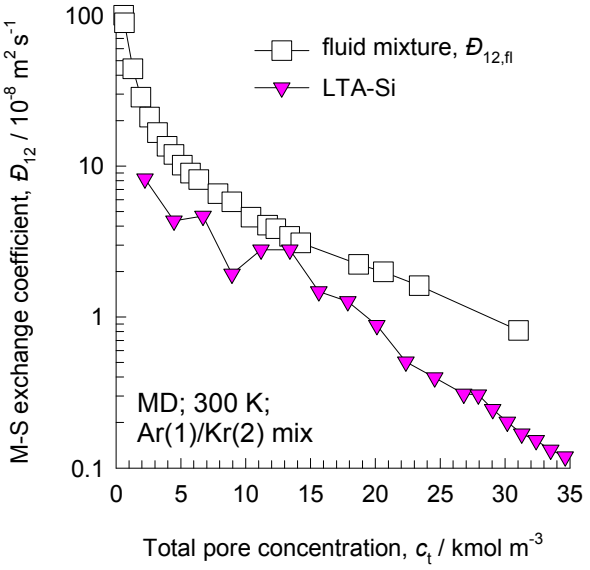


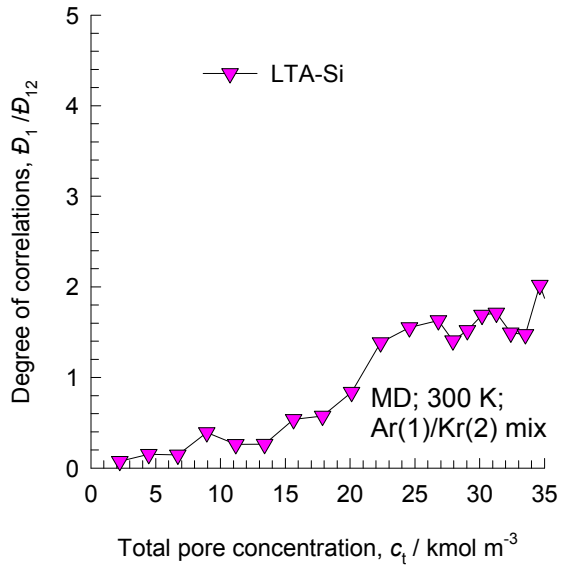


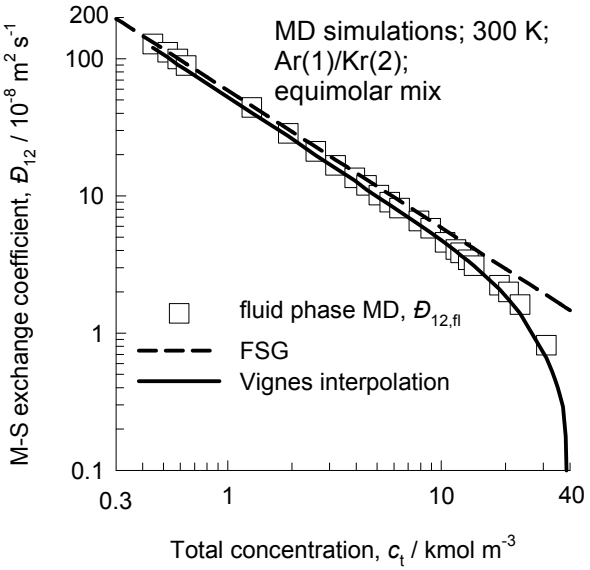


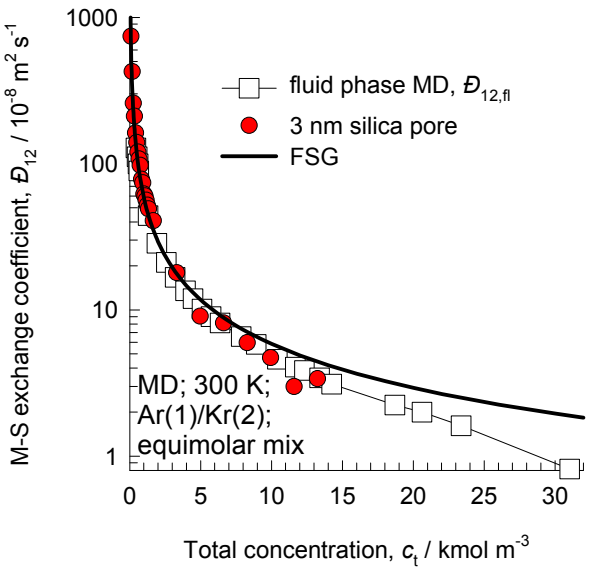

Figure B59

# Exchange coefficients as fraction of fluid phase $Đ_{12,fl}$

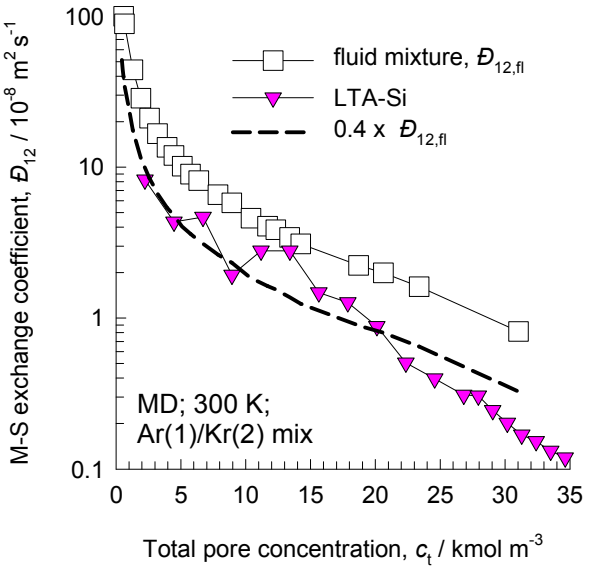

# Validation of the Vignes interpolation formula for $Đ_{12}$

Figure B60

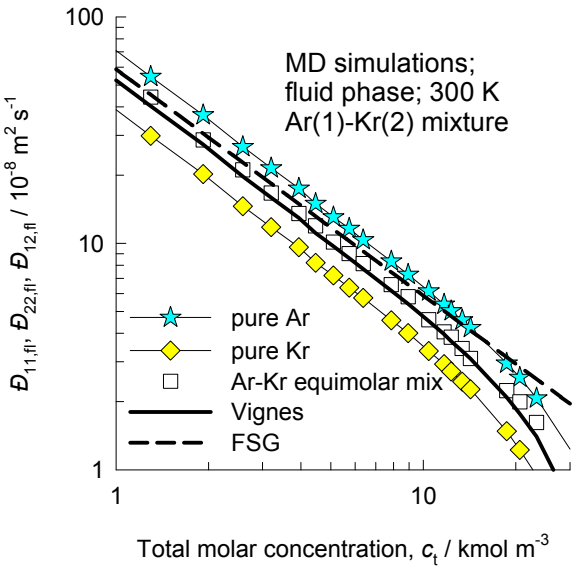

Figure B61

# Guest Mixture: water/ methanol, water/ethanol

Figure B62

# Diffusivities of water-methanol equimolar mixtures

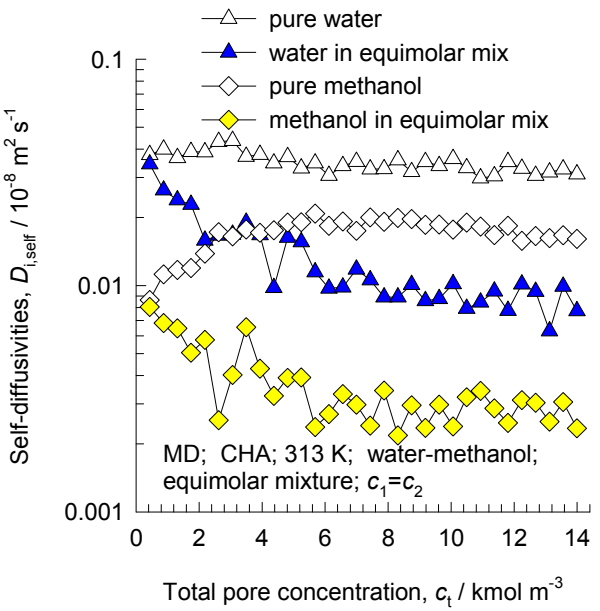


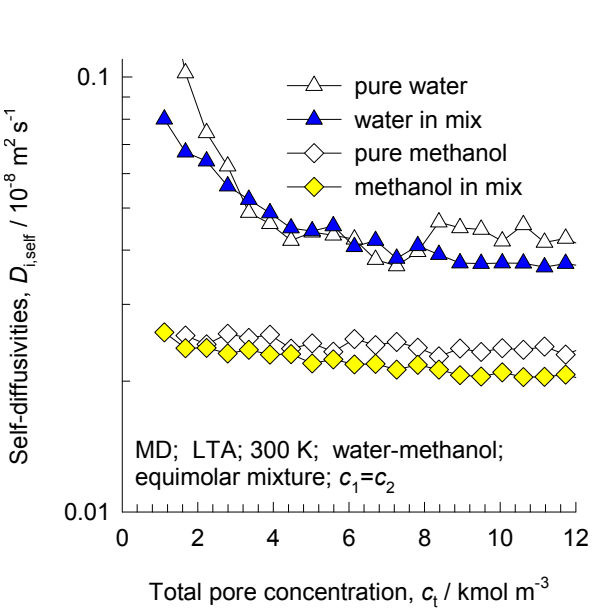


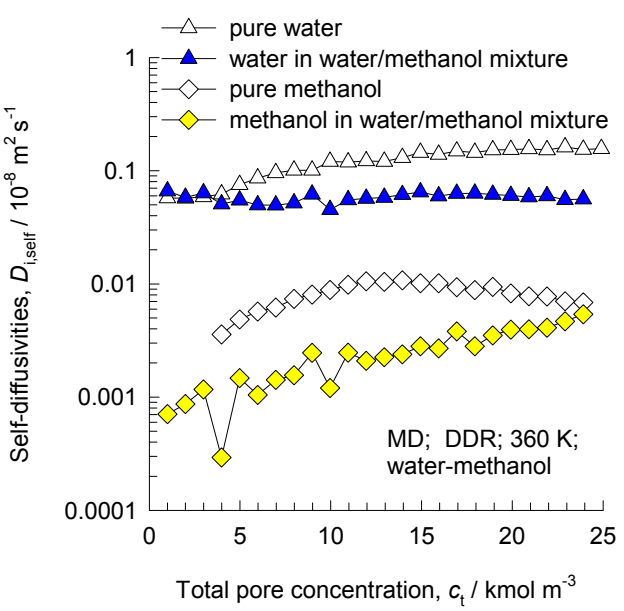


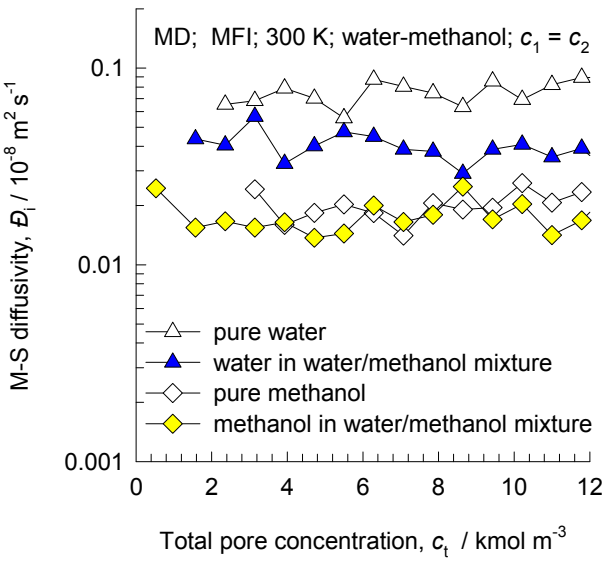


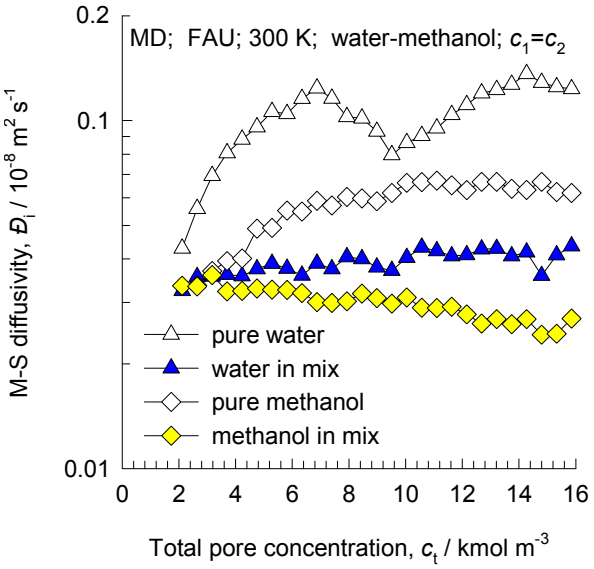


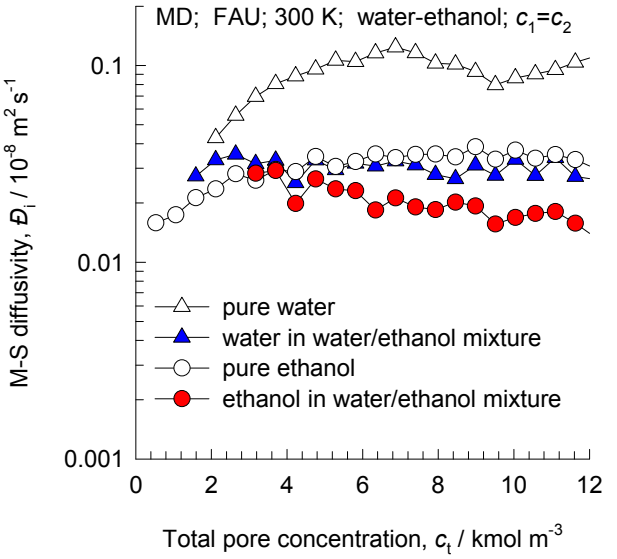

# FAU Comparing water/alcohol equimolar mixtures

Figure B63

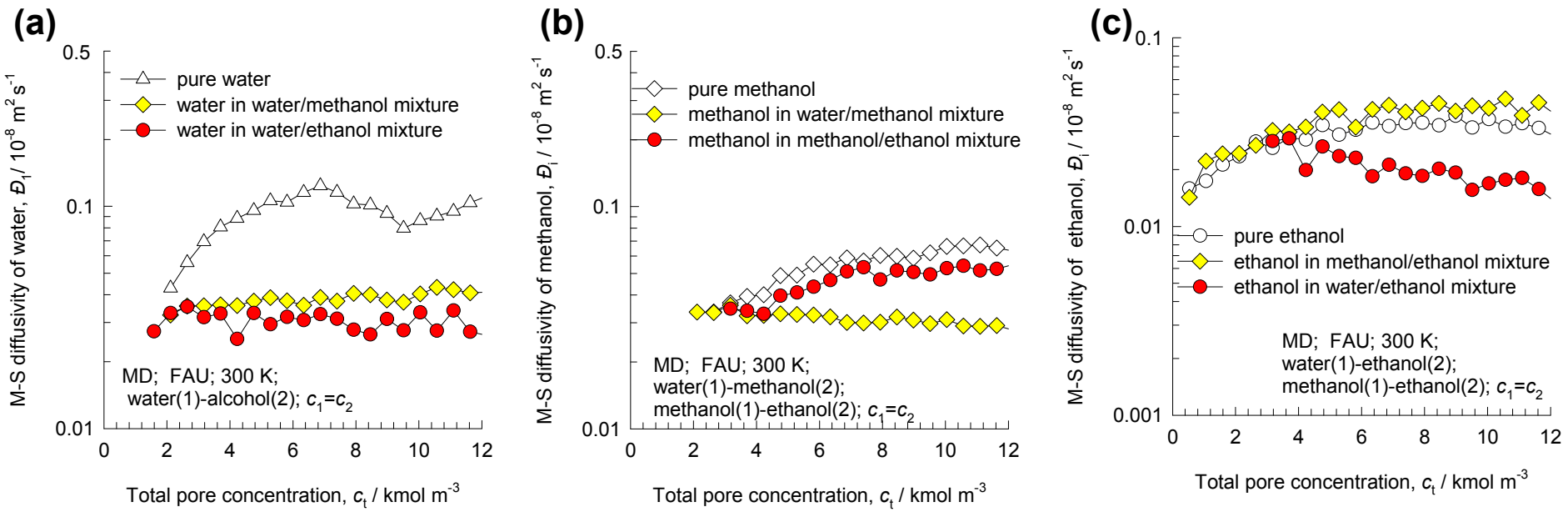


MD data on M-S diffusivities, $Đ_i$, of (a) water, (b) methanol, and (c) ethanol in equimolar ($c_1 = c_2$) water-methanol, water-ethanol and methanol-ethanol mixtures in FAU at 300 K. Also shown are the pure component $Đ_i$ determined at the same total pore concentration. From (a) it can be observed that the $Đ_i$ of water in mixtures with alcohols are significantly lower than that for pure water. The reason for this is that due to hydrogen bonding, water tends to cluster around alcohol molecules. The mobility of water molecules in the mixtures is significantly lowered due to cluster formation.

Interestingly, the $Đ_i$ of methanol in mixtures with water is also significantly lower than the value for pure methanol; see (b). In sharp contrast, the $Đ_i$ of methanol in mixtures with ethanol is practically the same as for pure methanol. The hydrogen bonding between methanol-ethanol and methanol-methanol is significantly weaker than for water-methanol pairs.

The results for the M-S diffusivity of ethanol are analogous to those for methanol; see (c). Compared with pure ethanol, the $Đ_i$ is significantly lowered in mixtures with water, but in remains practically the same in mixtures with methanol.

# FAU Comparing water/alcohol mixtures of varying composition

Figure B64

(a)

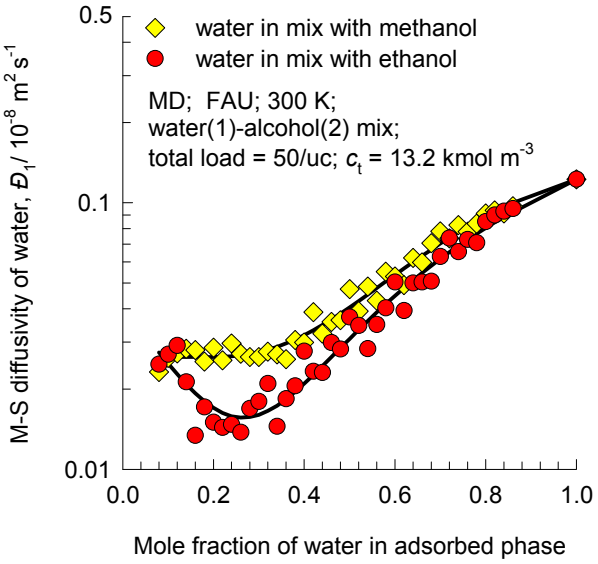


(b)

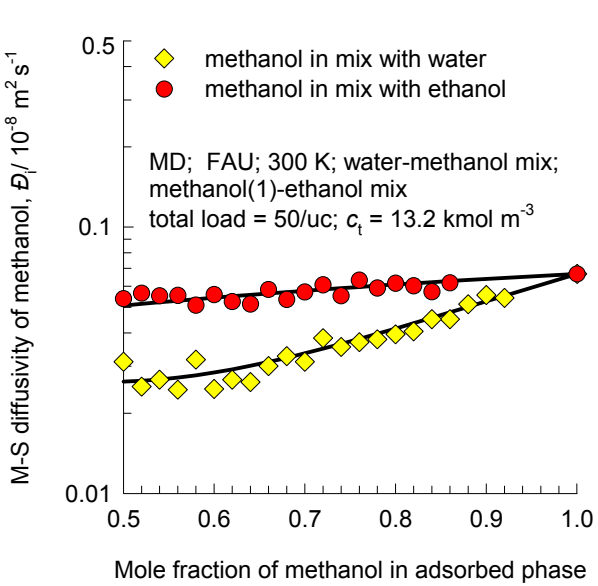


(a) presents data for $Đ_i$ of water in binary mixtures with methanol and ethanol. For both mixtures, we note a reduction in the $Đ_i$ of water with increasing alcohols concentration within the pores. Furthermore, the mobility of water in mixtures with ethanol is slightly lower than for water-methanol mixtures. (b) presents data for the M-S diffusivity $Đ_i$ of methanol in water-methanol and methanol-ethanol mixtures. For methanol-ethanol mixtures the M-S diffusivity $Đ_i$ is practically independent of composition, whereas in mixtures with water, the $Đ_i$ decreases significantly below the pure component value with increasing water concentrations. Water-methanol clustering is much more significant than methanol-ethanol clustering.

The results presented in (a) and (b) indicate that for a certain range of compositions of water-alcohol mixtures there is mutual hindering of both components in the mixture.

# **MFI** diffusion of water-methanol mixtures, varying composition

Figure B65

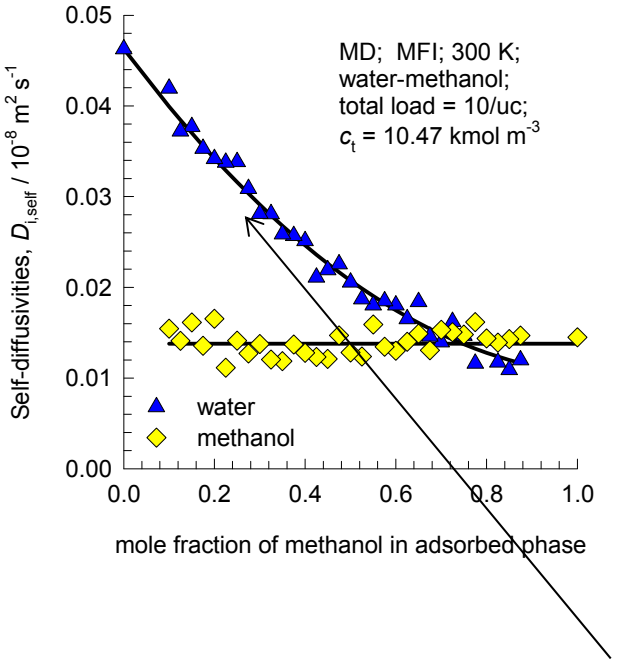


This reduction is due to hydrogen bonding

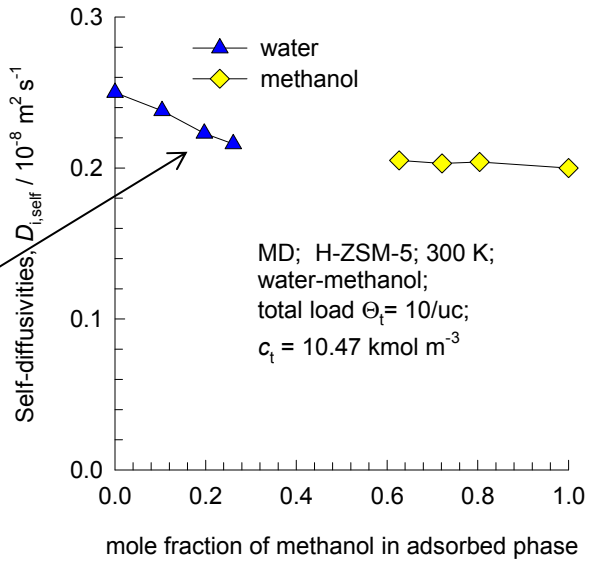


NMR data of Caro, J.; Bülow, M.; Richter-Mendau, J.; Kärger, J.; Hunger, M.; Freude, D. J. Chem. Soc., Faraday Trans. 1987, 83, 1843-1849.

# LTA water-methanol mixture snapshots showing clustering

Figure B66

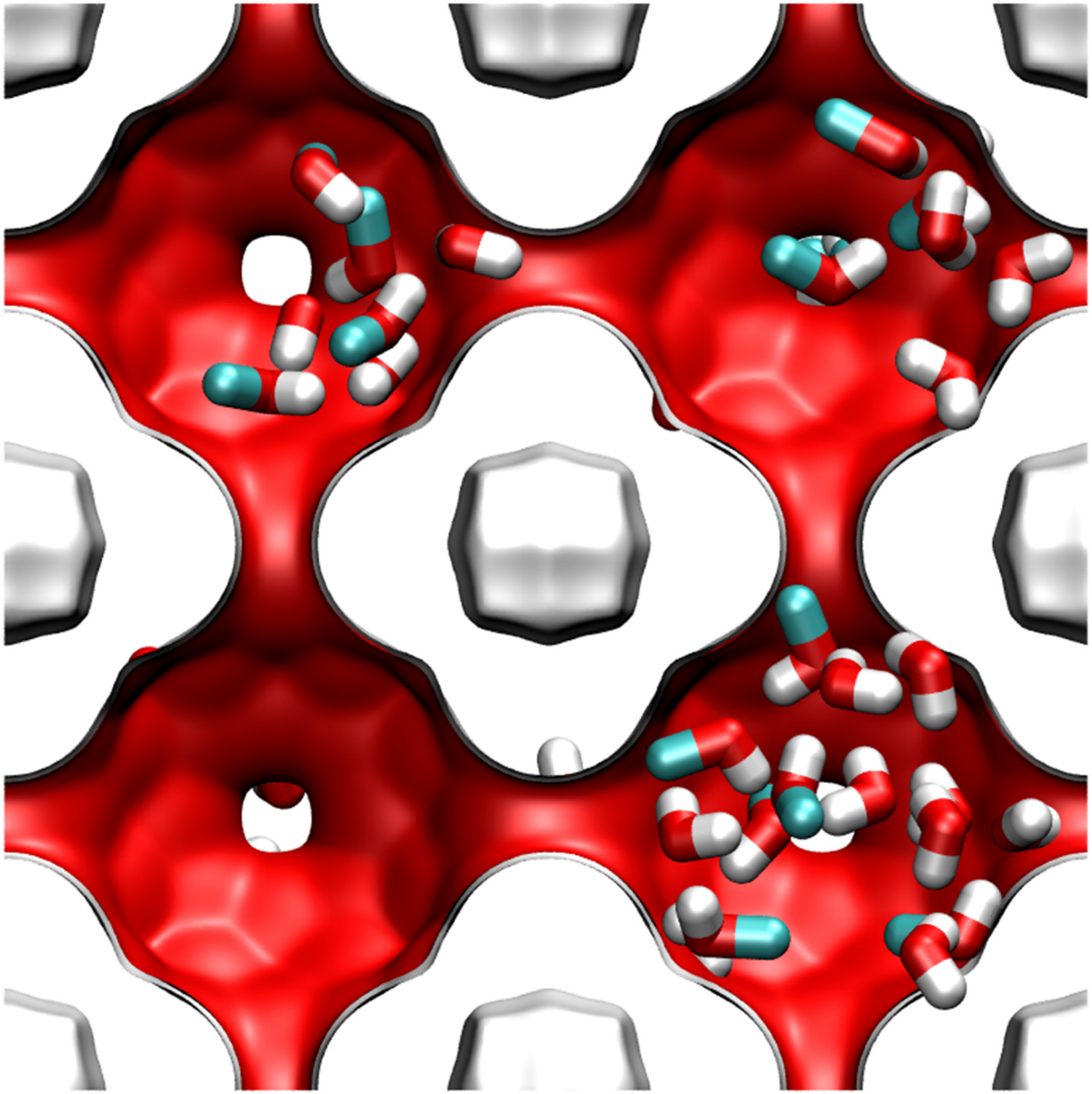

# **LTA** water-ethanol mixture snapshots showing clustering

Figure B67

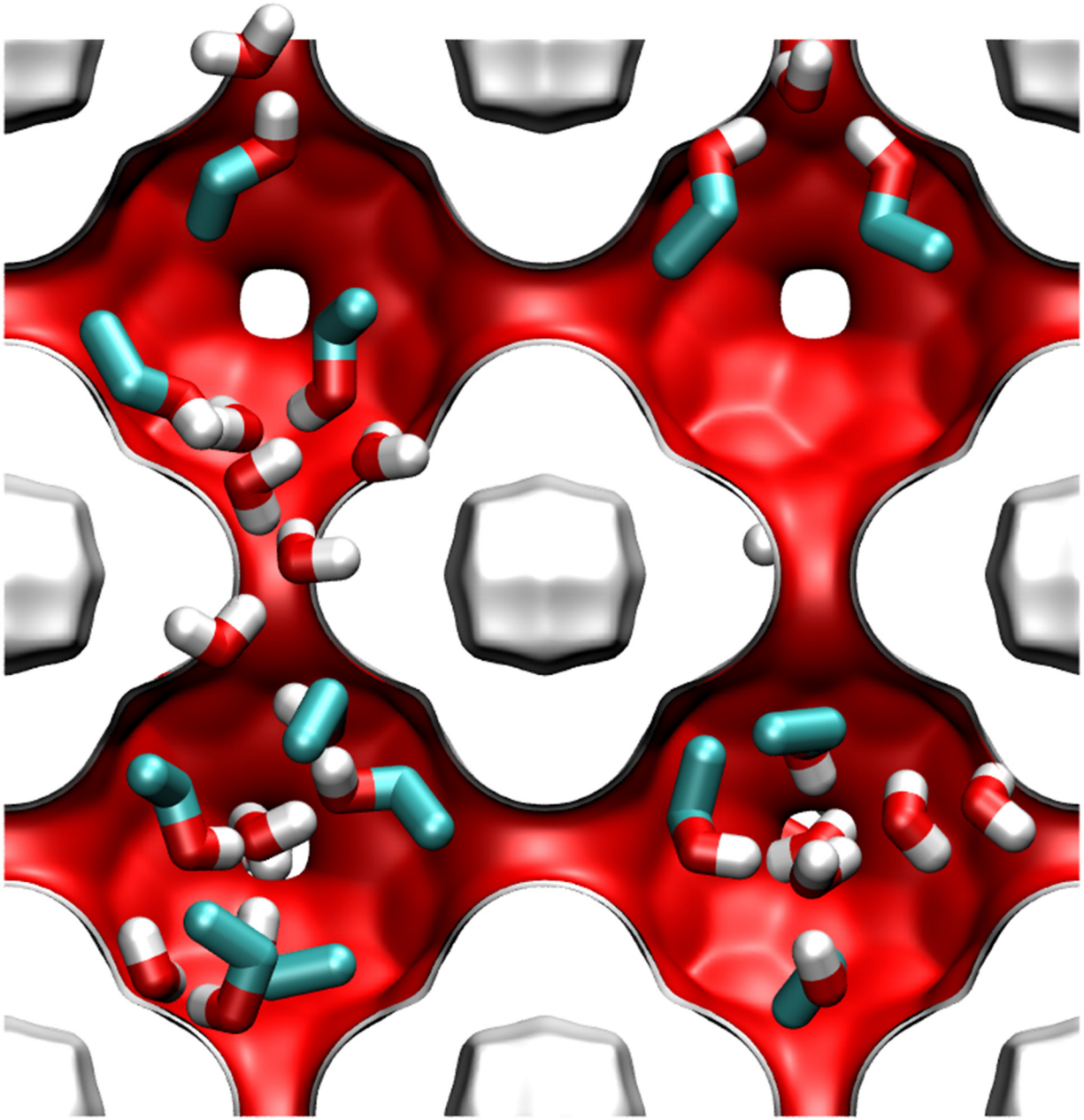

# **MFI** snapshot of a mixture of water and methanol

Figure B68

The snapshot shows some qualitative indication of clustering of water and methanol molecules caused by hydrogen bonding.

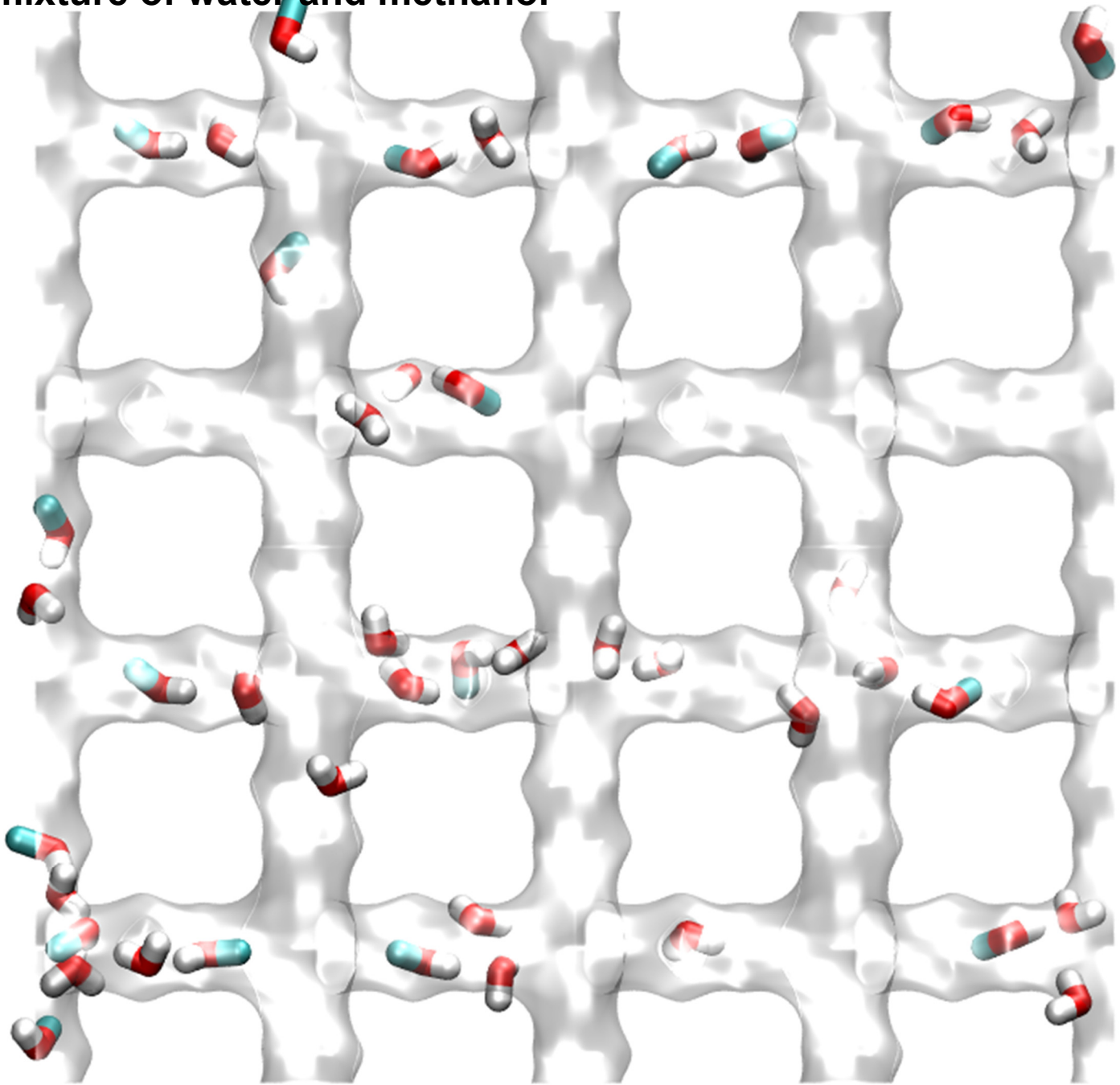

# **MFI** snapshot of a mixture of water and ethanol

Figure B69

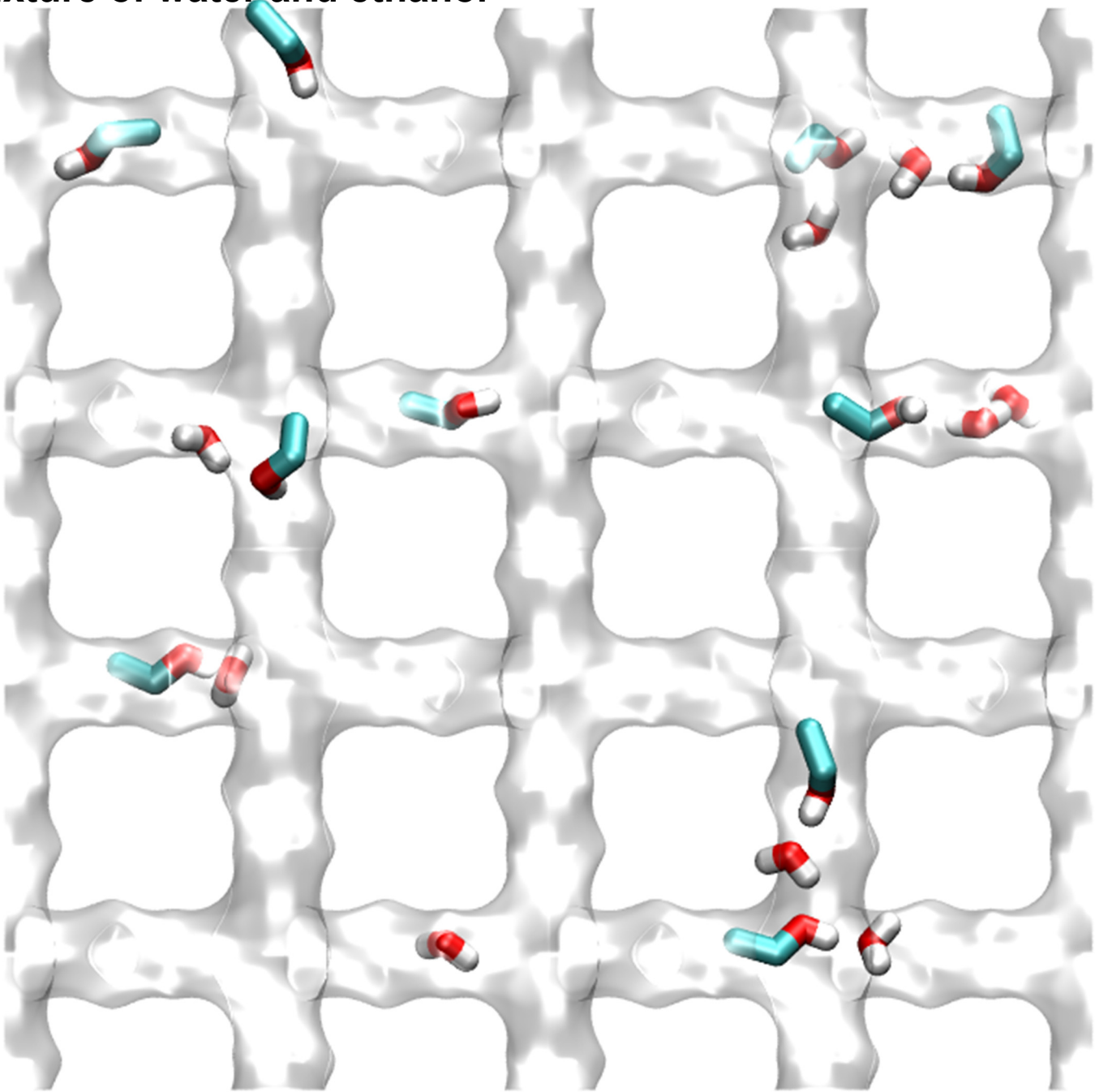

The snapshot shows some qualitative indication of clustering of water and ethanol molecules caused by hydrogen bonding.

Figure B70

# Guest Mixture in MFI zeolite: $CH_4/iC_4H_{10}$

Figure B71

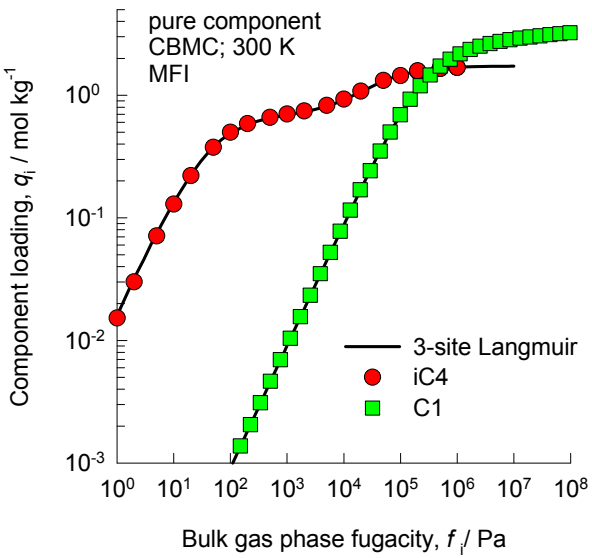


**Pure components adsorption**

# C1 - iC4 / MFI / 300K

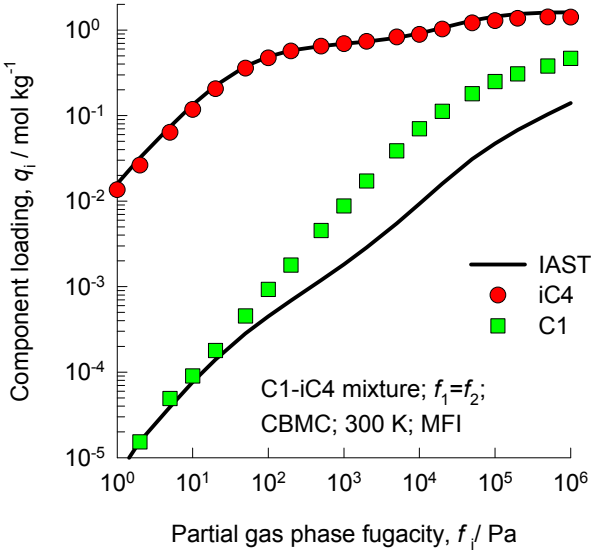


**mixture adsorption**

The failure of IAST to describe mixture adsorption accurately is because of segregation effects. The iC4 locates preferentially at the intersections. This implies that there is no homogeneous distribution of the mixture over the entire MFI framework. This non-homogeneous distribution of molecules causes departures from IAST.

The adsorption and diffusion characteristics are discussed in further details in:
R. Krishna, J.M. van Baten, Diffusion of hydrocarbon mixtures in MFI zeolite: Influence of intersection blocking, Chem. Eng. J. 140 (2008) 614-620.

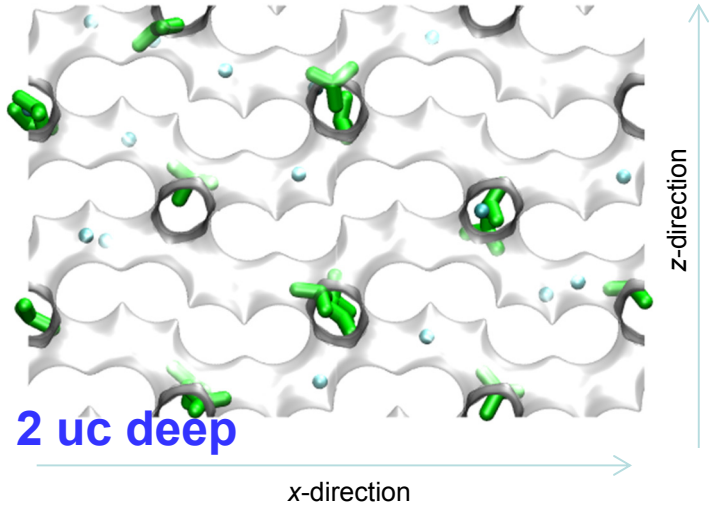


**2 uc deep**

**C1 = 2 molecules/uc**
**iC4 = 2 molecules/uc**

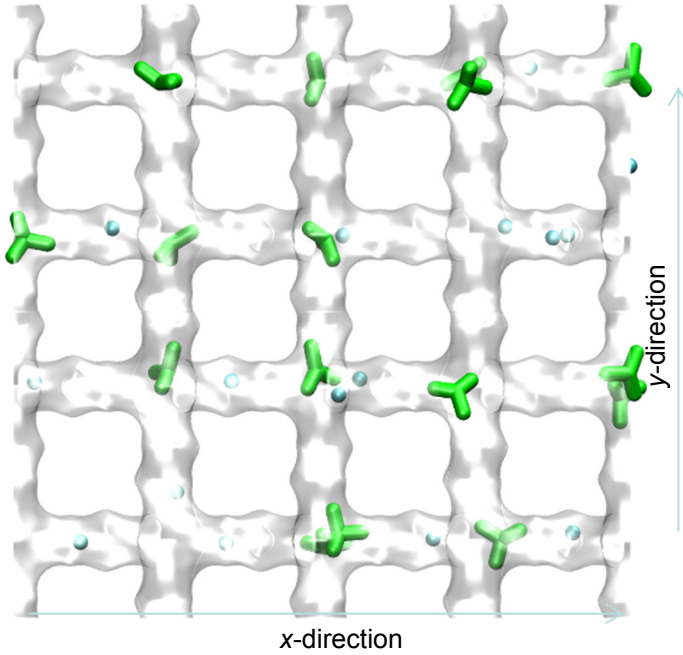


**2 uc deep**

# C1 - iC4 / MFI / 300K

## mixture diffusion

*y*-direction of yields highest diffusivity; this is a straight path

*x*-direction of yields intermediate; this is a zig-zag path

*z*-direction of yields lowest diffusivity

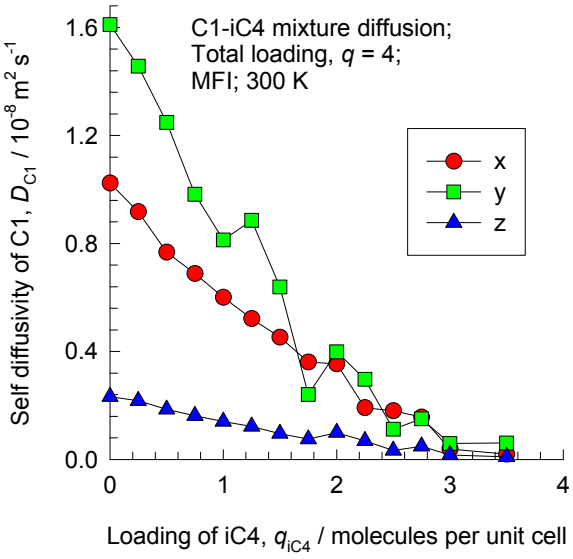


The adsorption and diffusion characteristics are discussed in further details in:
R. Krishna, J.M. van Baten, Diffusion of hydrocarbon mixtures in MFI zeolite: Influence of intersection blocking, Chem. Eng. J. 140 (2008) 614-620.

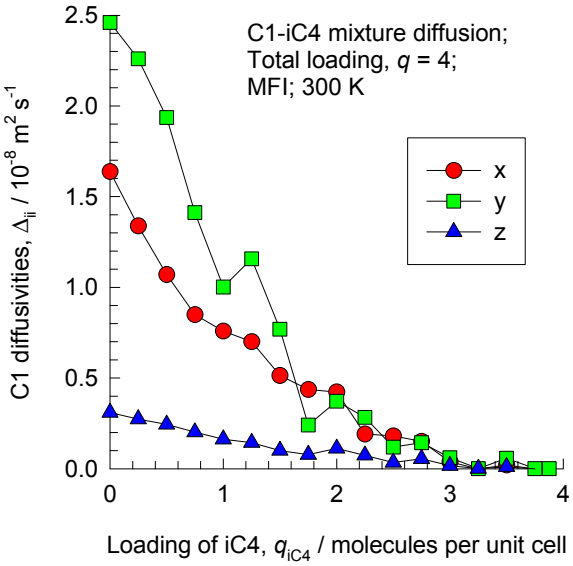

Figure B73

# Guest Mixture in MFI zeolite: $C_2H_6/iC_4H_{10}$

Figure B74

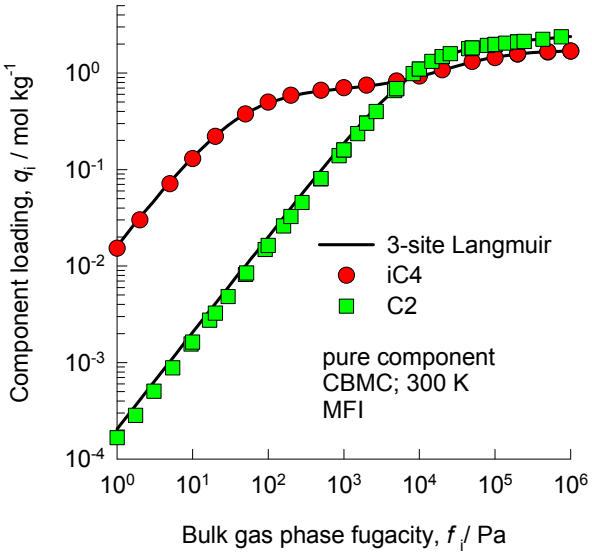


**Pure components adsorption**

# C2 - iC4 / MFI / 300K

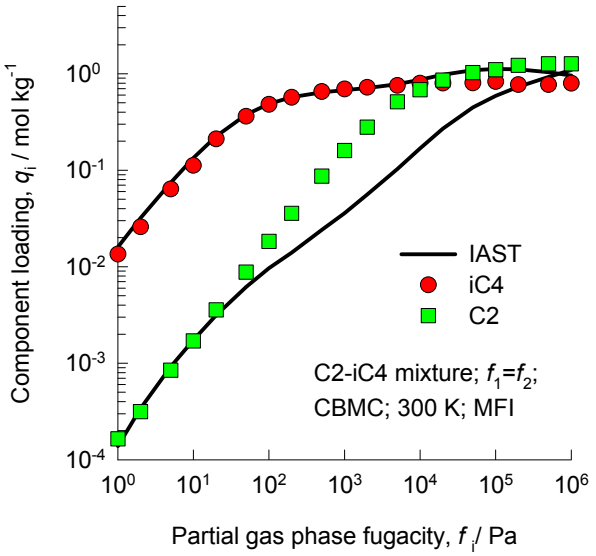


**mixture adsorption**

The failure of IAST to describe mixture adsorption accurately is because of segregation effects. The iC4 locates preferentially at the intersections. This implies that there is no homogeneous distribution of the mixture over the entire MFI framework. This non-homogeneous distribution of molecules causes departures from IAST.

The adsorption and diffusion characteristics are discussed in further details in:
R. Krishna, J.M. van Baten, Diffusion of hydrocarbon mixtures in MFI zeolite: Influence of intersection blocking, Chem. Eng. J. 140 (2008) 614-620.

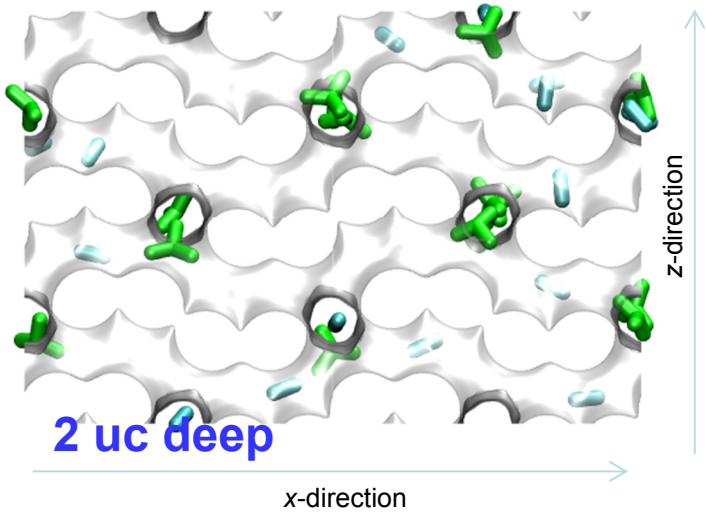


C2 = 2 molecules/uc

iC4 = 2 molecules/uc

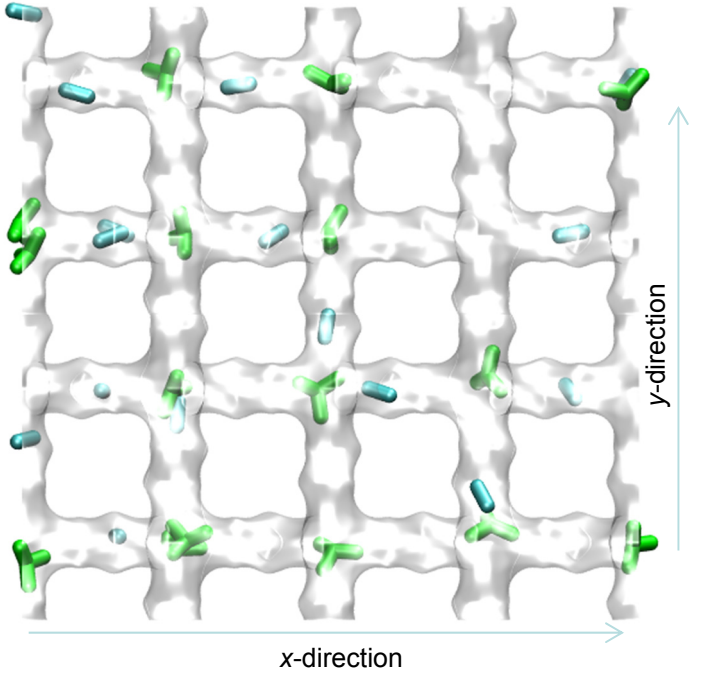


# C2 - iC4 / MFI / 300K

## mixture diffusion

*y*-direction of yields highest diffusivity; this is a straight path

*x*-direction of yields intermediate; this is a zig-zag path

*z*-direction of yields lowest diffusivity

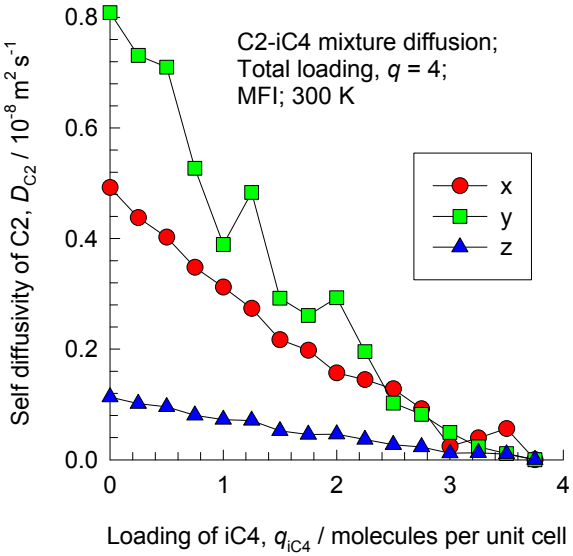


The adsorption and diffusion characteristics are discussed in further details in:
R. Krishna, J.M. van Baten, Diffusion of hydrocarbon mixtures in MFI zeolite: Influence of intersection blocking, Chem. Eng. J. 140 (2008) 614-620.

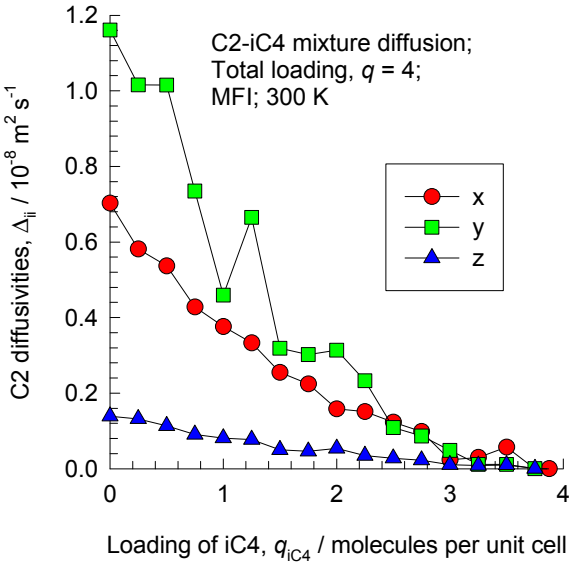

# Guest Mixture in MFI zeolite: $C_3H_8/iC_4H_{10}$

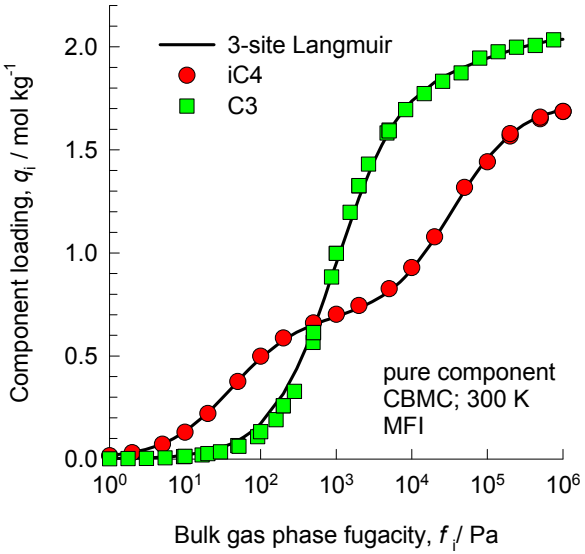


## Pure components adsorption

# C3 - iC4 / MFI / 300K

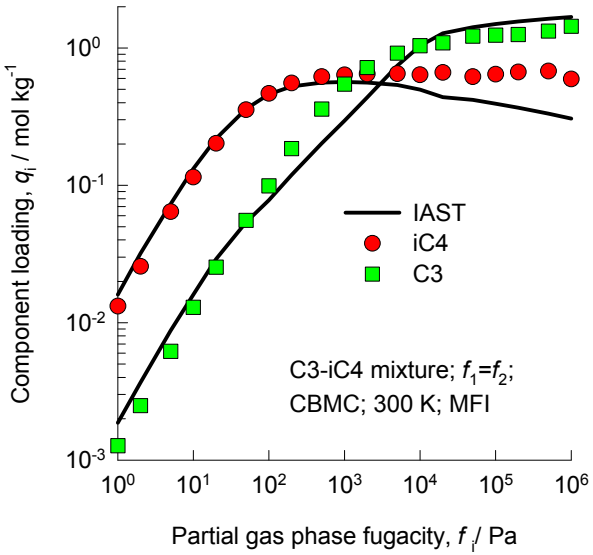


## mixture adsorption

The failure of IAST to describe mixture adsorption accurately is because of segregation effects. The iC4 locates preferentially at the intersections. This implies that there is no homogeneous distribution of the mixture over the entire MFI framework. This non-homogeneous distribution of molecules causes departures from IAST.

The adsorption and diffusion characteristics are discussed in further details in:
R. Krishna, J.M. van Baten, Diffusion of hydrocarbon mixtures in MFI zeolite: Influence of intersection blocking, Chem. Eng. J. 140 (2008) 614-620.

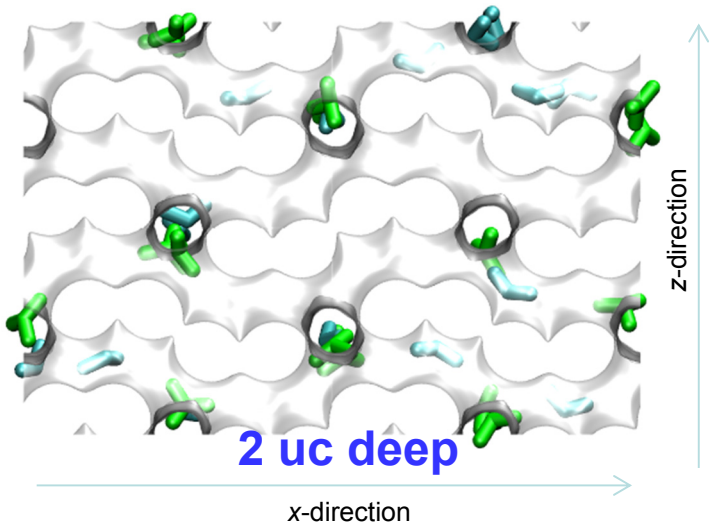


**C3 = 2 molecules/uc**
**iC4 = 2 molecules/uc**

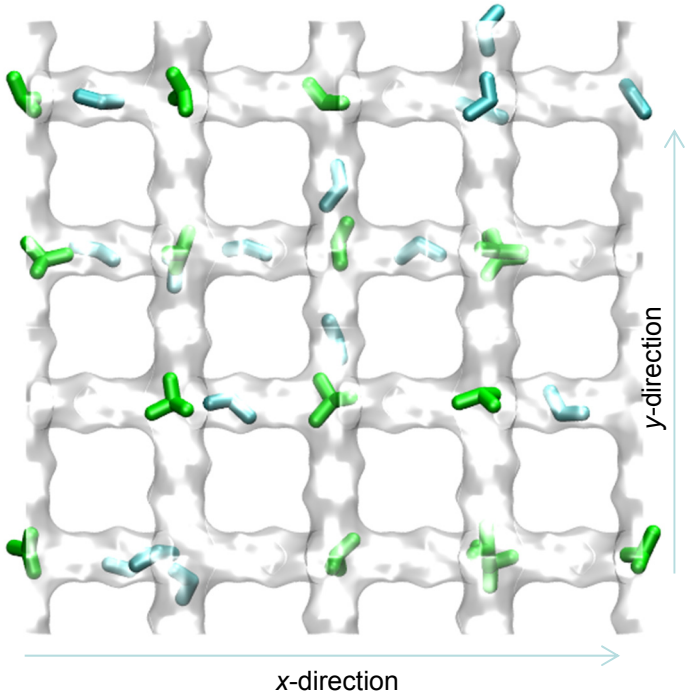


# C3 - iC4 / MFI / 300K

## mixture diffusion

*y*-direction of yields highest diffusivity; this is a straight path

*x*-direction of yields intermediate; this is a zig-zag path

*z*-direction of yields lowest diffusivity

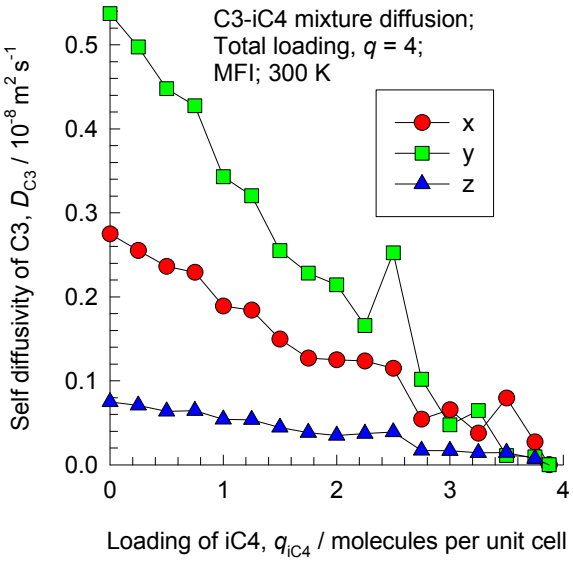


The adsorption and diffusion characteristics are discussed in further details in:
R. Krishna, J.M. van Baten, Diffusion of hydrocarbon mixtures in MFI zeolite: Influence of intersection blocking, Chem. Eng. J. 140 (2008) 614-620.

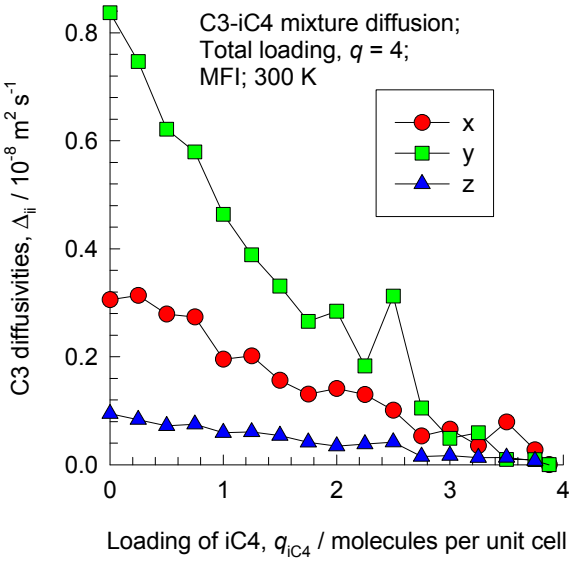

Figure B79

# Guest Mixture in MFI zeolite: $nC_4H_{10}/iC_4H_{10}$

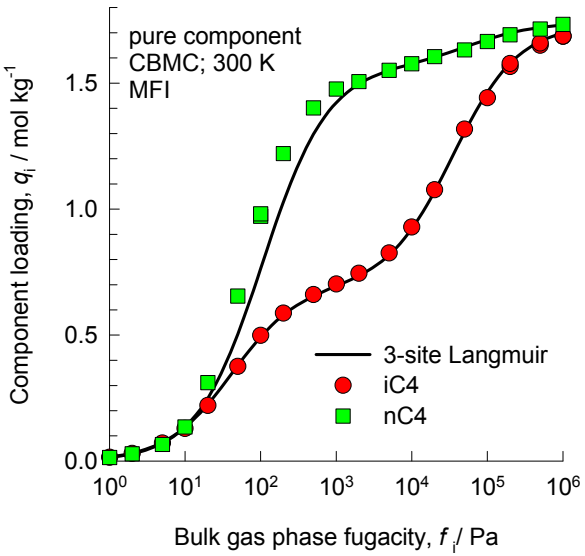


## Pure components adsorption

# nC4 - iC4 / MFI / 300K

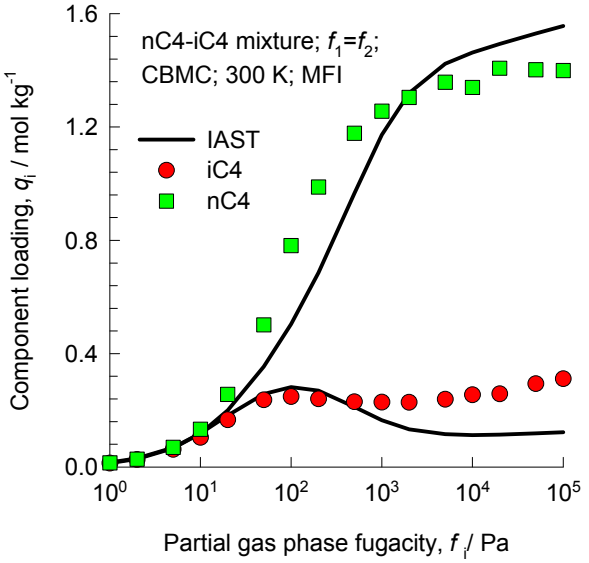


## mixture adsorption

The failure of IAST to describe mixture adsorption accurately is because of segregation effects. The iC4 locates preferentially at the intersections. This implies that there is no homogeneous distribution of the mixture over the entire MFI framework. This non-homogeneous distribution of molecules causes departures from IAST.

The adsorption and diffusion characteristics are discussed in further details in:
R. Krishna, J.M. van Baten, Diffusion of hydrocarbon mixtures in MFI zeolite: Influence of intersection blocking, Chem. Eng. J. 140 (2008) 614-620.

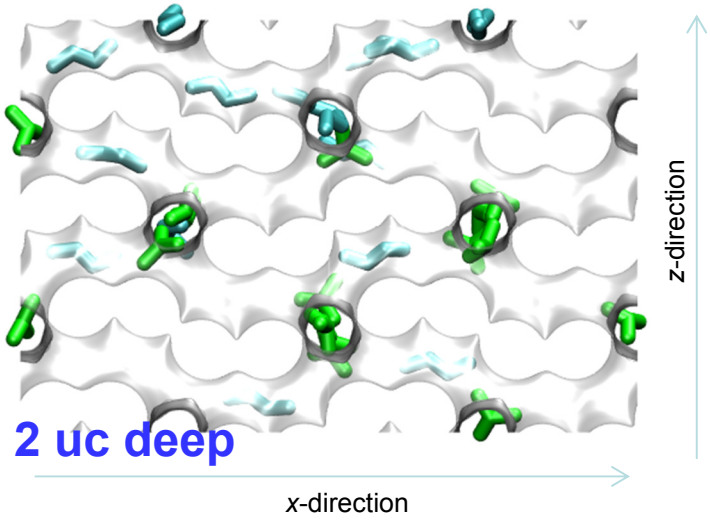


**2 uc deep**

**nC4 = 2 molecules/uc**

**iC4 = 2 molecules/uc**

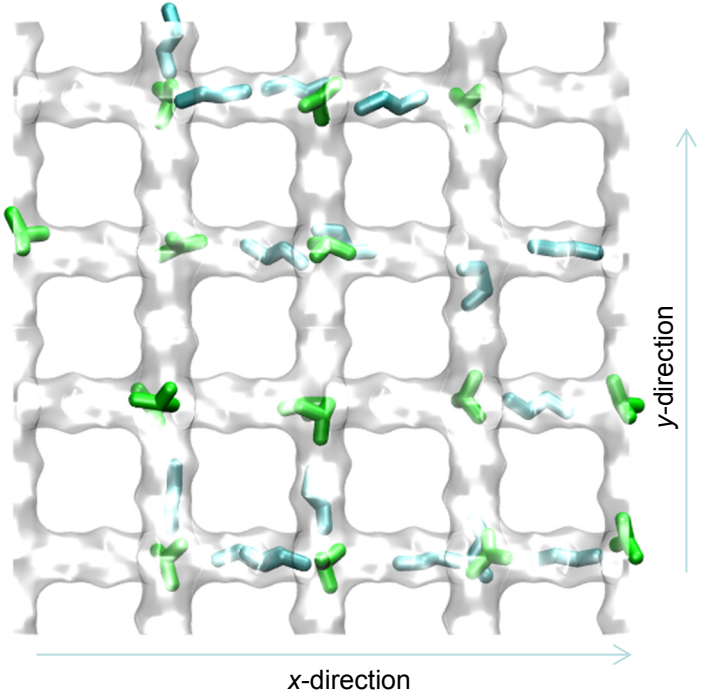


**2 uc deep**

# nC4 - iC4 / MFI / 300K

*y*-direction of yields highest diffusivity; this is a straight path

*x*-direction of yields intermediate; this is a zig-zag path

*z*-direction of yields lowest diffusivity

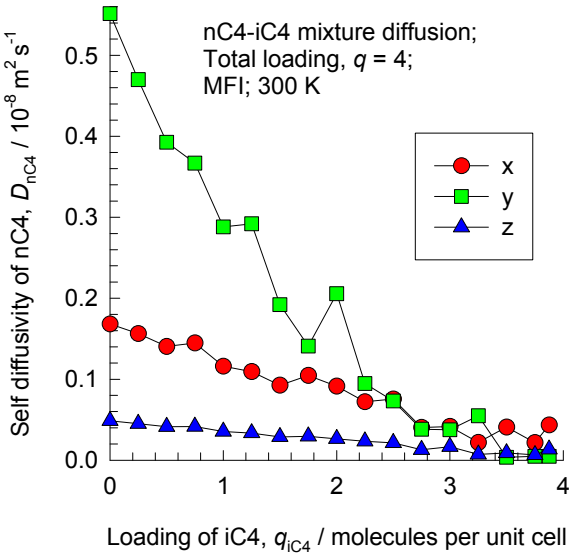


## mixture diffusion

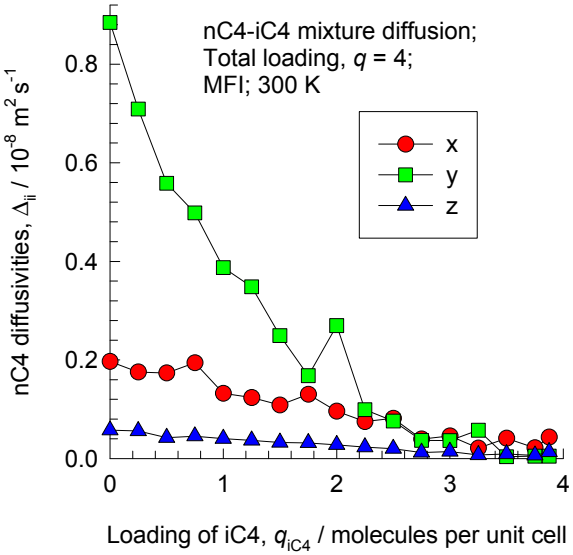


The adsorption and diffusion characteristics are discussed in further details in:
R. Krishna, J.M. van Baten, Diffusion of hydrocarbon mixtures in MFI zeolite: Influence of intersection blocking, Chem. Eng. J. 140 (2008) 614-620.

# MFI nC4/iC4mixture diffusion in MFI: PFG NMR experiments

Figure B82

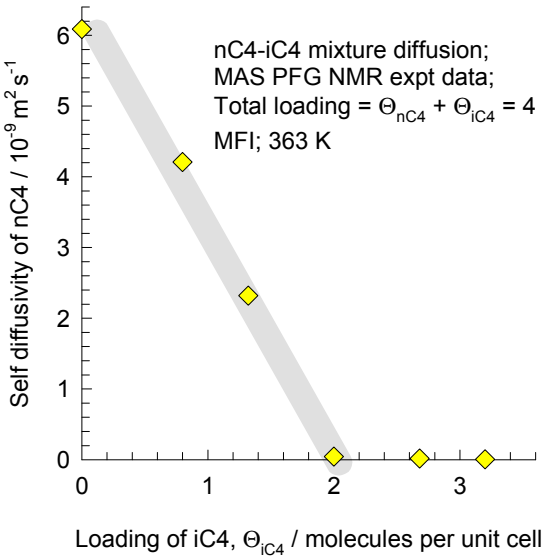


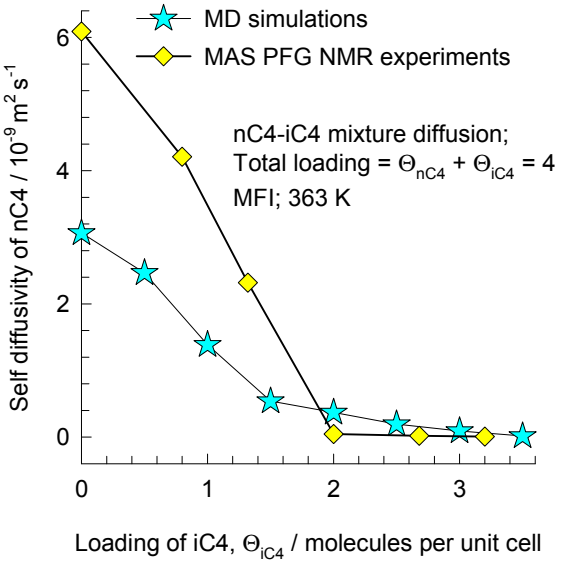


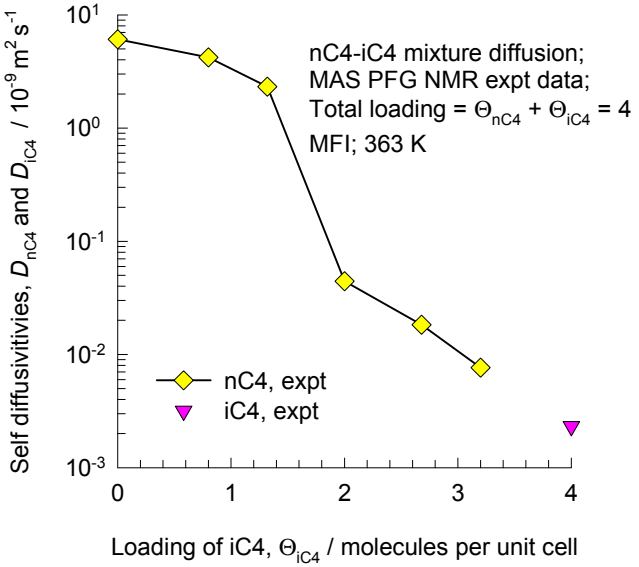


The data are re-plotted using the information in:
M. Fernandez, J. Kärger, D. Freude, A. Pampel, J.M. van Baten, R. Krishna, Mixture diffusion in zeolites studied by MAS PFG NMR and molecular simulation, Microporous Mesoporous Mater. 105 (2007) 124-131.

Figure B83

**Snapshots showing the location of molecules within MFI**

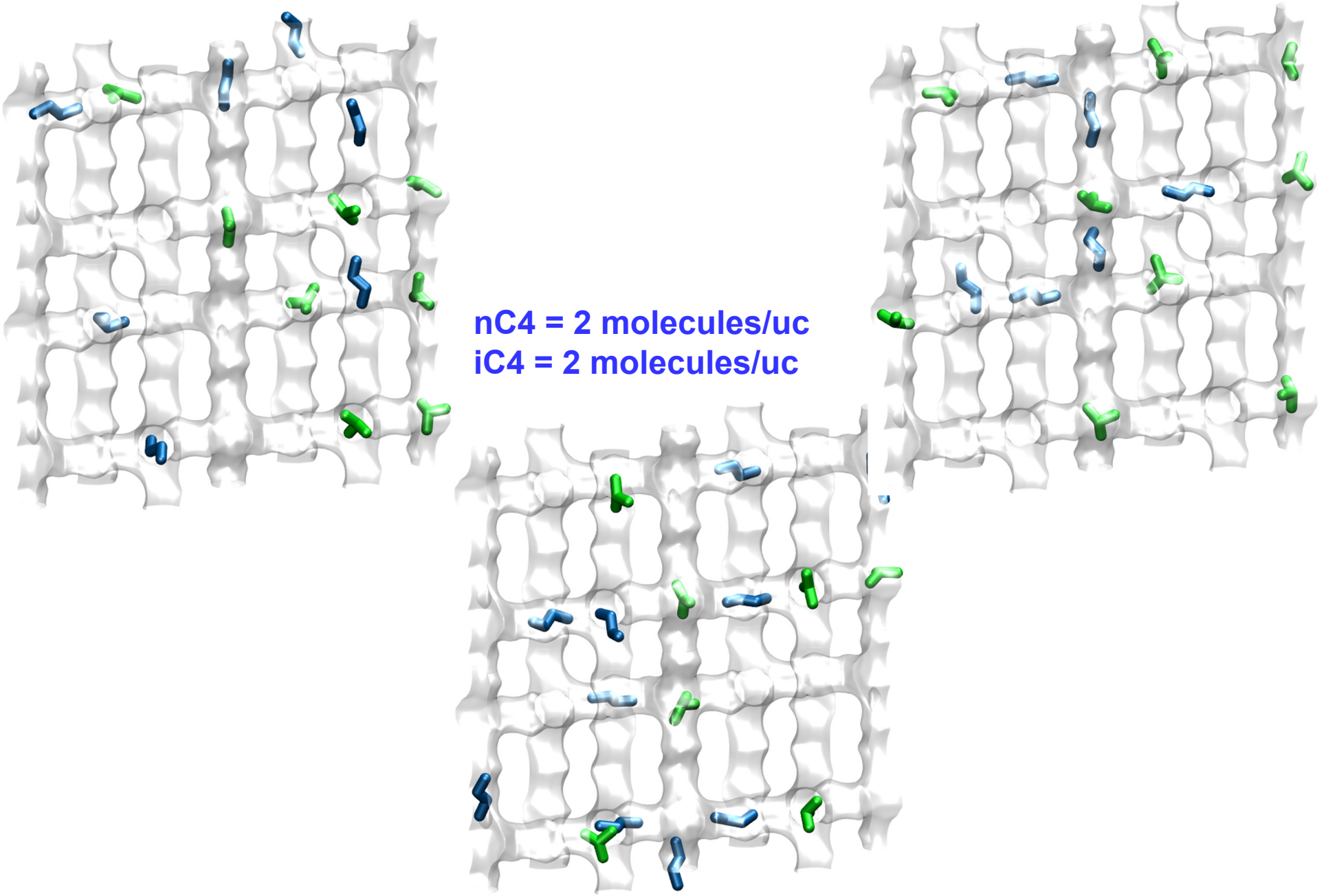

Figure B84

**Snapshots showing the location of molecules within MFI**

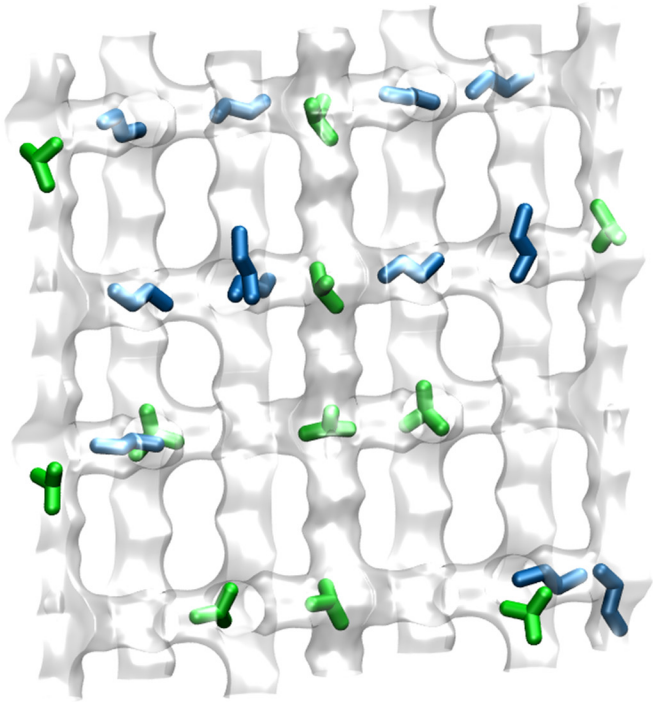

nC4 = 3 molecules/uc
iC4 = 3 molecules/uc

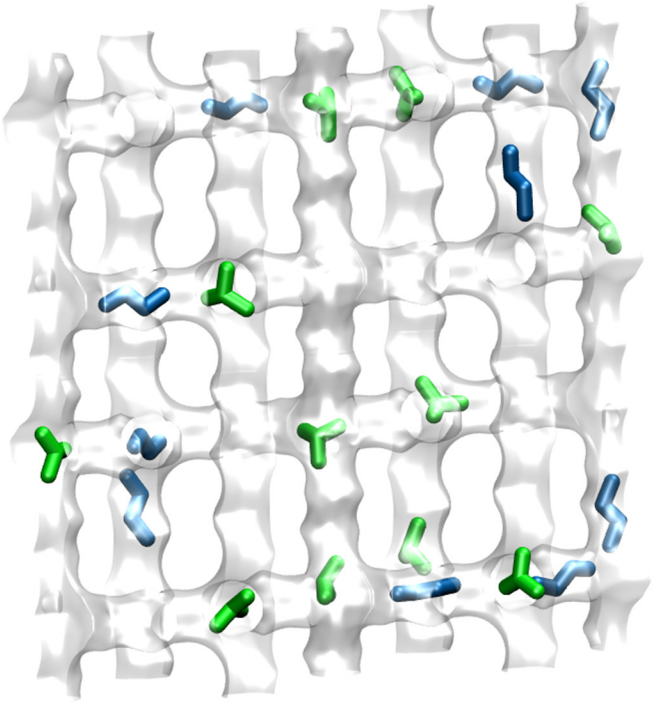

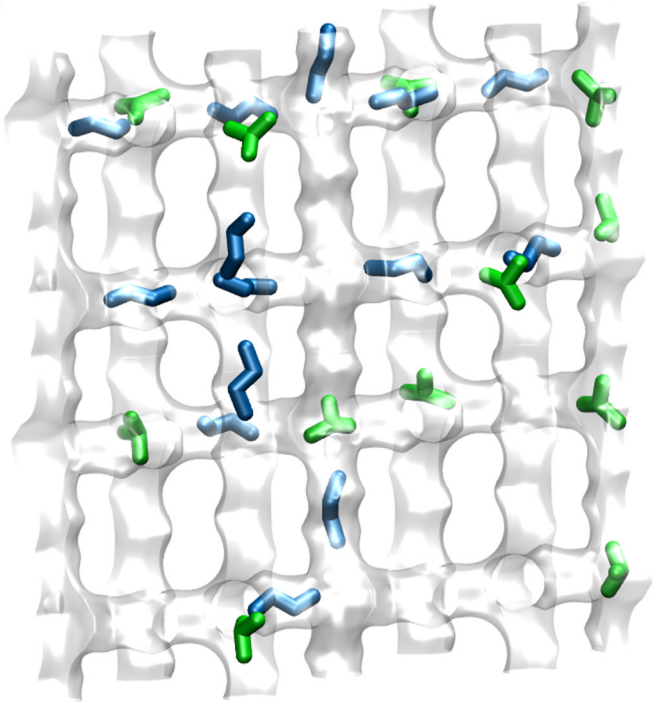

Figure B85

**Snapshots showing the location of molecules within MFI**

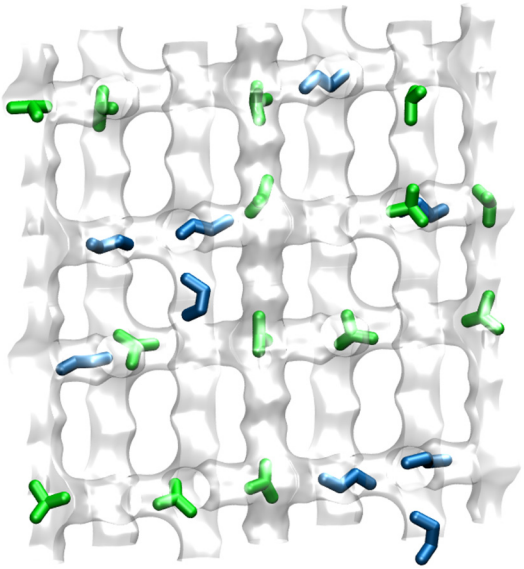

nC4 = 4 molecules/uc
iC4 = 4 molecules/uc

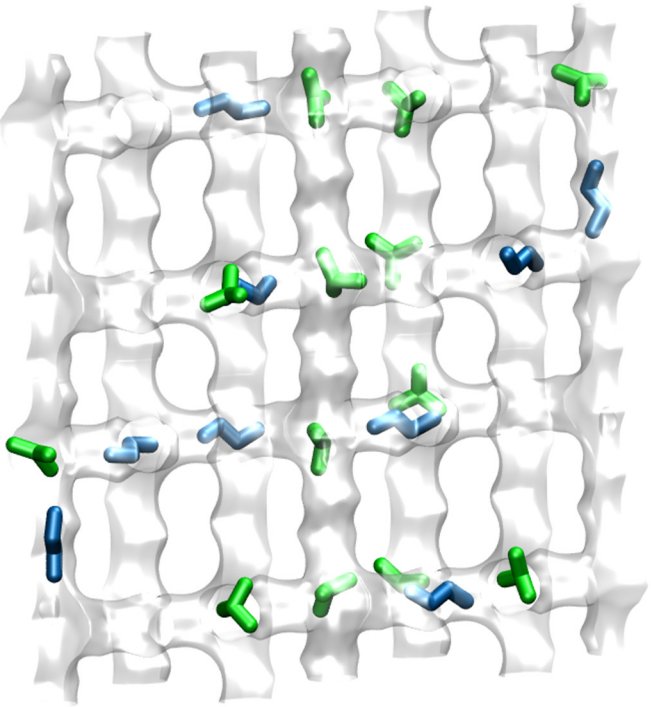

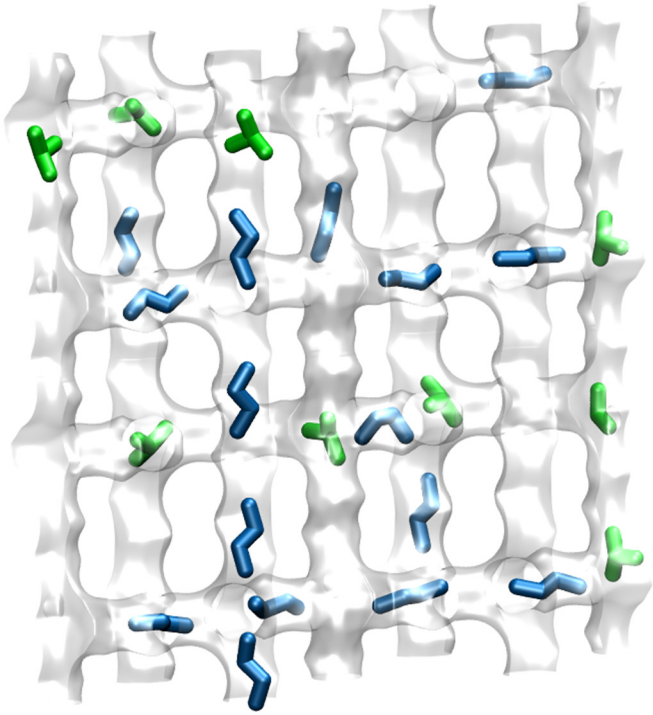

# Guest Mixture in MFI zeolite: $CH_4$/Benzene

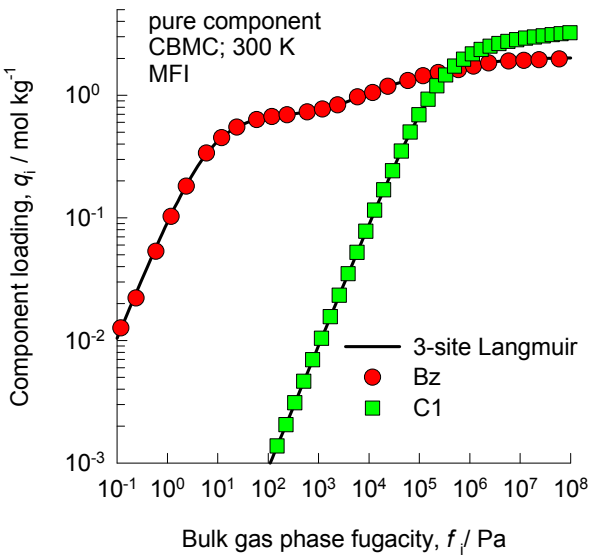


## Pure components adsorption

# C1 - Benzene/ MFI / 300K

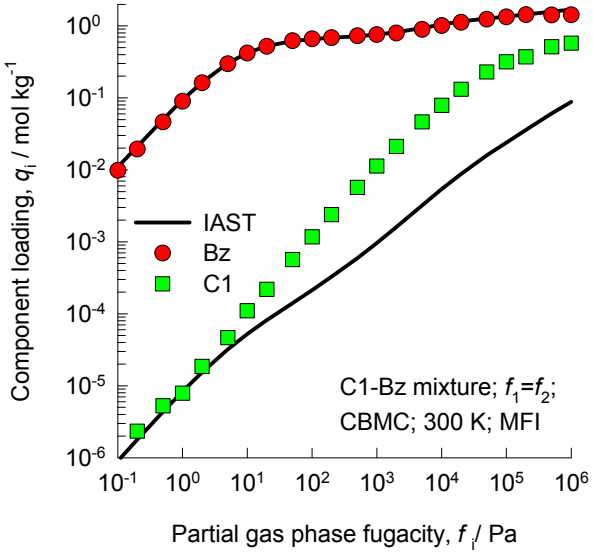


## mixture adsorption

The failure of IAST to describe mixture adsorption accurately is because of segregation effects. Benzene locates preferentially at the intersections. This implies that there is no homogeneous distribution of the mixture over the entire MFI framework. This non-homogeneous distribution of molecules causes departures from IAST.

The adsorption and diffusion characteristics are discussed in further details in:
R. Krishna, J.M. van Baten, Diffusion of hydrocarbon mixtures in MFI zeolite: Influence of intersection blocking, Chem. Eng. J. 140 (2008) 614-620.

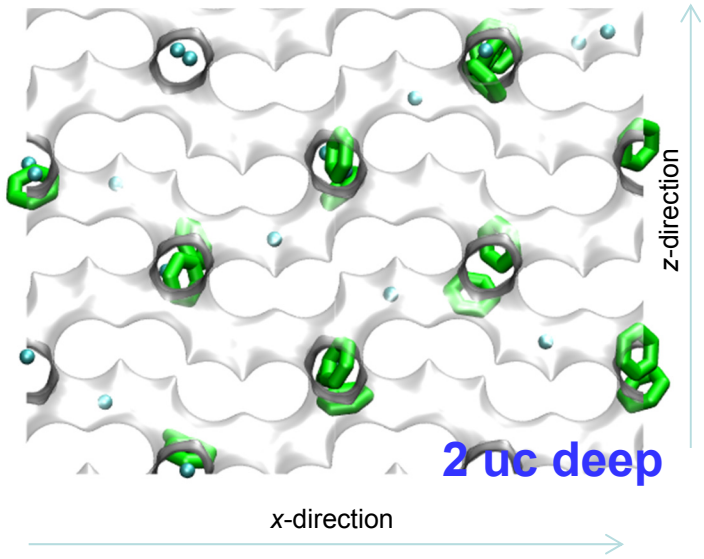


*y*-direction of yields highest diffusivity; this is a straight path

*x*-direction of yields intermediate; this is a zig-zag path

*z*-direction of yields lowest diffusivity

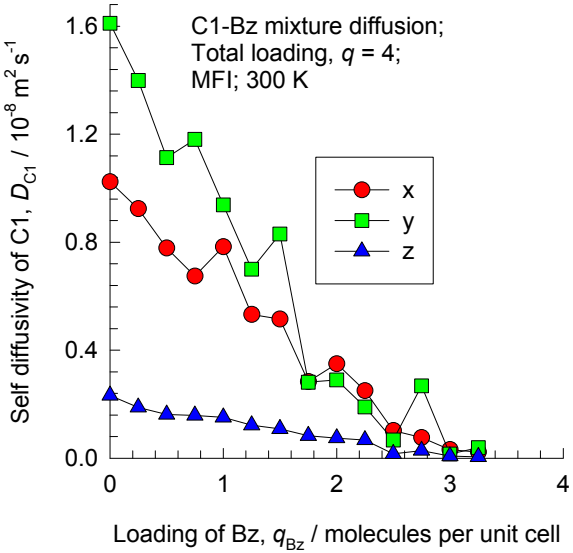


**C1 = 2 molecules/uc**

**Benzene = 2 molecules/uc**

# C1 - Benzene / MFI / 300K

## mixture diffusion

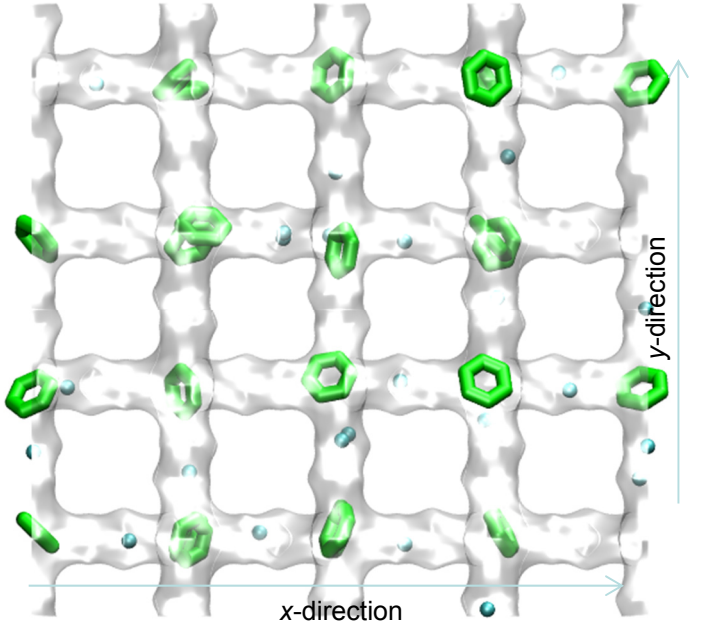


**3 uc deep**

The adsorption and diffusion characteristics are discussed in further details in:
R. Krishna, J.M. van Baten, Diffusion of hydrocarbon mixtures in MFI zeolite: Influence of intersection blocking, Chem. Eng. J. 140 (2008) 614-620.

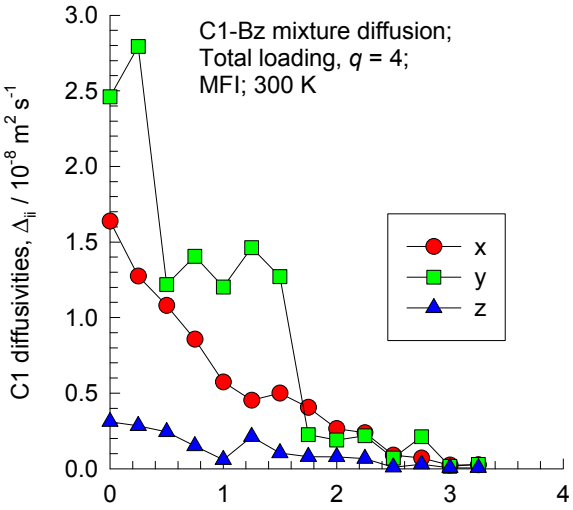

Figure B89

# MFI $CH_4$/Benzene mixture diffusion in MFI: PFG NMR experiments

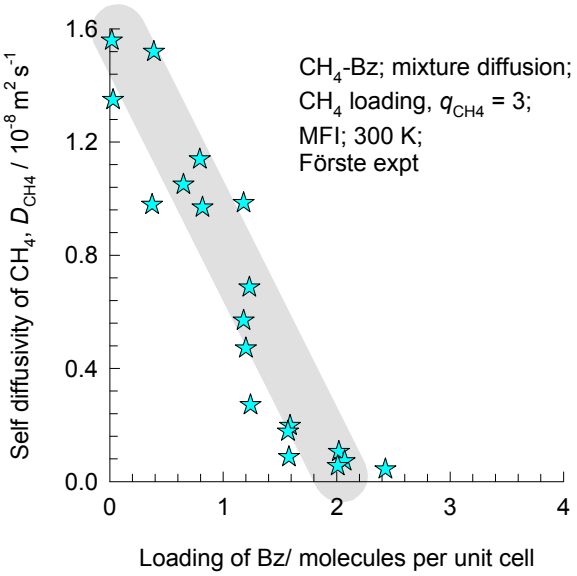


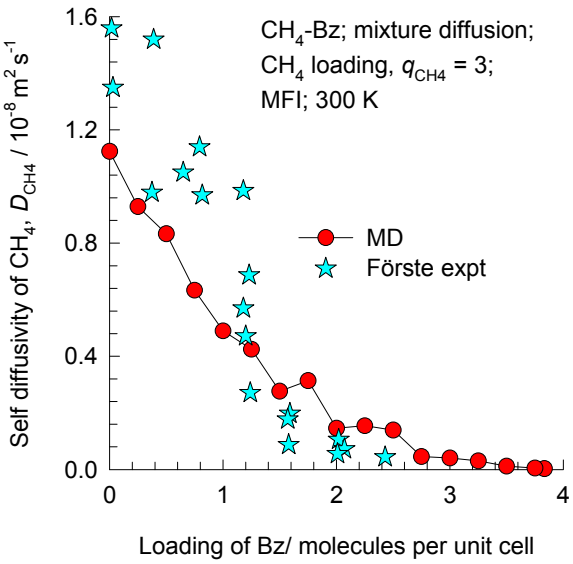


The experimental data are re-plotted using the information in:
C. Förste, A. Germanus, J. Kärger, H. Pfeifer, J. Caro, W. Pilz, A. Zikánová, Molecular mobility of methane adsorbed in ZSM-5 containing co-adsorbed benzene, and the location of benzene molecules, J. Chem. Soc., Faraday Trans. 1. 83 (1987) 2301-2309.

The MD simulation results are from:
R. Krishna, J.M. van Baten, Diffusion of hydrocarbon mixtures in MFI zeolite: Influence of intersection blocking, Chem. Eng. J. 140 (2008) 614-620.

# Guest Mixture in MFI zeolite: $CH_4$/22DMB

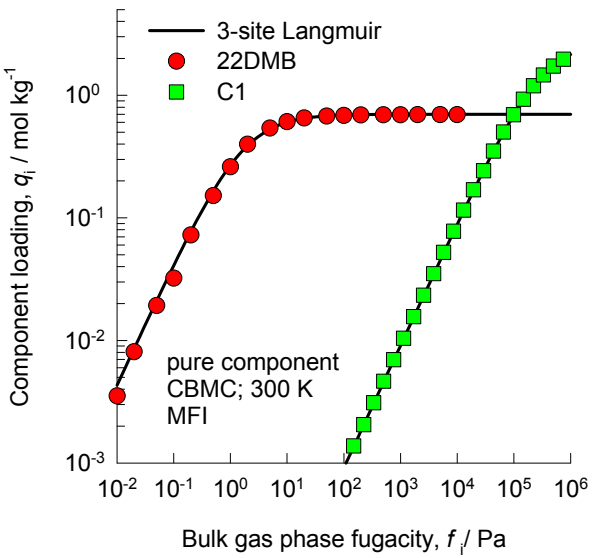


## Pure components adsorption

# C1 - 22DMB/ MFI / 300K

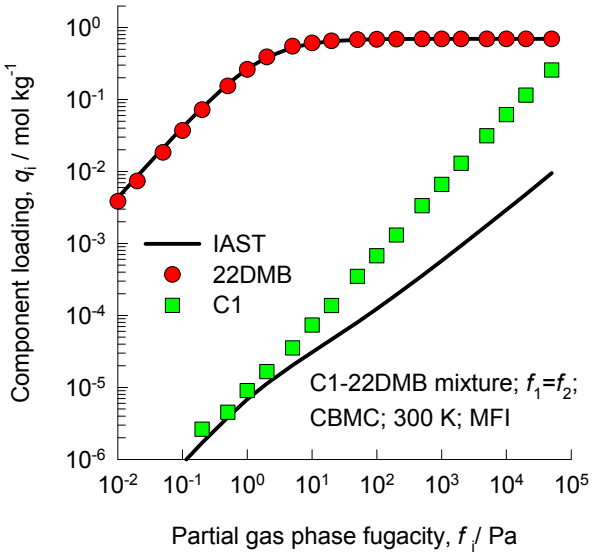


## mixture adsorption

The failure of IAST to describe mixture adsorption accurately is because of segregation effects. 22DMB locates preferentially at the intersections. This implies that there is no homogeneous distribution of the mixture over the entire MFI framework. This non-homogeneous distribution of molecules causes departures from IAST.

The adsorption and diffusion characteristics are discussed in further details in:
R. Krishna, J.M. van Baten, Diffusion of hydrocarbon mixtures in MFI zeolite: Influence of intersection blocking, Chem. Eng. J. 140 (2008) 614-620.

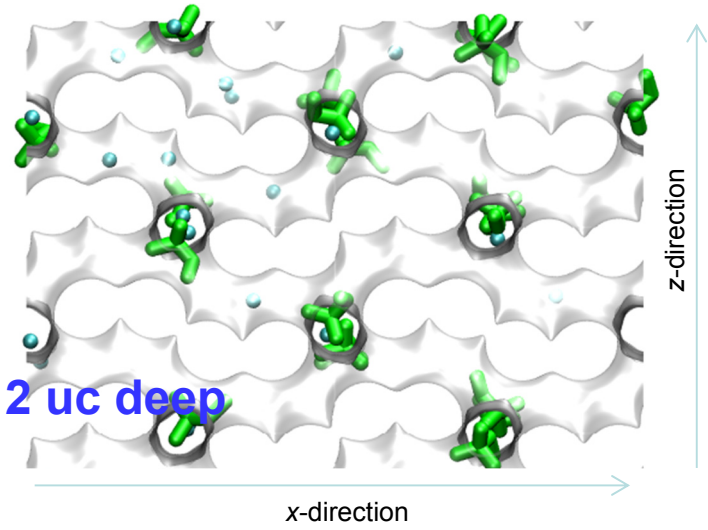


*y*-direction of yields highest diffusivity; this is a straight path

*x*-direction of yields intermediate; this is a zig-zag path

*z*-direction of yields lowest diffusivity

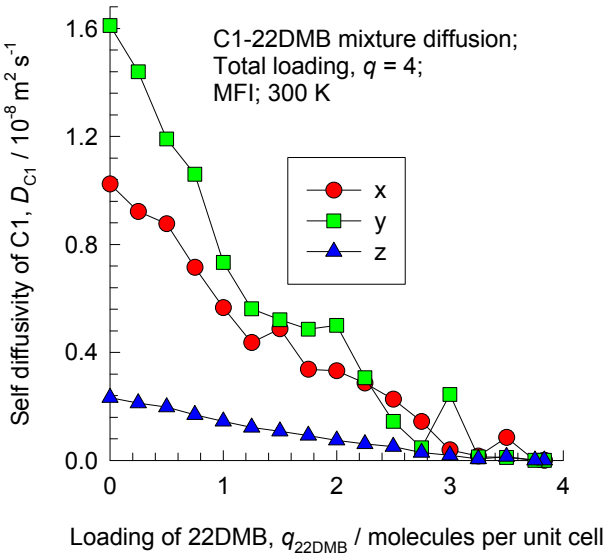


**C1 = 2 molecules/uc**
**22DMB = 2 molecules/uc**

# C1 - 22DMB / MFI / 300K

## mixture diffusion

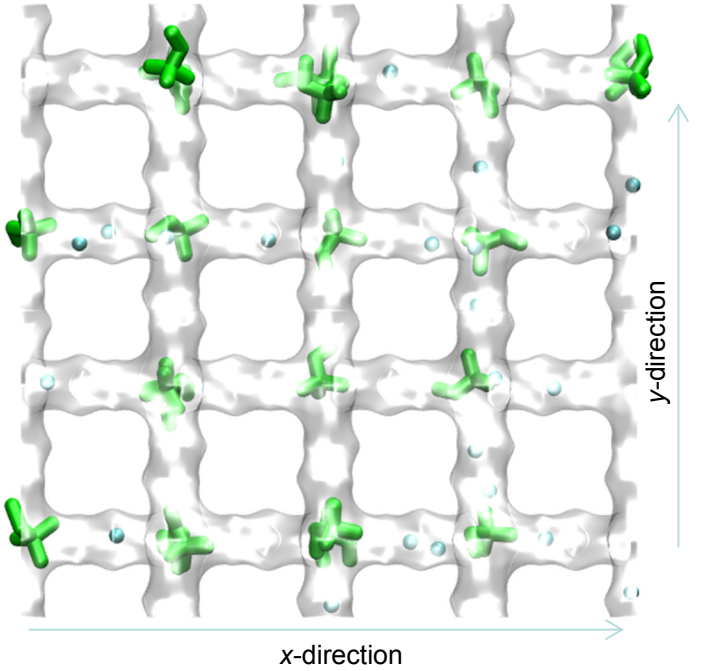


**3 uc deep**

The adsorption and diffusion characteristics are discussed in further details in:
R. Krishna, J.M. van Baten, Diffusion of hydrocarbon mixtures in MFI zeolite: Influence of intersection blocking, Chem. Eng. J. 140 (2008) 614-620.

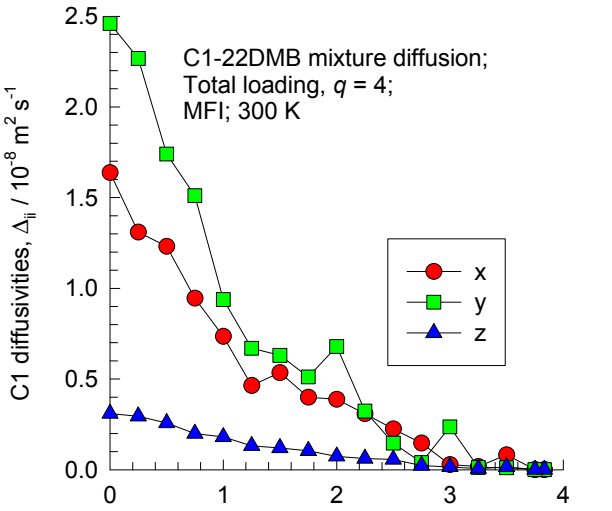

# Guest Mixture in MFI zeolite: $C_3H_8$/Benzene

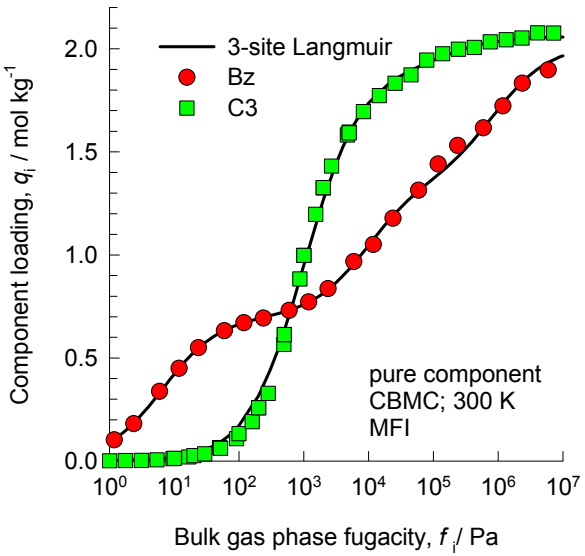


## Pure components adsorption

# C3 - Benzene/ MFI / 300K

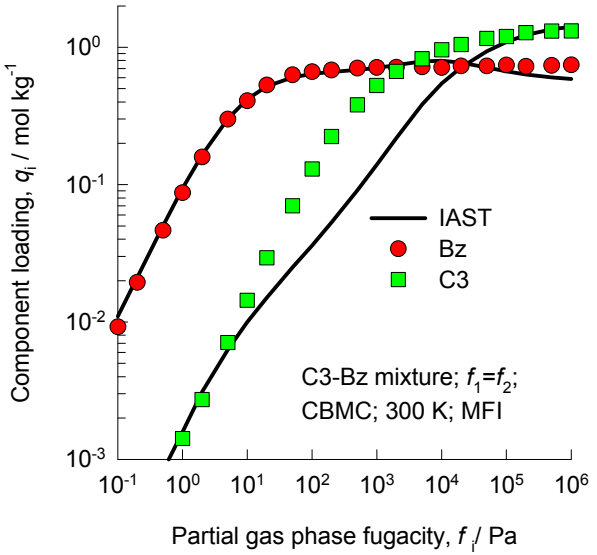


## mixture adsorption

The failure of IAST to describe mixture adsorption accurately is because of segregation effects. Benzene locates preferentially at the intersections. This implies that there is no homogeneous distribution of the mixture over the entire MFI framework. This non-homogeneous distribution of molecules causes departures from IAST.

The adsorption and diffusion characteristics are discussed in further details in:
R. Krishna, J.M. van Baten, Diffusion of hydrocarbon mixtures in MFI zeolite: Influence of intersection blocking, Chem. Eng. J. 140 (2008) 614-620.

# C3 - Benzene / MFI / 300K

## mixture diffusion

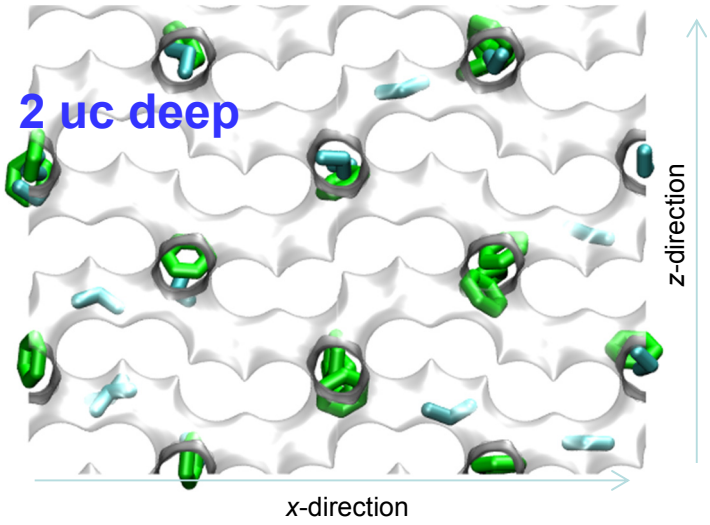


*y*-direction of yields highest diffusivity; this is a straight path

*x*-direction of yields intermediate; this is a zig-zag path

*z*-direction of yields lowest diffusivity

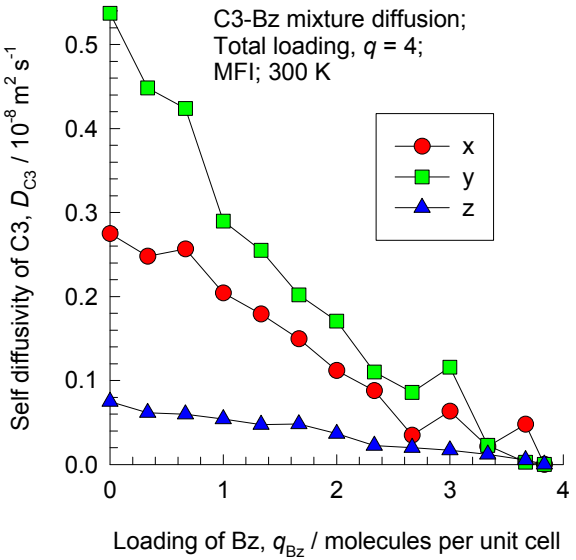


**C3 = 2 molecules/uc**
**Benzene = 2 molecules/uc**

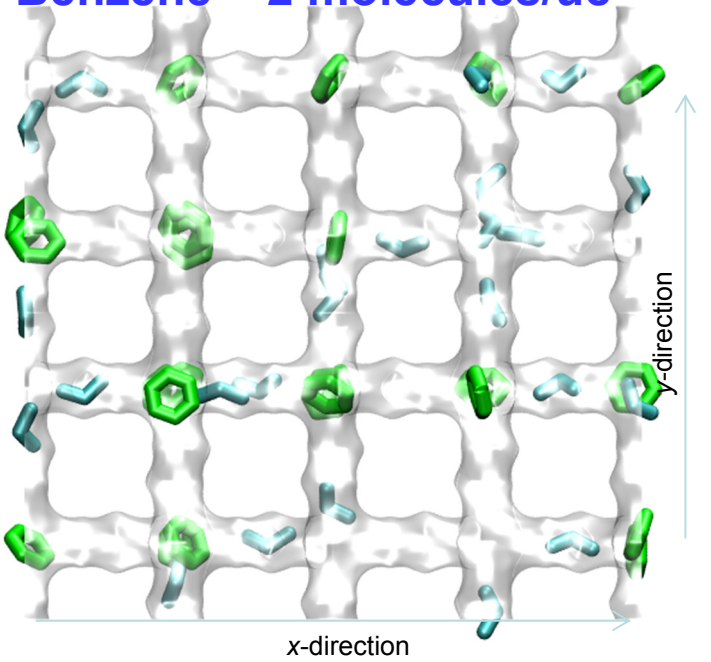


**3 uc deep**

The adsorption and diffusion characteristics are discussed in further details in:
R. Krishna, J.M. van Baten, Diffusion of hydrocarbon mixtures in MFI zeolite: Influence of intersection blocking, Chem. Eng. J. 140 (2008) 614-620.

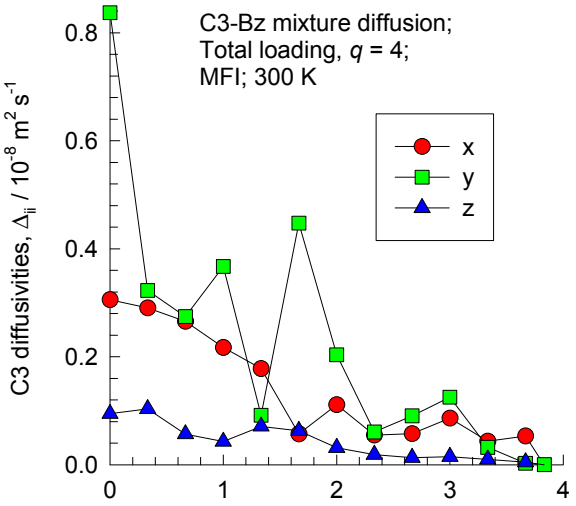

Figure B96

# Guest Mixture in MFI zeolite: nC6/22DMB

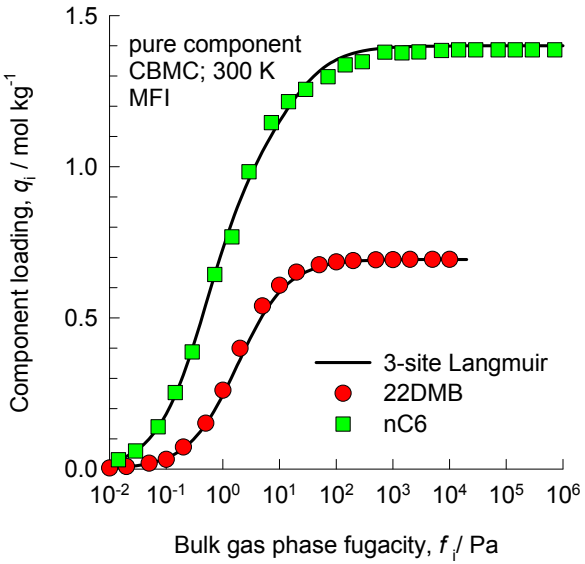


## Pure components adsorption

# nC6 -22DMB/ MFI / 300K

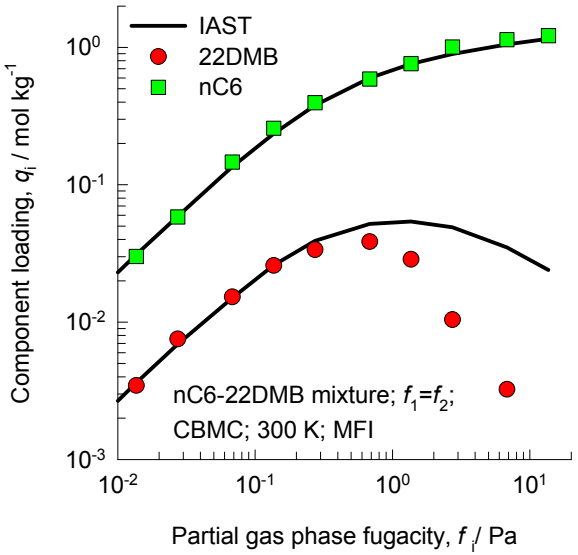


## mixture adsorption

The failure of IAST to describe mixture adsorption accurately is because of segregation effects. 22DMB locates preferentially at the intersections. This implies that there is no homogeneous distribution of the mixture over the entire MFI framework. This non-homogeneous distribution of molecules causes departures from IAST.

The adsorption and diffusion characteristics are discussed in further details in:
R. Krishna, J.M. van Baten, Diffusion of hydrocarbon mixtures in MFI zeolite: Influence of intersection blocking, Chem. Eng. J. 140 (2008) 614-620.

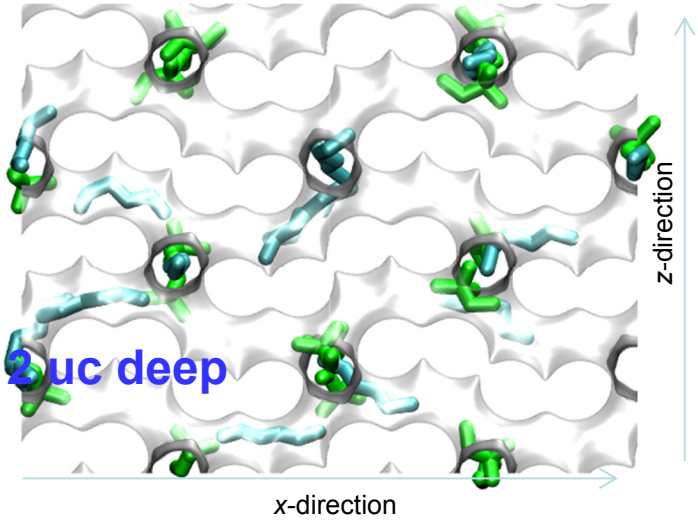


*y*-direction of yields highest diffusivity; this is a straight path

*x*-direction of yields intermediate; this is a zig-zag path

*z*-direction of yields lowest diffusivity

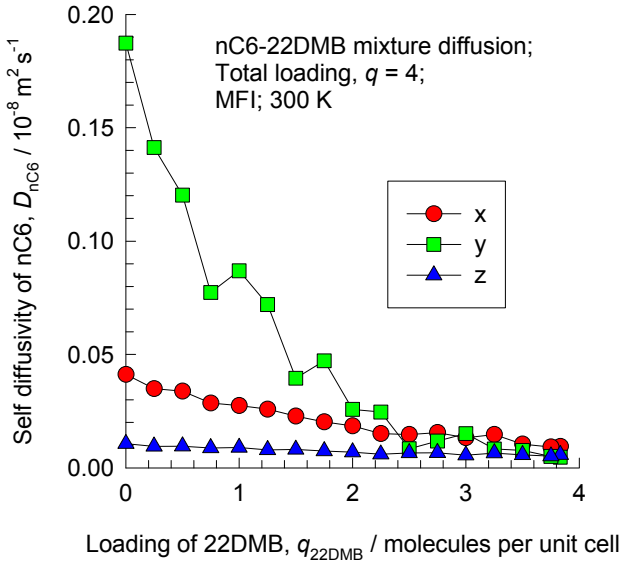


**nC6 = 2 molecules/uc**
**22DMB = 2 molecules/uc**

# nC6 - 22DMB / MFI / 300K

## mixture diffusion

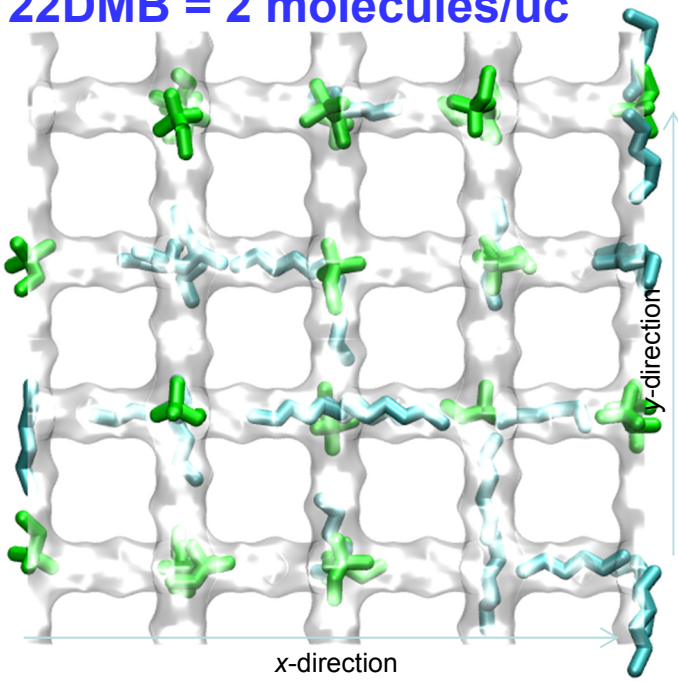


**3 uc deep**

The adsorption and diffusion characteristics are discussed in further details in:
R. Krishna, J.M. van Baten, Diffusion of hydrocarbon mixtures in MFI zeolite: Influence of intersection blocking, Chem. Eng. J. 140 (2008) 614-620.

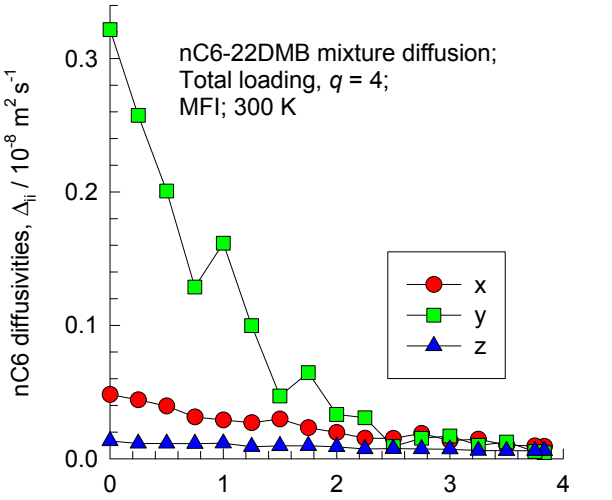

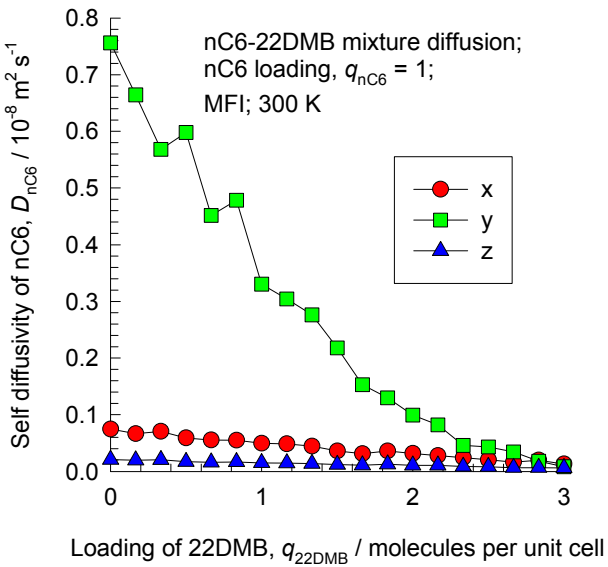


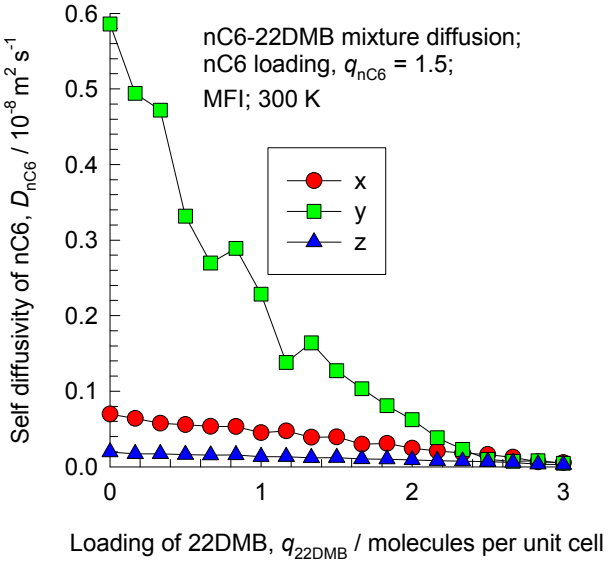


## mixture diffusion

# nC6 - 22DMB / MFI / 300K

## mixture diffusion

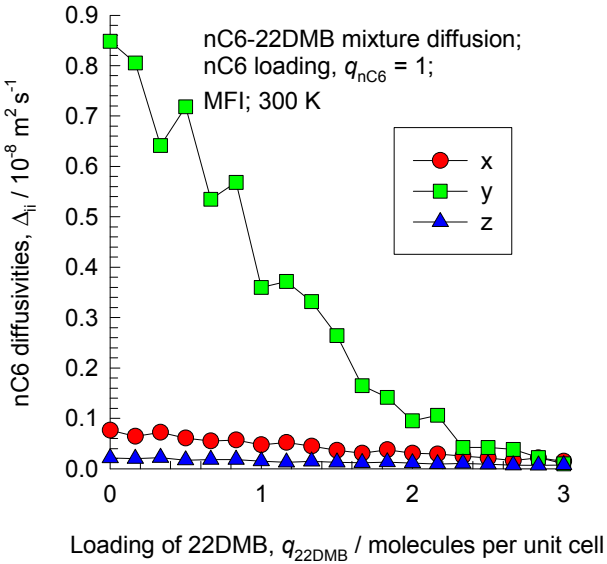


The adsorption and diffusion characteristics are discussed in further details in:
R. Krishna, J.M. van Baten, Diffusion of hydrocarbon mixtures in MFI zeolite: Influence of intersection blocking, Chem. Eng. J. 140 (2008) 614-620.

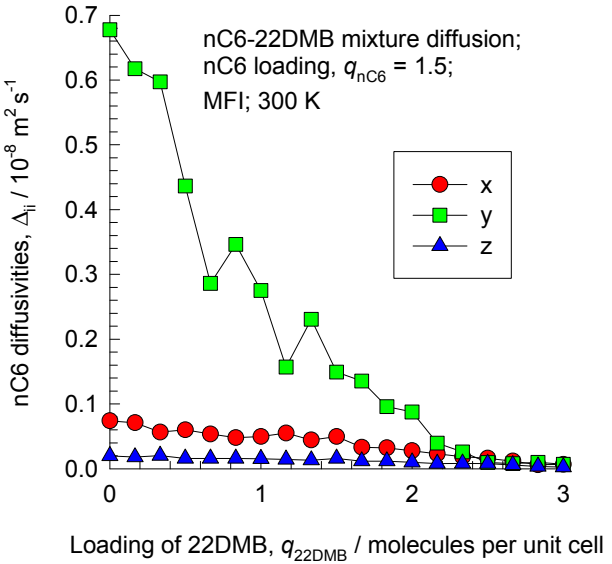

Figure B100

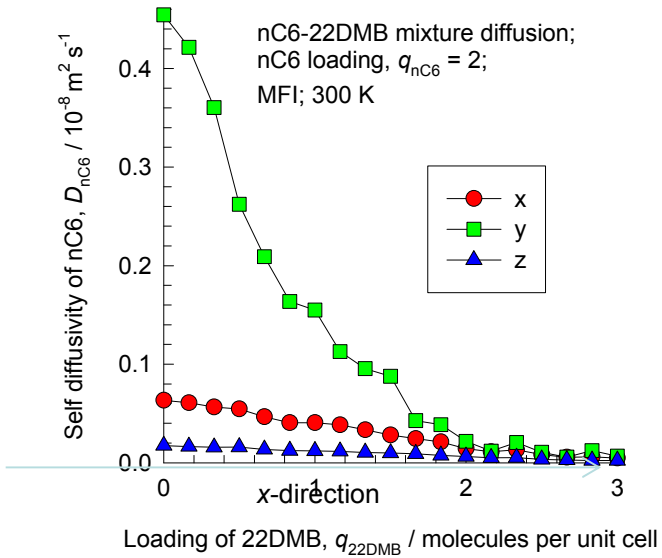


*y*-direction of yields highest diffusivity; this is a straight path

*x*-direction of yields intermediate; this is a zig-zag path

*z*-direction of yields lowest diffusivity

## mixture diffusion

# nC6 - 22DMB / MFI / 300K

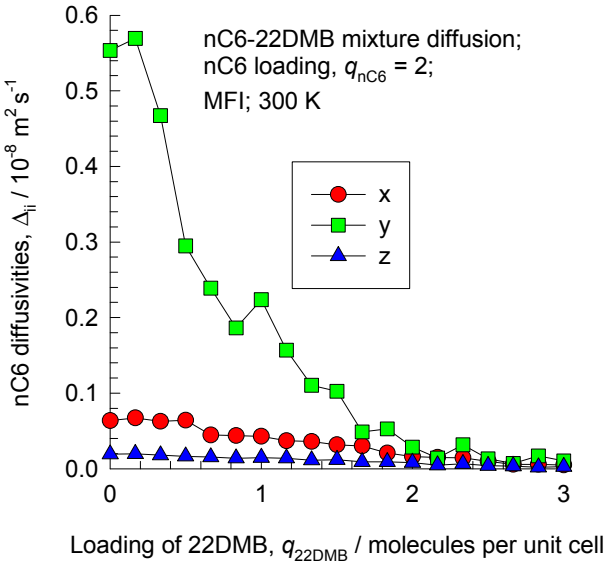


The adsorption and diffusion characteristics are discussed in further details in:
R. Krishna, J.M. van Baten, Diffusion of hydrocarbon mixtures in MFI zeolite: Influence of intersection blocking, Chem. Eng. J. 140 (2008) 614-620.

Figure B101

**Snapshots showing the location of molecules within MFI**

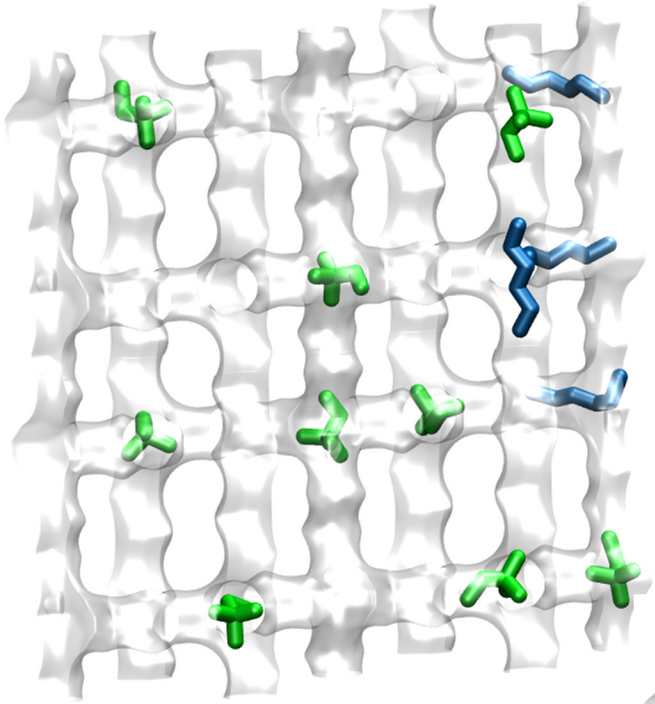

nC6 = 2 molecules/uc
22DMB = 2 molecules/uc

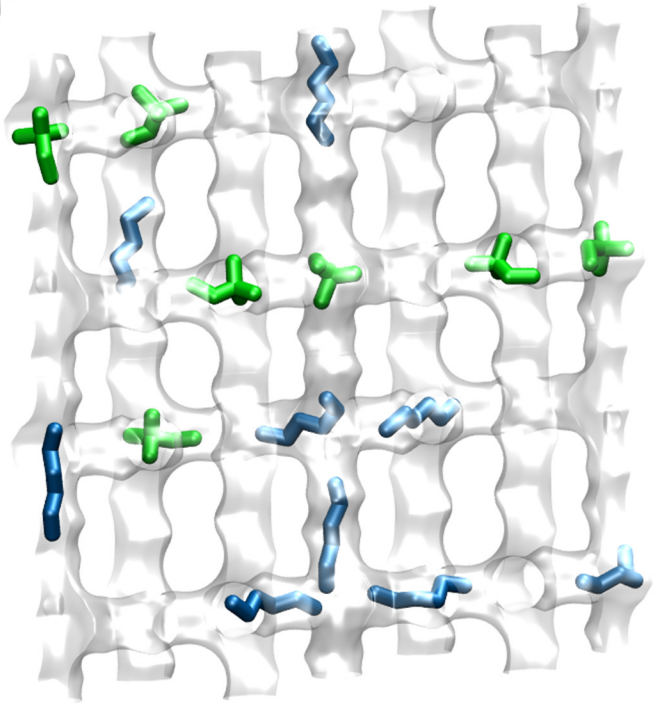

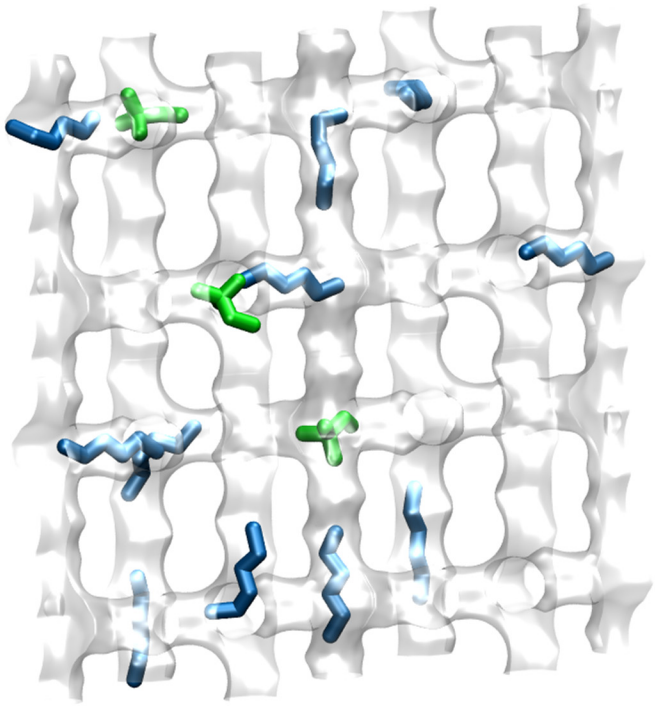

# Guest Mixture in MFI zeolite: nC6/2MP

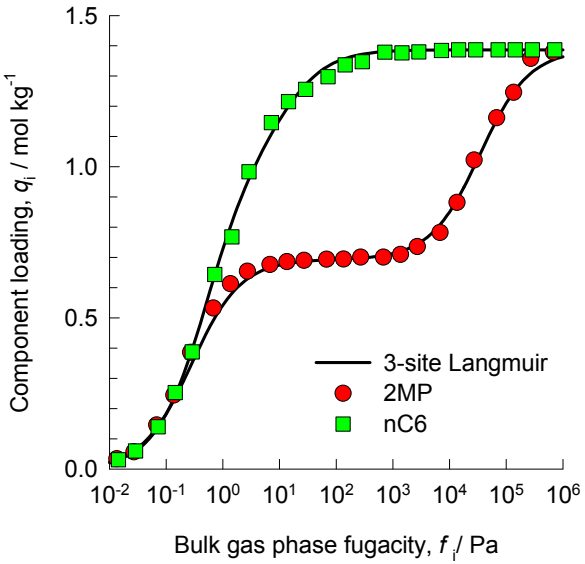


## Pure components adsorption

# nC6 -2MP/ MFI / 300K

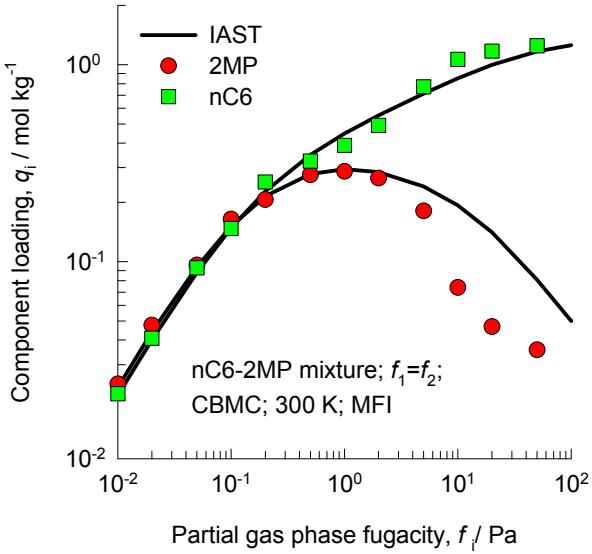


## mixture adsorption

The failure of IAST to describe mixture adsorption accurately is because of segregation effects. 2MP locates preferentially at the intersections. This implies that there is no homogeneous distribution of the mixture over the entire MFI framework. This non-homogeneous distribution of molecules causes departures from IAST.

The adsorption and diffusion characteristics are discussed in further details in:
R. Krishna, J.M. van Baten, Diffusion of hydrocarbon mixtures in MFI zeolite: Influence of intersection blocking, Chem. Eng. J. 140 (2008) 614-620.

# MFI nC6/2MP mixture diffusion in MFI

Figure B104

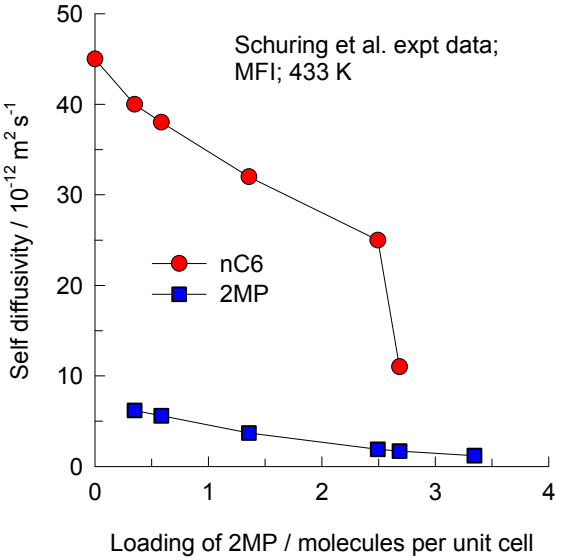


The data are re-plotted using the information in:
D. Schuring, A.O. Koriabkina, A.M. de Jong, B. Smit, R.A. van Santen, Adsorption and diffusion of n-hexane/2-methylpentane mixtures in zeolite silicalite: Experiments and modeling, J. Phys. Chem. B 105 (2001) 7690-7698.

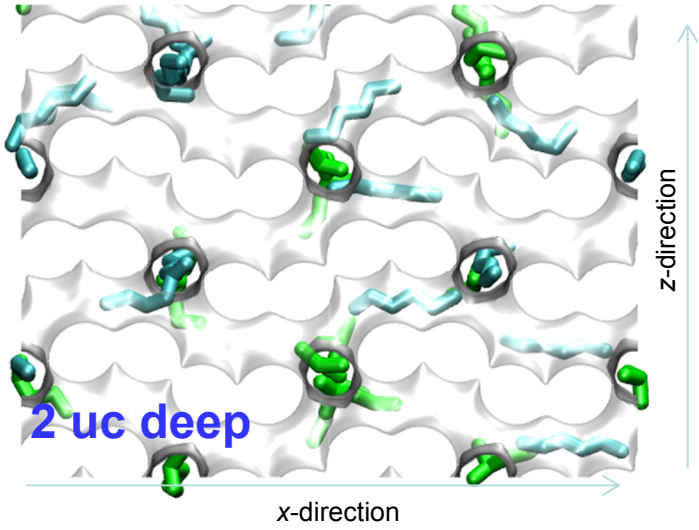


*y*-direction of yields highest diffusivity; this is a straight path

*x*-direction of yields intermediate; this is a zig-zag path

*z*-direction of yields lowest diffusivity

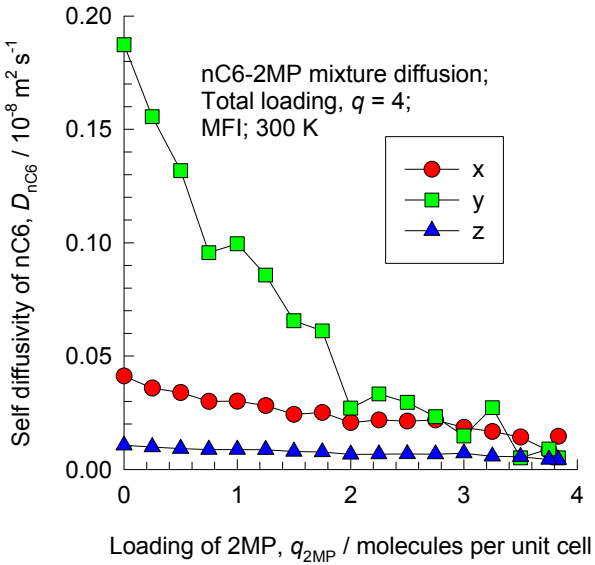


**nC6 = 2 molecules/uc**
**2MP = 2 molecules/uc**

# nC6 – 2MP/ MFI

## mixture diffusion

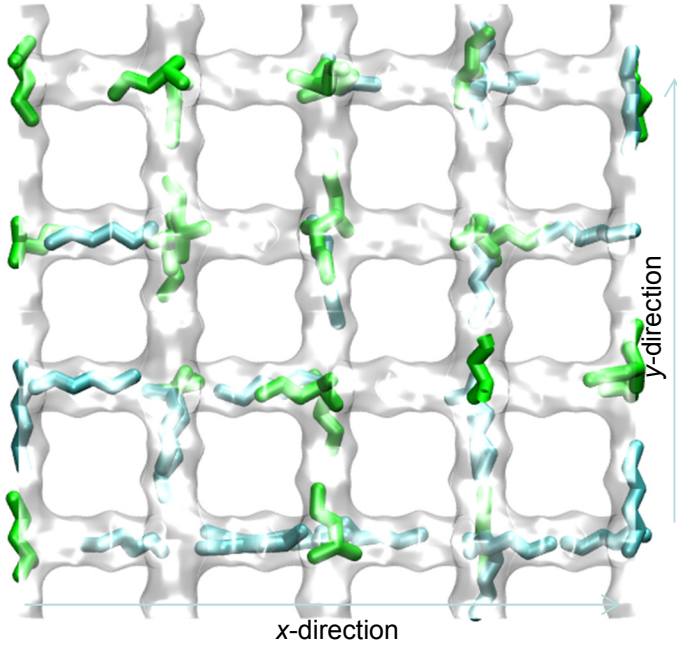


**3 uc deep**

The adsorption and diffusion characteristics are discussed in further details in:
R. Krishna, J.M. van Baten, Diffusion of hydrocarbon mixtures in MFI zeolite: Influence of intersection blocking, Chem. Eng. J. 140 (2008) 614-620.

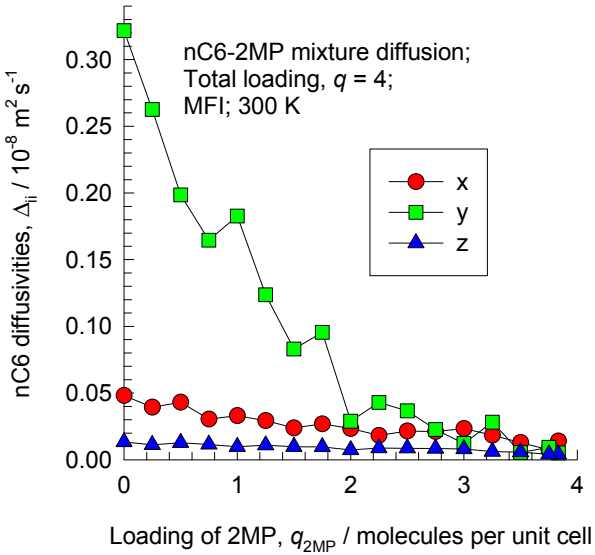

Figure B106

# Guest Mixture in MFI zeolite: nC6/3MP

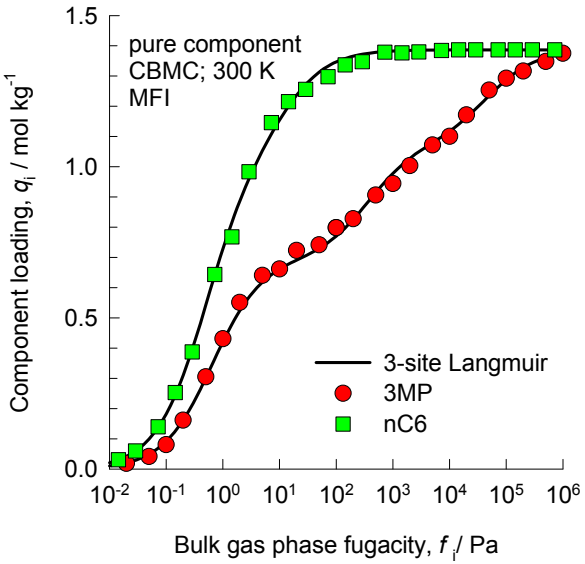


## Pure components adsorption

# nC6 -3MP/ MFI / 300K

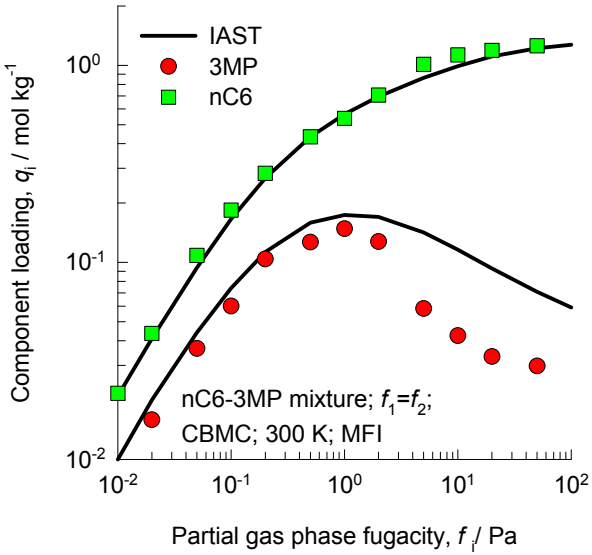


## mixture adsorption

The failure of IAST to describe mixture adsorption accurately is because of segregation effects. 3MP locates preferentially at the intersections. This implies that there is no homogeneous distribution of the mixture over the entire MFI framework. This non-homogeneous distribution of molecules causes departures from IAST.

The adsorption and diffusion characteristics are discussed in further details in:
R. Krishna, J.M. van Baten, Diffusion of hydrocarbon mixtures in MFI zeolite: Influence of intersection blocking, Chem. Eng. J. 140 (2008) 614-620.

Figure B108

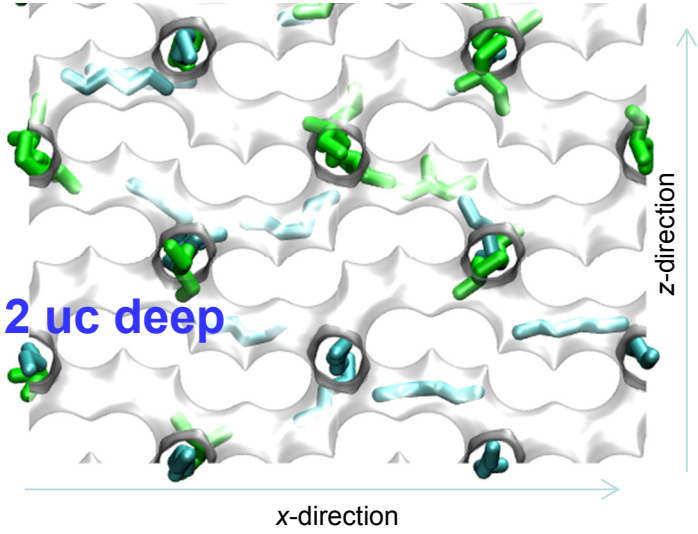


*y*-direction of yields highest diffusivity; this is a straight path

*x*-direction of yields intermediate; this is a zig-zag path

*z*-direction of yields lowest diffusivity

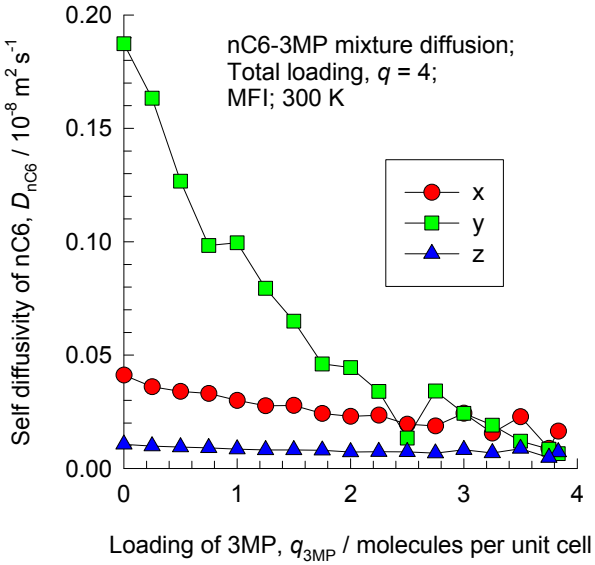


**nC6 = 2 molecules/uc**
**3MP = 2 molecules/uc**

# nC6 -3MP/ MFI / 300K

## mixture diffusion

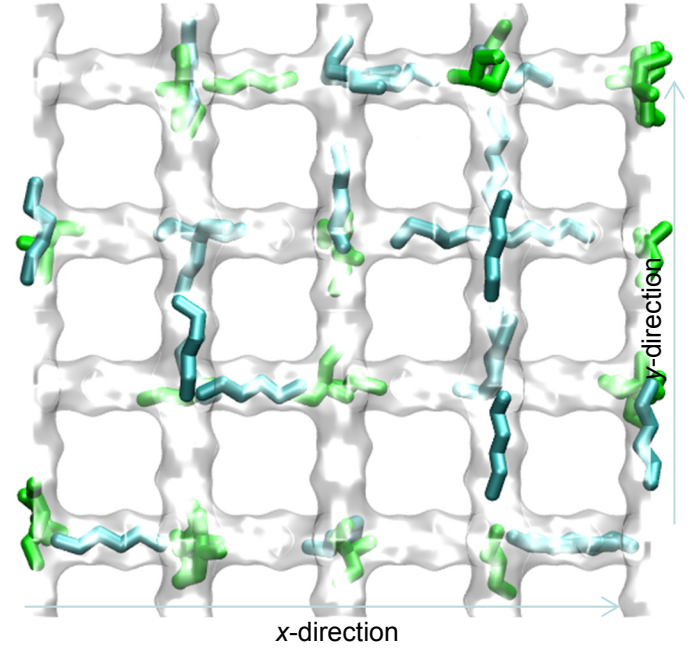


**3 uc deep**

The adsorption and diffusion characteristics are discussed in further details in:
R. Krishna, J.M. van Baten, Diffusion of hydrocarbon mixtures in MFI zeolite: Influence of intersection blocking, Chem. Eng. J. 140 (2008) 614-620.

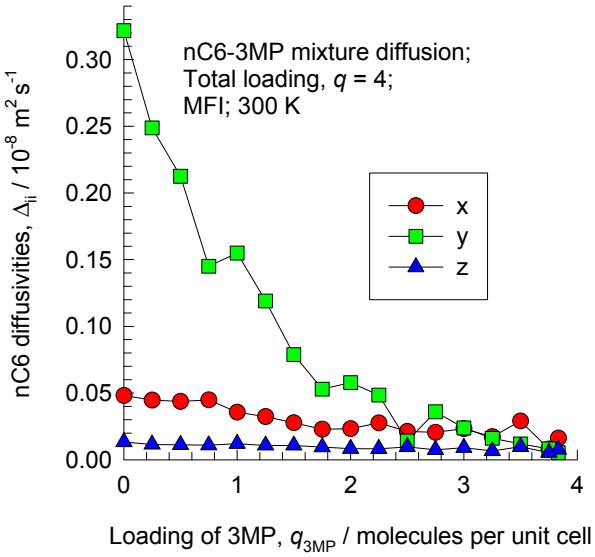

# Guest Mixture in MFI zeolite: nC6/Benzene

Figure B110

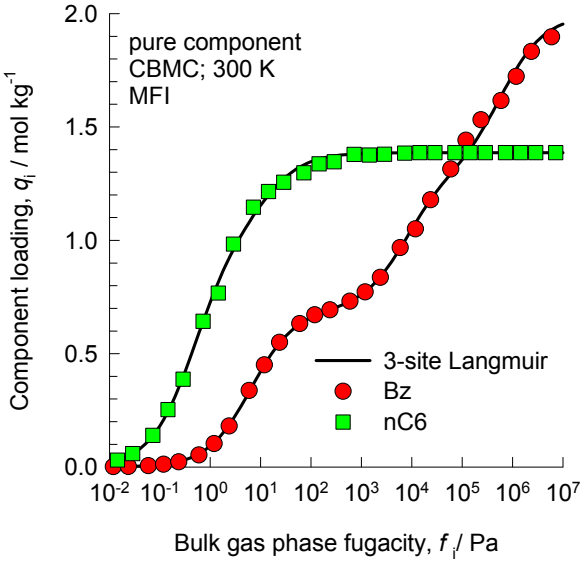


**Pure components adsorption**

# nC6 -Bz/ MFI / 300K

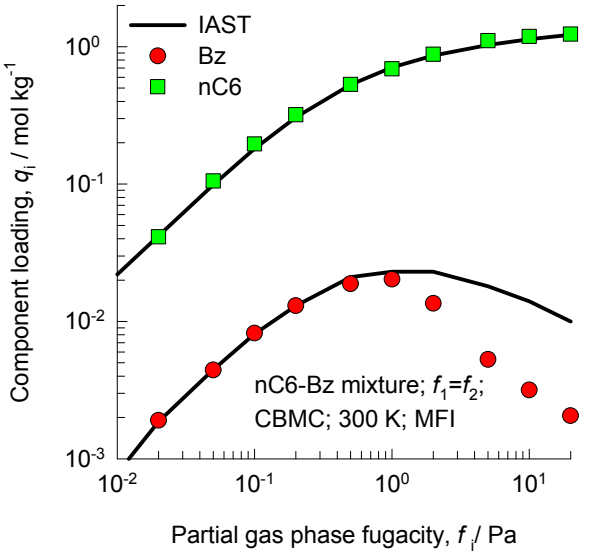


**mixture adsorption**

The failure of IAST to describe mixture adsorption accurately is because of segregation effects. Benzene locates preferentially at the intersections. This implies that there is no homogeneous distribution of the mixture over the entire MFI framework. This non-homogeneous distribution of molecules causes departures from IAST.

The adsorption and diffusion characteristics are discussed in further details in:
R. Krishna, J.M. van Baten, Diffusion of hydrocarbon mixtures in MFI zeolite: Influence of intersection blocking, Chem. Eng. J. 140 (2008) 614-620.

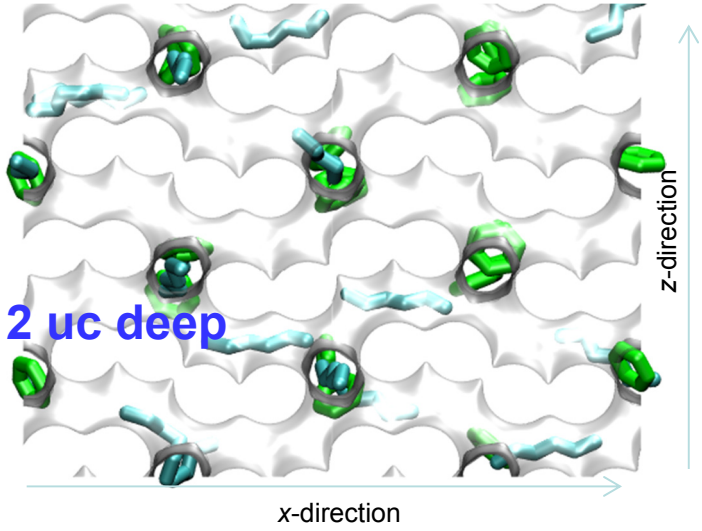


*y*-direction of yields highest diffusivity; this is a straight path

*x*-direction of yields intermediate; this is a zig-zag path

*z*-direction of yields lowest diffusivity

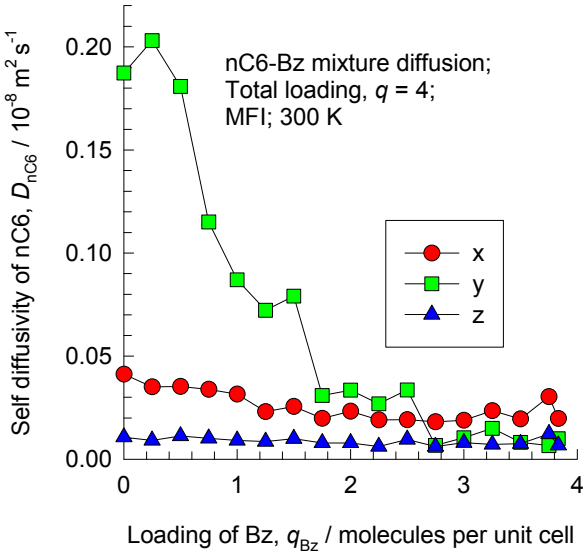


**nC6 = 2 molecules/uc**
**Bz = 2 molecules/uc**

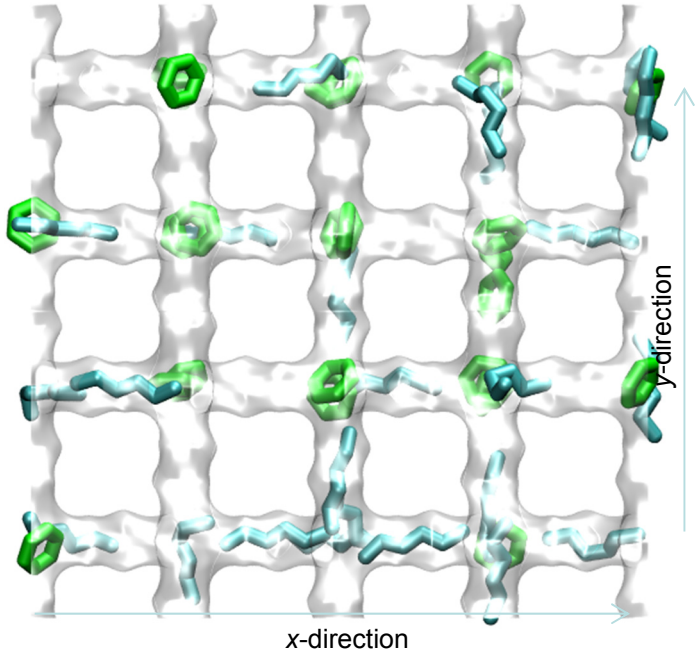


**3 uc deep**

# nC6 -Bz/ MFI / 300K

## mixture diffusion

The adsorption and diffusion characteristics are discussed in further details in:
R. Krishna, J.M. van Baten, Diffusion of hydrocarbon mixtures in MFI zeolite: Influence of intersection blocking, Chem. Eng. J. 140 (2008) 614-620.

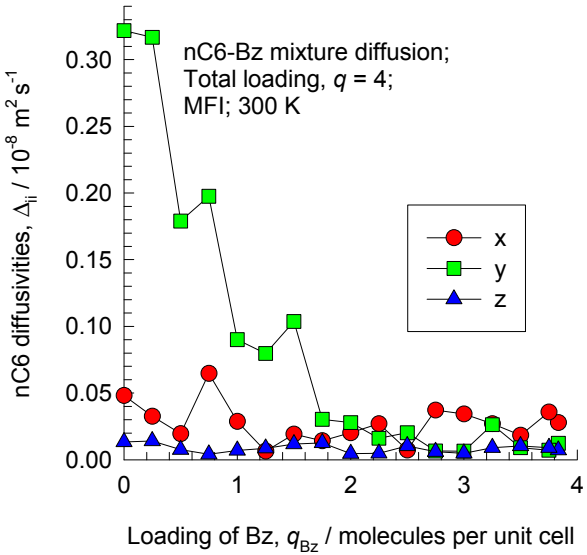

# Guest Mixture in MFI zeolite: $C_2H_4$/Benzene

The adsorption and diffusion characteristics are discussed in further details in:
N. Hansen, R. Krishna, J.M. van Baten, A.T. Bell, F.J. Keil, Analysis of Diffusion Limitation in the Alkylation of Benzene over H-ZSM-5 by Combining Quantum Chemical Calculations, Molecular Simulations, and a Continuum Approach, J. Phys. Chem. C 113 (2009) 235-246.
N. Hansen, R. Krishna, J.M. van Baten, A.T. Bell, F.J. Keil, Reactor simulation of benzene ethylation and ethane dehydrogenation catalyzed by ZSM-5: A multiscale approach, Chem. Eng. Sci. 65 (2010) 2472-2480.

Figure B113

**Snapshots showing the location of molecules within MFI**

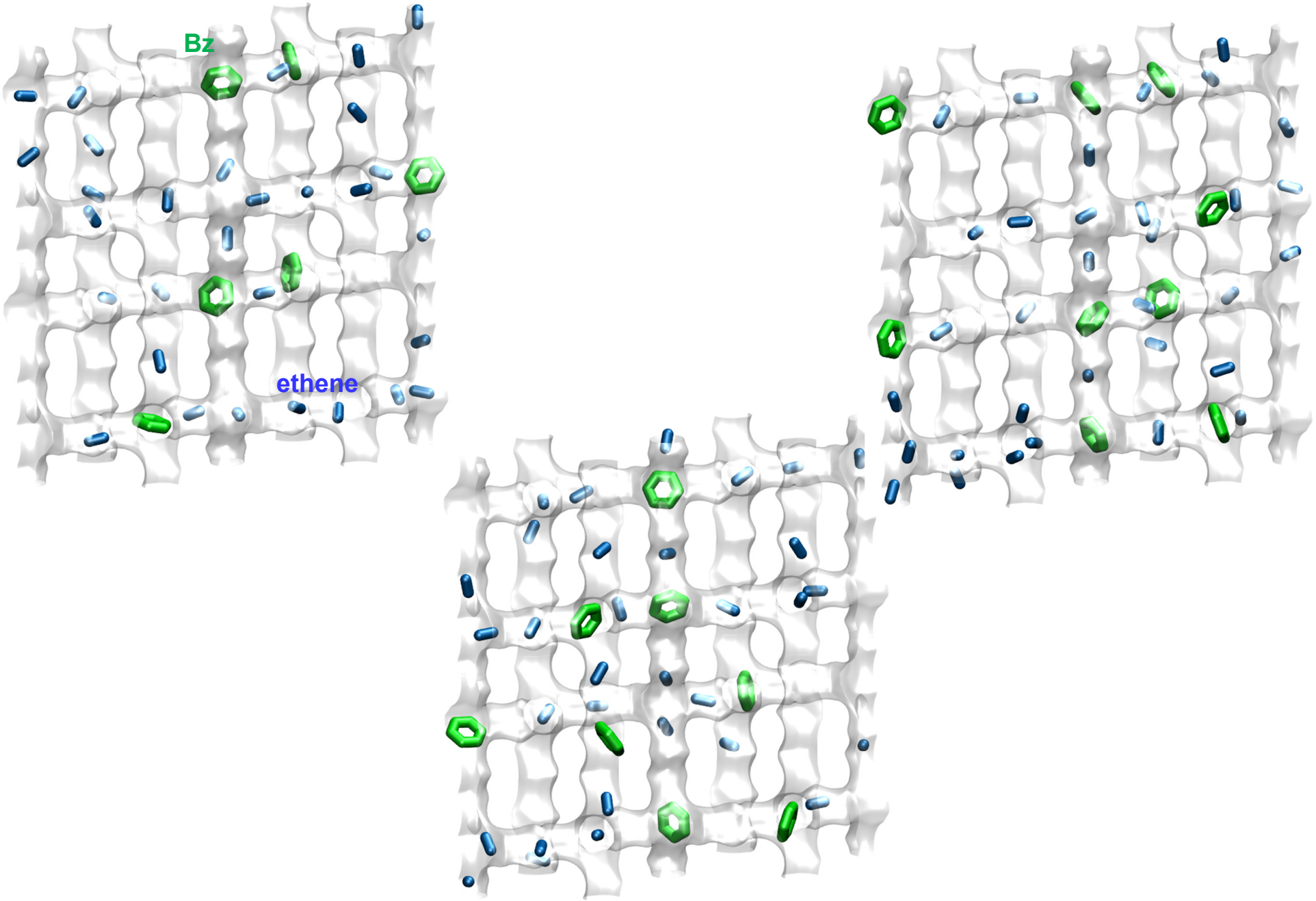

# Guest Mixture in MFI zeolite: nC6/3MP/22DMB

The adsorption characteristics are discussed in further details in:
Krishna, J.M. van Baten, In silico screening of metal-organic frameworks in separation applications, Phys. Chem. Chem. Phys. 13 (2011) 10593-10616.

Figure B115

**Snapshots showing the location of molecules within MFI**

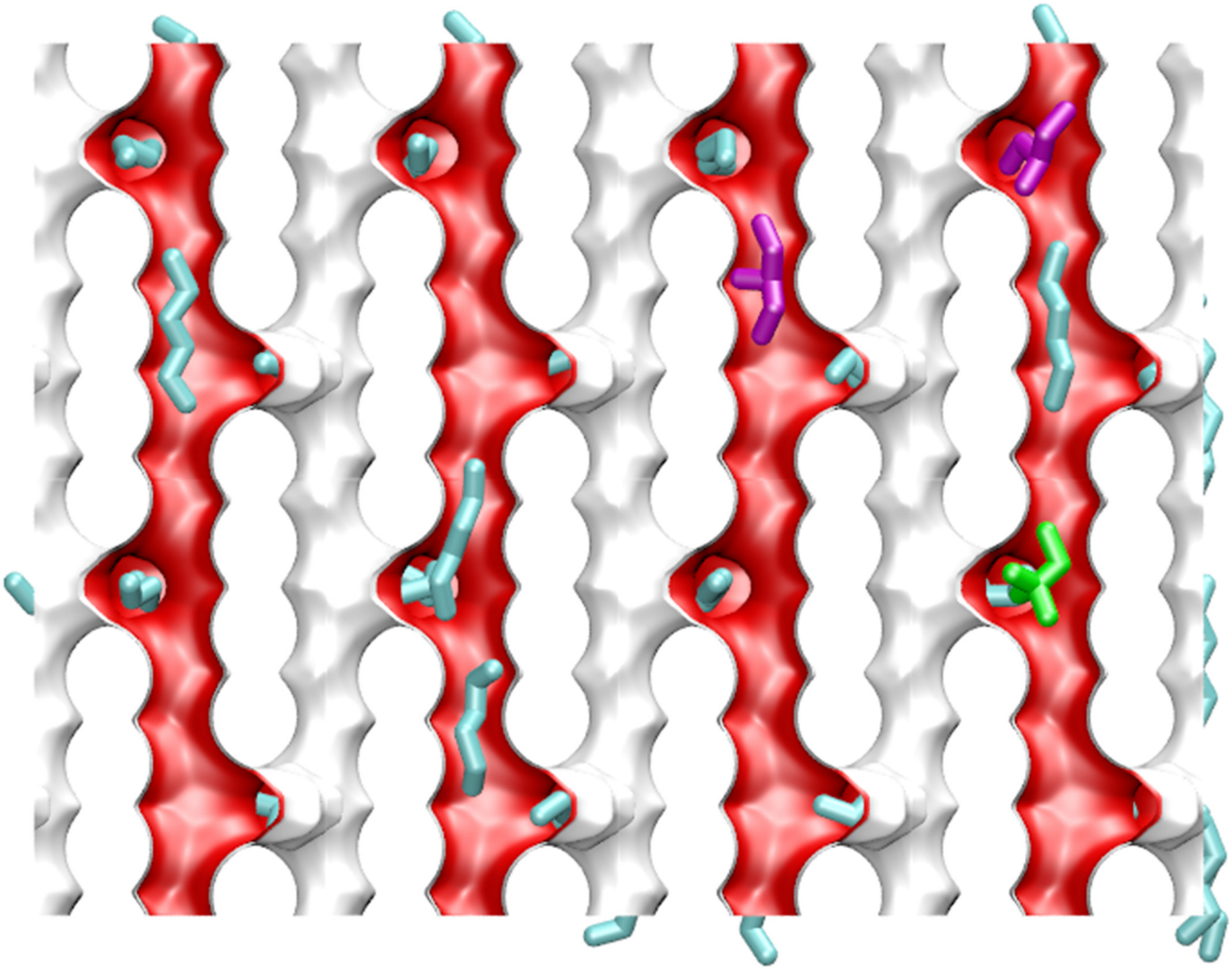

Figure B116

**Snapshots showing the location of molecules within MFI**

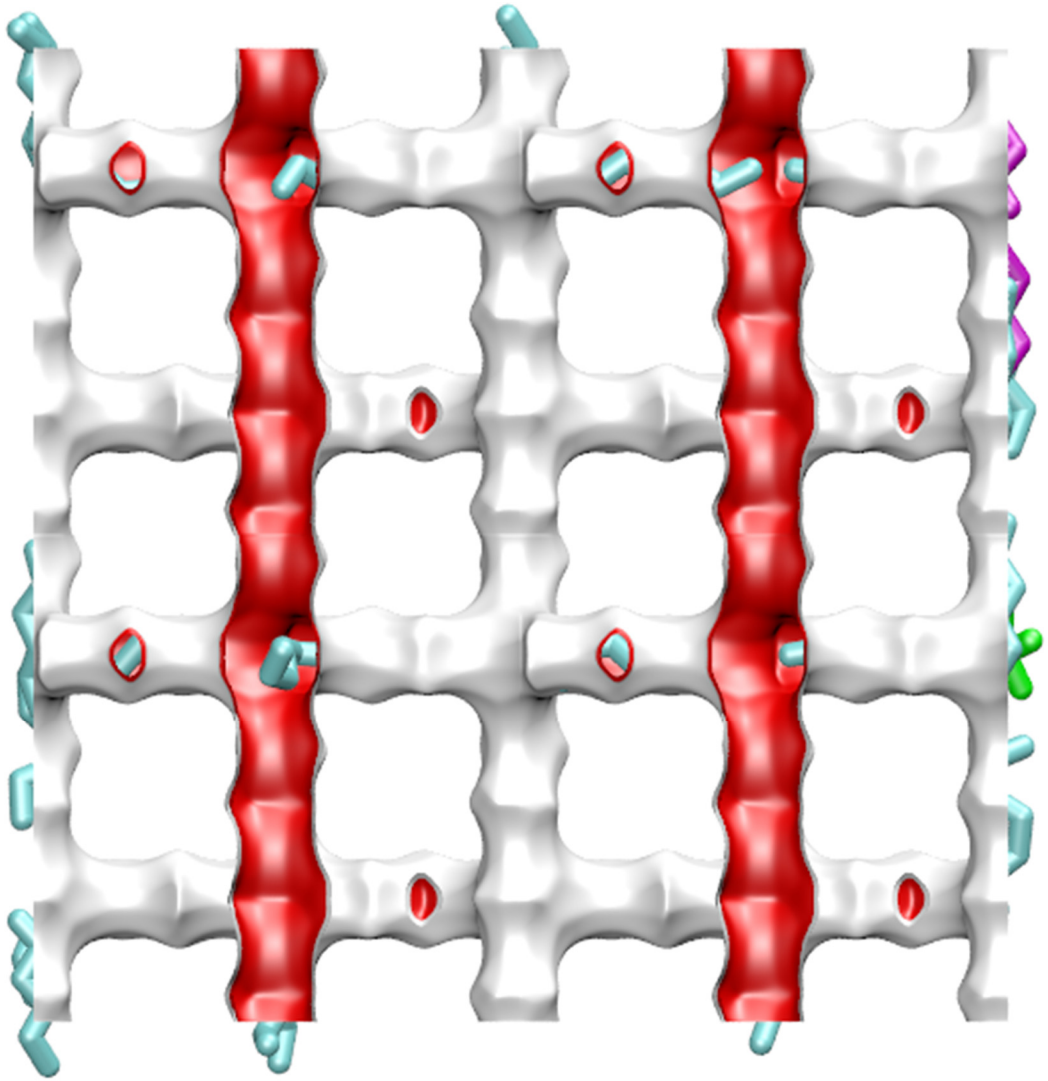

# Guest Mixture in MFI zeolite: $C_2H_4$/Benzene/Ethylbenzene

The adsorption and diffusion characteristics are discussed in further details in:
N. Hansen, R. Krishna, J.M. van Baten, A.T. Bell, F.J. Keil, Analysis of Diffusion Limitation in the Alkylation of Benzene over H-ZSM-5 by Combining Quantum Chemical Calculations, Molecular Simulations, and a Continuum Approach, J. Phys. Chem. C 113 (2009) 235-246.
N. Hansen, R. Krishna, J.M. van Baten, A.T. Bell, F.J. Keil, Reactor simulation of benzene ethylation and ethane dehydrogenation catalyzed by ZSM-5: A multiscale approach, Chem. Eng. Sci. 65 (2010) 2472-2480.

Figure B118

**Snapshots showing the location of molecules within MFI**